



UNIVERSIDAD CARLOS III DE MADRID

Ph. D. Thesis

Stable locomotion of humanoid robots based on
mass concentrated model

Author:
Mario Ricardo Arbulú Saavedra

Director:
Carlos Balaguer Bernaldo de Quiros, Ph. D.

Department of System and Automation Engineering

Leganés, October 2008

Ph. D. Thesis

Stable locomotion of humanoid robots based on
mass concentrated model

Author: Mario Ricardo Arbulú Saavedra

Director: Carlos Balaguer Bernaldo de Quiros, Ph. D.

Signature of the board:

President		Signature
Vocal		
Vocal		
Vocal		
Secretary		

Rating:

Leganés, de de

Contents

1	Introduction	1
1.1	History of Robots	2
1.1.1	Industrial robots story	2
1.1.2	Service robots	4
1.1.3	Science fiction and robots currently	10
1.2	Walking robots	10
1.2.1	Outline	10
1.2.2	Themes of legged robots	13
1.2.3	Alternative mechanisms of locomotion: Wheeled robots, tracked robots, active cords	15
1.3	Why study legged machines?	20
1.4	What control mechanisms do humans and animals use?	25
1.5	What are problems of biped control?	27
1.6	Features and applications of humanoid robots with biped loco- motion	29
1.7	Objectives	30
1.8	Thesis contents	33
2	Humanoid robots	35
2.1	Human evolution to biped locomotion, intelligence and bipedalism	36
2.2	Types of researches on humanoid robots	37
2.3	Main humanoid robot research projects	38
2.3.1	The Humanoid Robot at Waseda University	38
2.3.2	Honda robots	47
2.3.3	The HRP project	51
2.4	Other humanoids	54
2.4.1	The Johnnie project	54
2.4.2	The Robonaut project	55
2.4.3	The COG project	56
2.4.4	The Einstein-HUBO humanoid project	57
2.4.5	Toyota Partner Robots	58
2.4.6	The Rh-1 humanoid project	60
2.4.7	Humanoid entertainment robots	61
3	Human locomotion study. The stability of biped locomotion	65
3.1	Human biomechanics	66
3.1.1	Kinematics	66
3.1.2	Human locomotion	67

3.1.3	Anthropomorphic human dimensions, volume and weight distribution	71
3.1.4	Human walking trajectories	74
3.2	Biped locomotion stability criteria	77
3.2.1	Zero Moment Point (ZMP)	77
3.2.2	Foot-Rotation Indicator (FRI) Point	84
3.2.3	Universal stability criterion of the foot contact of legged robots: Contact Wrench Cone (CWC)	88
3.2.4	Comparison between the biped locomotion stability criteria	94
4	Study of humanoid robot gaits	96
4.1	Passive and active walking	97
4.1.1	Passive walking	97
4.1.2	Active walking	98
4.2	Static and dynamic gait	99
4.2.1	Static gait	99
4.2.2	Dynamic gait	100
4.3	Gait generation models	100
4.3.1	Joint space method	101
4.3.2	Virtual forces model	102
4.3.3	Mass distributed models	103
4.3.4	Pattern generator of a humanoid robot, taking into account the Contact Wrench Cone (CWC)	105
4.3.5	Two Masses Inverted Pendulum Mode (TMIPM)	108
4.3.6	The Multiple Masses Inverted Pendulum Mode (MMIPM)	110
4.3.7	Mass concentrated models	112
4.3.8	The 2D Inverted pendulum model	112
4.3.9	Laws of motion of a 3D Inverted pendulum model	115
4.3.10	Cart-table model	121
4.3.11	Discussion about inverted pendulum and cart-table models	125
5	Gait generation method	129
5.1	Outline	130
5.2	Layers of the “Gait generation” method	130
5.3	Layer 1: Global motion	131
5.4	Layer 2: Local motion - “Local Axis Gait” algorithm	132
5.4.1	Swing foot motion	132
5.4.2	Local axis gait algorithm	135
5.5	Layer 3: Motion Patterns Generation-“COG and ZMP” references	136
5.6	Cases of applying layers 1 to 3	137
5.7	Layer 4: Kinematics and dynamics modelling	139
5.7.1	Background of screw theory, Paden-Kahan subproblems and lie groups	140
5.7.2	Whole-body humanoid kinematics model	146
5.7.3	Forward kinematics	148
5.7.4	Inverse kinematics	150
5.7.5	Inverse dynamics	153
5.8	Layer 5: Off-line control	157
5.9	Acyclic Gait	163
5.9.1	Related work	164

5.9.2	Problem Statement	165
5.9.3	Overview of the Method	165
5.9.4	Upper body motion	167
5.9.5	Whole body motion	168
6	Results	173
6.1	Rh-1 specifications	174
6.2	HRP-2 specifications	176
6.3	Simulation and Experimental results	179
6.3.1	Simulation results on the Rh-1 humanoid robot platform .	179
6.3.2	Experimental results on Rh-1 humanoid robot platform .	184
6.3.3	Simulation and Experimental results on HRP-2 humanoid robot platform	204
7	Conclusions, contributions and future works	218
7.1	Conclusions	218
7.2	Contributions	223
7.3	Future work	225
	Appendices	228
	A Human COG projection and ZMP Measure system	229
	B Distribution of masses and inertias of medium human	239

List of Figures

1.1	Industrial robots working in a factory.	3
1.2	Estimated yearly supply of industrial robots at year's end in the world by main industries 2005 - 2006.	4
1.3	Some service robots.	5
1.4	Chart of service robots in Japan.	6
1.5	Examples of services robots. University Carlos III of Madrid, some Roboticslab service robots: ROMA 2 (climbing robot for inspection), Manfred (mobile manipulator), ASIBOT (Portable assistive robot), Maggie (Personal social robot).	7
1.6	Service robots in space.	8
1.7	The General Electric Walking Truck and Hirose Lab walking robots.	13
1.8	The General Electric Hardiman.	14
1.9	Humanoid robot cooperating with human in open-air tasks.	16
1.10	Wheels and tracks with external spokes.	16
1.11	Triangular clusters of wheels for stair climbing.	17
1.12	Variable geometry tracked vehicles.	17
1.13	Virtual K9 driving over a synthetic rock.	17
1.14	Artist's simulation of a Mars Exploration Rover at work on Mars.	18
1.15	The WorkPartner robot, with hybrid wheel-leg locomotion system.	19
1.16	Active Cord Mechanism - Revision 1 (ACM-R1), which is a wireless controlled snake-like robot.	20
1.17	Relative leg-length and maximum relative speed of various planar biped robots. (A) A copy of McGeer's planar passive biped robot walking down a slope. (B) "Mike", similar to McGeer's robot, but equipped with pneumatic actuators at its hip joints. Thus it can walk half-passively on level ground. (C) "Spring Flamingo", a powered planar biped robot with actuated ankle joints. (D) "Rabbit", a powered biped with four degree-of-freedom and point feet. (E) "RunBot". (F) The world record for the fastest human's walking speed (@Manoonpong et. al. [81]).	26
1.18	The human-like shape of a humanoid robot affords emotional feelings useful for friendly communication with humans.	29
1.19	A humanoid robot can work in an environment designed for humans. It can do dirty and demanding jobs, dangerous jobs (Bio-terror, SARS, etc.)	30
1.20	A humanoid can expand its ability by using machines and equipment that we use now.	30
1.21	Some applications of humanoid robots.	31

2.1	Metropolis and the Bicentennial Man.	36
2.2	The main humanoid robot research groups.	38
2.3	The bipeds WL-1 and WL-3.	39
2.4	The bipeds WAP-1, WAP-2 and WAP-3.	40
2.5	The bipeds WL-1, WL-5, WL-9 and WL-10.	41
2.6	The arms WAM-1, WAM-2 and WAM-4.	42
2.7	The arms WAM-7 and WAM-8L.	42
2.8	Computer-Aided Design System for Link Mechanisms, Artificial Limbs and Robotics.	43
2.9	The WABOT-1 and WABOT-2 humanoid robots.	44
2.10	The WABIAN and WABIAN RV humanoid robots.	46
2.11	The WABIAN 2R humanoid robot.	47
2.12	The ASIMO humanoid robot history [58].	48
2.13	A Honda humanoid robot P1 (1.820m and 210 Kg).	50
2.14	The New ASIMO humanoid robot.	51
2.15	The HRP-2P humanoid robot [3].	52
2.16	The HRP-2, HRP-3 and HRP-3P humanoid robots.	53
2.17	The Johnnie humanoid robot.	55
2.18	a) COG and b) Robonaut humanoid robots.	57
2.19	The Einstein-Hubo humanoid robot, the HUBO Lab humanoid. .	58
2.20	The Toyota Partner Robots concept.	59
2.21	The Toyota humanoid robots.	59
2.22	The Rh-1 humanoid robot, the University Carlos III of Madrid humanoid.	61
2.23	The QRIO robot, the SONY humanoid, and HOAP-3, the Fujitsu humanoid.	62
2.24	The evolution of HONDA humanoid robots.	63
2.25	The evolution of the Kawada-AIST humanoid robots.	64
2.26	The evolution of the WASEDA humanoid robots.	64
3.1	Human motion planes ©NASA [90].	66
3.2	The gait cycle, (<i>Reprinted, with permission, from a chapter by V.T. Inman et al., which appeared on page 26 of Human Walking, edited by Rose and Gamble and published by Williams Wilkins, Baltimore, MD; 1981.</i>)	67
3.3	The gait cycle has two phases: about 60-percent stance phase and about 40-percent swing phase with two periods of double support which occupy a total of 25 to 30 percent of the gait cycle.	68
3.4	Relationship between the tasks of gait and the phases of gait.	69
3.5	The vertical force shows the five phases of gait at stance event. Normally it exceeds body weight at two intervals, [21].	70
3.6	(a) Pelvic rotation effectively extends the trailing and advancing support points. (b) Pelvic tilt reduces vertical displacement of the center of mass, [21].	70
3.7	Anthropomorphic human dimensions, ©Winter, D., [125]	72
3.8	Whole body volume of American male crew member, ©NASA [90].	73
3.9	Human leg motion, sagittal view.	74
3.10	Human leg motion, top view.	75
3.11	Human leg motion, 3D view.	75
3.12	Human leg and shoulder ("red stick") motion during walking.	76

3.13	3D view of continuos stick chart of Human leg motion.	76
3.14	Sagital view of continuos stick chart of Human leg motion.	77
3.15	Biped mechanism and forces acting on its sole © Vukobratovic, et. al. [118].	79
3.16	Illustration of the determination of ZMP position © Vukobratovic, [118]: (a) Step 1, and (b) Step 2.	82
3.17	Possible relations between ZMP and CoP for a non-rigid foot: (a) dynamically balanced gait, (b) unbalanced gait where the ZMP does not exist and the acting ground reaction force point is CoP while the point where $M_x = 0$ and $M_y = 0$ is outside the support polygon (FZMP). The system as a whole rotates about the foot edge and overturns, and (c) tiptoe dynamic balance (“balletic motion”) © Vukobratovic, [118].	83
3.18	The sketch of a 3-D extended rigid-body biped robot (left), and a view with its support foot artificially disconnected from the shank to show the intervening forces (right). The CoP, GCoM, and the FRI point are denoted by P , C , and F , respectively, [51].	85
3.19	Condition for foot rotation when $\tau_1 = 0$. The figure sketches different lines of action of the force R_1 applied on the robot foot by the rest of the robot at ankle joint O_1 . If the line of action of a force intersects the ground beyond the footprint, there is a net moment applied on the foot and the foot rotates. Otherwise, the ankle joint forces may be supported by the foot/ground interaction forces, and the foot maintains static equilibrium in its stationary upright configuration, [51].	86
3.20	The locations of key points the ankle-joint location (O_1) and the support-polygon boundary (A and B), not its overall geometry are relevant for the behavior of the foot. The three examples of the robot foot shown in the figure have identical behavior, although their geometries are very different, [51].	87
3.21	The magnitude of the moment experienced by a point on the support boundary is linearly proportional to the distance of this point from the FRI point. The magnitudes of the moments at different points are shown by the length of the arrows. Clockwise (i.e., negative) moments are shown by upward-pointing arrows, and counterclockwise (i.e., positive) moments are shown by downward-pointing arrows. In the image, of the left the moments are precisely compensated, whereas in the image on the right they are not. The subscript n denotes the normal component of a force, © A. Goswami, [51].	88
3.22	Support polygon and an intersection of the polyhedral convex cone © Hirukawa et. al., [56].	89
3.23	Model of the system, [56].	90
3.24	Two feet on a horizontal plane, [56].	91
4.1	A chain of four rigid, inanimate links will walk by themselves down a shallow incline, ©T. McGeer, [84].	97
4.2	Active biped walking.	98
4.3	Static and dynamic gait, [10].	99
4.4	Five steps phases, [42].	101

4.5	Dual-leg example. Reaction frames A_l and A_r are assumed to be in the same orientation as reference frame O so that ${}^O_{A_l}R = {}^O_{A_r}R = I$. ©Pratt et. al. [97]	102
4.6	Distributed mass model. The computation cost is increased by the transformations of the whole-body dynamics model.	104
4.7	Concentrated mass model. The computations could be done in real-time.	104
4.8	Definitions of the coordinates ©Hirukawa et. al., [57].	105
4.9	Block diagram of the pattern generator, ©Hirukawa et. al. [57].	107
4.10	Mechanical model of the robot with two masses, where mass m_6^* represents the swinging leg and mass m_3^* represents the remaining masses of the robot ©A. Albert et. al., [57].	108
4.11	Mechanical model of the robot with multiple masses in order to respect the dynamic influence of the thigh, the shank and the foot of the swinging leg ©A. Albert et. al, [57].	110
4.12	Iterative algorithm for the calculation of the torso trajectory $x_3(t)$ when using a model for the swinging leg with three concentrated masses m_4^* , m_5^* and m_6^* ,© A. Albert et. al, [57]	111
4.13	The 2D Inverted Pendulum Model with motion in x-z plane.	112
4.14	Pendulum ball rolling in potentials.	114
4.15	Three-dimensional Inverted Pendulum Model.	115
4.16	Three-dimensional Inverted Pendulum Model.	117
4.17	3D-LIPM projected onto the XY plane on the local axis.	118
4.18	The laws of mass motion under inverted pendulum in the field of gravity.	119
4.19	Temporal mass pendulum motion in x and y direction.	120
4.20	A Cart-table model, on the x-axis, ($ZMP_x = p_x$).	121
4.21	Preview gain $G_p(j)$: (a) $Z_c=0.614m$, (b) $Z_c=0.814m$ (T=5 ms, $Q_e=1.0$, $Q_x=0_{3x3}$, $R=1.0 \times 10^{-6}$).	124
4.22	Pattern generated reference ZMP_x (black line), actual ZMP_x (blue line) and COG_x (red line).	125
4.23	Overlapping the patterns generated. It is observed and undershoot in the actual ZMP, due to the short preview time.	125
4.24	Pattern generated reference ZMP_y (black line), actual ZMP_y (blue line) and COG_y (red line).	126
4.25	Overlapping the patterns generated. It is observed and overshoot in the actual ZMP, due to the short preview time.	126
4.26	Comparison between Cart-table and 3D-LIPM.	127
5.1	Concept of gait generation method. For reaching the “Global goal”, a set of “Local motions” must be generated. Thus the local motion decide the better foot location for going ahead, go back, turn left, turn right, doing lateral step, climbing a stair or ramp.	130
5.2	Layers for humanoid gait motion generation.	131
5.3	Layer 1: Global motion of the humanoid robot.	132
5.4	Swing foot and reference frames for 3D planning motion in each step. In this case, the n^{th} step planning is shown.	133

5.5	Swing foot motion planning changing walking direction in real time. The n -th step trajectory is represented by the bold black line, which has two zones: climbing and landing. The swing foot is represented by the bold red rectangles, while the support foot is represented by the bold blue rectangle.	135
5.6	Convex hull (polygon with diagonal lines) between the feet (blue rectangles). The first and second ones are double support, the third one is a single support case. In any case, the ZMP must be inside to achieve stable walking.	137
5.7	ZMP and COG motion planning in the n -th step, Inverted pendulum model walking pattern.	138
5.8	Global motion with 3D-LIPM. Projection of COG motion planning (blue trajectory), foot motion (red trajectories); each rectangle is the feet.	139
5.9	Global motion with 3D-LIPM. Projection of COG motion planning (blue trajectory), foot motion (red trajectories); each rectangle is the feet.	139
5.10	ZMP and COG motion planning in the n -th step, Cart-table model.	140
5.11	Global motion with Cart-table. Reference ZMP (black line), actual ZMP (red line) and COG (blue line) trajectories in a plane parallel to the walking surface.	140
5.12	Time computation of inverse kinematics using D-H parameters and inverse Jacobian vs. POE	141
5.13	Screw motion of "p"	142
5.14	Rotation on single axis " ω " from point "p" to point "k"	144
5.15	Rotation on two subsequent axes " w_1 " and " w_2 " from "p" to "c" and from "c" to "k"	145
5.16	Rotation of point "p" to "k" which is a distance " δ " from "q"	146
5.17	Rh-1 kinematics configuration.	147
5.18	Four manipulator kinematics model.	147
5.19	Degrees of freedom (θ_1 to θ_{21}), position and orientation of hands ($\theta_{\theta_x}^{rh}$ to $\theta_{\theta_z}^{rh}$, $\theta_{\theta_x}^{lh}$ to $\theta_{\theta_z}^{lh}$), COG (θ_x^a , θ_y^a , θ_z^a , $\theta_{\theta_x}^a$, $\theta_{\theta_y}^a$, $\theta_{\theta_z}^a$) and feet (θ_x^r to $\theta_{\theta_z}^r$, θ_x^l to $\theta_{\theta_z}^l$).	149
5.20	Manipulator with three degrees of freedom.	155
5.21	Rh-1 mass distribution for dynamics modelling.	156
5.22	Flexion frontal angle " θ " due to the dynamics and effects of gravity.	158
5.23	Inverted pendulum with spring.	158
5.24	Inverted pendulum with spring-free body diagram.	159
5.25	Humanoid robot walking as a rigid body. The COG (green) follows the 3D-LIPM reference (red). The feet follow the splines references, too.	160
5.26	The theoretical pattern (bold black line) and the compensated pattern (dashed black line) of the right frontal ankle joint: q_1 . In the single support phase, the COG follows the 3D-LIPM, cart-table or another one, with combination of the pendulum with spring to compensate the defects of inertia, gravity, mechanics and terrain.	161
5.27	The theoretical pattern (bold black line) and the compensated pattern (dashed black line) of the left frontal ankle joint: q_{12}	162

5.28	The theoretical COG spatial pattern (black line) and the compensated pattern (red line). Feet patterns are shown, too.	162
5.29	Rh-0 humanoid robot walking with the proposed compensation. .	163
5.30	Motion from any statically stable posture to another one.	165
5.31	Flowchart of the method. X_i and X_g , are the initial and goal position, and θ_i and θ_g are the initial and goal orientation. Those are computed for the COG and feet by the forward kinematics. .	166
5.32	The upper body motion as an asynchronous way.	167
5.33	Preview gain $G_p(j)$: (a) $Z_c=0.614\text{m}$, (b) $Z_c=0.814\text{m}$ ($T=5\text{ ms}$, $Q_e=1.0$, $Q_x=0_{3\times 3}$, $R=1.0\times 10^{-6}$).	169
5.34	COG planning by compensating with the multi body ZMP . . .	170
5.35	One acyclic step. The ZMP trajectory on frontal plane with respect to the COG is always inside the support foot sole boundary. The swing foot motion is made while the ZMP is inside the foot sole boundary.	171
5.36	Two acyclic steps.	171
6.1	Rh-1 humanoid robot.	175
6.2	Rh-1 humanoid robot dimensions.	175
6.3	HRP-2 humanoid robot.	177
6.4	Walking patterns under the LAG algorithm. The blue rectangles are feet, the COG motion (blue patterns) and the feet motion (red patterns).	181
6.5	Snapshots of the Rh-1 walking under the LAG algorithm.	181
6.6	Walking patterns under the LAG algorithm.	182
6.7	Snapshots of the Rh-1 walking under the LAG algorithm.	182
6.8	The Rh-1 working in cooperation with a human carrying a construction ladder. (a) approaching. (b) grasping. (c) giving. (d) leaving. (e) and (d) back to the rest position.	183
6.9	Cooperation in disaster cases. In this case, the walking pattern and control system must deal with rough terrain during working cooperation tasks. Therefore, strong stability criteria such as the CWC could be used to prevent the humanoid from tipping over. .	183
6.10	VRML simulation and the Rh-1 without cover, static gait taking four steps forward.	184
6.11	Angular patterns of overlapped right leg joints. The red are ones the measured patterns and the blue ones are the reference patterns. .	185
6.12	Current of the right leg joints.	185
6.13	Snapshots of gait rotating on the vertical axis.	186
6.14	Three steps by dynamic walking patterns under the LAG algorithm, at 0.35Km/h	187
6.15	Walking reference patterns. COG pattern (black line), right foot (red line) and left foot (blue line).	188
6.16	Joint patterns of each leg, which are q_1 to q_6 for the right leg and q_7 to q_{12} for the left leg. The blue patterns are the reference patterns and the red patterns include the off-line compensation with delay.	189

6.17 Joint patterns of each leg, which are q_1 to q_6 for the right leg and q_7 to q_{12} for the left leg. The red patterns are the compensated reference patterns and the black patterns are measured by the encoders. The joint control allows the patterns to follow with a little error, but it is enough to obtain a stable walk.	190
6.18 Joint angular velocities of each leg, which are w_1 to w_6 for the right leg and w_7 to w_{12} for the left leg. Velocities during walking.	191
6.19 Joint currents of each leg, which are I_1 to I_6 for the right leg and I_7 to I_{12} for the left leg. Actual currents during walking motion.	192
6.20 Four steps by dynamic walking patterns under the LAG algorithm, increasing velocity about 0.7Km/h. Experimentally, the dynamic walking patterns are tested successfully. Higher velocity and continuity of walking patterns could be obtained by closing the loop of the whole body control system.	193
6.21 Joint patterns of each leg, which are q_1 to q_6 for the right leg and q_7 to q_{12} for the left leg. The red patterns are the compensated reference patterns and the black patterns are measured by the encoders. The joint control allows to track the patterns with a little error, but it is enough to obtain a stable walk.	194
6.22 Joint angular velocities of each leg, which are w_1 to w_6 for the right leg and w_7 to w_{12} for the left leg. Actual velocities during walking.	195
6.23 Joint currents of each leg, which are I_1 to I_6 for the right leg and I_7 to I_{12} for the left leg. Actual currents during walking motion.	196
6.24 Three steps by dynamic walking patterns under the LAG algorithm, velocity about 0.55Km/h. With onboard hardware, batteries and covers, the weight the Rh-1 increases from 35kg. to 48.5kg.	197
6.25 Joint patterns of each leg, which are q_1 to q_6 for the right leg and q_7 to q_{12} for the left leg. The red patterns are the compensated reference patterns and the black patterns are measured by the encoders. Joint control allows to track the patterns with a little error, but it is enough to obtain a stable walk.	198
6.26 Joint angular velocities of each leg, which are w_1 to w_6 for the right leg and w_7 to w_{12} for the left leg. Actual velocities during walking.	199
6.27 Joint currents of each leg, which are I_1 to I_6 for the right leg and I_7 to I_{12} for the left leg. Actual currents during walking motion.	200
6.28 Three steps by dynamic walking patterns in the hall under the LAG algorithm, velocity about 0.55Km/h. With onboard hardware, batteries and covers, the weight of the Rh-1 increases from 35kg. to 48.5kg.	201
6.29 Rh-1 humanoid robot making a greeting.	202
6.30 Spatial trajectory of the humanoid hand. The points p_1 , p_2 , p_3 and p_4 are the subgoals needed to make a gesture.	203
6.31 X, Y and Z temporal spatial trajectories of the humanoid hand.	203
6.32 θ_x^{lh} , θ_y^{lh} and θ_z^{lh} temporal orientation trajectories of the humanoid hand.	204
6.33 Temporal joints trajectories of the humanoid's left arm.	204
6.34 Simulation and actual acyclic step forward.	205

6.35 Actual results of angular joint patterns for taking one acyclic step forward, from the initial to the goal state. The right and the left side are shown. In both cases, the goal state is reached by a smooth and natural motion from the initial one (red dots).	206
6.36 ZMP_y , ZMP_x reference and measuring. COG_y , COG_x trajectory and vertical reaction forces on each foot.	207
6.37 Simulation and experimental result of one acyclic step backward and rotating.	208
6.38 Actual results of angular joint patterns for taking one acyclic step backward from the initial to the goal state. The right side and the left side of the humanoid are shown. In both cases, the goal state is reached by a smooth and natural motion from the initial one (red dots).	209
6.39 ZMP_y , ZMP_x reference and measuring. COG_y , COG_x trajectory and vertical reaction forces on each foot.	210
6.40 Simulation of two acyclic steps forward.	211
6.41 Experiment of two acyclic steps forward.	211
6.42 ZMP_y , ZMP_x reference and measuring. COG_y , COG_x trajectory and vertical reaction forces on each foot.	212
6.43 Torques on each joint of both legs while taking two acyclic steps forward.	213
6.44 Torques on each joint of both arms while taking two acyclic steps forward.	214
6.45 Torques on chest while taking two acyclic steps forward.	215
6.46 Horizontal force reactions on right foot.	215
6.47 Horizontal force reactions on left foot.	215
7.1 The evolution of HONDA humanoid robots.	219
7.2 The evolution of the Kawada-AIST humanoid robots.	219
7.3 The evolution of the WASEDA humanoid robots.	220
7.4 Cooperation tasks on construction.	226
7.5 Friction control of foot rotation.	226
7.6 Current consumption by left (q_{10}) and right (q_4) hips (Pitch direction, red rectangles). In red rectangles the currents are constant, because the load requires the motor current limit.	227
A.1 ZMP hardware measure system.	229
A.2 CAD design of the metal platform with load cells.	230
A.3 Acquisition card.	231
A.4 ZMP guide overview.	232
A.5 ZMP software structure.	232
A.6 Center of pressure computation, taking into account the forces of each corner on the platforms.	233
A.7 Experimental walking test.	234
A.8 ZMP_x computation, with mass concentrated model.	235
A.9 On-line measure of experimental walking test.	235
A.10 Off-line chart of preview experimental walking test.	236
A.11 Plotting sagittal CoP motion.	236
A.12 Plotting frontal CoP motion.	237
A.13 Acceleration in each direction.	237

A.14 ZMP evolution (black line).	238
A.15 Experimental walking test.	238
B.1 Planes of body segmentation.	239
B.2 Principal axis orientation for the head relative to the anatomical axis system.	240
B.3 Head link.	241
B.4 Neck link.	241
B.5 Thorax link.	241
B.6 Abdomen link.	241
B.7 Pelvis link.	242
B.8 Upper arm link.	242
B.9 Fore arm link.	242
B.10 Hand link.	243
B.11 Thigh link.	243
B.12 Calf link.	243
B.13 Foot link.	244
B.14 Body linkage and centers of mass for the mid-sized male aviator. Units are in centimeters.	244

List of Tables

1.1	Advantages and disadvantages of wheeled vs. legged locomotion.	23
1.2	Advantages and disadvantages of legged vs. biped locomotion.	24
3.1	Human volume distribution, ©NASA [90].	73
3.2	ZMP/FRI vs. CWC	94
4.1	3D-LIPM vs. Cart-table. (*SS: Single Support; **DS: Double Support)	128
6.1	Rh-1 humanoid robot degrees of freedom.	174
6.2	Rh-1 humanoid robot angular joint ranges vs human angular joint ranges.	176
6.3	HRP-2 humanoid robot degrees of freedom.	177
6.4	HRP-2 humanoid robot angular joint ranges vs. human angular joint ranges.	178
6.5	Walking parameters for taking many steps and changing direction.	180
B.1	Head properties. The principal axes are rotated -36 degrees on the Y_a axis.	241
B.2	Neck properties. The principal axes are rotated 22.2 degrees on the Y_r axis.	241
B.3	Thorax properties. The principal axes are rotated -12 degrees on the Y_r axis.	241
B.4	Abdomen properties. The principal axes are coincident with the reference axes.	241
B.5	Pelvis properties. The principal axes are rotated -24 degrees on the Y_r axis.	242
B.6	Upper arm properties. The Z_p axis is coincident with the Z_r axis and the X_p and Y_p axes are degenerate.	242
B.7	Forearm properties. The Z_p axis is coincident with the Z_r axis and the X_p and Y_p axes are degenerate.	242
B.8	Hand properties. The principal axes are coincident with the reference axes with the hand aligned, as shown in Figure 3.1.	243
B.9	Thigh properties. The Z_p axis is coincident with the Z_r axis and the X_p and Y_p axes are degenerate.	243
B.10	Calf properties. The Z_p axis is coincident with the Z_r axis and the X_p and Y_p axes are degenerate.	243

- B.11 Foot properties. The principal axes are coincident with the reference axes with the feet aligned as shown in Figure 3.1. 244

Acknowledgements

I want to give so much thanks to my wife Lina, children David, Almudena and Samuel, and family whose are the inspiration of this work. They have supported me during long time and they have motivated me to achieve any goal. Secondly I want to thank the Rh-0 and Rh-1 humanoid robot team: Prof. Carlos Balaguer (“Head of the humanoid robot project”), Luis Cabas (Mechanical designer), Dmitry Kaynov (Hardware and Software architecture), Pavel Staroverov (Interaction abilities), Jose Manuel Pardos (Path planning algorithms), Carlos, Paolo, Concha, Luis, our students and the Robotics lab members for their support during the last seven years. Thirdly, I want to thank the JRL-lab members (AIST, Tsukuba, Japan) for allowing me to use their resources and conclude this stage of my research specially Dr. Yokoi, Dr Kheddar, Dr. Kajita, Neo and Oliver for their helpful contribution to my research.

This research is supported by the CICYT (Comisión Interministerial de Ciencia y Tecnología), Ref.: DPI2004-00325.

Abstract

El estudio de la locomoción de robots humanoides es actualmente un área muy activa, en el campo de la robótica. Partiendo del principio que el hombre esta construyendo robots para trabajar juntos cooperando en ambientes humanos. La estabilidad durante la caminata es un factor crítico que prevee la caída del robot, la cual puede causar deterioros al mismo y a las personas en su entorno. De esta manera, el presente trabajo pretende resolver una parte del problema de la locomoción bípeda, esto es los metodos empleados para “La generación del paso” (“Gait generation”) y así obtener la caminata estable.

Para obtener una marcha estable se utilizan modelos de masa concentrada. De esta manera el modelo del “pendulo invertido simple” y el modelo del “carro sobre la mesa” se han utilizado para conseguir la marcha estable de robots humanoides.

En el modelo del pendulo invertido, la masa el pendulo conduce el movimiento del centro de gravedad (CDG) del robot humanoide durante la marcha. Se detallara que el CDG se mueve como una bola libre sobre un plano bajo las leyes del pendulo en el campo de gravedad.

Mientras que en el modelo del “carro sobre la mesa”, el carro conduce el movimiento del CDG durante la marcha. En este caso, el movimiento del carro es tratado como un sistema servocontrolado, y el movimiento del CDG es obtenido con los actuales y futuros estados de referencia del Zero Moment Point (ZMP).

El método para generar el paso propuesto esta compuesto de varias capas como son Movimiento global, movimiento local, generación de patrones de movimiento, cinemática inversa y dinámica inversa y finalmente una corrección off-line. Donde la entrada en este metodo es la meta global (es decir la configuracion final del robot, en el entorno de marcha) y las salidas son los patrones de movimiento de las articulaciones junto con el patrón de referencia del ZMP.

Por otro lado, se ha propuesto el método para generar el “Paso acíclico”. Este método abarca el movimiento del paso dinámico incluyendo todo el cuerpo del robot humanoide, desde desde cuquier postura genérica estéticamente estable hasta otra; donde las entradas son los estados inicial y final del robot (esto es los ángulos iniciales y finales de las articulaciones) y las salidas son las trayectorias de referencia de cada articulación y del ZMP.

Se han obtenido resultados satisfactorios en las simulaciones y en el robot humanoide real Rh-1 desarrollado en el Robotics lab de la Universidad Carlos III de Madrid. De igual manera el movimiento innovador llamado “Paso acíclico” se ha implementado exitosamente en el robot humanoide HRP-2 (desarrollado por el AIST e Industrias Kawada Inc., Japon). Finalmente los resultados, contribuciones y trabajos futuros se expondrán y discutirán.

Abstract

The study of humanoid robot locomotion is currently a very active area in robotics, since humans build robots to work their environments in common cooperation and in harmony. Stability during walking motion is a critical fact in preventing the robot from falling down and causing the human or itself damages. This work tries to solve a part of the locomotion problem, which is, the “Gait Generation” methods used to obtain stable walking.

Mass concentrated models are used to obtain stable walking motion. Thus the inverted pendulum model and the cart-table model are used to obtain stable walking motion in humanoid robots.

In the inverted pendulum model, the mass of the pendulum drives the center of gravity (COG) motion of the humanoid robot while it is walking. It will be detailed that the COG moves like a free ball on a plane under the laws of the pendulum in the field of gravity.

While in the cart-table model, the cart drives the COG motion during walking motion. In this case, the cart motion is treated as a servo control system, obtaining its motion from future reference states of the ZMP.

The gait generation method proposed has many layers like Global motion, local motion, motion patterns generation, inverse kinematics and inverse dynamics and finally off-line correction. When the input in the gait generation method is the global goal (that is the final configuration of the robot in walking environment), and the output is the joint patterns and ZMP reference patterns.

Otherwise, the “Acyclic gait” method is proposed. This method deals with the whole body humanoid robot dynamic step motion from any generic posture to another one when the input is the initial and goal robot states (that is the initial and goal joint angles) and the output is the joint and ZMP reference patterns.

Successful simulation and actual results have been obtained with the Rh-1 humanoid robot developed in the Robotics lab (Universidad Carlos III de Madrid, Spain) and the innovative motion called “Acyclic gait” implemented in the HRP-2 humanoid robot platform (developed by the AIST and Kawada Industries Inc., Japan). Furthermore, the results, contributions and future works will be discussed.

Chapter 1

Introduction

There is a driving force more powerful than steam, electricity and atomic energy: the Will.
(Albert Einstein)

The history of robots as a background for understanding current robotics research is outlined. The evolution to walking robotics deals with complex motion control, structural design and walking patterns. Are discussed the advantages of biped locomotion over wheeled locomotion, so the study of walking machines is justified. Although stability while walking is not a totally understood problem, some robotics researchers are developing biped machines, for working in cooperation in environments prepared for humans. An outline of the human and animals mechanism will be presented to understand the walking problem and prepare an embodiment, so, biped control problems are summarized in the proposed embodiment. Researchers have proposed many stability criteria for maintaining stability during the walking motion, which takes into account whole body biped dynamics. This work will focus on the stability criteria for generating Zero Moment Point (ZMP) based walking patterns. In this chapter, the objectives are proposed and detailed in order to clarify the subject of this thesis. One of them is that walking patterns could be generated by the distributed mass model or mass concentrated model. Experimentally, the mass concentrated model has obtained successful results and it could be apply in real time, because the computation time is considerably lower with respect to the distributed mass model and the complex non-linear dynamics are reduced to linear dynamics. Thus, the mass concentrated model will be used to generate stable walking patterns of humanoid robots. Finally, the thesis contents will be described.

1.1 History of Robots

As in any science or subject, an outline of the history of robots will be explained in order to detail a background of robotics research and machines. Some questions about robots will be asked in this chapter, such as when were robots invented, who designed the first industrial robot and how did the major robotics companies started.

The imagination of researchers and storytellers for many centuries have been captured by the robots. Since the Greeks, the first industrial robots were not produced until the 1970's. Today's cutting edge humanoid robots are the result of years of trial and error.

It is possible to classify such robots as industrial robots and Service robots. In the following paragraphs, some details about them will be explained.

1.1.1 Industrial robots story

The industrial workplace have been revolutionized by the robots. Thousands of manufacturers rely on the productivity, high performance and savings provided by modern-day industrial automation.

However, the six-axis manipulator robot equipped with a controller and driver console, took time to evolve. Currently, industrial robot is the product of many minds and numerous experiments.

Outline of the Industrial robot

The first industrial robot was invented by George Charles Devol in 1954 (he is called the father of robotics), and it was called Unimate. J. F. Engelberger and Devol funded Unimation, the first robot company. The next year General Motors installed the Unimate for die casting handling and spot welding in 1961.

In order to assist handicapped people the Rancho Arm was created in 1963. After that, in 1968, the tentacle arm was invented and it could lift a human and it had 12 degrees of freedom. It was designed by M. Minsky.

In 1969, the Stanford Arm was introduced to serial production. It achieved high dexterity when it has assemble a Model T water pump.

Next, the Silver arm was created in 1974 in the MIT. It performs precise assembly using touch and pressure sensors and microcomputer. These arms led Victor Scheinman, the inventor of the Stanford Arm, to form Vicarm, Inc. in 1974 to manufacture industrial robotic arms. Scheinman was instrumental in the creation of the PUMA (programmable universal manipulator for assembly) for Unimation. In 1977, the European robot company ASEA built two sizes of industrial robots (Fig. 1.1). In the 1980's, ASEA was one of the top ten companies in the world in power technology. After that in 1988, ASEA and BBC merged to form ABB (Asea Brown Boveri Ltd.), one of the largest electrical engineering companies in the world. Currently, strong markets and a focus on operational efficiency help ABB meet key financial targets three years ahead of schedule. ABB is the leader in industrial robot supply, service and modular manufacturing systems which have installed more than 160000 robots around the world.

Although it is difficult to give data accurately, the total worldwide stock of operational industrial robots at the end of 2006 was between a minimum of

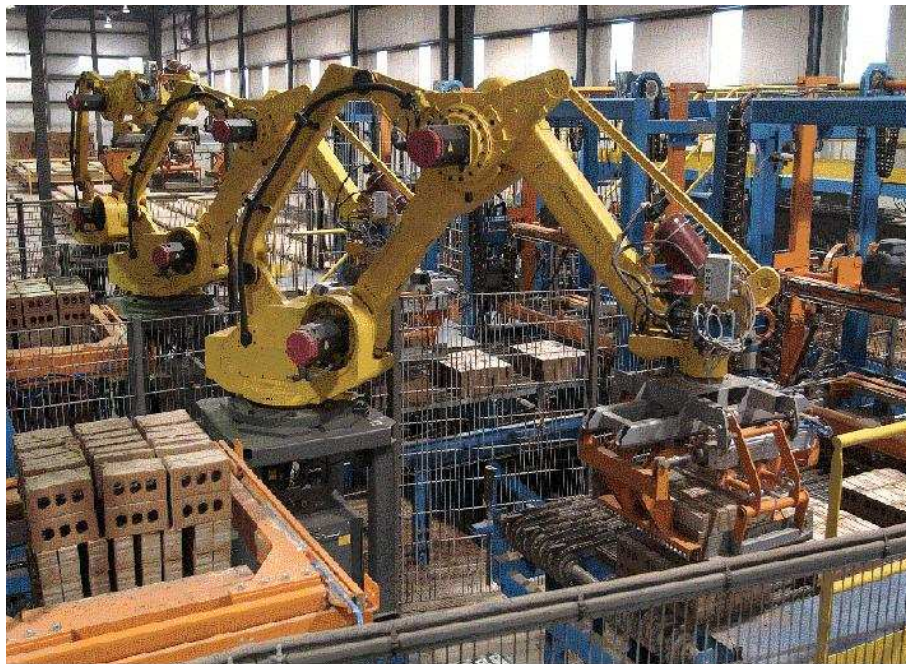


Figure 1.1: Industrial robots working in a factory.

951,000 units and a possible maximum of 1'200,000 units (International Federation of Robotics - IFR). Japan is the leader with 350,000 installed robots; Spain has about 20,000, so it is one of the seven most robotized countries of the world [11]. Spanish Industry has a high robot density, nearly 70 robot for every 10,000 workers, and the car industry has 65-70 percent of this (Fig. 1.2).

The development of the computer directly influenced the advancement of industrial robotics. The automotive industry was another contributor. In the 1980's, automotive companies showered robotic companies with investments.

However the enthusiasm and funding were not always matched with understanding. The General Motors Corporation spent more than 40 billion dollars on new technology in the 1980's, but a lack of understanding led to costly robot fiascos. In 1988, robots at the Hamtramck Michigan plant wreaked havoc, smashing windows and painting one another.

The premature introduction of robotics created financial instability. The robotics industry has only recently regained mid-1980 revenue levels. The American robotics market disappeared as Japanese and European bought up companies.

Industrial robots advantages:

The factories and enterprises has been evolve by the automation around the world. The industrial robots offer many advantages. Recent developments have made industrial robots more user-friendly, affordable, and intelligent than ever before.

- About the Product: greater accuracy is achieved by robots to perform

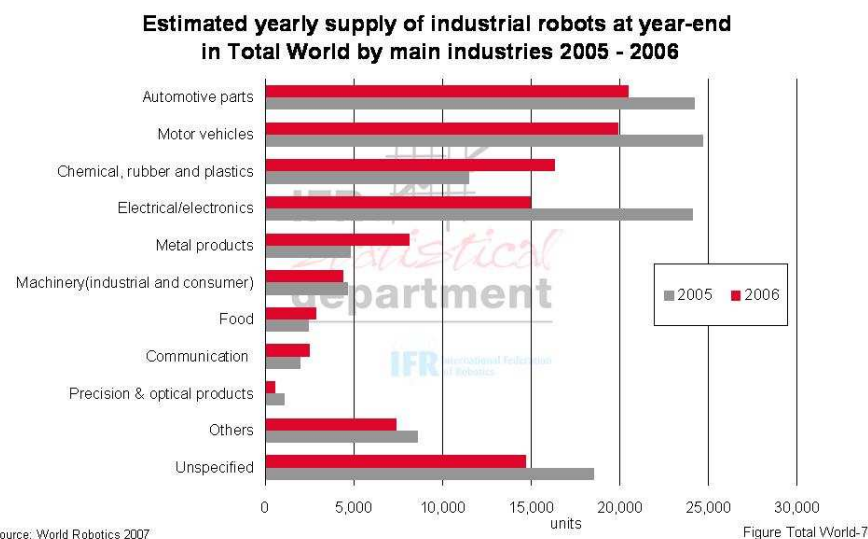


Figure 1.2: Estimated yearly supply of industrial robots at year's end in the world by main industries 2005 - 2006.

applications with precision and consistency. The product quality improves because of these increases.

- About the Environment: The arduous and dangerous tasks of workers could be avoided, because robots handle toxic substances, repetitive and detail-driven jobs, and lift, carry and select products without tiring or stopping. Many accidents and waste could be avoided by robots, so it allows to save money. The workers could learn new tasks such as programming due the introduction of robots has led many .
- About the Company: For an industrial robot, the typical return on investment is substantial and quick. Robots are leading to increased productivity and manufacturing cost cuts; otherwise they are tireless. Management control has been increased as well.

The future of the Industrial Robots:

Current developments in industrial robotics are focused in artificial intelligence. Future industrial robots will be equipped with advanced learning, vision, and sensory capabilities. Increased application flexibility will lead to increased productivity. Smarter robots will be able to perform complicated tasks perfectly.

1.1.2 Service robots

A service robot is which operates semi or fully autonomously to perform services useful to the well being of humans and equipment, excluding manufacturing operations, (From, IFR-International Federation of Robotics). It could be classified such as:



Figure 1.3: Some service robots.

- Servicing humans (personal safeguarding, entertainment etc.)
- Servicing equipment (maintenance, repair, cleaning etc.)
- Others performing an autonomous function (surveillance, transport, data acquisition, etc.) and/or service robots that cannot be classified in the two groups above.

Service Robots are key products, showing the way to the Future

This statement is based on the definition suggested by the Fraunhofer Institute for Manufacturing Engineering and Automation (IPA) in 1994: "A service robot is a freely programmable mobile device carrying out services either partially or fully automatically. Services are tasks that do not serve the direct industrial manufacture of goods, but the performing of services for humans and equipment". (see Fig. 1.3).

Certainly neither definition is all-inclusive. One thing is clear, though: the areas of application of service robots are not easily defined, as were those of the industrial robot [103].

Service robots have growth potential

A service robot in every household? A service robot as a part of the basket of available commodities in 2015? Service robots as mass products of the twenty-first century? These questions concern engineers throughout the world who have devoted their work to this fascinating field.

The examples listed at the beginning of this section show that it is almost impossible to give global potential estimates for the use of service robots. Due

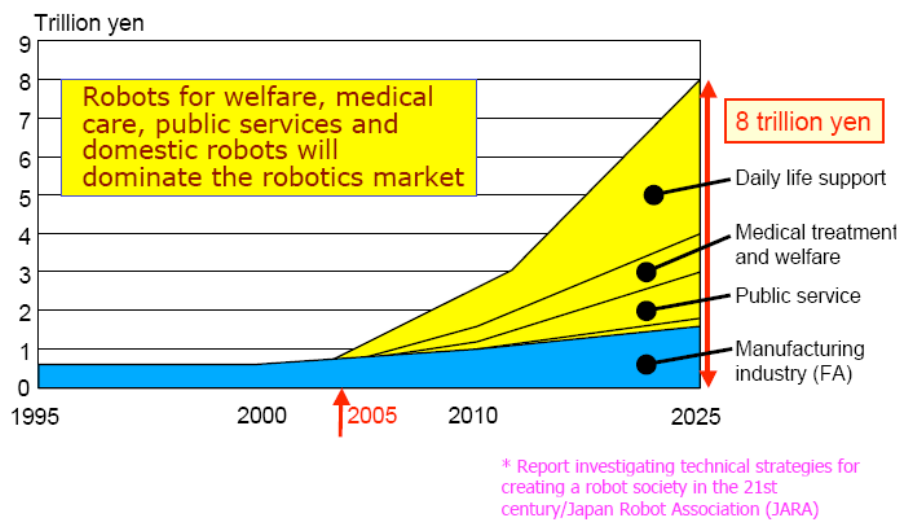


Figure 1.4: Chart of service robots in Japan.

to the comparatively high diversity and the small number of service robots installed to date, statistics, such as they exist in the area of industrial robots, have only been recorded occasionally.

If one sees the service robot as a midway point in the evolution of industrial robots towards personal robots, then this product indeed has all the prerequisites for becoming a key product in the near future.

Just like the locomotive, electrical engineering, the automobile, plastics and television and mobile phones, the service robot could establish itself in the mainstream of information and communication technologies as a mass product by the beginning of the twenty-first century.

On flat surfaces, wheels are most efficient. For rough terrain or the anthroposphere (characterized by stairs, etc.) leg locomotion seems to be more advantageous. Approaches are mainly taken from nature, where quadruped and six-legged creatures are common. The control of bipeds is usually more complicated, but they are more flexible in their motion and better adapted to the human environment.

Some research aims at the development of service robots for use in human environments. In the course of this research, various wheel-based and leg-based robots have been developed with a main focus on bipedal robots and full autonomy. Other research is based on uses of space. An example of service robots in Japan is shown in (Fig. 1.4), where the perspective is that they will dominate the robotics market.

The applications could be described as (IEEE Robotics and Automation Society), some examples are shown in the Figure 1.5, which have been developed in the Robotics lab of the University Carlos III of Madrid:

- Cleaning Housekeeping
- Edutainment
- Humanoids



Figure 1.5: Examples of services robots. University Carlos III of Madrid, some Roboticslab service robots: ROMA 2 (climbing robot for inspection), Manfred (mobile manipulator), ASIBOT (Portable assistive robot), Maggie (Personal social robot).

- Humanitarian Demining
- Rehabilitation
- Inspection
- Agriculture Harvesting
- Lawn Mowers
- Surveillance
- Medical Applications
- Mining Applications
- Construction
- Automatic Refilling
- Guides Office
- Fire Fighters
- Picking Palletising
- Food Industry
- Search Rescue

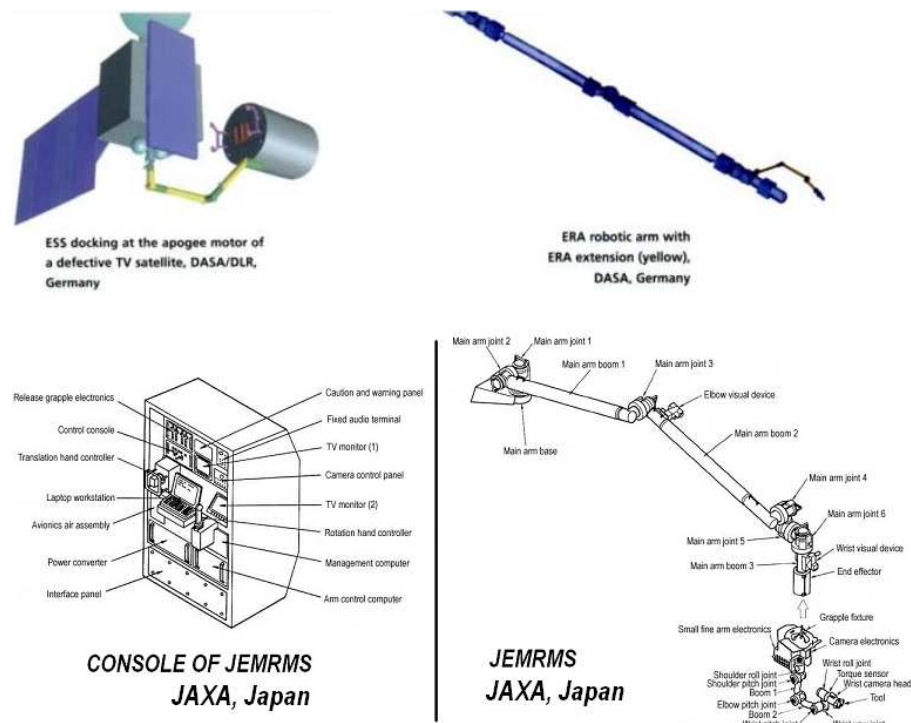


Figure 1.6: Service robots in space.

The future of service robots

Many services to human society are the current research of service robots. The following paragraphs will describe some of them.

Reviving the TV satellite?

The ESS (Experimental Servicing Satellite) project, initiated by Daimler-Chrysler Aerospace (DASA), is aimed at the preliminary development of free-flying telerobots. They fly to space systems to inspect them and carry out maintenance. On reaching its objective, the capture tool draws in the satellite in need of repair and clasp it with a simple gripping mechanism. When the arm was free again, by way of an interchangeable adapter, it picked up a pair of electromechanical clippers, which had also been newly developed during the project, and cut the clamps blocking the TV satellite's solar panel.

Mechanic in Space

Commissioned by the European Space Agency ESA, the European robotic arm, ERA, is currently being built, integrated, and tested by, among others, the companies Fokker, DASA-RI, and TS. The ERA was intended to be used for assembly and maintenance work on the Russian segment of the International Space Station (ISS) and should be ready for use in space by the year 2009.

The ERA is a robotic arm approximately 11 meters in length possessing seven degrees of freedom which have been constructed symmetrically. It can move around a space station independently and can be affixed to defined docking adapters. For future developments (ERA extension), it is intended that the arm will be equipped with additional smaller robotic arms (approximately 1.5 meters long) to enable it to carry out more complex repairs on the space station.

The Remote Manipulator System (JEMRMS) serves as an arm to support experiments conducted on the exposed facility, developed by the JAXA.

The main arm handles large items for delicate tasks. A small fine arm can be attached at the end of the main arm. The main arm is equipped with a TV camera which allows astronauts to monitor the operation from inside the pressurized module. The JEM Remote Manipulator System (JEMRMS) is a robot system intended for operation in space. It will be attached to the Pressurized Module (PM), which is a part of the Japanese Experiment Module (JEM). JEMRMS will be utilized for experiments being conducted on JEM or for supporting JEM maintenance tasks.

The JEMRMS is going to be the third space manipulator system Japan has flown.

During the Manipulator Flight Demonstration (MFD) conducted in August 1997 during mission STS-85 (Discovery), using an arm equivalent to the small fine arm (SFA) of the JEMRMS, some JEMRMS functions were proven satisfactory. Also, using Engineering Test Satellite-7 (EST-7; nicknamed Orihime-Hikoboshi and launched in November 1997), various experiments have been conducted in order to accumulate basic technology for space robots including remote operation from the ground.

The uses include exchanging experiment payloads or devices located on JEM components, EF and ELM-ES; supporting experiments or maintenance tasks; moving maximum seven-ton objects with the ten-meter main arms and performing precise operations with the small fine arm two-meter to handle orbital replacement units (ORU). An astronaut inside the JEM can manipulate, control and manage these two robot arms by operating and monitoring the RMS console.

The JEMRMS will be used for more than ten years in orbit. This means it should be capable of being exchanged or repaired in case of trouble. In emergencies, it has been designed to be repaired by intravehicular or extravehicular activities.

Since astronauts use the JEMRMS for a long term, the man-machine interface had to be designed carefully, so that astronauts can operate it with ease (Fig. 1.6).

The Astronaut's Third Hand

To assist astronauts inside the space station, stationary or mobile robots will be introduced to operate the individual scientific experiments. Here, the ability of the robot's kinematics to adapt to various task requirements is particularly important. Also, the robotic arm should weight as little as possible but be able

to carry heavy weights.

Spin-off for Civilian Use

Cost and investment returns are not the main issue in the prestige of space travel. However, this field is of particular interest in the development of robotics technology because space robotic developments will soon enrich earthly service robot developments, where practical use comes before fascination.

1.1.3 Science fiction and robots currently

The connection between science fiction and actual robots is closer than someone might think.

Isaac Asimov, (Russian-American biochemist and author), written science fiction story about robots. His novel deals with the robot performance laws that have become a reference point throughout the world. In one of his stories was the first time when the word “robotics” appeared, and his ideas have inspired inventors and thinkers.

Laws of Robotics of Asimov:

- Law Zero: A robot may not injure humanity, or, through inaction, allow humanity to come to harm.
- Law One: A robot may not injure a human being, or, through inaction, allow a human being to come to harm, unless this would violate a higher order law.
- Law Two: A robot must obey orders given it by human beings, except where such orders would conflict with a higher order law.
- Law Three: A robot must protect its own existence as long as such protection does not conflict with a higher order law.

When discussing ethical questions about the future of robots, the Asimov's laws are considered as common ground. As an example, the first law is totally opposite to the creation of armed military robotic machines.

1.2 Walking robots

Walking robots have many choices of locomotion systems for walking over any terrain. This section tries to explain the well-known locomotion possibilities in order to give a background of current locomotion systems, such as legged, wheeled, hybrid wheeled-legged and active cord mechanisms for walking.

1.2.1 Outline

The Baron von Drais invented a walking machine in 1817, which would help him go around the royal gardens faster. It is composed by two same-size in-line wheels, the front one steerable, mounted in a frame which you straddled.

This device was propelled by pushing your feet against the ground, thus rolling yourself and the device forward in a sort of gliding walk (that is the bicycle). This machine was known as the hobby horse or Draisienne.

The Draisienne was made entirely of wood. It enjoyed a short-lived popularity as a fad, not being practical for transportation in any place other than a well-maintained pathway such as in a park or garden.

From here the concept of walking robot covers the legged and wheeled robots or combination of both.

The original manipulator-type robots does not need locomotion and they are mostly mounted in a fixed position. The robots have slowly moved from factories to more open areas, such as train stations, hospitals and mines, during the last twenty years. These robots, called service and field robots, have to move and act on ordinary environments or in partly closed working sites; so, the significance of their locomotion has increased.

The hybrid of the main land locomotion principles, wheeled and legged locomotion, can be combined to help find an optimal solution for greatly varying ground conditions. The hybrid locomotion can also be called roiking (rolling-walking). This kind of robot can move using different locomotion modes; it can drive with wheels, rolk (use wheels and legs at the same time) or even walk.

The earliest walking machines were mechanical toys. (The history of automata and mechanical toys is beyond the scope of this chapter.) Their legs were driven by cranks or cams from a source of rotary power, usually clockwork, and executed a fixed cycle [113].

In passing, the steam elephant in one of Jule Verne's novels warrants attention, as this seems to anticipate one of the most successful methods in robotics, namely the use of pneumatic or hydraulic actuation of individuals joints.

The main event which led to the consideration of practical walking machines was the invention of the internal combustion engine, which made possible all sorts of new vehicles. One line of development consisted of extending wheels and caterpillar tracks by attaching feet spikes or posts to the rim or to sections of the track. Several "legged" machines of this kind are described by Thring (1983) [112]. However, these might not be considered true walking machines as they do not have legs separately attached to the body.

Another line of development has been the production of giant excavators such as walking draglines. An example is the Ransomes Rapier walking dragline which, in 1962, held the world weight record at 1800 tons. While excavating, it sits on a large flat circular base. To move, it drives its two flat feet, one on each the side and each size of a large bulldozer, until they take enough weight to drag the machine backwards. However, such excavators provide few lessons for the design of more agile vehicles.

A third branch of mobile robot has been the invention of machines to move in specific environments, such as within pipes, up trees or on orbiting structures.

The history of robots give to researchers the background of the evolution of robots in many subjects such as design, control, modelling, hardware and software, which could be applied to advanced robots. It is shown that humans trend to create machines with ever greater abilities by developing machines as automatic tool with a human shape in order to cooperate in their environments. The first step in this kind of research is the development of walking robots. Research in walking robotics began in the 1950s. Since the beginning of the research, [109], various types of walking machines have been developed: one

leg, two leg, three leg, four leg, six leg machines and so on. Those traditional research interests were related to how to design efficient legged mechanisms and develop stable walking control algorithms. Currently, there are some new trends in walking robotics research. Some new trends can be seen in the advancement of humanoid research and some proposals of walking systems based on the combination of wheels and legs and cellular type systems. Also, the other trends can be seen in the application possibility of walking systems. The way of legged walking has been considered to be useful for moving over rough surfaces. Recently, the new application possibility can be seen in some kinds of entertainment robots. In such an application, legged walking is used to draw the user's interest and make robot behavior more attractive. The walking robot is one of the most popular topics in robotics. It had more than 40 years of history. From 1950-1970, there were several robot projects carried out and several types of walking robots were experimentally constructed with different numbers of legs, two, four, six and eight, in USA, Europe and Japan.

In the early history, one of the most well-known examples of research in walking robots was the quadruped walking robot project carried out by Professor McGhee, University of Southern California (USC) and his group, the name of which was called "California Horse Project". They analyzed the gait of horses to know which gait patterns were suitable for the quadruped robot and, with the results in mind, developed several experimental walking robots. After, Prof. McGhee moved to Ohio State University (OSU), their group established the ASV project, which was the research to develop a practical six-legged walking robot driven by a human operator. This was demonstrated in impressive ways in an outdoor environment [123].

The other remarkable walking robot was the six-legged robot developed by Odetics, Inc., which was one of the most practical systems developed so far [100]. As well as this research and developed systems, there a lot of fundamental research. However, as long as we consider walking robotics a kind of technology which realizes new mobile functions useful, we can not be sure if it has achieved successful results. There are few research results being currently used in spite of a lot of research that has been carried out. In Japan, there was a lot of walking robotics research in universities, industries and national and public institutes in 1980s. Even in industries, they spent a lot of their own budgets for the research. However, in the 1990s, there were few companies which had research activities on walking robots.

Anyway, it seems that Japanese industries have almost no interest in walking robots, though some universities and national institutes still have interests in the area. The reason why is related to no practical results being produced from research activities done in the 1970s and 1980s. If robotics is just a pure scientific area, no practical applications and little interest on the part of industry will produce no problems. As long as robotics is insisted to be a science and technology which contributes to solving some kind of practical problems, improving this situation must be considered. In order to do so, some new efforts for the research and re-consideration of the goal of walking robotics will be required. As an example of the walking robot research in Japan, the well known results in the Hirose Lab, which are based in quadruped robots (KUMO-I in 1976 and PV-II in 1979, see Fig. 1.7). They have the next filosphy about walking, [54]: *"However, walking machines, because they can move while separately selecting the point of leg contact with the ground by adapting to the shape of the terrain,*

are fully practical, depending on the use, because they have such characteristics as: 1) Can move stably over a rugged surface, and can pass over fragile objects on the ground surface without touching them. 2) Can make holonomic omnidirectional motion without slipping or damaging the ground surface. 3) Utilizing the degrees of freedom of the legs it can become a stable and active platform even on a rugged surface when stopped for some manipulation task.”

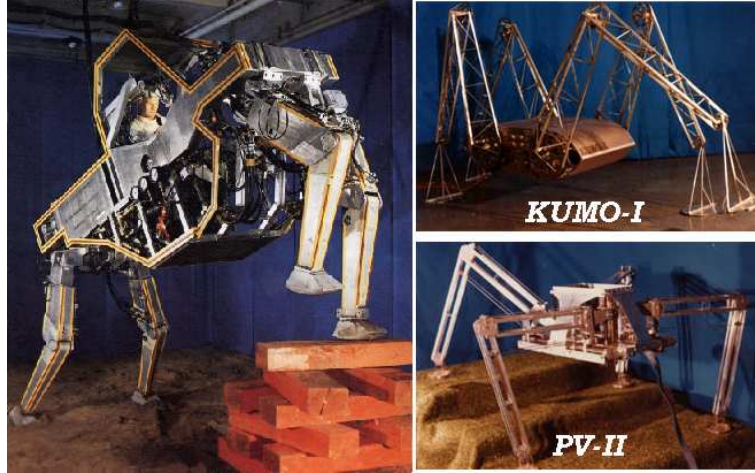


Figure 1.7: The General Electric Walking Truck and Hirose Lab walking robots.

1.2.2 Themes of legged robots

It is possible to identify two principal themes of legged robot research. The three main themes are:

1. Rough-terrain transport.
2. Prosthetic or orthotic bipeds.
3. Bipeds for human cooperation.

There is not an absolute distinction between these. The bipedal exoskeleton worn by a person has been seen not just as an aid for the disabled but as a strength amplifier, and there is one application of this in transport. The General Electric Walking Truck is a hybrid, in that it walked as a quadruped but was controlled as a sort of exoskeleton attached to its driver. Of the subsidiary themes, perhaps the most important has been the study of animal and human locomotion.

In the beginning, most research was aimed at military transport and prostheses.

1. Rough-terrain transport.

The earliest serious attempt to build a walking machine with independently controlled legs was made in Britain in 1940 by A.C. Hutchinson and F.S. Smith. Hutchinson, [60] who worked for the W.H. Allen Company Ltd., suggested that for a every large armoured vehicle, the 1000 ton



Figure 1.8: The General Electric Hardiman.

class, legs would be better than tracks. Hutchinson and Smith decided on four legs and the quadruped crawl gait. They studied a variety of leg mechanisms mainly intended to allow a pair of hydraulic actuators to produce easily separable vertical and horizontal movement. They chose a design with a rolling thigh joint, which acted as a kind of inverted wheel, and a telescopic leg.

The proposed control mechanism consisted of a feedback loop per leg, with the four legs each being controlled by the hand or foot of the driver: essentially the solution to be adopted by General Electric for the Walking Truck in the 1960s (see Fig. 1.7). After the project was halted, some research was undertaken about this time by Aerojet General Corporation, it includes the second series of walking machines developments on behalf of the US Army, and also for NASA which at this time was getting interested in the problems of mobility in space, on the Moon and other planets. At least three applications were envisaged: planetary exploration, a walking chair for the disabled, and military transport. Variants of the basic vehicle had six and eight legs and executed an alternating tripod and an alternating tetrapod gait, respectively. In the military transport role, a train of these vehicles walking behind and steered by a soldier on foot was envisaged. The leading vehicle was powered and towed the rest of the train. In this form, it was known as the Iron Mule Train. The basic design used a fixed-leg cycle produced by a mechanical linkage of cams and levers.

2. Prosthetic or orthotic bipeds.

The history of these machines emerges gradually from that of unpowered

prosthetic and orthotic aids, which are extremely ancient in origin. It is also closely associated with the development of prosthetic arms. In addition to the medical application, exoskeletons were seen at one time as “man-amplifiers”. A third strand of this research has been the quest for more or less anthropomorphic bipedal robots. Although in principle this could be regarded as a separate subject, it has always been intimately linked with the prosthetic-orthotic application.

It is uncertain when powered leg prostheses were first tried. In 1948, N. A. Bernstein [29] in the USSR suggested a design for an above-knee prosthesis with powered knee joints, but this seems not to have been the focus of much immediate research. One of the earliest practical efforts relating to bipeds was that of the Cornell Aeronautical Laboratory (CAL).

General Electric built a high-strength exoskeleton called Hardiman during the same period as the Walking Truck (see Fig. 1.8). The performance and servo control methods available seem not to have been adequate to make the exoskeleton a practical tool.

An early interest in walking machines was also shown in Yugoslavia. In 1961, R. Tomovic, [114] from the University of Belgrade, wrote a finite-state control paper which influenced the development of walking machines in the US. This work was presumably known to Vuckobratovic, [121] who subsequently did research on bipedal walking and prosthetics at the Mikhail Pupin Institute, Belgrade.

3. Bipeds for cooperating with humans.

The legged robots studied above deal with the trends from the USA in this field; otherwise the trends from Japan and Oriental countries are to develop bipeds for cooperating and living in harmony with humans.

These bipeds are well-known as humanoid robots, which will be detailed in chapter 2.

The goal of this kind of robot is to develop a “service robot” for working in human environments (see Fig. 1.9).

Currently, some human-size humanoid robots are working as hosts of museums (i.e., ASIMO, Honda Mo. Co. Ltd.), playing musical instruments (i.e., TOYOTA partner robots), or can cooperate with humans (i.e., HRP-2, Kawada Inc.-AIST).

There are low-scale humanoid robots used for entertainment activities. The most important prototype was invented by SONY, which has developed the QRIO with high mobility and dexterity movements.

Some examples will be shown and discussed in the Section 1.6.

1.2.3 Alternative mechanisms of locomotion: Wheeled robots, tracked robots, active cords

This section is primarily an outline of locomotion with legs, but it would be incomplete without some mention of certain alternative locomotion mechanisms



Figure 1.9: Humanoid robot cooperating with human in open-air tasks.

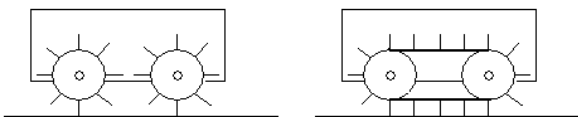


Figure 1.10: Wheels and tracks with external spokes.

which have been tried for vehicles. The use of legs is only one of several approaches to achieving high mobility, and may not always be the best. Some alternative mechanisms for vehicles will now be considered.

Variable geometry wheeled and tracked robots

Most mobile robots use wheels or tracks. Wheels have the advantages of engineering simplicity, low friction when on a smooth surface and, sometimes, integral springiness. Tracks are a way of extending the use of wheels to soft and rough ground by laying down a track for wheels to run on.

Not surprisingly, given the enormous success of wheels and tracks, many attempts have been made to retain their advantages while overcoming their weaknesses. The main weakness is their poor performance when faced with vertical steps or discontinuous surfaces. Of course, the problem can be solved by making the wheel large compared with the step or gap, but there may be factors limiting wheel size.

The simplest approach to improving a wheel or track is to give it some of the characteristics of a leg by attaching leg-like spokes to the rim. These methods work, after a fashion, but give a lurching, unstable motion on stairs, particularly if required to turn at the same time (see Fig. 1.10).

An alternative approach is to introduce extra joints so that when one wheel comes to a discontinuity, another wheel can be placed beyond the obstacle while

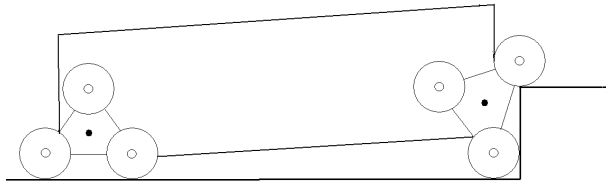


Figure 1.11: Triangular clusters of wheels for stair climbing.

the first is lifted over it. One way of doing this can sometimes work well on stairs, and is sometimes used in hand-carts or sack trolleys (see Fig. 1.11). The wheels are in triplets, each triplet being free to rotate about a central axle. The vehicle is shown encountering a stair, with the front triplet rotating to bring a new wheel onto the first step. Methods of driving the individual wheels and the common axle vary.

Tracked vehicles have also been designed with extra joints. The purposes of this are several: it can allow a sudden change from a flat surface to a very steep slope; a transition is possible between a compact posture and a long but stable one; mobility on soft soil may be enhanced; and the ability to cross crevasses may be improved (see Fig. 1.12).

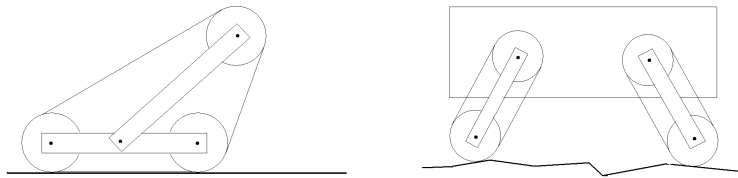


Figure 1.12: Variable geometry tracked vehicles.

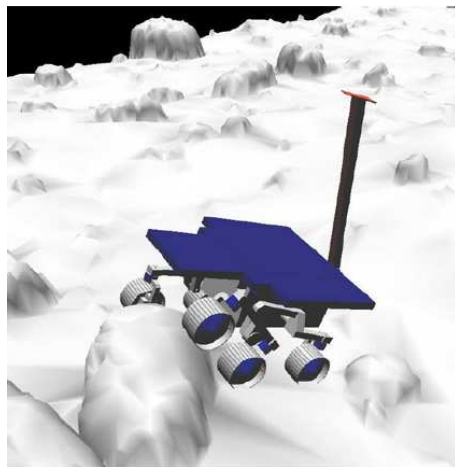


Figure 1.13: Virtual K9 driving over a synthetic rock.

Rovers use this kind of technology for exploring the planets and the moon;

that is the case of the rovers developed by the NASA (see Fig. 1.13 and 1.14, [62]). The design began with some basics from Sojourner, the rover on NASA's 1997 Mars Pathfinder mission. Some of the carried-over design elements are six wheels and a rocker-bogie suspension for driving over rough terrain, a shell of airbags for cushioning the landing, solar panels and rechargeable batteries for power, and radioisotope heater units for protecting batteries through extremely cold martian nights.

However, at 174 kilograms (384 pounds), each Mars Exploration Rover is more than 17 times as heavy as Pathfinder. It is also more than twice as long (at 1.6 meters or 5.2 feet) and tall (1.5 meters or 4.9 feet). Pathfinder's lander, not the Sojourner rover, housed that mission's main communications, camera and computer functions. The Mars Exploration Rovers carry equipment for those functions onboard.

Their landers enfolded them in flight and performed crucial roles on arrival, but after Spirit and Opportunity rolled off their unfolded landers onto martian soil, the landers' jobs were finished.

NASA's Jet Propulsion Laboratory, Pasadena, Calif., designed and built the two new rovers plus the lander and the cruise stage for each. The cruise stage provided capabilities needed during the journey from Earth to Mars. In early 2003, the hardware arrived at NASA's Kennedy Space Station in Florida for final assembly, testing and integration with Boeing Delta II launch vehicles.

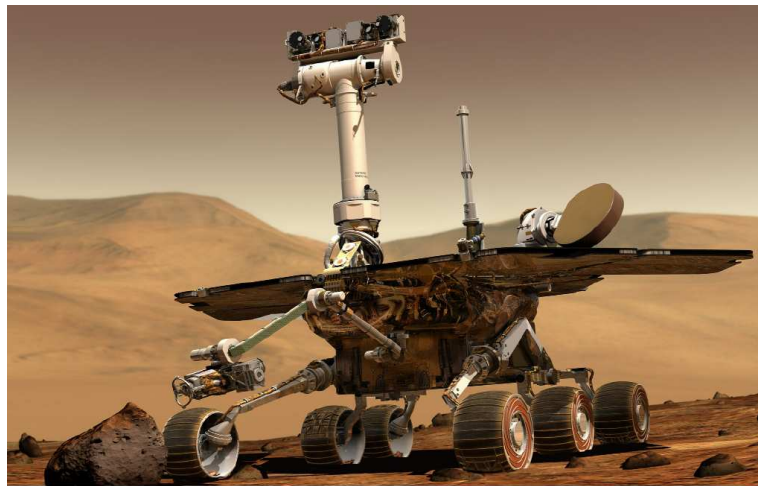


Figure 1.14: Artist's simulation of a Mars Exploration Rover at work on Mars.

While the twin spacecraft were being built, scientists and engineers winnowed a list of 155 candidate landing sites to a final pair best suited to the mission's goals and safety. More than 100 Mars experts participated in evaluating the sites. They made heavy use of images and other data from NASA's Mars Global Surveyor and Mars Odyssey orbiters.

The scientific goal of the rover project has been to assess the history of environmental conditions at sites that may once have been wet and favorable to life. Each of the two selected landing sites showed evidence detectable from orbit that it may have once been wet.

For Spirit, NASA chose Gusev Crater, a basin the size of the U.S. State of



Figure 1.15: The WorkPartner robot, with hybrid wheel-leg locomotion system.

Connecticut that appears to have once held a lake, judging from the shapes of the landscape. A wide channel, now dry, runs downhill for hundreds of kilometers or miles to the crater and appears to have been carved by water flowing into the crater. For Opportunity, NASA chose part of a broad plain named Meridiani Planum based on a different type of evidence for a possibly watery past. A mineral-mapping instrument on the Mars Global Surveyor had identified there an exposure of gray hematite, a mineral that usually forms in the presence of liquid water, the size of the U. S. State of Oklahoma.

Wheel-leg hybrids

Some machines may be regarded as variable geometry wheeled vehicles or alternatively as walking machines with wheeled feet. An example is the remote controlled robot for maintenance in nuclear power stations.

Another example is the WorkPartner, which is a futuristic service robot designed for outdoor use. It is presently under development at HUT (Helsinki University of Technology) automation Technology Laboratory, [127]. Mobility is based on a hybrid locomotion system, which combines benefits of both legged and wheeled locomotion to provide at the same time good terrain negotiating capability and large velocity range. Figure 1.15 illustrates the mobile platform on which the manipulation and tooling system has been built. The platform has an active body joint and four legs equipped with wheels. The weight is about 200 Kg, including all mechanical components and the components of the energy system, the actuating system and the computing system. The payload is about 40 Kg, which is mainly taken by the two-hand manipulator system. The actuation system is fully electrical and the power system a hybrid one with batteries and 3 KW combustion engine. The locomotion system allows motion by legs only, by legs and wheels powered at the same time or by wheels only.

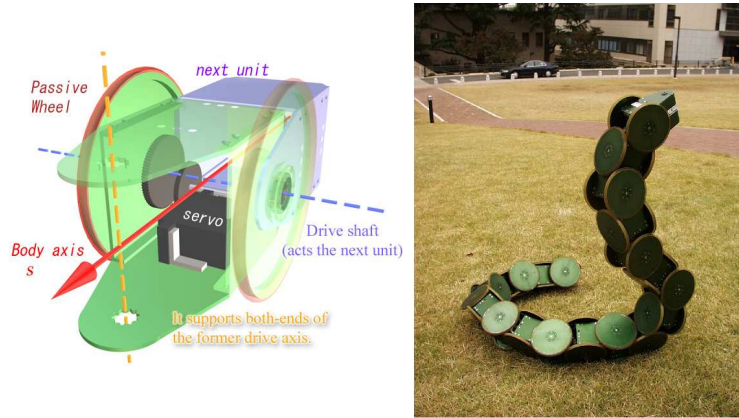


Figure 1.16: Active Cord Mechanism - Revision 1 (ACM-R1), which is a wireless controlled snake-like robot.

With wheels, the machine can obtain 7 Km/h speed on a hard ground.

Active cord mechanisms

The most radical departure from previous methods of mechanical locomotion has been that of Hirose and Umetani, [55] at the Tokyo Institute of Technology. The potential utility of flexible structures like the snake, the elephant's trunk and the tentacle of the octopus has long been recognized, but these rely on large numbers of actuators, which if reproduced with current engineering methods, would be heavy and bulky. Hirose and Umetani have found several ways in which potentially useful flexible active structures (which they term active cord mechanisms'). They have designed flexible-fingered grippers on the principle, and a series of experimental locomotion machines resembling a snake or centipede. An early one of these consisted of a train of short segments connected by hinge or ball joints, with a single azimuth actuator at each joint. (The machine was constrained to travel on a more or less plane surface.) It could travel between obstacles and through a labyrinth by thrusting backwards against the walls with waves of the body in the same way as a snake.

A more active cord mechanism can control its shape in three dimensions: for example, it can rear up while stabilized by a flat loop of the back part of its body. It uses axial joints alternating with oblique-axis joints, (see Fig. 1.16, Mori and Hirose, [85]).

The designers suggest that for the relatively small number of segments which is practicable, the snake mechanism of generating thrust is unsatisfactory and it is better to provide a separate method, such as a pair of powered wheels at each joint.

1.3 Why study legged machines?

Aside from the sheer thrill of creating machines that actually run there are two serious reasons for exploring the use of legs locomotion (Raibert, M. [99]) :

1. One reason is mobility. There is a need for vehicles that can travel over dif-

ficult terrain, where existing vehicles cannot go. Wheels excel on prepared surfaces such as rails and roads, but most places have not yet been paved. Only about half the earth's land mass is accessible to existing wheeled and tracked vehicles, whereas a much larger fraction can be reached by animals on foot. It should be possible to build legged vehicles that can go to the places that animals are already able to reach.

One reason legs provide better mobility on rough terrain than do wheels or tracks is that they can use isolated footholds that optimize support and traction, whereas a wheel requires a continuous path of support. As a consequence, the mobility of a legged system is generally limited by the best footholds on reachable terrain and a wheel is limited by the worst terrain. A ladder provides a good example: its steepest parts prohibit ascent on wheels, while the flattest parts, the rungs, enable ascent using legs.

Another advantage of legs is that they provide an active suspension that decouples the path of the body from the paths of the feet. The payload is free to travel smoothly despite pronounced variations in the terrain. A legged system can also step over obstacles. In principle, the performance of legged vehicles can, to a great extent, be independent of the detailed roughness of the ground. A legged system uses this decoupling to increase its speed and efficiency on rough terrain.

The construction of useful legged vehicles depends on progress in several areas of engineering and science. Legged vehicles will need systems that control joint motions, cycle the use of legs, monitor and manipulate balance, generate motions to use known footholds, sense the terrain to find good footholds, and calculate negotiable foothold sequences. Most of these tasks are not well understood yet, but research is under way. If this research is successful, it will lead to the development of legged vehicles that travel efficiently and quickly over terrain where softness, grade, or obstacles make existing vehicles ineffective. Such vehicles will be useful in industrial, agricultural, and military applications.

2. A second reason for exploring machines that use legs for locomotion is to understand human and animal locomotion. One need watch only a few instant replays on television to be awed by the variety and complexity of ways athletes can carry, swing, toss, glide and otherwise propel their bodies through space, maintaining orientation, balance, and speed as they go. Such performance is not limited to professional athletes; behavior at the local playground is equally impressive from a mechanical engineering, sensory-motor integration, or computational point of view. Perhaps most exciting is the sight of one's own child advancing rapidly from creeping and crawling to walking, running, hopping, jumping, and climbing.

Animals also demonstrate great mobility and agility. They move quickly and reliably through forest, swamp, marsh, and jungle, and from tree to tree. Sometimes they move with great speed, often with great efficiency.

The advantages for using wheeled, multi-legged and biped locomotion are summarized in Table 1.1 and Table 1.2, Kathib et. al. [105], Raibert M. H. [99], Balaguer C. [24].

From the tables it is clear that biped robots are the more complicated design and control systems, but they have more advantages compared to the wheeled robot and multi-legged robots in human environment applications. Furthermore, if biped robots are equipped with arms, they are called humanoid robots. The main advantage is that they could be used in human cooperation jobs human tasks, operating human tools, devices machines, doing dangerous human tasks and looking like a human; that is, it is easier to do human-humanoid cooperation work as a friendly partner. It is possible to summarize the humanoid's features as follows:

- The human-like shape of a humanoid robot affords emotional feelings useful for friendly communication to humans.
- The humanoid robot can work in environments designed for humans.
- The humanoid can expand its ability by using machines and equipment that we use.
- The humanoid's motion is easy for humans to understand and predict.
- The humanoid can be a multi-purpose machine.

Despite the excellence of using our own legs for locomotion, understanding the control principles that underlie walking and running is still at a primitive stage.

Wheeled	Advantages	Disadvantages
	Easy locomotion	No Difficult terrain (soft, uneven), only rails and roads
	Easy design	Need continuous path of support
	Consume less energy	Difficult manoeuvre
	High velocity on structured terrains	Increase the numbers of wheels for omnidirectional motion
	Less control effort because of their simple mechanisms	
	Reduced stability problems	
Legged	Advantages	Disadvantages
	Difficult terrain (soft, uneven)	Complex design (because it is a complex mechanism)
	Omnidirectional motion	High power consumption
	Isolated footholds, optimize support and traction	Complex control
	Decouples the path of the body from the paths of the feet	Slow velocity on structured terrain
	The payload does not know the variations of the terrain	Synchronization of many joints
	A legged system can also step over obstacles and up and down stairs	
	Can walk independent of the detailed roughness of the ground	
	It can achieve a smooth ride on rough ground by varying the effective length of its legs to match the undulations of the ground.	
	The construction of useful legged vehicles depends on progress in several areas of engineering and science	
	Less damage to the terrain	
	Behavior at the local playground is equally impressive from a mechanical engineering, sensory-motor integration, or computational point of view	
	Natural, animal type	
	Human environments	
	Better energetic performance	
	They have fewer problems of binding and sliding	

Table 1.1: Advantages and disadvantages of wheeled vs. legged locomotion.

1.3 Why study legged machines?

24

Legged	Advantages	Disadvantages
	Difficult terrain (soft, uneven)	Complex design (because, it is a complex mechanism)
	Omnidirectional motion	High power consumption
	Isolated footholds optimize support and traction	Complex control
	Decouples the path of the body from the paths of the feet	Slow velocity on structured terrain
	The payload does not know the variations of the terrain	Synchronization of many joints
	A legged system can also step over obstacles and up and down stairs	
	Can walk independent of the detailed roughness of the ground	
	It can achieve a smooth ride on rough ground by varying the effective length of its legs to match the undulations of the ground.	
	The construction of useful legged vehicles depends on progress in several areas of engineering and science	
	Less damage to the terrain	
	Behavior at the local playground is equally impressive from a mechanical engineering, sensory-motor integration, or computational point of view	
	Natural, animal type	
	Human environments	
	Better energetic performance	
	They have fewer problems of binding and sliding	
Biped	Advantages	Disadvantages
	The legs coordination of the is more simple; only two footholds must be managed	Control system is more complex, because stability in the single support phase is not easy to control
	It is possible to walk in a narrow space	Robust mechanical design with light materials, normally expensive
	Consume less energy	
	The adaptability to human environments is better (i.e., sitting in a chair)	
	A biped can generate yaw moments on the body when the legs counteroscillate, swinging fore and aft	
	The human-like shape of biped robots affords emotional feeling useful for friendly communication to humans	
	If a biped is to recover a leg during stance, then it must be able to shorten that leg during recovery	
	When the stance and recovery motions overlap in time, the duration of flight does not uniquely determine the time available for the recovery motion	

Table 1.2: Advantages and disadvantages of legged vs. biped locomotion.

1.4 What control mechanisms do humans and animals use?

There are many ways to learn more about the mechanisms for animal locomotion, one of them is to build machines that locomote using legs. Due that an animal and a machine perform similar locomotion system, their control and mechanical structures have similar problems. Because humans are building machines, they could get new insights into these problems, and they could learn about possible solutions. Specific theories and algorithms can guide biological research by suggesting specific models for experimental testing and verification. This sort of interdisciplinary approach is already becoming popular in other areas where biology and robotics have a common ground, such as vision, speech, and manipulation [98].

Biological nervous systems have many different kinds of neurons, and this heterogeneity is important for their function. An example is provided by insects, which have nervous systems that are orders of magnitude more complex than the most advanced artificial neural nets. As they walk, insects solve the problem of coordination of their six multi-segmented legs in real time in the presence of variations in terrain. In addition, because of the heterogeneity and architecture of their nervous systems, insects display remarkable coordination when they first reach their adult stage; they do not require learning to perform basic functions. Also, insect nervous systems are extremely robust; after suffering some types of severe damage, insects can immediately function surprisingly well (Delcomyn, F. [43]).

Manoonpong and coworkers [81] underlie the following analysis about the control mechanisms of humans and animals: The humans can adapt quickly to any terrain, when walking; furthermore they can learn to walk on any kind of surface. So, in similar surface and boundary conditions, the humans can walk stably with respect of the first time, because, they terrain is known.

The combination of their neuronal control and biomechanics allows the stable walking motion, this has been revealed by Neurophysiological studies. As example, some animals (e.g. horses, bulls) could stand up and walk some steps, but their biomechanical design do not allow to make stable gait with two feet.

It is possible to assure (by Neuronal control), that many kind of gaits can first be learned, for being applied quickly next.

Bernstein (Russian physiologist, 30's) [28], [29], [30] had explained that due the redundancy of effective movements ("The Bernstein Problem", also discussed in [115]), the coordination of the cooperation between the differents functional levels of the motor system, including controlled forms of motor learning, is a complex problem.

Over this problem, Sporns and Edelman [106] proposed that a successful developmentally guided coordination between neuronal activity and the biomechanics of the musculoskeletal system can be achieved without determining a desired trajectory. Instead, it is based on variations of neuronal and biomechanical structures and is the result of somatic selection processes within brain circuits. The concept was applied to solve the arm-reaching problem, which was demonstrated with an artificial sensorimotor system.

A theoretical framework that combines some features of inverse dynamic computations with the equilibrium-point hypothesis for controlling a wide reper-

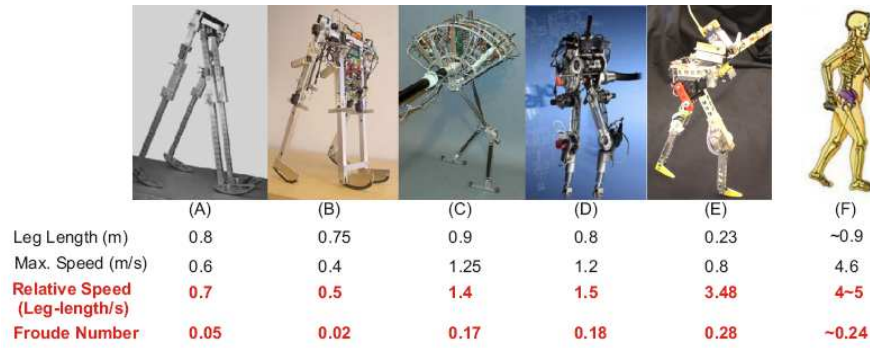


Figure 1.17: Relative leg-length and maximum relative speed of various planar biped robots. (A) A copy of McGeer’s planar passive biped robot walking down a slope. (B) “Mike”, similar to McGeer’s robot, but equipped with pneumatic actuators at its hip joints. Thus it can walk half-passively on level ground. (C) “Spring Flamingo”, a powered planar biped robot with actuated ankle joints. (D) “Rabbit”, a powered biped with four degree-of-freedom and point feet. (E) “RunBot”. (F) The world record for the fastest human’s walking speed (©Manoonpong et. al. [81]).

toire of motor behaviors also involving motor learning, has been proposed by Mussa-Ivaldi and Bizzi [87], [31]. By force fields as motor-primitives, the motion control of two degrees of freedom robot is obtained.

The central pattern generator (CPG), which have been proposed by Nakanishi et. al. [89], introduces one suitable example of biped locomotion control with motor learning. There, a central pattern generator (CPG) was employed to generate dynamical primitives movement while the desired trajectories for walking behavior were learned by imitating demonstrated movements of humans.

Currently, many problems still unsolved, specially the problem of adaptive and fast biped walking based on self-stabilizing dynamic processes. As well known a biped has only one foot touching the ground during most of a gait cycle, this poses huge difficulties for dynamic control as the biped always tends to trip or fall. As an alternative of biped motion control, this paragraph show that minimal adaptive neuronal control based on the reflexive mechanism [40] coupled with appropriate biomechanics can generate fast and adaptive biped walking gaits by a self-stabilizing process. As a result, the biped system (“RunBot”, Manoonpong et. al. [81]) can perform like in natural human walking (as shown by similar Froude numbers, see Figure 1.17) where the maximum walking speed is comparable to that of humans.

In general, a hierarchical structure [37] is followed by a neuronal walking control. At the bottom level there are direct motor responses, often in the form of a local, sometimes monosynaptic reflex driven by afferent signals, which are elicited by sensors in the skin, tendons, and muscles, like the knee tendon reflex. It is called the spinal (reflex) level; can already produce reproducible, albeit unstable gaits and seem to play a more dominant role in non-primate vertebrates and especially in insects. This level is often also augmented by central pattern generators (CPGs) in the spinal cord. For example some researchers have shown that the generation of motor patterns as well as the coordination of motor

behavior in both, vertebrates and invertebrates, is basically achieved by CPGs. Although CPGs provide the basis for generation of motor patterns, this does not mean that sensory inputs are unimportant in the patterning of locomotion. In fact, the sensory input is crucial for the refinement of CPG activity in response to external events.

Notice that especially in humans, CPG functions seem to be less important for walking and they had been hard to unequivocally verify, because they can strongly be influenced and, thus, superseded by sensory influences and by the activity of higher motor centers. In general, higher motor centers modulate the activity of the spinal level and their influence leads to our flexibility and adaptivity when executing gaits under different conditions. As an example, inputs from peripheral sensors (e.g.; eye, vestibular organ) can be used to adapt a gait to different terrains and also to change the posture of the walker, moving its body, to compensate a disturbance. Reflexes play also a role at this level, called here the postural (reflex) level, but these long-loop reflexes are always polysynaptic and can be much influenced by plasticity. Infants also use such peripheral sensor signals to learn the difficult task of adjusting and stabilizing their gaits which many times amounts to the learning of how to avoid reflexes by earlier compensatory motor actions. The Cerebellum seems to play a fundamental role in this type of motor learning for reflex-avoidance or reflex-augmentation.

Finally, Manoonpong et. al. [81] summarize that there are three important requirements for basic walking control:

1. Biomechanical level: The walker requires an appropriate biomechanical design, which may use some principles of passive walkers to assure stability [39].
2. Spinal reflex level: It needs a low-level neuronal structure, which creates dynamically stable gaits with some degree of self-stabilization to assure basic robustness.
3. Postural reflex level: Finally, it requires higher levels of neuronal control, which can learn to use peripheral sensing to assure flexibility of the walker in different terrains.

The next section is related of the previous items and it detail the biped control problems.

1.5 What are problems of biped control?

The main control problems for coping with a complex control system are the stability to avoid falling down in any posture, the capacity of the mechanism to absorb impact during foot landing and the adaptation to any surface, the attitude for maintaining the reference biped body orientation . Adequate sensors and control algorithms should be employed to obtain stable walking motion from the reference patterns. The combination of inertial (such accelerometers and gyroscopes) and force sensors are used to feed back external disturbances, due to terrain irregularities, structure imperfections, inertial and gravity effects by measuring the actual attitude and forces on each foot and hands during the double support phase, walking motion or cooperation tasks.

Otherwise, structural compliances should be mounted in order to mechanically reduce the impact effects (due to working precision, design and terrain imperfections), normally in the soles of the feet.

Furthermore, suitable reference walking patterns in order to distribute the biped mass during walking motion to maintain stability (by taking into account the dynamics effects) and reduce the impacts are required. These walking patterns are the starting point of the mechanical design and the control system of the biped robot, because they define the number of degrees of freedom and working angles of each joint, which are the input of the kinematics and dynamics models and the references of the control system. This is the objective of this thesis.

From the previous section, the control problems of a biped machine, which are included in the “Postural reflex level” and will be detailed in other work from a colleague of the humanoid team, could be summarized as following:

1. *The stability problem*

Stability is maintained by controlling a non-physical degree of freedom, which is called “Zero Moment Point” (ZMP). This criteria was proposed thirty years ago by Professor Miomir Vukobratovic. The dynamics of the whole body is taken into account. The criteria affirms that the biped does not fall down if the ZMP is maintained inside of the convex hull during the walking motion. Therefore, it is necessary to have a control loop of the ZMP to obtain stable walking motion. To compute the ZMP online, six axis force/torque sensors are used; this information is feedback to the respective control loop.

2. *The absorbing impact and adapting to any surface problem*

Imperfections or changes in the walking surface and changing the support foot while walking drastically cause force variations on the landing foot. Those facts degenerate the biped structure. Thus, the compliance control loop should be implemented to adapt the biped to these changes. Furthermore, the compliance structural design should be developed in order to cushion the impacts. The force/torque sensors are used to feedback the external reaction on each foot and hand.

3. *The attitude problem*

During the walking motion, the dynamics and gravitational effects cause tipping torques which cause the biped to fall down. Furthermore, structural imperfections cause important flexion on some joints. As the reference patterns include the attitude because the biped should walk upright all the time, a control attitude loop must be implemented to obtain stable walking motion. Suitable gyros and accelerometers are used to compute the actual robot attitude and it is feedback to the biped control system, which allows the biped to walk upright.



Figure 1.18: The human-like shape of a humanoid robot affords emotional feelings useful for friendly communication with humans.

1.6 Features and applications of humanoid robots with biped locomotion

Because this work deals with humanoid robots as a kind of “service robot”, some features and applications will be outlined in this section in order to justify the framework of the humanoid research. Among the features subjects related to anthropomorphic appearance will be detailed, while in the applications the possible uses of humanoid robots with biped locomotion will be explained.

The main features for developing humanoid robots with biped locomotion are, (see Fig. 1.18 to Fig. 1.20, Yokoi, K. [128]):

1. The human-like shape of a humanoid robot affords emotional feeling useful for friendly communication with human. Therefore, it is more suitable to work in cooperation with a machine of human appearance instead of an of one any shape one.
2. A humanoid robot can work in an environment designed for humans. All human environments are based on anthropomorphic measures, so a humanoid robot with biped locomotion is a good solution for human-machine cooperation.
3. A humanoid can expand its ability by using machines and equipment that humans use now. The humanoid robot is a machine that could drive any machine which has been designed to be driven by humans.
4. A humanoid’s motion is easy for humans to understand and predict. In order to prevent falling, avoid obstacles, etc., as the motion and performance is similar to a human’s, by intuition it is possible to recognize the next action of the humanoid robot. This feature is very useful, specially in the case of human-humanoid cooperation tasks.

As for the applications of humanoids robots, some examples could be described:

1. Building and Home Management. The humanoid could operate home tools and devices.

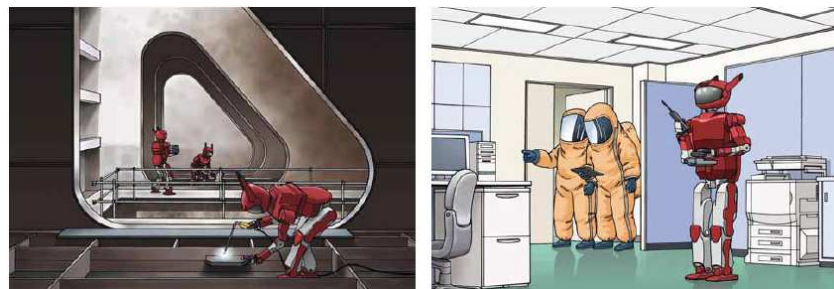


Figure 1.19: A humanoid robot can work in an environment designed for humans. It can do dirty and demanding jobs, dangerous jobs (Bio-terror, SARS, etc.)



Figure 1.20: A humanoid can expand its ability by using machines and equipment that we use now.

2. Plant Management. Some industrial plant devices could be operated by humanoid robots, especially dangerous ones.
3. Collaborative Outdoor Work. Human-humanoid cooperation work such as in construction environments could be implemented.
4. Industrial Vehicle Operation. As the dexterity of the humanoid is not similar to that of the human, but it is enough, it is possible to operate an industrial vehicle.
5. Care Support Services. Aid services in hospitals or nursing homes could be implemented with humanoid robots.

1.7 Objectives

The objectives of this research are:

1. *Develop a study of the kinematics and dynamics of humanoid robots.*
2. *Develop a study of gait locomotion.*



Figure 1.21: Some applications of humanoid robots.

3. *Develop a study of gait control algorithms.*
4. *Develop stable walking patterns for humanoid robots and implement them in real humanoid robot platforms.*

The following paragraphs deal with the explanation of the objectives in order to detail them.

1. *Develop a study of the kinematics and dynamics of humanoid robots*

To introduce humanoid robot mobility, many aspects should be taken into account. Some of them do not include the field of gravity or forces of inertia. These aspects are related to the number of joints and joint motion ranges for reaching any local or global goal. Furthermore the motion planning is constrained to physical velocity limits of the actuators, so the suitable kinematics model must be developed. This model computes the joint pattern references (position and velocity) of the control system.

Furthermore, physical constraints include gravity and inertial effects, which must be modeled in order to control the total system. This is the reason for developing a robust dynamic model, because the constraints of the actuators include the acceleration and torque limits, as the structure of the robot also has external acting forces and torques as constraints. This model computes the whole body attitude, joint torque and external forces references of the control system.

There are a few proposals for the kinematics modeling of humanoid robots because it is a complex problem with high redundancy. To avoid the redundancy, null-space projections could be used (Nakamura et. al. [88]), as a well known suitable approach. Other approaches divide the humanoid robot in many manipulators, so all the kinematics theory developed could

be implemented, with the constraints that each manipulator end effector must follow the motion of common parts (such as hip, spine, neck). This work deals with the second approach and it uses the screw theory (R. S. Ball et. al. [25]) in order to analyze the kinematic problem, because meaningful, analytic and closed solutions are obtained at the position level.

Likewise, the dynamics modeling of humanoid robots is an other complex problem, because it is a system with multi-body masses and inertias, which represents a complex analysis and high computation time. Normally, recursive methods are used for solving the inverse and forward dynamics problem (Featherstone et. al. [48], Murray et. al. [86]). The constraints in this case are not so easy as the kinematic model, because the gravitational and inertial effects make a non-linear model, so it is not enough to follow the common parts motion as a constraint. However, the mass distribution on double support, the reaction forces and torques and others constraints should be taken into account to solve the dynamic problem in a recursive way.

2. *Develop a study of gait locomotion*

The word “gait” has various meanings, for example (as selected from a dictionary): “A particular way or manner of moving on foot.”

It is clear that this meaning is suitable for studying humanoid robot gait locomotion. The researchers in this field first studied the human gait to develop stable walking patterns. Certainly, imitating is a good approach the human gait in order to make a humanoid robot walk stably . The passive walkers (McGeer et. al. [84]) make a walking motion under the field of gravity and the swing foot motion looks like the human one. The main characteristic of the swing foot motion is that it falls down from the effect of gravity. It is one difference with the current humanoid robot walking motion (Honda, [10], HRP-2, [70], Johnnie, [80]), because in order to reduce the force impact when the swing foot is landing, the planned swing foot pattern does not fall down.

Otherwise, gait stability is controlled by center of gravity (COG) motion. Studies of biomechanics demonstrates that, when the human walks, the human center of gravity follows the laws of motion of the inverted pendulum (Winter et. al. [125]). That way stable gait is obtained, because the COG is concentrated near the support foot during the swing motion, and the COG quickly changes its position during the change of support foot.

3. *Develop a study of gait control algorithms*

The gait control algorithms proposed by a few researchers, after about fifteen years of research, such as by HONDA Mo. Co. Ltd., are the reference for the next humanoid robot prototypes [53]. This kind of research introduces a new algorithm based on human gait control and combining classical control theories with new ones. This research proposed three control loops: the attitude control, the foot force reaction control, and the Zero Moment Point (ZMP) control. In the first control loop, as a human uses the inner ear for controlling balance, a humanoid uses inertial sensors (accelerometers, gyros) for maintaining the reference attitude. The second loop, as a human reduces the reaction forces of the swing leg on

landing by adapting the heel, sole and toes to the terrain with a complex muscle and bone mechanisms, a humanoid must adapt the swing leg while it is landing by a compliance mechanical structure and compliance control system. That way, the mechanical loads on the humanoid are reduced considerably, and that follows its references. The ZMP control loop, like a human dynamic stability parameter during the motion of walking, the ZMP must be inside the support polygon (more details about this parameter will be explained later. Vukobratovic et. al. [118]). It is possible to define a reference of the ZMP motion and this loop must follow it by whole body robot control.

Other interesting and effective research was proposed by Huang et. al. [59] by combining the reference planned patterns with online modifications. At first, a method of generating a highly stable, smooth walking pattern is presented. Then, a method of real-time modification consisting of body posture control, actual ZMP control and landing time control based sensor information is proposed. By combining the proposed offline walking pattern with real-time modification, the biped robot can walk smoothly and adapt to unknown environments.

4. *Develop stable walking patterns for humanoid robots and implement them in real humanoid robot platforms*

Many walking pattern generation methods are studied in order to obtain stable humanoid robot walking motion. Some of them deal with the distributed mass model when it is not possible to be applied in real time, because of the high complexity of the multibody dynamics [9], [57]. Other methods deal with the mass concentrated models, which could be applied in real time, [63], [96], because the whole body dynamics are simplified to one mass motion in space under the field of gravity. The mass concentrated models for generating dynamics and stable walking patterns of humanoid robots were selected, they are: the “Three dimensional Inverted Pendulum Model, (3D-LIPM)” and the “Cart-table Model, (CTM)” (Kajita et. al. [64]). These models are successfully tested on the Rh-1 humanoid robot platform. Otherwise, the new walking pattern generation method in order to generate an “acyclic gait” is proposed and successfully tested in the HRP-2 humanoid robot platform, currently the most advanced humanoid robot platform.

1.8 Thesis contents

This work deals with mass concentrated model locomotion generation patterns in order to obtain stable walking motion according to ZMP-based criteria. In order to know the humanoid research groups and results, in Chapter 2, a brief discussion is presented. The study starts with the human locomotion study (Chapter 3) and it is concluded that the concentrated mass model allows us to accurately approximate the walking human motion (see Appendix A). After that, biped robot gaits introduce the way to apply the principles of human locomotion to humanoid robots (Chapter 4). The gait generation method is detailed (Chapter 5); when the input and output are presented in the proposed algorithm. For computing the output, the algorithm is divided in many layers to

simplify the problem; so the “global goal” (goal humanoid configuration) is the input and the “joint and the ZMP reference patterns” are the output. A special case of walking motion is developed and implemented in the HRP-2 humanoid robot platform, that is, the “Acyclic gait” an it is presented at last of Chapter 5. Successful results are obtained with the Rh-1 [36], [73], [16], [107] and HRP-2 [70] humanoid robot platforms (Chapter 6). Finally conclusions, contributions and future works are discussed in Chapter 7.

Additionally, in the Appendices, the COG projection on flat surface and ZMP measure system are detailed (Appendix A) and finally the distribution of masses and inertias of human will be shown in the (Appendix B).

Chapter 2

Humanoid robots

Movement is the passage of power to act.
(Aristotle)

This chapter deals with the history of some human-size humanoid robots developed by a few groups around the world, mainly concentrated in Japan. When the walking robot is discussed, humanoid robots are one of the most popular topics. Historically, humanoid research has been carried out by Professor Ichiro Kato's group at Waseda University in Japan since 1970. They developed a humanoid called "WABOT". Also, in 1990, they launched the "humanoid project" as a collaboration project between Waseda University and some companies. This project is now under way to develop several component technologies and integrated systems for the humanoid. In addition the Waseda Group, there has been much research on humanoids started especially since 1990, MIT, NASA (USA), University of Tokyo, ERATO, ATR and so on. These groups are based on intelligence algorithms for humanoid robots, so as it is not the topic of this research the description of these robots will not detailed, also, a special feature we can observe recently in this area is that companys' interests in humanoids are increasing and their technologies have advanced significantly. In Japan, Honda announced a humanoid P2 in 1996, a humanoid with very reliable biped walking capability. From the Honda results, the Humanoid Robot Project (HRP) in Japan, launched around 1998, the most important results have been obtained by the AIST with Kawada Industries. Currently the HRP-3 version of the humanoid robot is high mobile and water resistant, designed for open air collaborative work with humans. However, Honda has presented the ASIMO robot running and working in closed human environments. Inspired in this active area, there are other small groups like the Technical University of Munich which has developed the humanoid robot Johnnie, which has an advanced locomotion system. After that in the KAIST, the Hubo Lab developed the humanoid robot Einstein-Hubo with an innovative face and motion abilities; TOYOTA has developed the partner robots including a musician humanoid robot. Following this robotics trend, the University Carlos III of Madrid has developed the Rh-1 humanoid robot for work in human environments. The trend after this study demonstrate that the height and weight decrease; otherwise the increasing of degrees of freedom is a challenge to obtaining a stable walking motion and dexterous posture changes including arm manipulation, building small but powerful actuators and electronics components, and developing efficient computation algorithms.

The dream of robotics researchers has been developed by science fiction in comics and films, such as the well known “Metropolis” in 1926 and current films such as “The Bicentennial Man” (see Fig. 2.1, 1999). The first case is a story in which machines are revealed to humans. The second case deals with an ideal assistant robot, which wants to be a human, and after two hundred years of life, it is transformed into a person, as at this time technology develops artificial feelings, skin, human behaviour and even aging.

Since Greek mythology, there has been an idea of machines with human appearance. In the Cretan tales incorporated into Greek mythology, Talos (Latin Talus) or Talon was a giant man of bronze who protected Europa in Crete, circling the island's shores three times daily while guarding it. The god was identified with the Tallaia, a spur of the Ida range in Crete. The ideas of Talos vary widely, with one consistent detail: in Greek imagery outside Crete, Talos is always being vanquished. He seems to have been an enigmatic figure to the Greeks themselves.

Talos is described by Greeks as a gift, either a gift from Hephaestus to Minos, forged with the aid of the Cyclopes in the form of a bull or a gift from Zeus to Europa.

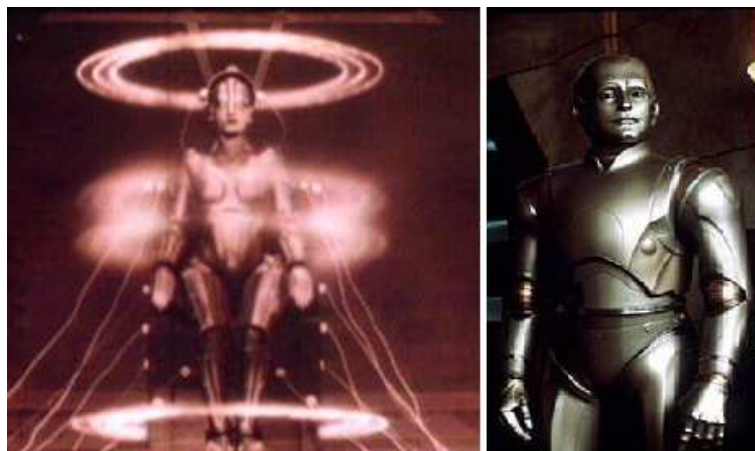


Figure 2.1: Metropolis and the Bicentennial Man.

2.1 Human evolution to biped locomotion, intelligence and bipedalism

Is it possible to develop intelligence without bipedalism? Bipedalism frees the hands from locomotion and to develop intelligence. This would permit the carrying of tools. It also allows an increased precision of grasping with a more gracile structure of the hands.

There are at least twelve distinct hypotheses as to how and why bipedalism evolved in humans, and also some debate as to when. Evidence points to bipedalism evolving before the expansion of the human brain size. The different hypotheses are not necessarily mutually exclusive and a number of selective

forces may have acted together to lead to human bipedalism, as refers Balaguer, C. at [23].

Various reasons have been proposed for the evolution of human bipedalism, including freeing the hands for tool use and carrying, sexual dimorphism in food gathering, changes in climate and habitat (from jungle to savanna) and to reducing the amount of skin exposed to the tropical sun. The first two explanations have been criticized for projecting modern social concerns and prejudices onto ancestral species. The latter two have been criticized for not making sense in the context of the forest and woodland biomes occupied by human ancestors. An alternative explanation is the mixture of savanna and scattered woods forced proto-humans to travel between clusters of trees and bipedalism offered greater efficiency for slow, long-distance travel between these clusters than knuckle-walking quadrupedism.

Robotics researchers, in order to imitate human intelligence, have the way by developing biped robots, because they are following natural human evolution. It is the everytime paradigm that the human tries to imitate her own creation by developing a machine with similar capabilities for working in her environments (humanoid robots), to create an anthropomorphic partner or assistant. At first step, some groups are developing humanoids for implementing intelligence algorithms; other groups are concentrated on implementing stable locomotion algorithms including humanoid-human cooperation. This thesis is inspired in the latter group.

At this time, some humanoid robot projects of a few robotics researchers groups around the world have been launched.

2.2 Types of researches on humanoid robots

The humanoid has drawn a lot of attention from robotics researchers as their research target. Also, it made people imagine various dreamy applications. However, because of the difficulty of achieving a stable and reliable biped walking function, a humanoid was considered just a dreamy research target for researchers. Since Honda developed a reliable humanoid, the reputation of humanoids has been changed from just a research target to a machine which can be used for practical applications.

There are mainly two types of research on Humanoids. The first one is related to scientific interests. In this research, humanoid is pursued to investigate what human intelligence is and to understand human behavior in computational scientific ways. MIT, NASA, ERATO and the ATR group are working on humanoids from this point of view (those kind of humanoids are not our reference). The second type is to develop a humanoid to use it practically. The new trend of humanoid research has been made from the second type of research. In such a trend, the Ministry of Economy, Trade and Industry (METI) in Japan started the Humanoid Robotics Project (HRP) to find real practical applications [110], after that, HONDA demonstrated the feasibility of this kind of robot, which is based on preliminary studies at Waseda University.

This thesis is based on the second type of humanoid robot, which is for practical use, such as an assistant in daily human environments, working in dangerous plants, or in cooperation with humans.

2.3 Main humanoid robot research projects

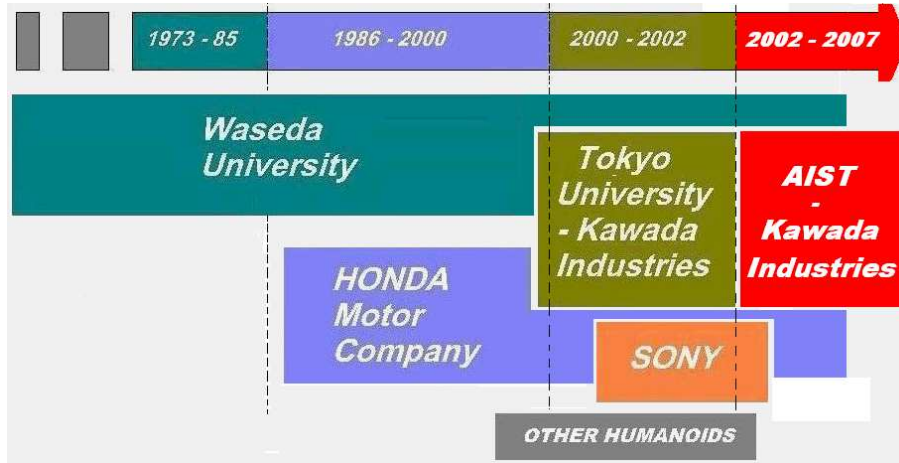


Figure 2.2: The main humanoid robot research groups.

As a background of humanoid robot research, there are few groups around the world, most of them concentrated in Japan (Fig. 2.2). The pioneer group is at Waseda University, started in the 1970's. In 1973, they presented the WABOT-1 [72], (Fig. 2.9), which could walk, speak, and recognize voice commands. More abilities couldn't be implemented because of the absence of adequate computers. After that, the WABIAN presented in the 1980's and currently the WABIAN 2R (Fig. 2.11), [91] as one of the more advanced humanoid robot.

2.3.1 The Humanoid Robot at Waseda University

Waseda University has been one of the leading research sites for anthropomorphic robots since the late Prof. Ichiro Kato and his colleagues started the WABOT Project in 1970 [7]. Since then, just about ten years, by integrating the latest key technologies, they have developed a variety of humanoid robots including the WABOT-1, which is the first full-scale human-like robot made in 1973, the musician robot WABOT-2 in 1984, Hadaly-2, which works together with a human partner, and the biped walking robot WABIAN in 1997. Not only a lot of fundamental technology was created but also many talented engineers and scientists were nurtured from these activities.

Based on the results above, Waseda University established the Humanoid Robotics Institute in April 2000 to promote research activities which aim to construct a new relationship between humans and machines in the advanced information society. Essentially, it is expected that a robot will provide assistance in housework, for aged people and for entertainment to keep up the amenity of life and the human environment in the next century. A type of human robot, a humanoid is expected to work together with human partners in our living environment, and it will share the same working space and will experience the same thinking and behavior patterns as a human being. The robot will integrate information from sensors and show coordinated actions which realize a

high level of communication with a human without any special training using multimedia such as speech, facial expression and body movement.

This section introduces the recent results of individual research groups. Although Robotics is essentially an interdisciplinary engineering, it is vital that humanoid research be done in cooperation with biology, psychology, sociology and medicine. The Humanoid Robotics Institute will open the door for researchers from both inside and outside of the university to serve not only the academic and industrial worlds but also society as a whole.

The Biped Walking Robot

The study of artificial arms and hands began in 1967 incorporating the technological assets gained from developing the active prostheses started three years earlier. The studies had at first aimed only to develop machines to perform manual labor in lieu of persons and emphasized development of artificial hand mechanisms. Recently the aim has been to develop robots which can perform intelligent work as well as manual labor.

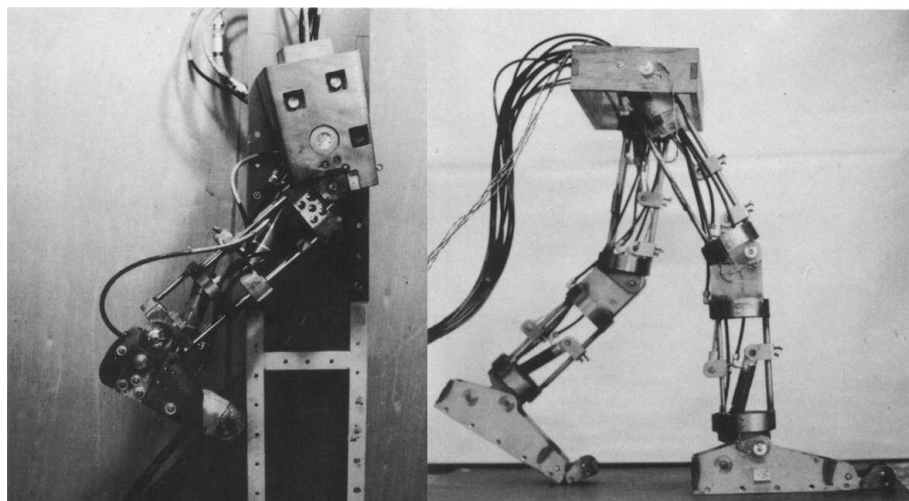


Figure 2.3: The bipeds WL-1 and WL-3.

Lower Limb Model: WL-1 (1966-1967)

The artificial lower-limb WL-1 was constructed on the basis of the analysis of locomotion of lower limbs. It resulted in the creation of the fundamental functions of biped locomotion.

Master/Slave-Type Walking Machine: WL-3 (1968-1969)

The mechanical model of lower limbs, the WL-3, which had an electro-hydraulic servo-actuator and was controlled by using a master-slave method, was constructed. It managed human-like movement in a swing phase and a

stance phase. It was also able to stand up and sit down, (Fig. 2.3).

Introduction of Artificial Muscle Made of Rubber: WAP-1 (1969)

The anthropomorphic pneumatically-activated pedipulator WAP-1 was developed. In it, artificial muscles made of rubber were attached as actuators. Planar biped locomotion was realized by teaching-playback control of its artificial muscles.

Introduction of the Pouch-Type Artificial Muscle: WAP-2 (1970)

In the second mode, the WAP-2, the powerful pouch-type artificial muscles were used as actuators. Automatic posture control was obtained by implanting pressure sensors under the soles.

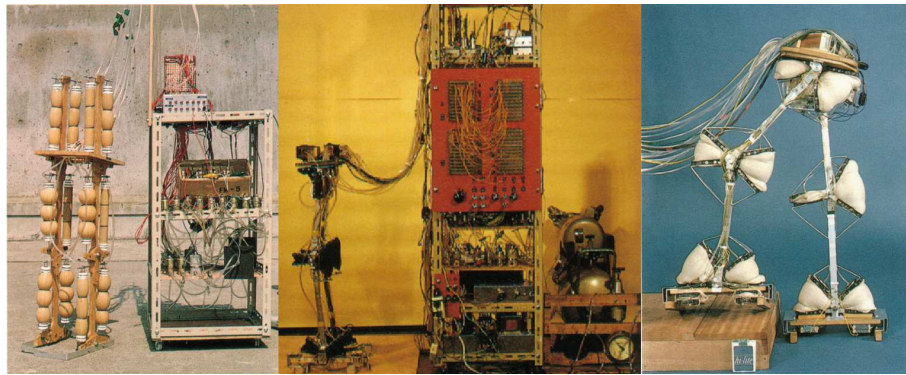


Figure 2.4: The bipeds WAP-1, WAP-2 and WAP-3.

Realization of Biped Walking in a Light -Weight Model: WAP-3 (1971)

The WAP-3, a refined model of the WAP-2, was able to move its center of gravity on the frontal plane so that it was able not only to walk on a flat surface but also descend and ascend a staircase or slope and turn while walking. A controller based on memory directed the WAP-3, and its actuator was driven by PWM. The three-dimensional automatic biped walking realized by the WAP-3 was the first in the world (Fig. 2.4).

Realization of Static Walking by a Heavy Model: WL-5 (1970-1972)

The minicomputer controlled model WL-5 was developed. It had a laterally bendable body through which it could move its center of gravity on a frontal plane. Automatic biped walking and the ability to change the direction it was walking in were made possible through the use of a mini computer. The WL-5 was used as the lower limbs of the WABOT-1 (45sec/step).

Realization of Quasi-Dynamic Walking: WL-9DR (1979-1980)

Quasi-dynamic walking was realized for the first time in the world by the model WL-9DR which used a 16-bit microcomputer as its controller instead of a minicomputer, enabling versatile control. The number of points where the WL-9DR's sole touched the floor was increased from three to four. This, in

turn, made the mathematical solution of a particular walking pattern much more easily attainable (10sec/step).

Realization of Plane Walking: WL-10, 10R (1982-1983)

The model WL-10R is a refined type of WL-10, in which the rotaries type servo-actuator (RSA) was introduced and carbon fiber-reinforced plastic (CFRP) was used in its structural parts. The WL-10R added one more degree of freedom at the yaw axis of the hip joint. Consequently, the WL-10R acquired the function of walking laterally, turning and walking forward and also backward, which is called plane walking (4.4sec/step).

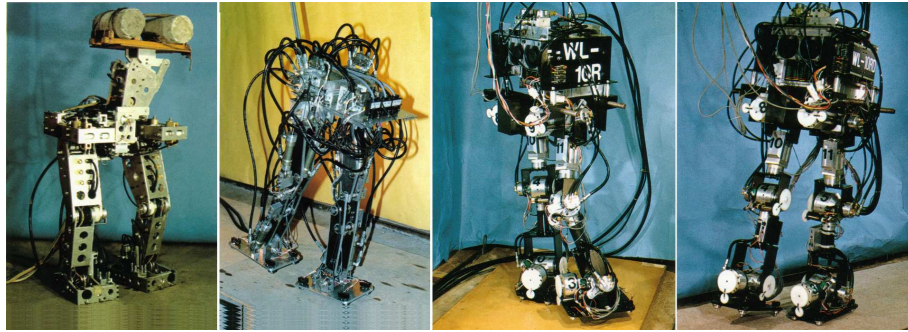


Figure 2.5: The bipeds WL-1, WL-5, WL-9 and WL-10.

Realization of Dynamic Walking: WL-10RD (1984)

In the model WL-10RD, a refined WL-10R, torque sensors were attached to the ankle and the hip joint to allow flexible control of a change-over phase (transition-phase from standing on one leg to standing on the other leg) using torque feedback. Consequently, complete dynamic walking was realized, the first successful such walking in the world. (1.3sec/step), ref. Figure 2.5.

Artificial Arms and Hands

The study of artificial arms and hands began in 1967 incorporating the technological assets gained from developing the active prostheses started three years earlier. The studies had at first aimed only to develop machines to perform manual labor in lieu of persons and emphasized development of artificial hand mechanisms. Recently the aim has been to develop robots which can perform intelligent work as well as manual labor.

First Stage WAM Series: WAM-1, 2, 3 (1967-1970)

WAM-1 was first developed in 1967. WASEDA-type artificial muscles made of rubber were used. The WAM-1 featured seven degrees of freedom (DOF), four in the hand and three in the arm. In 1969, the computer-controlled WAM-2 was assembled, featuring five electrically actuated DOFs in the arm. The WAM-3, a further refinement of the WAM-2, was developed in 1970. WAM-2 and 3 had the position sensors and the pressure sensors on their fingers so that

they could automatically grasp and transport objects.

Expansion to the WABOT-1 (1971-1972)

The development of the WAM-4 was started on the basis of the previously developed models, the WAM-1, 2 and 3, and was completed in 1972. The WAM-4 consisted of six DOFs in the arm and one DOF in the hand. The right and left hands were both developed as the upper limbs of the intelligent robot WABOT-1. WAM-4 detected objects using a visual sensor and tactile sensors attached to its fingers, and grasped and transferred or shifted objects from one hand to the other using symmetric bilateral control (Fig. 2.6).

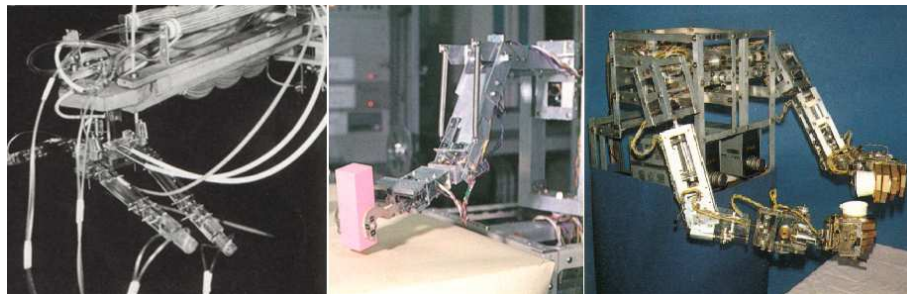


Figure 2.6: The arms WAM-1, WAM-2 and WAM-4.

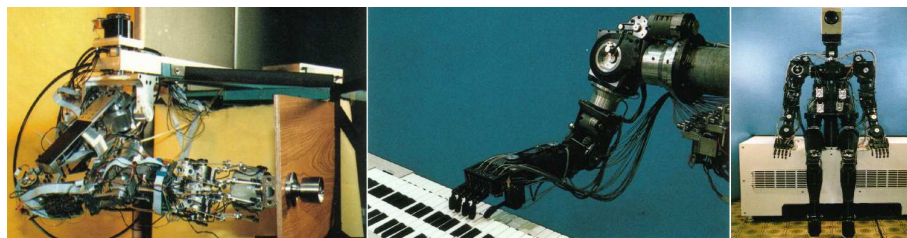


Figure 2.7: The arms WAM-7 and WAM-8L.

Force Control and a Redundant DOF (1973-1980)

Studies of an anthropomorphic artificial arm having a redundant DOF like a human arm were started in 1973. In 1974, one concept for control adaptable to external constraints, named the "Torque Position Control", was proposed. The development of the WAM-6, which had seven DOFs in the arm and two DOFs in the hand, was started in 1975 and completed in 1979. Electro-hydraulic servo-actuators, the RSA (Rotary Servo Actuator) were introduced and torque feedback was managed by the strain gauges attached to each joint of the WAM-6. In 1980, three-dimensional Torque-Position Control was applied to the WAM-6, making it possible for it to open a door and paint a curved surface.

Keyboard Playing Robot (1981-1989)

The task of developing a dexterous robot that could move quickly and act intelligently began with the challenge of trying to construct a robot that could

play a keyboard. In 1982, tapping a key ten times per second was realized by artificial fingers to which the driving force was transmitted through cables. In 1983, the WAM-7, with seven DOFs in the arm and fourteen DOFs in the fingers was developed and it could play simple tunes. Four limbs, the WAM-7R (left arm), the WAM-8 (right arm), the WAM-8L (legs) were successively developed in 1984. They had fifty DOFs total and played the electronic organ, tapping fifteen times per second. The software algorithm, based on artificial intelligence software that could read a musical score automatically determined the cooperative movement of the fingers and arms. The WAM-8 had the ability to perform middle-level tunes (Fig. 2.7).

Model for Postural Control (1967-1968)

A biped-walking machine will be required to sustain its stability while standing and walking unassisted. Hence as a first step in developing a biped walking machine, a two-bar linked inverted pendulum was constructed and control strategies for holding its balance while standing were investigated.

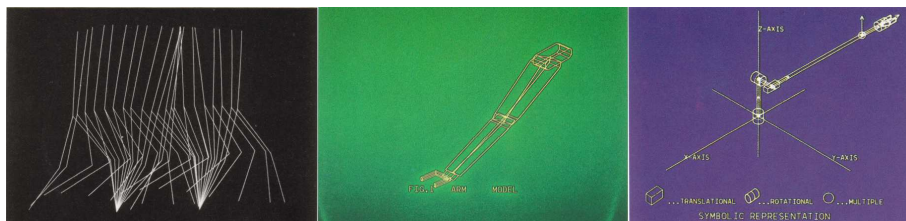


Figure 2.8: Computer-Aided Design System for Link Mechanisms, Artificial Limbs and Robotics.

Computer-Aided Design System for Robotics

Robots are mathematically considered a system that consists of multi-links with multi-degrees of freedom. The development of a software system for analyzing and also designing universal multi-link systems was started in 1979.

Computer-Aided Design System for Link Mechanisms (1979)

A simulation system for the dynamic analysis and the design of mechanisms was constructed on a main frame computer. This study aimed to design machines effectively and rapidly. Using this system, the movement of a machine could be graphically displayed by inputting just the shape of its parts, the mechanical structure and the external forces.

Computer-Aided Design System for Artificial Limbs (1980-1981)

An interactive computer system was developed to aid the design of artificial limbs. It simulated limbs as link mechanisms with multi-degrees of freedom and then calculated the force of each joint by giving their trajectories or calculated

the trajectory of each joint by giving the external forces.

Computer-Aided Design System for Robotics (1982-1983)

Researchers built an interactive software system in which the modeling and the dynamic equations of a robot having arbitrary degrees of freedom were automatically created and solved. This system could also be applied to a link mechanism having a control system.

Computer-Aided Composition System for Walking Pattern:
WALK MASTER-2 (1984)

The interactive software-system WALK MASTER-2 was written for a personal computer to analyze and compose the walking pattern of a walking biped robot. This system enables the analysis of the ZMP (zero moment point) when the biped robot is walking, and the composition of a walking pattern combined with the robot's actuator characteristics in three-dimensional graphics (Fig. 2.8).

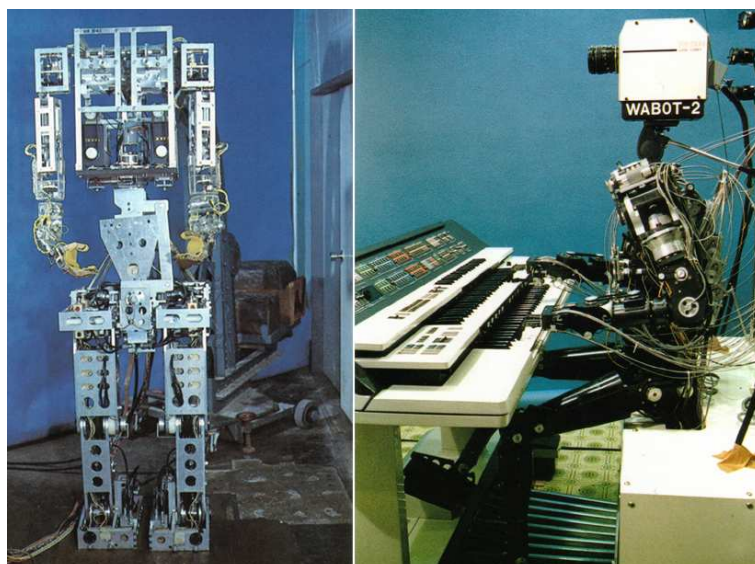


Figure 2.9: The WABOT-1 and WABOT-2 humanoid robots.

WABOT -WAseda roBOT-

It has been forecast that robots will penetrate society in the 21st century, not only in secondary industry but also in the service industry, that is, the tertiary industry field. In that case, robots will be required to have an anthropomorphic appearance and faculties. In other words, since robots that play active roles in the secondary industry are assessed as substitutions of human labor power, the robots being developed for the future should have an ability to deal with information as well as a person does. Developing the anthropomorphic intelligent robot WABOT (WAseda roBOT) was then started with the aim to finally develop a

"personal robot" which resembled a person as much as possible. Four laboratories in the School of Science Engineering of Waseda University joined to set up "The Bio-engineering group", which started the WABOT project in 1970. Our laboratory has taken charge of the limb-control system in the WABOT, which consists of artificial limbs and their control system.

WABOT-1 (1970-1973)

The WABOT-1 was the first full-scale anthropomorphic robot developed in the world. It consisted of a limb-control system, a vision system and a conversation system. The WABOT-1 was able to communicate with a person in Japanese and to measure distances and directions to the objects using external receptors, artificial ears and eyes, and an artificial mouth. The WABOT-1 walked with its lower limbs and was able to grip and transport objects with hands that used tactile sensors. It was estimated that the WABOT-1 has the mental faculty of a one-and-a-half-year-old child. WABOT-1 consisted of the WAM-4 (its artificial hands) and the WL-5 (its artificial legs).

WABOT-2 (1980-1984)

In 1980, our laboratories joined in a joint project again and commenced the WABOT-2 project. Playing a keyboard instrument was set up as an intelligent task that the WABOT-2 aimed to accomplish, since an artistic activity such as playing a keyboard instrument would require human-like intelligence and dexterity. Therefore the WABOT-2 was defined as a "specialist robot" rather than a versatile robot like the WABOT-1. The robot musician WABOT-2 can converse with a person, read a normal musical score with its eye and play tunes of average difficulty on an electronic organ. The WABOT-2 is also able to accompany a person while it listens to the person singing. The WABOT-2 was the first milestone in developing a "personal robot". (Fig. 2.9).

WABIAN(WAseda BIpedal humANoid) Series

WABIAN was developed under the following design plan to investigate a cooperative dynamic walk and collaborative work with humans. (1) The size of the biped robot should be the average size of an adult Japanese woman to do collaborative work with humans. (2) The robot should be able to walk at about the speed of a human. (3) The robot should have 3 DOF trunks and 6 DOF arms. (4) The joints of the robot should use electric servomotors. (5) A control computer and motor drives except power supply should be installed. WABIAN had a total of thirty-five mechanical DOFs; twelve DOF legs, fourteen DOF arms, a two DOF neck, four DOFs in the eyes and a torso with a three DOF waist. They have realized various kinds of walking such as dynamic forward and backward walking, marching in place, dancing, carrying a load, emotional walking, etc.

The next version, WABIAN-RV, can perform various walking motions by online generating and outputting motion pattern on every step. It is based on the online pattern generation method and this method improves environmental adaptability. (Fig. 2.10). It include "the methods of generating and teaching macro command by voice command" for more interactive human-robot interface. Using "macro command" and a voice recognition system developed in this research, a walking motion is generated in the on-motion-mode and the

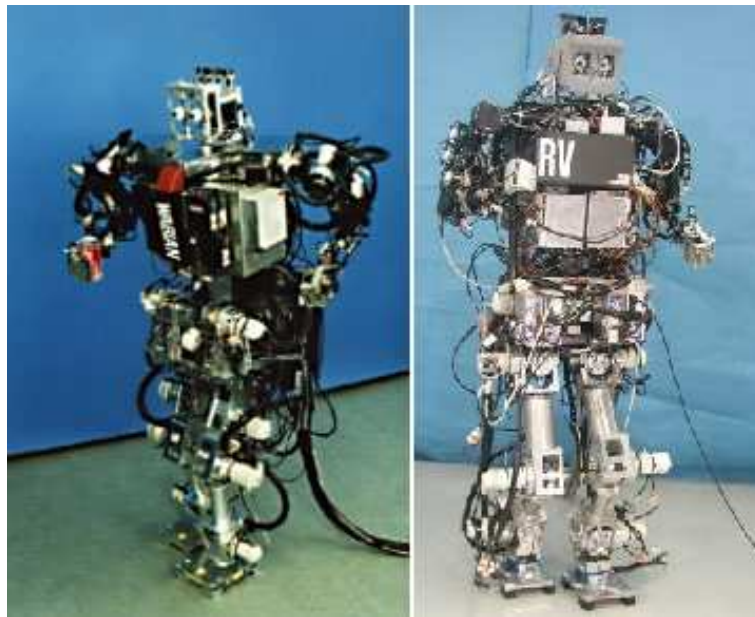


Figure 2.10: The WABIAN and WABIAN RV humanoid robots.

off-motion-mode. WABIAN-RV has a total of forty-three mechanical DOFs and control systems.

The Wabian 2R project

The WABIAN-2R has been designed accordingly in order to develop a humanoid robot with a height of 1475[mm], and a weight of 64.5[kg]. This robot was developed in order to mimic the various motions which a human does usually. It consisted of 41-DOFs. (6-DOFs Legs, 2-DOFs Waist, 2-DOFs Trunk, 7-DOF Arms, 3-DOF Hands, and 3-DOF Neck, 1-DOF Feet(Passive one)). Movable range is designed in reference to human motion measurement in rehabilitation. 2-DOFs (Roll, Yaw) at the waist enables more human-like walking motions. In the hip joint a new mechanism has an advantage which allows this robot to walk with in a knee the stretched position due to the independent orientation of the trunk movement. At the foot, when a biped humanoid robot walks on the ground, its heel and toe reaches the ground at the same time. Therefore, it is difficult for the robot to walk with long steps and mimic various walking gaits of a human. To solve the problem, they have developed a new biped foot system having one passive toe joint based on human gaits analyzed by a motion capture system. The control system is controlled by a computer mounted on its trunk. The control computer consists of a PCI CPU board , which is connected to I/O boards through a PCI bus. For I/O boards, they used an HRP Interface Board which has 16ch D/As, 16ch Counters and 16ch PIOs, and a six axis force/torque sensor receiver board (Fig. 2.11).

The operating system installed on the control computer is QNX, which is a real time system. Each actuator system is equipped with an incremental encoder attached to the motor shaft and a photo sensor attached to the joint shaft in

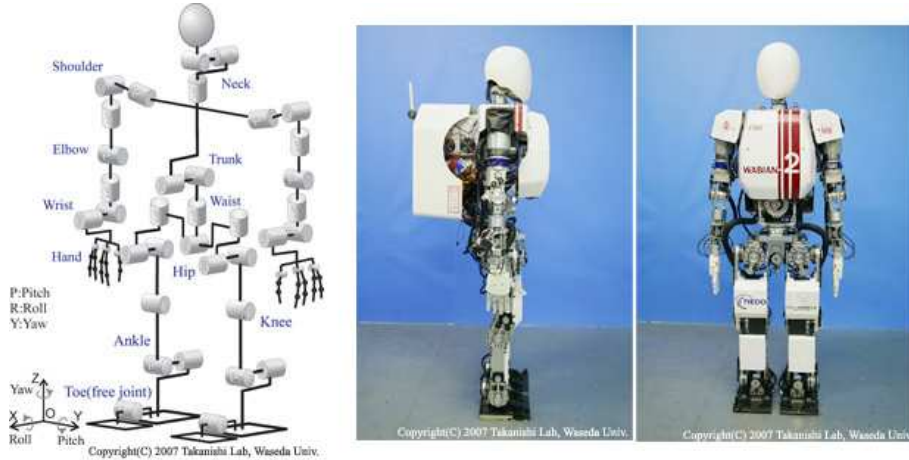


Figure 2.11: The WABIAN 2R humanoid robot.

order to detect the initial posture. (Also, each ankle is equipped with a six axis force/torque sensor which is used to measure floor reaction force and ZMP(Zero Moment Point)). About the power supply, WABIAN-2R can use an external power supply and the batteries which are received in a body exclusively. They tune-up WABIAN-2R with the external power supply and measure the experimental data with the batteries. The WABIAN-2R can seamlessly switch the external power supply and the batteries to realize an effective experiment as a human motion simulator. Furthermore, the WABIAN-2R can charge the batteries during the external power supply use by using an Li-ion battery without memory effect. By these functions, they realize the effective experiment system which can tuneup with the external power supply, and measure the experimental data with the batteries. Afterwards, they charge the batteries that they used while adjusting the WABIAN-2R with the external power supply.

2.3.2 Honda robots

Further on, in 1986, Honda Mo. Co. Inc. started to develop the ASIMO robot (Sakagami et. al. [101]). It was presented in 2000. (Fig. 2.12) it's currently one of the most advanced humanoid robots; it can walk like a human in any direction, climb stairs and recognize faces, voice and gesture commands, etc. The last version presented in 2005 can additionally run up to 6 Km/h and it is used as museums guide, and a host in the Honda offices (Fig. 2.14).

The Start of Humanoid Robot Research

In December of 1996, Honda publicly presented a humanoid robot with two legs and two arms. The research and development of this robot was initiated 24 years ago in 1984 (Hirai et. al. '97, [52]).

The key words were “intelligence and mobility”, and our direction and thoughts were ”to coexist and collaborate with a human, to perform things that a human is unable to do and to create a mobility which brings additional value to human society.” That is to say, they aimed at developing a new type



Figure 2.12: The ASIMO humanoid robot history [58].

of robot to meet consumer needs but not a robot for a special limited purpose.

They first planned a practical wheeled robot with two arms and a video camera installed on the upper body for recognition research, which they thought would be very convenient for studying such intelligence as judgment and recognition research. However, as they gave careful thought to the meaning of a consumer type robot which they initially intended to develop, they came to the conclusion that it does not meet one of our key words, “mobility”. They then looked into a type of consumer robot which will better meet their initial objective.

If they were to look at a “Domestic Robot” for an example of a type of robot that consumers may use, it would be necessary for the robot to walk around the furniture and walk up and down the staircase inside of a house. They found that a human with two legs is best suited for such movements. At the same time, if they were able to develop a two-legged (biped) robot technology, they believed that the robot should be able to move around the majority of ground environments including rough terrain.

Consequently, they reached a conclusion that the configuration of the lower part of the robot would be better if it had two legged mobile mechanism which can walk like human than if it were the wheeled type and therefore decided to develop a robot by concentrating our effort on that objective. Once they established their direction, the next step was how to realize it.

They then began to conduct a study on two legged walking mechanism by first analyzing actual human walking by taking themselves as a model.

Study on Robot's Leg Mechanism

Following 7 subjects were selected to study the leg mechanism:

1. Effectiveness of leg joints relating to the walking.
2. Locations of leg joints.

3. Movable extent of leg joints.
4. Dimension, weight and center of gravity of a leg.
5. Torque placed on leg joints during the walking.
6. Sensors related to the walking.
7. Grounding impact on leg joints during the walking.

Progress toward Humanizing

The next step is to create a humanoid robot. They defined the functions of this humanoid robot as follows. The robot should be of such a type that it can automatically perform a certain type of work under the known environment and perform an uncertain type of work with assistance from a human operator under an unknown environment. The first experimental humanoid robot had an overall length of 1,915mm and a weight of 185Kg.

Researchers of Honda had first concentrated their study on how to realize the coordinated movement of legs and arms and therefore the computers for image processing and action plan, electric power supply, etc., were not installed on the first robot. Through the experiment with this robot, they studied a coordinated movement of the robot to perform such tasks like turning a switch on and off, grasping and turning a door knob and holding and carrying an object.

In the next stage, they developed a wireless humanoid robot, as shown in Fig. 2.13 which was publicly revealed by Honda as mentioned earlier. The overall length was 1,820mm with a weight of 210Kg. Computers, a motor driver, batteries as a power source and a transmitter were installed inside the robot. The main functional specifications are listed below.

Mobility Performance:

1. Be able to move around on normal flat surfaces. Example: Plastic tiles, paved road, grazing, etc.
2. Be able to pass through a narrow opening: the width of the opening is 850 mm.
3. Be able to step over and cross over steps and mounds. Example: Step over steps with a height of about 200mm. Cross over steps 150mm high and 150mm long.
4. Be able to walk up and down the staircase of general buildings at a normal human speed. Example: a staircase with steps 200 mm high and 220 mm deep.
5. Be able to walk on a known slope of about 10.

Working Ability:

1. Be able to grasp and hold an object that weights about 5Kg
2. Be able to perform light work using a tool such as a wrench by a remote control.

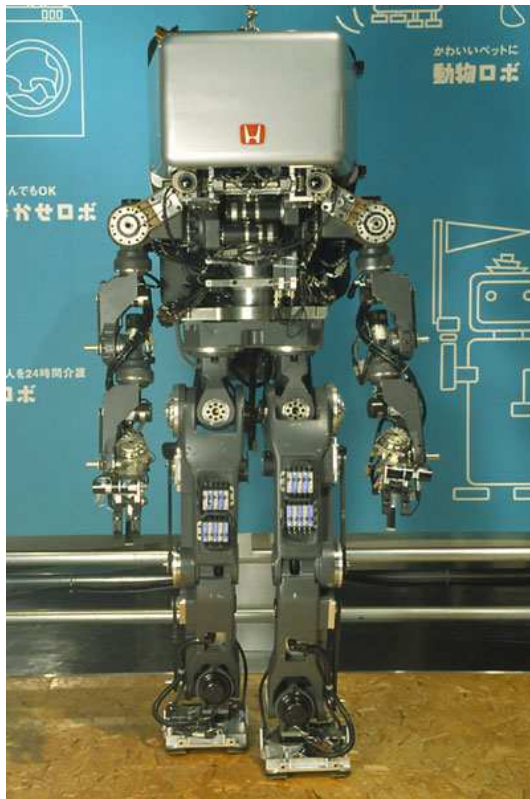


Figure 2.13: A Honda humanoid robot P1 (1.820m and 210 Kg).

The next development had been divided into a short-term and long term plan.

For the short term, emphasis will focused on the hardware improvement, which are:

1. A smaller, more compact robot
2. Mobility performance improvement
3. Operability performance improvement

For the long term, ASIMO researchers believe that increasing physical versatility by way of mobility improvement and environmental adaptability, made possible by hardware and software technology advancement, as well as improving autonomous mobility without detailed human instructions are important.

On the contrary, they also hope to develop technologies so that the humanoid robot can function not only as a machine, but blend in our social environment and interact with people, and play more important roles in our society.

In this background the ASIMO humanoid robot was born in 2000. Four years later, the New ASIMO was presented (Fig. 2.14) with more abilities, such as running up to 6Km/h, making human cooperation and interaction tasks, etc.

The University of Tokyo and Kawada Industries started with the H series up to H7. Next, the AIST (Advanced Institute of Science and Technologies) with



Figure 2.14: The New ASIMO humanoid robot.

Kawada Industries, supported by the Japanese government in the humanoid robot project (HRP), developed the HRP-2L, HRP-2P, HRP-2, HRP-3P and HRP-3 humanoid robots (Fig. 2.15 and Fig. 2.16). These humanoid robots have a wide range of joint motion and can lie down and stand up. The HRP-3 is water resistant and can walk on low-friction surfaces.

2.3.3 The HRP project

The HRP project is introduced as a question in the discussion on humanoid applications: What is the effectiveness of a “human-shaped” robot?. There are many people who say that almost applications designed for robots will not require a human shape and the functions will be more important than the shape (Inoue et. al [61]).

When they consider the practical meaning of humanoid research, they should recognize the practical importance of the human shape. There will be three benefits a “human shaped” robot produces:

1. There are several areas requiring a human shape” machine. A human shape creates new robot application possibilities in such areas.
2. A human shape produces emotional feelings useful for friendly communication between a robot and a human.
3. A human shape is one of the best shapes for a remotely controlled robot, because it makes easier to control for the operator.

There are some businesses which require human shaped devices and machines like entertainment business, prothesis and orthosis, commercial advertisements and so on. In those areas, human shape robotic technologies have traditionally

been pursued. Humanoid technology will have the possibility of being a powerful new tool to activate those areas.



Figure 2.15: The HRP-2P humanoid robot [3].

The behaviour of a humanoid seems to produce some kinds of feelings which make people imagine it was friendly to humans. It is a special effect which they will not have when they see the behavior of the conventional industrial robot. Such a feature is thought to be very effective for constructing the service robot, especially one which works in a human living environment. In telerobotics, one of the most important problems to be solved is to design a robot which can be controlled easily by a human operator. The human shape is one of the best shapes for remotely controlled robots. In the history of telerobotics research, the human-shaped robot has been investigated. Humanoid technology will provide an efficient tool for constructing an excellent telerobotic system.

As mentioned above, humanoid technology has several possibilities for practical applications. Therefore, the HRP project in Japan is promoted with the emphasis on the application aspect. The objective of the project is to develop a safe and reliable, human-friendly robot system capable of carrying out complicated tasks and supporting humans within human living and working environments. The leader of the project was Prof. Hirochika Inoue and the sub-leader Prof. Susumu Tachi, both of whom are from the University of Tokyo. The NEDO (The New Energy and Industrial Technology Development Organization) is responsible for the administration of the project with the METI, and the MSTC (Manufacturing Science and Technology Center) is the secretary of the project.

The project is run on a new scheme called a platform-based approach. The platform uses a humanoid prototype for common uses in the project. The platform is developed at phase one and it is utilized by contributors of the project as an infrastructure for RD at phase two. The approach is an antithesis of the ordinary way of robotics projects where elemental technologies are developed



Figure 2.16: The HRP-2, HRP-3 and HRP-3P humanoid robots.

first and they are integrated in the final phase of the projects. The project was run from 1998FY to 2002FY for five years, consisting of phase one for the first two years and phase two for the last three years. The total budget of the project is expected to be about 5 billion JPY.

The platform consisted of a humanoid robot, a remote control cockpit to control the robot and an equivalent virtual robot. Honda RD Co. Ltd. has produced the humanoid robot platform (the well known P3). Kawasaki Heavy Industries, Ltd., Matsushita Electric Works, Ltd., Fanuc, Ltd., and the University of Tokyo have developed the remote control cockpit system. By using the developed cockpit system, they can obtain realistic kinesthetic sensation of a humanoid robot's motion. Fujitsu, Hitachi, the University of Tokyo, Electrotechnical Laboratory (ETL), and Mechanical Engineering Laboratory, where ETL and MEL are currently a part of the Intelligent Systems Institute, AIST, have developed the virtual robot as the software counterpart of the platform robot. It has the equivalent dynamics and geometric model of the humanoid robot as well as that of its working environment.

In phase two (FY2000-2002), research and development are carried out on the applications of humanoid robots with consideration given to needs of industries in which such robots might be used. Improvement and addition of elemental technologies will be carried out using the platforms developed in phase one. The applications include maintenance tasks of industrial plants, tele-driving of construction machines, human care, security services and construction work. At the selection of those applications, how the human shape is effective for each application is deeply considered.

2.4 Other humanoids

Other groups the Technical University of Munich (TUM) developed the Johnnie. It has an advanced feedback gait control and can walk and rotate; furthermore, it has been built with light materials that weight about 40 kg and high 1.80m [80], Fig. 2.17. In the USA, the research is concentrated on learning abilities and arm dexterity, so the COG [33] and Robonaut projects by the MIT and NASA, respectively, are the main robots in this field Fig. 2.18. There are other groups in the USA like the SARCOS project, whose aim is to develop a human-like humanoid robot. More groups like the Hubo Lab from the KAIST, TOYOTA, SONY and the robotics lab of the University Carlos III of Madrid started their humanoid robot project in 2002 between others. The result is the Rh-1 humanoid robot platform. It is 1.50m of high, has 21 degrees of freedom, weights 50Kg [36], has onboard hardware, [73] and can walk at 0.8 km/h. [17], [16] recognize faces and gestures. [107] Some results of this will be shown later [12].

2.4.1 The Johnnie project

The Johnnie project, (Fig. 2.17) developed and build an autonomous biped walking robot. The main objective was to realize an anthropomorphic walking machine with a human-like, dynamically stable gait. The robot is able to walk on even and uneven ground and around curves. Furthermore, a jogging motion which is characterized by short ballistic phases where both feet are not in contact with the ground is planned. The robot is autonomous in terms of actuators, sensors and computational power, while the energy is supplied by a cable [1].

Johnnie's structure resembles the human locomotor apparatus and has a total of 17 actively driven joints. The overall weight is about 49kg and the height is 1.80m. Each leg incorporates six driven joints. Three of them are located in the hip, one actuates the knee and another two drive the ankle joint (pitch and roll). Furthermore, the upper body is equipped with a rotational degree of freedom about the body's vertical axis. Two arms with two DOFs each are employed to compensate the overall momentum about the body vertical axis. The joints are driven by brush DC-motors in combination with lightweight gears. Joint angles and velocities are measured by incremental encoders. Furthermore, two six-axis force sensors in the feet measure the ground reaction forces. An inertial measurement unit consisting of a three-axis accelerometer and three gyroscope sensors determine the spacial orientation of the upper body. A PCI-I/O-board interfaces the main computer (Pentium IV 2.8GHz) with the sensors and motor drivers. The control algorithms run on the PC as RT-Linux kernel modules.

Johnnie's control system is subdivided into three layers. The top layer handles the computation of the trajectories and switches between different walking patterns and phases of gait. One step is composed of various different phases such as the stance and swing phases. For each of these phases, the robot's motion is computed such that the planned trajectory does not lead to a tilt or lift-off of the stance foot. On the second level the system dynamics are controlled so that the robot can keep its balance. Even when the reference trajectories are ideal, the upper body may deviate from its reference due to ground inclination or external forces. The inclination of the robot is measured with the inertial

measurement unit and the trajectories are adapted such that the upper body is stabilized in an upright position.

The balancing control uses a reduced system model which can be computed in real time. Simultaneously, a force-torque control ensures that the feet do not tilt, which is necessary in order to maintain controllability.

The resulting motion of the robot is mapped onto the joint angles, which are controlled on the lowest layer. The position, velocity and acceleration of each joint is controlled by a PID controller with friction observer.

The control scheme has been tested intensively using a multibody simulation program. Standing, walking and jogging can be controlled stably and external disturbances are eliminated effectively. Today, Johnnie can walk with a speed of 2.2km/h. Future work will focus on realizing a faster walking motion. At the Hannover Fair 2003, Johnnie was presented with a visual guidance system developed by the Institute of Automatic Control Engineering of the Technical University Munich. With this vision system, the robot is able to detect obstacles and to decide whether to step on, over or walk around them. The project was supported by the Deutsche Forschungsgemeinschaft (German Research Foundation) within the Priority Program Autonomous Walking.

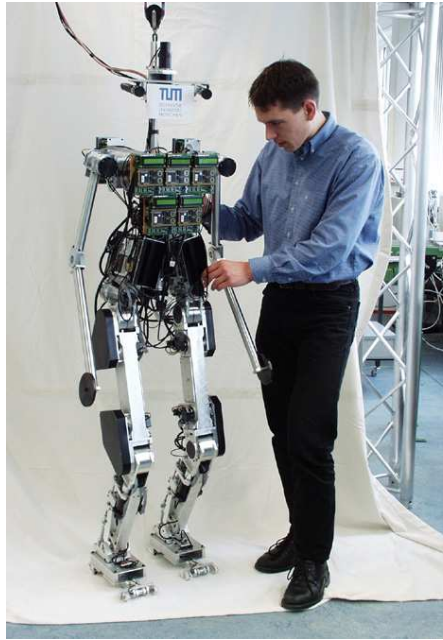


Figure 2.17: The Johnnie humanoid robot.

2.4.2 The Robonaut project

Robonaut is a humanoid robot designed by the Robot Systems Technology Branch at NASA's Johnson Space Center in a collaborative effort with DARPA, (Fig. 2.18). The Robonaut project [32] seeks to develop and demonstrate a robotic system that can function as an EVA astronaut equivalent. Robonaut jumps generations ahead by eliminating the robotic scars (e.g., special

robotic grapples and targets) and specialized robotic tools of traditional on-orbit robotics. However, it still keeps the human operator in the control loop through its telepresence control system. Robonaut is designed to be used for "EVA" tasks, i.e., those which were not specifically designed for robots.

Our challenge is to build machines that can help humans work and explore in space. Working side by side with humans, or going where the risks are too great for people, machines like Robonaut will expand our ability for construction and discovery. Central to that effort is a capability they call dexterous manipulation, embodied by an ability to use ones hand to do work, and our challenge has been to build machines with dexterity that exceeds that of a suited astronaut. The resulting robotic system called Robonaut is the product of collaboration between NASA and DARPA, supporting the hard work of many JSC engineers that are determined to meet these goals.

They are using a humanoid shape to meet NASA's increasing requirements for Extravehicular Activity (EVA, or spacewalks). Over the past five decades, space flight hardware has been designed for human servicing. Space walks are planned for most of the assembly missions for the International Space Station, and they are a key contingency for resolving in-orbit failures. Combined with our substantial investment in EVA tools, this accumulation of equipment requiring a humanoid shape and an assumed level of human performance presents a unique opportunity for a humanoid system.

While the depth and breadth of human performance is beyond the current state of the art in robotics, NASA targeted the reduced dexterity and performance of a suited astronaut as Robonaut's design goals, specifically using the work envelope, ranges of motion, strength and endurance capabilities of space walking humans.

2.4.3 The COG project

To explore issues of developmental structure, physical embodiment, integration of multiple sensory and motor systems, and social interaction, it has constructed an upper-torso humanoid robot called COG, Brooks et. al. [34]. The robot has twenty-one degrees of freedom and a variety of sensory systems, including visual, auditory, vestibular, kinesthetic, and tactile senses. It has a variety of implemented visual-motor routines (smooth-pursuit tracking, binocular vergence, and vestibular-ocular and opto-kinetic reflexes), orientation behaviors, motor control techniques, and social behaviors (pointing to a visual target, recognizing joint attention through face and eye finding, imitation of head nods, and regulating interaction through expressive feedback). It also further outline a number of areas for future research that will be necessary to build a complete embodied system.

As Prof. Brooks from the MIT save, avoiding flighty anthropomorphism, you can consider COG (Fig. 2.18) to be a set of sensors and actuators which try to approximate the sensory and motor dynamics of a human body. Except for legs and a flexible spine, the major degrees of motor freedom in the trunk, head, and arms are all there. Sight exists in the form of video cameras. Hearing and touch are on the drawing board. Proprioception in the form of joint position and torque is already in place; a vestibular system is on the way. Hands are being built as you read this, and a system for vocalization is also in the works. COG is a single hardware platform which seeks to bring together each of the

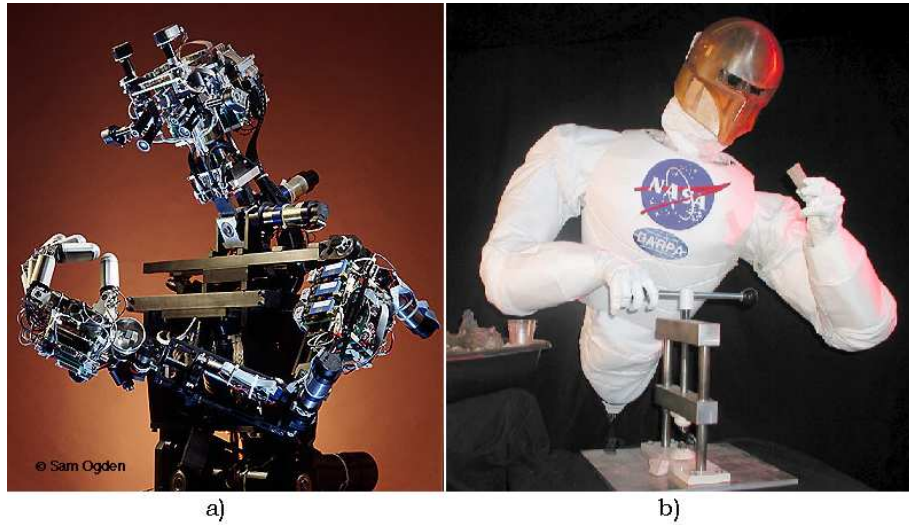


Figure 2.18: a) COG and b) Robonaut humanoid robots.

many subfields of Artificial Intelligence into one unified, coherent, functional whole.

2.4.4 The Einstein-HUBO humanoid project

From its preview versions, KHR-1 to KHR-3, Albert HUBO is an android robot. It is composed of a head, which is modelled after Dr. Albert Einstein's, and HUBO's body. The development period took about 3 months, and it was finished in November, 2005. The head part was developed by Hanson-Robotics. Its skin is a special material, Frubber, often used in Hollywood [2].

The head has 35 joints, so it can impersonate various facial expressions using independent movements of eyes and lips. It has 2 CCD cameras to do vision recognition. Also, the body of Albert HUBO can perform all the HUBO's performances, so it is possible to express more natural features and movements. In the body, there are lithium polymer batteries which can get about two and a half hours of operating time. By using a remote network, it is possible to access the Albert HUBO from an external computer. Albert HUBO (Fig. 2.19) was announced first at the 2005 APEC Summit in Busan, Korea. It was praised by many world leaders, such as the US president, the Japanese Prime Minister and so on.

Expected Effect

- Guaranteeing humanoid robot techniques.
- Entertaining people.
- Helping old or feeble people.

Long-term Plan

- Increasing the walking speed.
- Walking on a sloping road.
- Climbing stairs.



Figure 2.19: The Einstein-Hubo humanoid robot, the HUBO Lab humanoid.

2.4.5 Toyota Partner Robots

From the late 1970s to the 1980s, Toyota began collaborating with robot manufacturers to develop industrial robots for use in welding and painting processes in automobile manufacturing plants [6]. Then after the turn of the century, Toyota started developing Toyota Partner Robots by combining industrial robot technologies with the latest control technologies used in automobiles. The basic concept behind the partner robot project is the creation of robots that can use tools, assist people, and live in harmony with us. Based on this concept, it was set out to develop two types of robots, to be demonstrated at EXPO 2005 AICHI, JAPAN. One of these is a robot that can play the trumpet and walk on its two legs, and is meant to be entertaining especially to children. The other is a mountable robot called “i-foot” that was conceived by young engineers based on their childhood dreams. One of the notable features of the Toyota Partner

Robots is their ability to collaborate with each other. That is, multiple robots can move in synchronization rather than moving individually as stand alone units. Furthermore, these robots have artificial lips and fingers that allow them to play the trumpet like a human being. Currently, it is also developing robots that can provide elderly care to help Japan cope with its rapidly aging population. Our dreams are boundless and they plan to strive to develop partner robots that can enrich people's lives by working in harmony with society and assisting with people's activities.

Concept

Since Toyota's founding, their corporate spirit has been "to enrich society through making things." Based on this spirit, Toyota has been developing human-assisting partner robots (Fig. 2.20). Their goal is to build robots that embody kindness and intelligence and that will be able to assist with human activities in applications such as assistance, elderly care, manufacturing, and mobility in the near future.

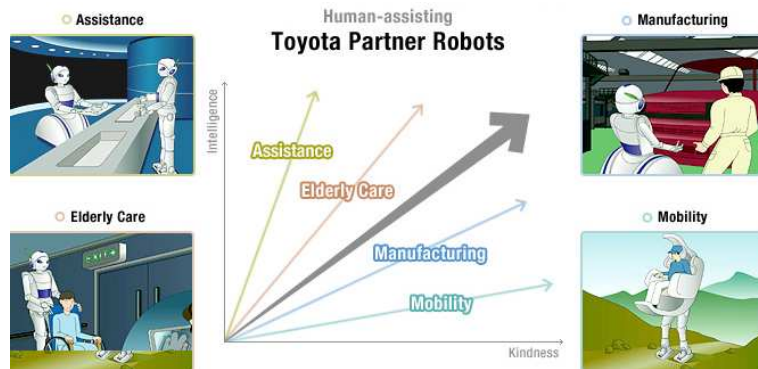


Figure 2.20: The Toyota Partner Robots concept.

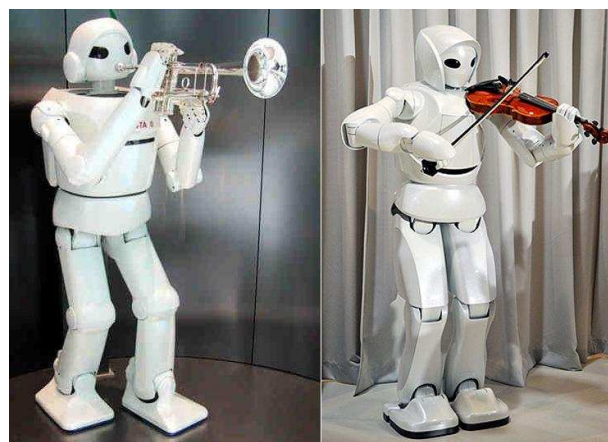


Figure 2.21: The Toyota humanoid robots.

The main features of Toyota walking robots are stable movement, artificial

lips capable of playing a musical instrument, robot hands, and a lightweight body. The technologies replicate the vibration of human lips. It has the ability of human fingers to operate valves on a musical instrument. The main specifications are 1.45m of height, 40kg of weight and 31 DOF (Fig. 2.21).

2.4.6 The Rh-1 humanoid project

Inspired by this active area, the Robotics lab of the University Carlos III of Madrid launched the humanoid robot project (under the direction of Prof. Carlos Balaguer), the Rh-0 in its first phase (2002-2004), the Rh-1 (2005-2007) and currently the Rh-2 (2007-2009). The Rh-1 humanoid robot is 1.45mm tall, weight 48.5 kg, has 21 DOFs, can walk about 0.8 Km/h, recognize faces, and responds to voice commands (Fig. 2.22).

The Control level is divided into 3 layers represented as a controller centered on its own task such as external communications, motion controller's network supervision or general control. At on the Device level, each servo drive not only closes the servo loop but calculates and performs trajectory online, synchronizes with other devices and can execute different movement programs located in its memory. These kinds of devices are located near the motors, gaining the benefit of less wiring that is one of the requirements for energy efficiency. They are lightweight and require less effort in cabling. Advanced and commercially available motion controllers were implemented in order to reduce development time and cost. Continuous evolution and improvements in electronics and computing have already made it possible to reduce the industrial controller's size for using it in the humanoid development project. Furthermore, it has the advantage of applying well supported and widely used devices from the industrial control field, and brings the commonly used and well supported standards into a humanoid robot development area.

On the Control level, the Main controller is a commercial PC/104+ single board computer because of its small size and low energy consumption. It was used instead of a DSP controller because it has a different peripheral interface such as Ethernet and RS-232, and an easy programming environment. Also, there is a great variety of additional extension modules for the PC/104+ bus, like CAN-bus, digital and analog input-output, and PCMCIA cards. Selecting criteria were fast CPU speed, low consumption and availability of expansion interfaces. The Main Controller provides general synchronization, updates sensory data, calculates the trajectory and sends it to the servo controllers of each joint. It also supervises data transmission for extension boards like the Supervisory Controller and ZMP Estimation Controller via PC/104+ bus. The Communication Supervisory Controller uses a network bus to reliably connect distributed intelligent motion controllers with the Main Controller.

According to the Server-Client model, the humanoid robot is controlled by the passive Server, which waits for requests and upon their receipt, processes them and then serves replies for the Client. On the other hand, the Server controls all Control Agents which reside in the CAN bus network. In that case, the Control Server is no longer a slave. It is a network master for Control Agents which perform their operations (motion control or sensing) and reply for the Server.

More detailed description of the Rh-1 humanoid robot will be shown in Chapter 6.

It is clear that the Japanese results on biped walking robots are the best in the world, at least in locomotion facts. Because of this, this thesis is focused on the subject of locomotion. It is based on walking pattern models developed in Japan. Successful results in two experimental humanoid robot platforms will be shown and discussed (Rh-1 and HRP-2 humanoid robots).

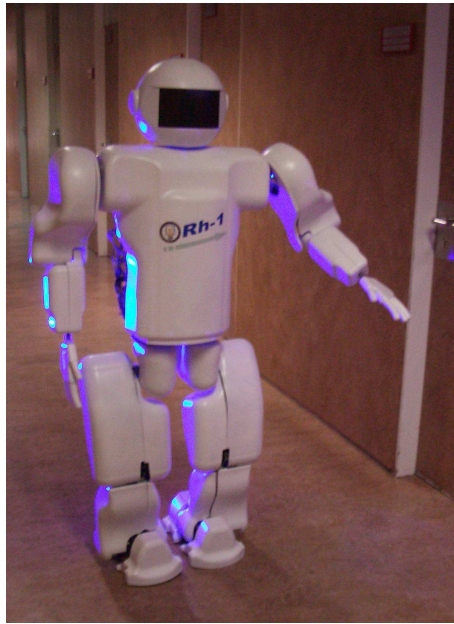


Figure 2.22: The Rh-1 humanoid robot, the University Carlos III of Madrid humanoid.

2.4.7 Humanoid entertainment robots

A brief detail about Sony robots is presented in this section, because they are not the topic of this thesis, which is constrained to human-size humanoid robots.

Sony has developed the “SDR” series of humanoid robots and finally presented the “QRIO” with high mobility ranges [5], in 2000 with future commercial uses in mind, but the production was closed a few years ago (Fig. 2.23). It is the most advanced entertainment humanoid robot.

QRIO is Sony’s new corporate ambassador who embodies the company’s vision of dreams, entertainment and technology around the world. A product of cutting edge artificial intelligence and dynamic technology, it serves as Sony’s technology platform to promote advancements by combining Sony’s expertise in these technologies. It is a small biped (two-footed) entertainment robot that aims to live with you in the future, makes life fun and makes you happy. QRIO is curious about many things in the world - for example, technology, microelectronics and robotics to the rhythm of hip-hop. The everyday occurrences in people’s lives are magical wonders to QRIO. The entertainment Robot’s Partial Features are autonomy, singing in a simple, clear voice and dancing in a fluid motion, the ability to memorize and detect up to 10 individual faces, recognition

of speech, as well as the ability to learn and memorize new words, short and long-term memory (can temporarily memorize objects and individuals, and through continued interaction, commit faces, names and emotions to its long-term memory), expressing an array of emotions through speech and body language, and walk on flat, irregular and tilted surfaces. This humanoid robot incorporates other Sony technology such as steady-shot technology sensors to provide the robot a posture sensor acting like the inner ear balance feature (from the video camera), effective actuators to support motion, delicate and smooth movements from the manufacturing technology of precise machinery assembly (from the CD player), and a jam detecting sensor which is a basic safety technology (from the AIBO robot).

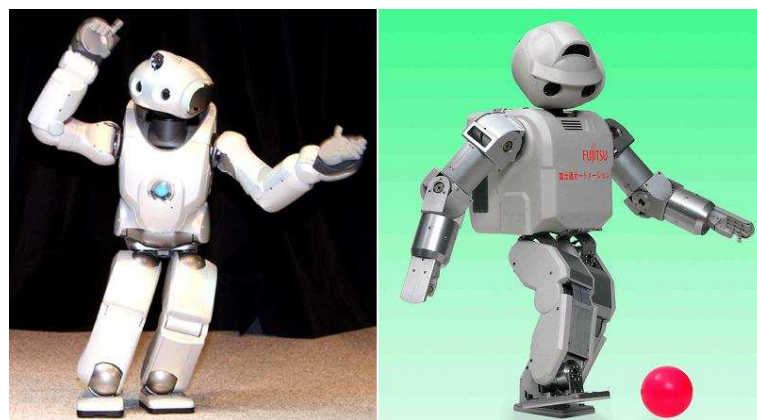


Figure 2.23: The Qrio robot, the SONY humanoid, and HOAP-3, the Fujitsu humanoid.

Another well known entertainment humanoid robot is the Fujitsu Automation's HOAP-3, (Fig. 2.23). Short in stature at 60cm and weighing in at 8.8kg, image recognition and various sensors have been added. With a 1.1GHz Pentium M processor that runs on RT-Linux inside, HOAP-3 would be a prime target for homebrew application developers. Fujitsu Automation has announced that the internal interface information of the hardware/software for the unit will be released. Simulation software for pre-confirmation of control programs is included for those who are into self-programming.

With no price tag attached to it at the moment, Fujitsu Automation is currently accepting orders for HOAP-3. HOAP-3 has gone through 2 previous iterations since 2001, aptly named HOAP-1 and HOAP-2. With progress in movement capabilities, external recognition and communication functionality, HOAP-3 is the culmination of 4 years' worth of intense research and development work.

A camera, microphone, speaker, expression LED, audio recognition function, voice synthesis function, and image recognition function have been added. This makes it viable for research involving human communication and hand-eye co-ordination. HOAP-3's distance sensor, grip sensor, and acceleration sensor are controllable through a wired or wireless LAN.

Conclusions

Human evolution to bipedalism is an option for developing intelligent machines. That way, some progress on walking robotics was explained with the emphasis on the results in the few research groups around the world. Though walking robotics is an important and attractive research area in robotics, not enough applications have been made yet. For the future of walking robotics, considering how to improve this situation will be necessary. This was briefly discussed and reconsideration of the goal of walking robotics research was pointed out for the improvement of the situation. As an example of the trends about humanoid size, weight and structural complexity, the evolution of HONDA robots is shown in Fig. 2.24.

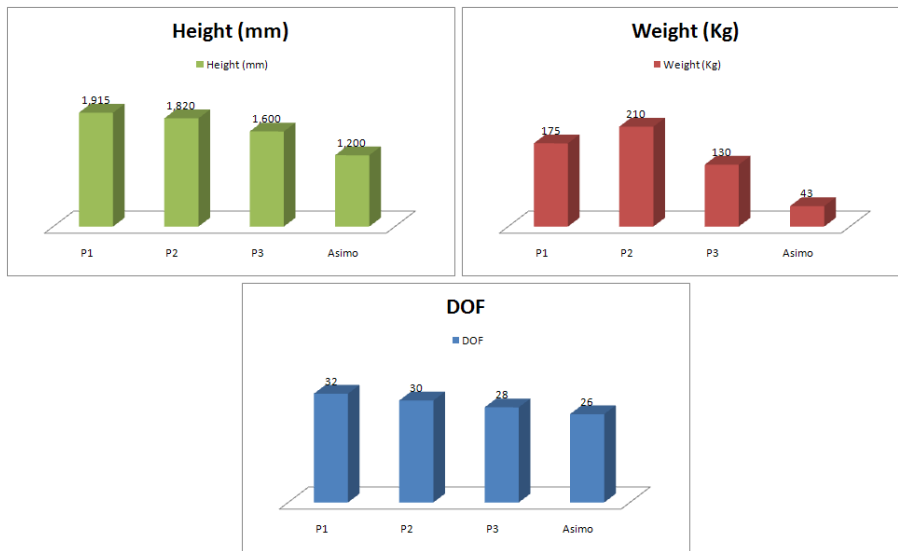


Figure 2.24: The evolution of HONDA humanoid robots.

From the picture above, in order to reduce power consumption and increase motion stability, the weight and height are reduced throughout the construction of humanoid robot prototypes. The degrees of freedom (DOFs) are the minimum for high dexterity by using strong, light materials, small electronic but powerful devices, high torque motors, powerful modelling and control algorithms.

Other important groups such as Kawada-AIST and Waseda have developed high dexterity humanoid robots, so the arms and body DOF increase, the height is about 1.60m and the weight is maintained around 60Kg. In these cases, the height and weight end to human measurements, (as seen in Fig. 2.25, Fig. 2.26).

From this analysis of the most important humanoid robot projects, the mechanical size and configuration of the Rh-1 and Rh-2 prototypes are explained as following: the Rh-1 was developed for cooperating at indoor environments, that way the selected dimensions take as an approach the ASIMO robot ones; that is, Rh-1 could attend to a sitted person. For that, the height of 1.35m is enough. Otherwise, the current Rh-2 prototype will be designed for cooperating at outdoor environments, so the trend is to approach the HRP-2 platform; because, it was

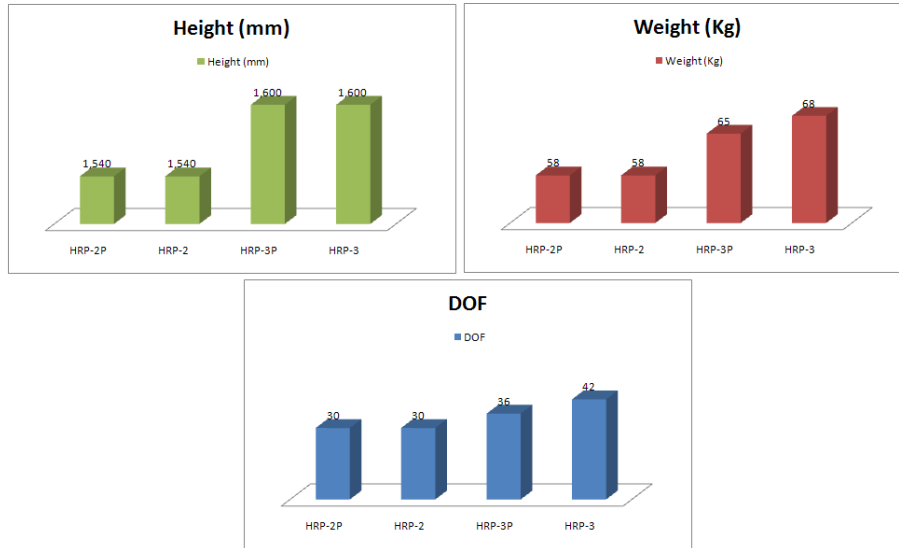


Figure 2.25: The evolution of the Kawada-AIST humanoid robots.

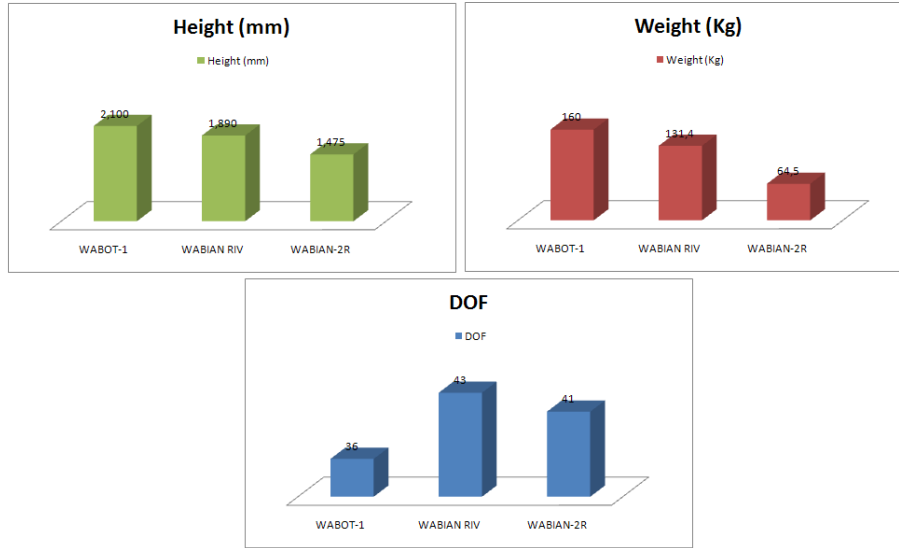


Figure 2.26: The evolution of the WASEDA humanoid robots.

developed for working in cooperation with a stand up person. Thus, the height selected is about 1.50m and more complex kinematics will be developed, specially in the arms, in order to increase its manipulability.

Chapter 3

Human locomotion study. The stability of biped locomotion

If I have seen further it is by standing on the shoulders of giants.
(Isaac Newton)

Biomechanics of human movement can be defined as the interdisciplinary which describes, analyzes and assesses human movement. A wide variety of physical movements are involved - everything from the gait of the physically handicapped to the lifting of a load by a factory worker to the performance of superior athlete. The physical and biological principles that apply are the same in all cases. What changes from case to case is the specific movement task and the level of detail that is required for the performance of each movement. The list of professionals and semiprofessionals interested in applied aspects of human movement is quite long: orthopedic surgeons, athletic coaches, rehabilitation engineers, therapists, kinesiologists, prosthetists, psychiatrists, orthotists, sports equipment designers, current biped robot researchers and so on. Biomechanics, as an outgrowth of both life and physical sciences, is built on the basic body of knowledge of physics, chemistry, mathematics, physiology and anatomy. It is amazing to note that the first real "biomechanicians" date back to Leonardo Da Vinci, Galileo, Lagrange, Bernoulli, Euler, and Young. All these scientists had primary interests in the application of mechanics to biological problems.

The biped locomotion stability will be studied, from many criteria, such as "Zero Moment Point (ZMP)", "Foot Rotation Indicator (FRI)" and "Contact Wrench Cone (CWC)". This work is based on the ZMP criterion, because it is the most used and studied in the last thirty years by many researchers and it has obtained successful results with the most advanced humanoid robots.

3.1 Human biomechanics

The humanoid design starts from its motion requirements, so the dimensions, joint range motion, joint velocities, forces and wrench should be studied. After that, the link design could start. This first humanoid robot prototype deals with the study of locomotion, so human locomotion will be analyzed. First, human biomechanics anthropometry is studied; next, the human walking motion is analyzed.

3.1.1 Kinematics

Interests in the actual patterns of movement of humans and animals goes back to prehistoric times and was depicted in cave drawings, statues and paintings. Such replications were subjective impressions of the artist. It was not until a century ago that the first motion picture cameras recorded locomotion patterns of both humans and animals. Marey, the French physiologist, used a photographic "gun" in 1885 to record displacements in human gait and chronophotographic equipment to get a stick diagram of a runner. About the same time, Muybridge in the United States triggered 24 cameras sequentially to record the patterns of a running man. Progress has been rapid during this century, and we now can record and analyze everything from the gait of a child with cerebral palsy to the performance of an elite athlete (Winter et. al. [125]).

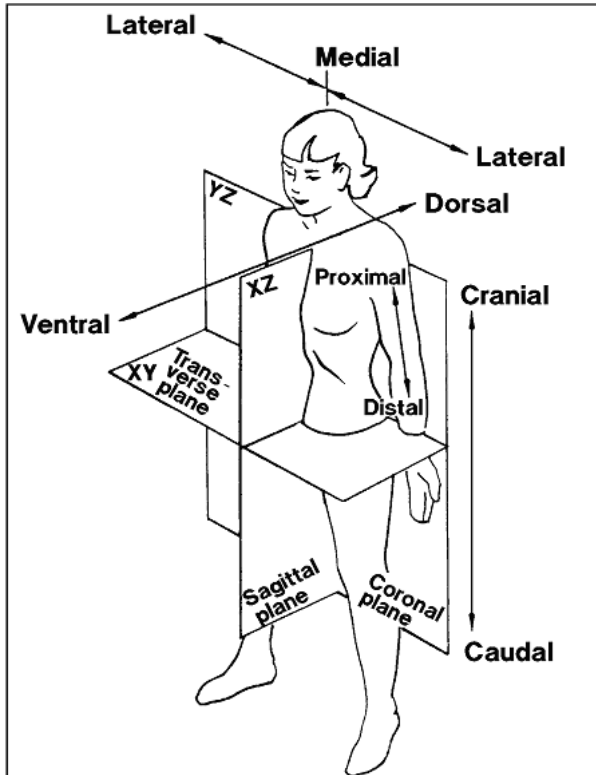


Figure 3.1: Human motion planes ©NASA [90].

The term used for these descriptions of human movement is *kinematics*. Kinematics is not concerned with the forces, either internal or external, that cause the movement, but rather with the details of the movement itself. A complete and accurate quantitative description of the simplest movement requires a huge volume of data and a large number of calculations, resulting in an enormous number of graphic plots. For example, describing the movement of the lower limb in the sagittal plane during one stride can require up to 50 variables. These include linear and angular displacements, velocities and accelerations. It should be understood that any given analysis may use only a small fraction of the available kinematic variables. An assessment of a running broad jump, for example, may require only the velocity and height of the body's center of gravity. On the other hand, a mechanical power analysis of an amputee's gait may require almost all the kinematic variables that are available.

In order to keep track of all the kinematic variables, it is important to establish a convention system. Thus if we wish to analyze movement relative to the ground or the direction of gravity, we must establish a spatial reference system (Fig. 3.1). Such conventions are mandatory when imaging devices are used to record the movement. However, when instruments are attached to the body, the data become relative, and we lose information about gravity and the direction of movement.

3.1.2 Human locomotion

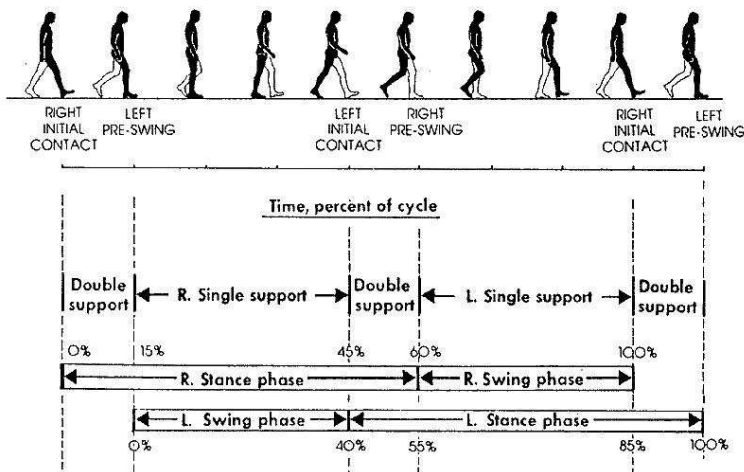


Figure 3.2: The gait cycle, (Reprinted, with permission, from a chapter by V.T. Inman et al., which appeared on page 26 of *Human Walking*, edited by Rose and Gamble and published by Williams Wilkins, Baltimore, MD; 1981.)

Study of Gait Cycle

Ed Ayyapa describes the “Gait cycle” systematically as following paragraphs [21]: the main factors which cause influence on the “gait cycle” are the shape, position and function of neuromuscular and musculoskeletal structures as well

as by the ligamentous and capsular constraints of the joints (see Fig. 3.2). As main goal of the locomotor apparatus (lower limbs with pelvis) is save energy during the act of walk.

For dividing the gait cycle in many stages or events, some considerations are taking into account such as: the gait cycle is the period of time between any two identical events in the walking cycle. As the gait cycle could be divided in events and the continuity between each other must be maintained, any event could be selected as the starting of the gait cycle (it is in the ideal case, because the terrain imperfections and human postures make gait cycle not periodic). So, the initial contact is currently called as the starting and finishing event.

Otherwise, the gait stride is defined as the distance between two initial contacts of one foot.

The stance and swing are the events of the gait cycle. Stance is the event when the foot is in contact with the ground, (around 60 percent of the gait cycle). Swing is the event when the foot is in the air, (around 40 percent of the gait cycle).

The phase when both feet are in contact with the ground is called double support (as shown in Figure 3.3). The double support happens two times in the gait cycle, that is, at the beginning and at the end of stance event. When the human is running the double support phase disappears.

The initial and final double support take up about 15 percent of the gait cycle, when the human is walking normally. So, the two periods of double support represent about 30 percent of the gait cycle (it could be seen in the Fig. 3.2; the double support is included in the stance phase).

The period of time when only one foot is in contact with the ground is called single support. While the human is walking, the single support time is equal to the swing event of the other leg.

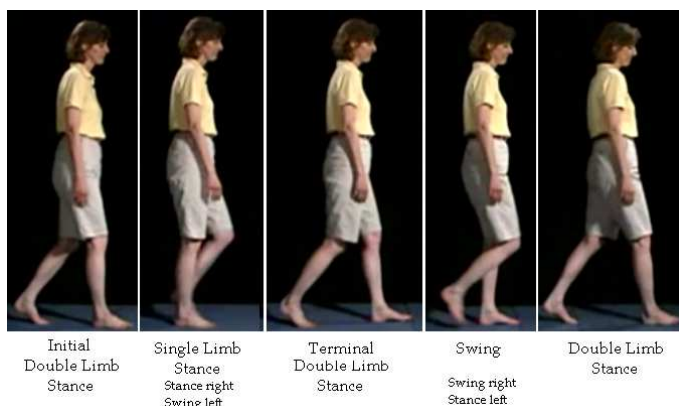


Figure 3.3: The gait cycle has two phases: about 60-percent stance phase and about 40-percent swing phase with two periods of double support which occupy a total of 25 to 30 percent of the gait cycle.

Tasks of Gait

Three tasks constitute the gait cycle, those are included in the stance and swing events. Thus, the swing event includes the body advancement and the

stance event includes the weight acceptance and single support (Fig. 3.4).

The weight acceptance is the first task. The initial contact and loading response perform this task. Both actions must be compensated in order to maintain the kinetic stability while walking.

The single limb support is the second task. This task is composed by: midstance and terminal stance. Additionally, the preswing is the transition between the single support to body advancement. While the support foot supports the body weight the stability is obtained.

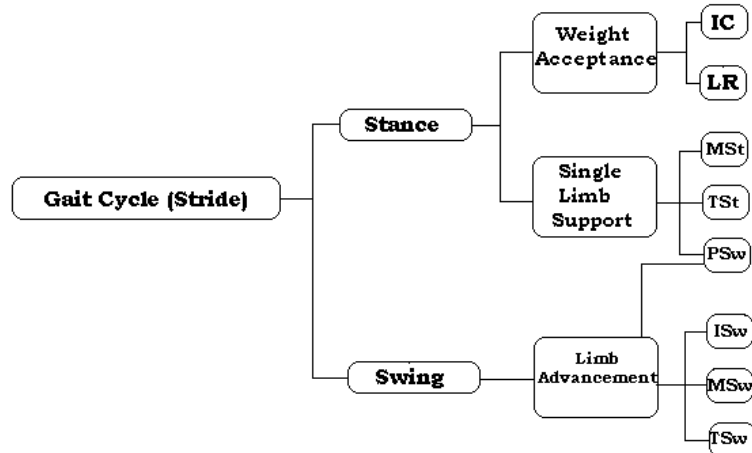


Figure 3.4: Relationship between the tasks of gait and the phases of gait.

The body or limb advancement is the third task. It is constituted by the following phases: preswing, initial swing, midswing and terminal swing. In this task the stance body advances to the posture of the next initial contact.

Phases of Gait

The phases of the gait cycle are detailed as following (see Figure 3.4)::

- Initial contact (IC)
- Loading response (LR)
- Midstance (MSt)
- Terminal stance (TSt)
- Preswing (PSw)
- Initial swing (ISw)
- Midswing (MSw)
- Terminal swing (TSw)

It is clear that the stance event has five phases and the swing event has three phases. The preswing phase adapts the body for going ahead, so it is included in the swing event.

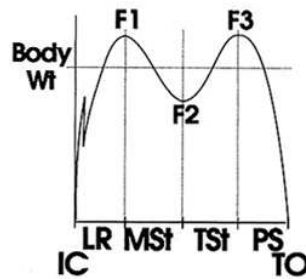


Figure 3.5: The vertical force shows the five phases of gait at stance event. Normally it exceeds body weight at two intervals, [21].

The vertical force reaction on one foot, at normal walking, shows information about each phase of the stance event. (see Figure 3.5).

From the research of Ed. Ayyappa [21], the next paragraph is reproduced in order to detail the walking concept:

Saunders et al. defined walking as “the translation of the center of mass through space in a manner requiring the least energy expenditure”. They identified six determinants or variables that affect that energy expenditure, [102]. Variations in pelvic rotation, pelvic tilt, knee flexion at mid-stance, foot and ankle motion, knee motion, and lateral pelvic displacement all affect energy expenditure and the mechanical efficiency of walking (see Figure 3.6).

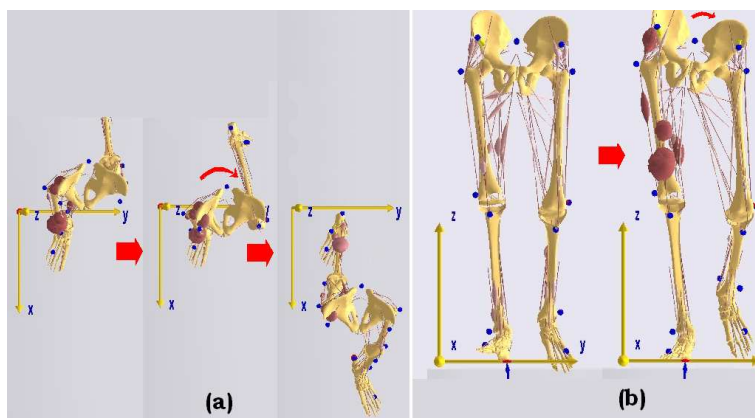


Figure 3.6: (a) Pelvic rotation effectively extends the trailing and advancing support points. (b) Pelvic tilt reduces vertical displacement of the center of mass, [21].

As a functional basis for understanding energy efficiency in gait, these principles have stood the test of time. These determinants of gait are based on two principles: 1) Any displacement that elevates, depresses or moves the center of mass beyond normal maximum excursion limits wastes energy, and 2) Any abrupt or irregular movement will waste energy even when that movement does not exceed the normal maximum displacement limits of the center of mass. A successful long-distance runner intuitively takes advantage of these principles.

By contrast, the unsuccessful runner lumbers from side to side and lurches up and down in a vicious spiral of exhaustion followed by increased energy expenditure.

Of the six determinants of gait, three provide mechanical advantages that limit vertical displacement of the center of mass. The term center of mass is synonymous with the term center of gravity (COG). Without these mechanical advantages that limit displacement, the center of mass would displace vertically 7.5 cm on a person of average height. Resulting from these three determinants, the center of mass is said to displace vertically only 5 cm.”

3.1.3 Anthropomorphic human dimensions, volume and weight distribution

Human dimensions are taken into account as a reference, because their proportions allow for stable walking and optimal distribution of the forces actuating while a human is walking. Biomechanics give us a relationship between human height and each link, furthermore, in the same way as the mass.

Anthropometry is the major branch of anthropology that studies the physical measurements of the human body to determine differences in individuals and groups. A wide variety of physical measurements are required to describe and differentiate the characteristics of race, sex, age, and body type. In the past, the major emphasis of these studies has been evolutionary and historical. However, more recently, a major impetus has come from the needs of technological developments, especially man-machine interfaces: workspace design, cockpits, pressure suits, armor, and so on. Most of these needs are satisfied by basic linear, area, and volume measures. However, human movement analysis requires kinetic measures as well: masses, moments of inertia, and their locations. There is also a moderate body of knowledge regarding the joint centers of rotation, the origin and insertion muscles, the angles of pull of tendons, and the length and cross-sectional area muscles.

The most basic body dimension is the length of the segments between each joint. These vary with body build, sex, and racial origin. Dempster and co-workers (1955, 1959), [44] have summarized estimates of segment lengths and joint center locations relative to anatomical landmarks. An average set of segment lengths expressed as a percentage of body height was prepared by Drillis and Contini (1966), [45] and is shown in (Fig. 3.7). These segment proportions serve as a good approximation in the absence of better data, preferably measured directly from the individual (Winter D., [125]).

The following are considerations that must be made when using and applying anthropometric data; [90], they are from the NASA space program for designing modules 3.1:

- Percentile Range - Design and sizing of space modules should ensure accommodation, compatibility, operability, and maintainability by the user population. Generally, design limits are based on a range of the user population from the 5th percentile values for critical body dimensions, as appropriate. The use of this range will theoretically provide coverage for 90% of the user population for that dimension.
- User Population Definition - Anthropometric data should be established from a survey of the actual user population. In the case of space programs,

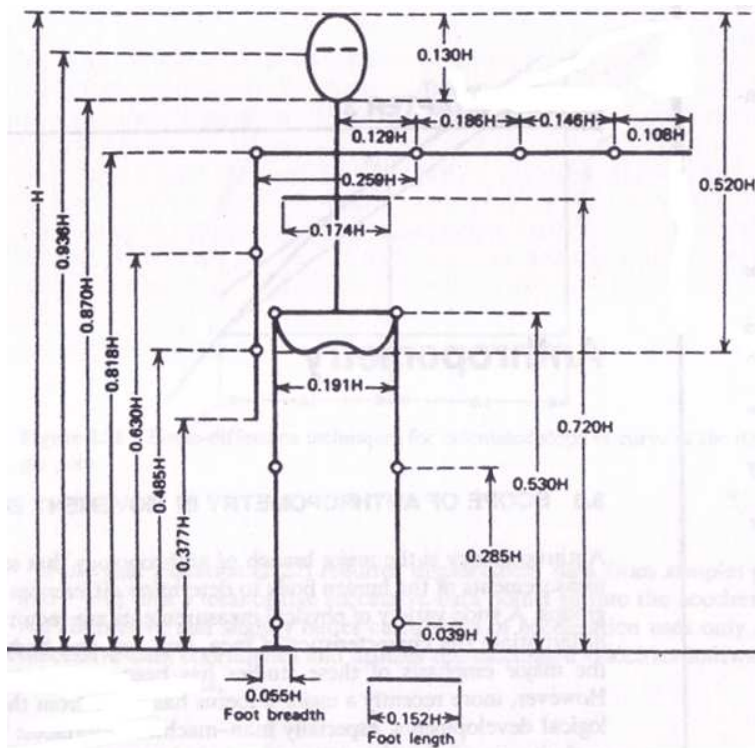


Figure 3.7: Anthropomorphic human dimensions, ©Winter, D., [125]

it is difficult to define the user population. Past space programs have involved a small, select, and easily defined group. As the space program expands, the user population will expand and change. With improved environmental controls, physical fitness will be a less important criterion. Skills and knowledge will be more of a factor in selection. International participation will also influence the character of the user population. In this document, the user population has not been defined. Data are provided for the 5th percentile Asian Japanese and the 95th percentile White or Black American male projected to the year 2000. This does not necessarily define the 5th and 95th percentile of the user population. The data in this document are meant only to provide information on the size ranges of people of the world. The Japanese female represents some of the smallest people in the world and the American male some of the largest. Development of a predicted user population size range requires a statistical combination of an estimated mix of these data.

- Misuse of the 50th Percentile - There is an erroneous tendency to consider the 50th percentile dimensional data as sufficient to accommodate the majority of users. This must not be done. The 50th percentile dimensions will accommodate only a narrow portion of the population, not a majority of the users. The full size range of users must be considered.

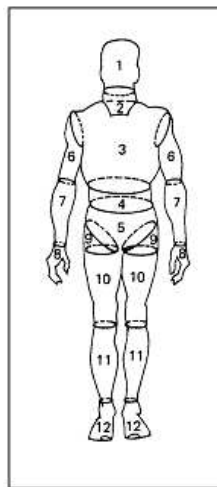


Figure 3.8: Whole body volume of American male crew member, ©NASA [90].

Segment	Vol. (cm ³)	Vol. (cm ³)	Vol. (cm ³)
	5th perc.	50th perc.	95th perc.
1 Head	4260	4400	4550
2 Neck	930	1100	1270
3 Thorax	20420	26110	31760
4 Abdomen	2030	2500	2960
5 Pelvis	9420	12300	15150
6 Upper arm	1600	2500	2500
7 Forearm	1180	1450	1720
8 Hand	460	530	610
9 Hip flap	2890	3640	4380
10 Thigh minus flap	5480	6700	7920
11 Calf	3320	4040	4760
12 Foot	840	1010	1180
5+4+3 Torso	31870	40910	49870
9+10 Thigh	8360	10340	12300
7+8 Forearm plus hand	1640	1980	2320

Table 3.1: Human volume distribution, ©NASA [90].

- Summation of Segment Dimensions - Caution must be taken when combining body segment dimensions. The 95th percentile arm length, for instance, is not the addition of the 95th percentile shoulder-to-elbow length plus the 95th percentile elbow-to-hand length. The actual 95th percentile arm length will be somewhat less. The 95th percentile individual is not composed of 95th percentile segments. The same is true for any percentile individual.
- Percentiles within a category of data are exclusive. For example, a person

who is 5th percentile body size does not necessarily have 5th percentile reach or joint movement.

The mass and inertia distribution will be detailed in the appendix B.

3.1.4 Human walking trajectories

The human walking motion is studied in order to analyze the right motion of each link and joint during the step. The swing leg and hip motions must assure stable walking in any direction and speed. In this work, only walking motion is detailed (Fig. 3.9 to 3.14). Earlier biomechanical studies had the sole purpose of describing a given movement, and any assessments that were made resulted from visual inspection of the data. A total description in the plane of the movement is the stick diagram, in which each body segment is represented by a straight line or stick (Fig. 3.9 to 3.14), [125]. Joining the sticks together gives the spatial orientation of all segments at any point in time. Repetition of this plot at equal intervals of time gives a pictorial and anatomical description of the dynamics of the movement. The full page of coordinate data is required to make this complete plot for the description of the event. The coordinate data can be used directly for any desired analysis: reaction forces, muscle moments, energy changes, efficiency, and so on. A trained observer, for example, can scan a stick diagram and extract useful information that will give some directions for training or therapy, or give the researcher some insight into basic mechanisms of movement.

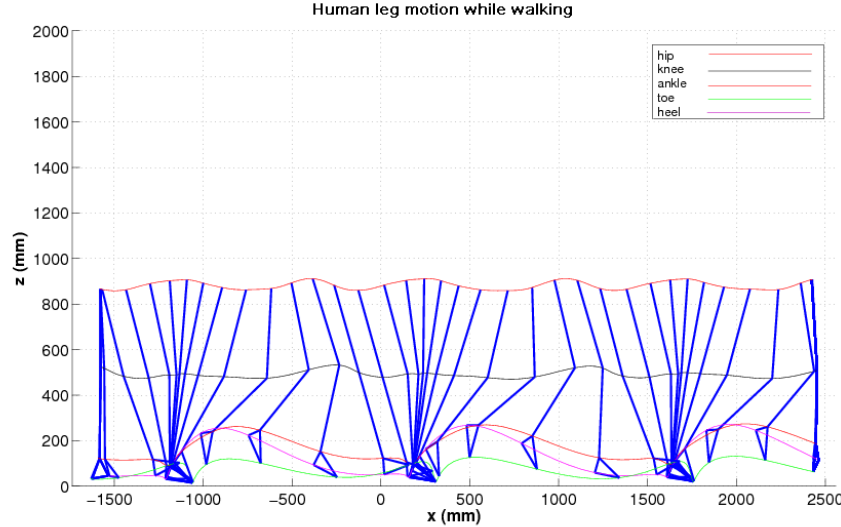


Figure 3.9: Human leg motion, sagittal view.

The joint angular evolution during a walk should be measured with the appropriate devices, or by introducing the swing leg and hip trajectories as inputs of a kinematic model. For the humanoid robot, the joint angular evolution is the inputs for walking. The human swing foot normally falls to the ground while walking, while for a humanoid robot it is an issue that must be avoided

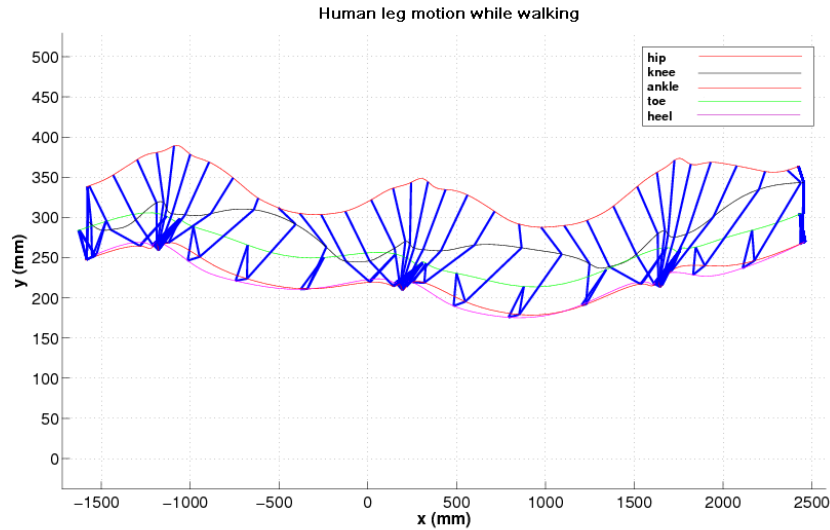


Figure 3.10: Human leg motion, top view.

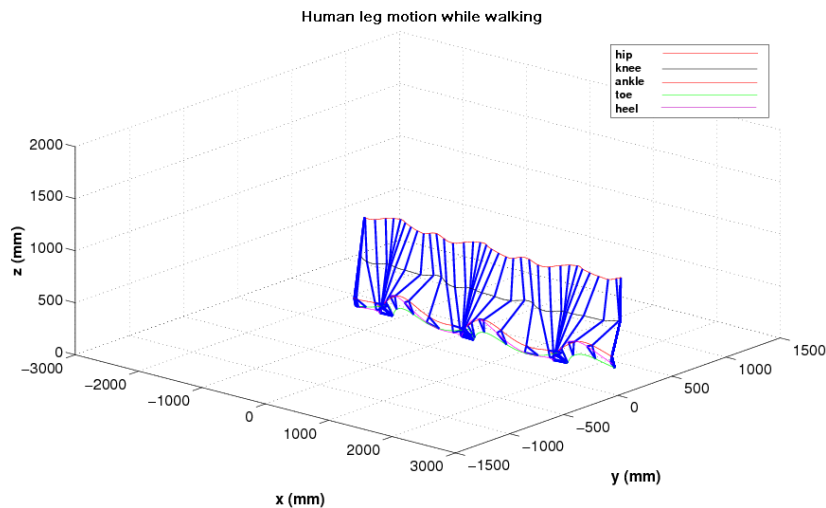


Figure 3.11: Human leg motion, 3D view.

in order to protect the robot structure and force sensors of the soles. Thus, the adequate walking pattern should be generated, for the COG and the swing foot. Normally, the human COG follows the laws of the inverted pendulum in the field of gravity during the walking motion, which is an hyperbolic orbit. It is suitable for doing a smooth walking motion at the jerk level. However, the humanoid robot's swing foot motion should be faster than the human one in order not to fall while walking.

Figures 3.9 and 3.10 show the leg motion and the hip, knee and feet trajectories (including the ankle, toe and heel). The hip trajectory is quite similar to

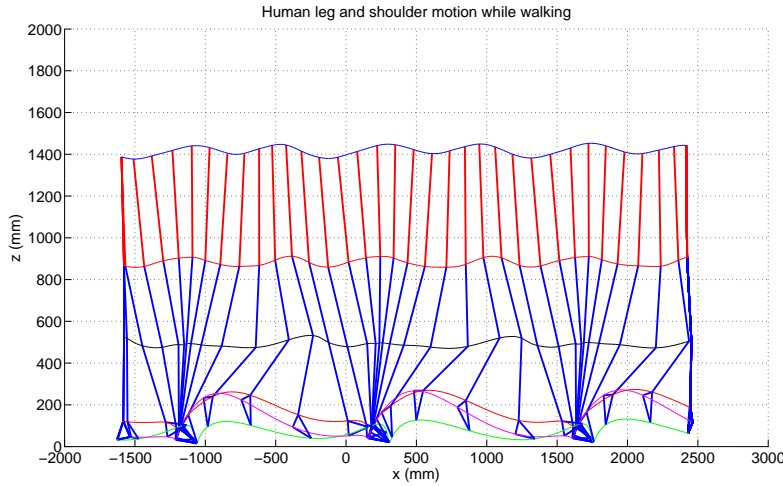


Figure 3.12: Human leg and shoulder ("red stick") motion during walking.

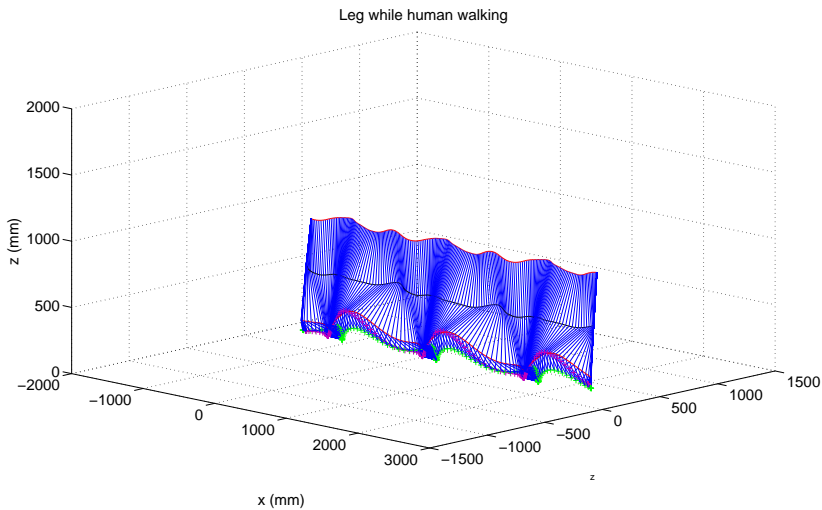


Figure 3.13: 3D view of continuos stick chart of Human leg motion.

the COG trajectory. In the sagittal view, that trajectory climbs and descends cyclically. The falling motion increases the sole reaction force, so in the humanoid robot, it is better to have a motion on a horizontal plane; furthermore, the trajectory shape looks like the inverted pendulum motion (top view), so we could approximate the humanoid robot in this way. In Fig. 3.11, the 3D swing leg motion is shown in order to have an idea of spatial leg motion.

Fig. 3.12 includes the shoulder motion. In this case, we have an idea of how the upper body cooperates in the walking motion in order to maintain stability. Clearly, the shoulder turns backward at start of the walking motion and forward at the end of walking. However, at the frontal plane, the motion always is upright and in the horizontal one, the motion looks like that of the

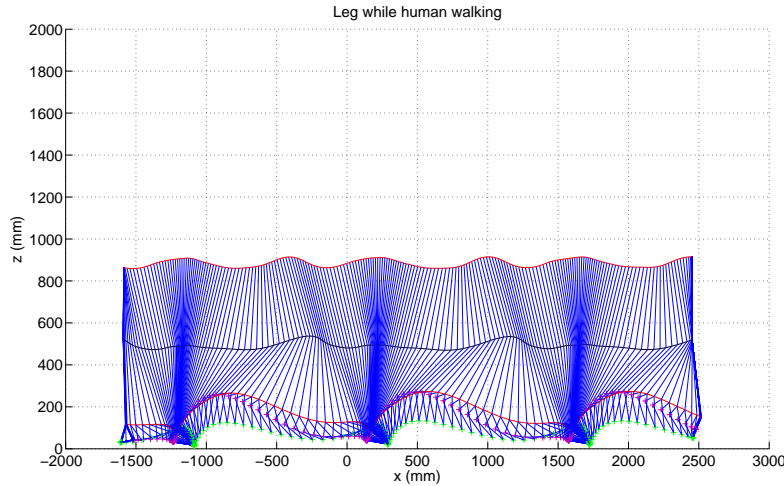


Figure 3.14: Sagittal view of continuous stick chart of Human leg motion.

hip.

Finally, in Figures 3.13 and 3.14, the stick chart gives us an idea of continuous human leg motion during walking. When the swing leg starts its motion, the hip moves backward while the knee is bending and the tiptoe goes up. Next, the foot falls freely to the ground, landing with the heel.

3.2 Biped locomotion stability criteria

Since the study of biped locomotion started, the dynamic stability criteria for obtaining a stable walking motion has been the main feature. The most popular stability criteria proposed by Professor Miomir Vukobratovic (1970), the “Zero Moment Point” (ZMP), is the base of almost all walking biped robot stability control. However, other researchers have proposed other ones, such as Dr. Ambarish Goswami (1999). He proposed the “Foot Rotation Indicator” (FRI), which performs such an extension on the ZMP, in the sense that it is not necessary to maintain it inside the convex hull to obtain dynamic walking stability. Currently, the research tends to cover a more robust stability criteria, with multicontact points and over rough terrain, so the “Contact Wrench Cone” (CWC) is proposed, by Dr. Hirohisa Hirukawa and coworkers from the AIST.

In this section, an explanation and conceptual studies developed by the Prof. Miomir Vukobratovic and coworkers will be detailed. The other stability criteria such as “FRI” and “CWC” will be outlined.

3.2.1 Zero Moment Point (ZMP)

In this section, an explanation of the Professor Vukobratovic and coworkers will be detailed [119], [120], in order to understand the ZMP concept. Theoretical studies from various aspects have been accompanied by a lot of simulation work and various practically realized systems, from the simplest cases of pla-

nar mechanisms to the Honda, Kawada (with the AIST) and Sony humanoid robots, the most advanced biped locomotion robots designed up to now. Irrespective of their structure and number of degrees of freedom (DOFs) involved, the basic characteristics of all biped locomotion systems are: (i) the possibility of rotation of the overall system about one of the foot edges caused by strong disturbances, which is equivalent to the appearance of an unpowered (passive) DOF, (ii) gait repeatability (symmetry), which is related to regular gait only, and (iii) regular interchangeability of single and double-support phases. During the act of walking, two different situations arise in sequence: the statically stable double-support phase in which the mechanism is supported on both feet simultaneously, and the statically unstable single-support phase, when only one foot of the mechanism is in contact with the ground while the other is being transferred from the back to front positions. Thus, the locomotion mechanism changes its structure during a single walking cycle from an open to a closed kinematic chain. All these circumstances have to be taken into account in artificial gait synthesis.

All of the biped mechanism joints are powered and directly controllable except for the contact between the foot and the ground (which can be considered as an additional passive DOF), where the interaction of the mechanism and environment takes place. This contact is essential for the walk realization because the position of the mechanisms with respect to the environment depends on the relative position of the foot/feet with respect to the ground.

The foot cannot be controlled directly but in an indirect way, by ensuring the appropriate dynamics of the mechanism above the foot. Thus, the overall indicator of the mechanism behavior is the point where the influence of all forces acting on the mechanism can be replaced by one single force. This point was termed the Zero-Moment Point (ZMP). Recognition of the significance and role of ZMP in the artificial biped walk was a turning point in gait planning and control. The seminal method for gait synthesis (semi-inverse method) was proposed by Vukobratovic and Juricic. It should be noted that despite the limitation that the motion can be synthesized only for as many joints as the zero-moment conditions can be preset, this method has remained for a long time the only procedure for biped gait synthesis. The ZMP is also indispensable in biped control for establishing the practically unavoidable feedback with respect to dynamic ground reaction forces.

In this section some basic issues related to biped locomotion is reviewed with particular attention paid to the ZMP because of its crucial importance for gait analysis, synthesis and control. Despite the fact that the notion of ZMP has never been introduced in the form of a formal definition, in the course of almost three and a half decades this concept has been involved in very diverse applications related to numerous anthropomorphic locomotion mechanisms of different degrees of complexity.

The ZMP notion

Apart from the realization of the relative motion of the mechanism's links, the most important task of a locomotion mechanism during the gait is to preserve its dynamic balance, which is achieved by ensuring the whole area of the foot, and not only the edge, is in contact with the ground. The foot relies freely on the support and the only contact with the environment is realized via the

friction force and vertical force of the ground reaction.

Let us consider the locomotion mechanism in the single-support phase (Fig. 3.15(a)), with the whole foot being on the ground. To facilitate the analysis we can neglect the part of the mechanism above the ankle of the support foot (point A) and replace its influence by force F_A and moment M_A (Fig. 3.15(b)), whereby the weight of the foot itself acts at its center of gravity (point G). The foot also experiences the ground reaction at point P , whose action keeps the whole mechanism in equilibrium. In general, the total ground reaction consists of three components of the force R (R_x, R_y, R_z) and moment M (M_x, M_y, M_z).

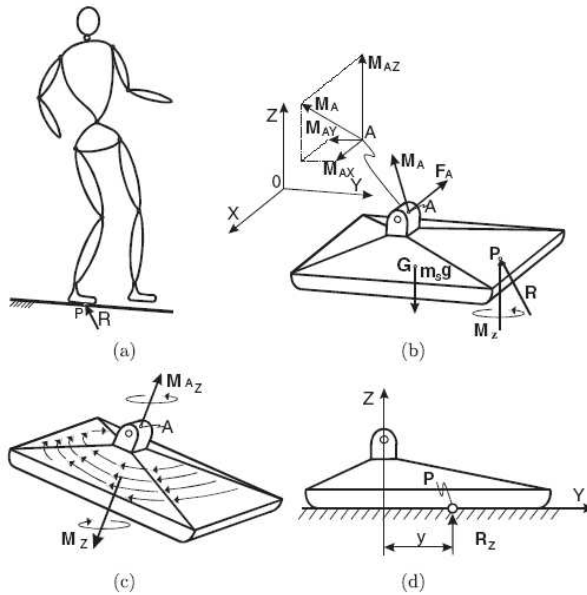


Figure 3.15: Biped mechanism and forces acting on its sole © Vukobratovic, et al. [118].

Since the friction force acts at the point of contact of the foot with the ground, and the foot on the ground is at rest, those components of force R and moment M that act in the horizontal plane will be balanced by friction. Therefore, the horizontal reaction force (R_x, R_y) represents the friction force that is balancing the horizontal component of the force F_A , whereas the vertical reaction moment M_z represents the moment of friction reaction forces (Fig. 3.15(c)) that balance the vertical component of moment M_A and the moment induced by force F_A . Thus, if we assume the foot-floor contact is without sliding, static friction will compensate for the horizontal force components (R_x, R_y) and vertical reaction torque (M_z). The vertical reaction force R_z represents the ground reaction that balances vertical forces. It remains to consider the balancing of the horizontal component of the foot load moment. However, due to a unidirectional nature of the connection between the foot and the ground (it is obvious that the ground reaction force induced by foot action is always oriented upwards), horizontal components of all active moments can be compensated for only by changing position of the reaction force R within the support polygon. Therefore, the horizontal component of moment M_A will shift the reaction force

to the corresponding position to balance the additional load. This is illustrated in Fig. 3.15(d), where, for the sake of simplicity, we present a simple planar case in the $y-z$ plane. Moment M_{Ax} is balanced by shifting the acting point of force R_z , whose intensity is determined from the equation of balance of all the forces acting on the foot by the corresponding distance y . It is necessary to emphasize that all the time the reaction force is within the area covered by the foot, the increase in the ankle moment will be compensated for by changing the position of this force, and no horizontal components of the moments M_x and M_y will exist. This is the reason why in Fig. 3.15(b) at point P only the M_z component exists.

However, if the real support polygon is not large enough to encompass the appropriate position of force R to balance the action of external moments, force R will act at the foot edge and the uncompensated part of the horizontal component of the reaction moment will cause the mechanism's rotation about the foot edge, which can result in the mechanism's overturning. Therefore, we can say that the necessary and sufficient condition for the locomotion mechanism to be in dynamic equilibrium is that for point P on the sole where the ground reaction force is acting,

$$\begin{aligned} M_x &= 0 \\ M_y &= 0 \end{aligned} \quad (3.1)$$

Since both components relevant to the realization of dynamic balance are equal to zero, a natural choice for naming this point was "Zero-Moment Point". In other words, the reaction of the ground due to the foot resting on it can always be reduced to force R and the vertical component of moment M_z ; point P on which the reaction force is acting represents ZMP. Now, a logical question can be posed: given the mechanism dynamics, what should the ZMP position be that would ensure dynamic equilibrium? It should be noted that in view of the fact that the entire mechanism is supported on the foot, a prerequisite for the mechanism's dynamic equilibrium is that the foot rests fully on the floor. Thus, to answer the previous question, let us state the static equilibrium equations for the supporting foot (Fig. 3.15(b)):

$$R + F_A + m_s g = 0 \quad (3.2)$$

$$\overrightarrow{OP} \times \overrightarrow{R} + \overrightarrow{OG} \times m_s g + M_A + M_Z + \overrightarrow{OA} \times F_A = 0 \quad (3.3)$$

where \overrightarrow{OP} , \overrightarrow{OG} and \overrightarrow{OA} are radius vectors from the origin of the coordinate system O_{xyz} to the ground reaction force acting point (P), foot mass center (G), and ankle joint (A), respectively, while the foot mass is m_s .

If we place the origin of the coordinate system at point P and project Eq. 3.3 onto the z -axis, then the vertical component of the ground reaction moment (actually, it is the ground friction moment) will be

$$M_Z = M_{fr} = - \left(M_A^Z + (\overrightarrow{OA} \times F_A)^Z \right) \quad (3.4)$$

In a general case, this moment is different from zero and can be reduced to zero only by the appropriate dynamics of the overall mechanism. However, the projection of Eq. (3.3) onto the horizontal plane gives

$$\left(\overrightarrow{OP} \times \overrightarrow{R}\right)^H + \overrightarrow{OG} \times m_s g + M_A^H + \left(\overrightarrow{OA} \times F_A\right)^H = 0 \quad (3.5)$$

This equation is a basis for computing the position of the ground reaction force acting point (P). Equation 3.5, representing the equation of the foot equilibrium, answers the above question concerning the ZMP position that will ensure dynamic equilibrium for the overall mechanism dynamics, but it does not answer the inverse question: whether for the given motion the mechanism is in dynamic equilibrium. To answer this question we have to consider the relationship between the computed position of P and the support polygon. If the position of point P , computed from Eq. 3.5, is within the support polygon, the system is in dynamic equilibrium.

However, in reality, point P cannot exist outside the support polygon, as in that case the reaction force R cannot act on the system at all. From this follows a straightforward but very important conclusion: in reality, in order to ensure dynamic equilibrium, a point P that satisfies Eq. 3.5 must be within the support polygon. If we suppose for a moment that point P is outside the support polygon, let us consider what would then be the meaning of this point. In view of the fact that this position of P was obtained from the condition $M_x = M_y = 0$, we can consider it a fictitious ZMP (FZMP). Therefore, in reality, ZMP can exist only within the support polygon, and this point we can term regular ZMP, or ZMP for short, and all the calculated positions of point P outside the support polygon represent fictitious locations.

Let us explain this in more detail. It is clear from Eqs. 3.2 and 3.3 that the ZMP position depends on the mechanism dynamics (i.e., on F_A and M_A). In the situation when the mechanism dynamics changes so that the ZMP approaches the support polygon edge (in either single-support or double-support phases) let us focus our attention on the moment when the ZMP is just reaching the support polygon edge. The corresponding point will remain the ZMP only if no additional moments are acting at this point. However, if an additional moment appeared, the locomotion mechanism would start to rotate about the foot edge and the mechanism would collapse. In such a situation, the acting point of ground reaction force would be on the foot edge, but this point would not be the ZMP any more, since both conditions $M_x = 0$ and $M_y = 0$ would not be fulfilled simultaneously.

To further clarify the meaning of the ZMP outside the support polygon (FZMP), let us be reminded that there are two different cases in which the ZMP plays a key role:

1. in determining the proper dynamics of the mechanism above the foot to ensure a desired ZMP position,
2. in determining the ZMP position for the given mechanism motion.

Case (1) belongs to the task of gait synthesis [122] and will not be further elaborated here, whereas Case (2) refers to gait control, where the ZMP position is a key indicator of the dynamic equilibrium of the mechanism. Thus, a crucial question is how to determine the ZMP position. In the case of a real walking mechanism, information about the ZMP position can be obtained by measuring forces acting at the contact of the ground and the mechanism, [120] with the aid of force sensors on the sole of the mechanism. However, if the biped gait is

investigated using a dynamic model, the ZMP position must be computed. For a given mechanism motion, the force and moment at the ankle joint (F_A and M_A) can be obtained from the model of the mechanism dynamics, [120] and all elements in Eq. 3.5 except for \overrightarrow{OP} will be known.

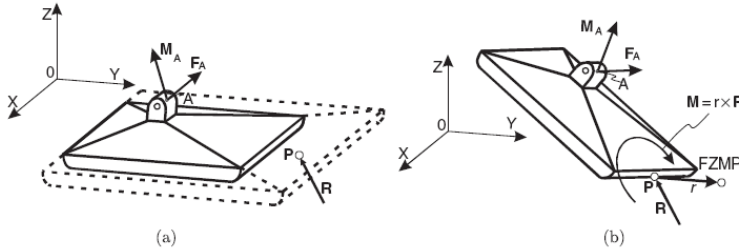


Figure 3.16: Illustration of the determination of ZMP position © Vukobratovic, [118]: (a) Step 1, and (b) Step 2.

The procedure for determining the ZMP position consists of two steps.

Step 1. Compute \overrightarrow{OP} from Eq. 3.5 (see Fig. 3.15). Let us call the obtained position of point P *computed ZMP position*. Note again that at this moment we actually do not know whether this position of point P (see Fig. 3.16(a)) will be within the real support polygon or outside it.

Step 2. The computed ZMP position is just a candidate to be a regular ZMP and its position should be compared with the real support polygon size. If the computed ZMP is outside the support polygon, this means that the ground reaction force acting point (P) is actually on the edge of the support polygon and the mechanism rotation about the support polygon edge will be initiated by the unbalanced moment, whose intensity depends on the distance from the support polygon edge to the computed position of ZMP, i.e., to the FZMP position.

The above procedure is illustrated in Fig. 3.16. In Step 1, we obtain an answer to the question concerning the ZMP location for the given dynamics not taking into account the real foot size (see Fig. 3.16(a)), whereas in Step 2, we obtain the answer whether, regarding the foot size (more precisely, the support polygon size), the mechanism is really balanced or not, and where the regular ZMP (provided it exists) is located. If the computed acting point of the ground reaction force is within the real support polygon, this point is the ZMP and the mechanism is in equilibrium. If this is not the case, the ground reaction force acting point will be on the support polygon border and the distance from it to the computed ZMP position is proportional to the intensity of the perturbation moment that acts on the foot (Fig. 3.16(b)).

The ZMP concept has been properly comprehended by researchers, widely used, and very frequently cited. It can be noted that, although being essentially correct, all the ZMP definitions differ significantly in the extent of their detail.

Here Prof. Vukobratovic and coworkers have to point out another important issue, and this is the difference between the center of pressure (CoP) and ZMP, as it is very important to make a clear distinction between the two notions, which must not generally be regarded as identical. The pressure between the foot and

the ground can always be replaced by a force acting at the center of pressure - CoP. If this force balances all active forces acting on the mechanism during the motion (inertia, gravitation, Coriolis and centrifugal forces and moments) its acting point is ZMP. Thus, in the case of a dynamically balanced gait, CoP and ZMP coincide. When the gait is not dynamically balanced, ZMP does not exist and the mechanism collapses about the foot edge. To make the ZMP notion and its relationship with CoP perfectly clear, they will summarize their previous discussion in three characteristic cases for a non-rigid foot in contact with the ground, as sketched out in Fig. 3.17.

In a balanced gait, the ZMP coincides with CoP (Fig. 3.17(a)). In the case of a disturbance that brings the acting point of the ground reaction force to the foot edge, the perturbation moment will cause rotation of the biped system about the foot edge (as we already mentioned, the foot edge is in fact a very narrow strip as the shoe sole is not totally rigid) and its overturning. In that case, we can speak only of the fictitious ZMP, whose distance from the foot edge represents the intensity of the perturbation moment (Fig. 3.17(b)). However, it is possible to realize the biped motion, for example, on the toe tips (Fig. 3.17(c)) with special shoes having a pinpoint area (balletic motion), while keeping the ZMP position within the pinpoint area.

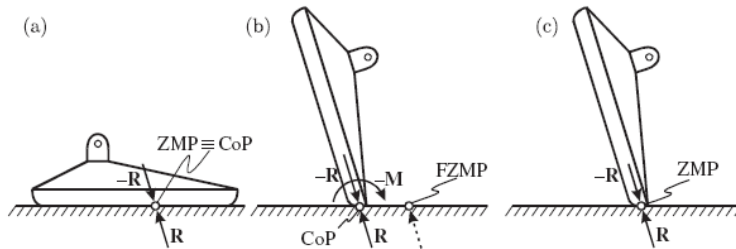


Figure 3.17: Possible relations between ZMP and CoP for a non-rigid foot: (a) dynamically balanced gait, (b) unbalanced gait where the ZMP does not exist and the acting ground reaction force point is CoP while the point where $M_x = 0$ and $M_y = 0$ is outside the support polygon (FZMP). The system as a whole rotates about the foot edge and overturns, and (c) tiptoe dynamic balance (“balletic motion”) © Vukobratovic, [118].

Although the ZMP now coincides with CoP, it is not a regular gait, and the person should be specially trained to perform it. Here, it is necessary to be reminded that the task of deriving a model of nominal dynamics of a humanoid robot is concerned with satisfying a certain number of dynamic connections. This is in fact the so-called mixed type of task, when the link’s motion and the driving torques are both partly known and their complements are sought. In the case of investigating the dynamics of biped structure, the motion of the links performing a given type of gait is known, while the known moments are equal to zero. The latter follows from the equilibrium conditions holding for a selected point within the support polygon and for the joints of passive links. Therefore, there are two types of zero-moment points. Both of them serve to form the model of nominal dynamics of the humanoid robot, but those within the support polygon are practically unavoidable in gait synthesis as well as for the overall control of a dynamically balanced gait.

To relate the ZMP notion only to CoP is not correct as the ZMP can exist at some other points in the system, e.g., at the shoulder joints if we consider arms as freely-swinging pendulums with no actuators at the joints. In summary, the ZMP always coincides with the CoP (dynamically balanced gait), but the CoP is not always the ZMP (dynamically unbalanced gait). However, the FZMP never coincides with the CoP because the CoP cannot, naturally, exist outside the support polygon.

3.2.2 Foot-Rotation Indicator (FRI) Point

The Dr. A. Goswami, [51] introduces the “Foot-Rotation Indicator” (FRI) and he describes the detail of this concept as following: to formally introduce the FRI point, we first treat the entire biped robot -a general *n-segment* extended rigid-body kinematic chain (see the sketch in Fig. 3.18 on the left)-as a system, and determine its response to external force/torque. We may employ Newton’s or d’Alembert’s principle for this purpose. The external forces acting on the robot are the resultant ground reaction force/torques, R and M , acting at the CoP (denoted by P ; see Fig. 3.18, on the right), and gravity. The equation for rotational dynamic equilibrium (we deal with rotational equilibrium only, and do not discuss translational equilibrium: “sliding”, assuming that the foot/ground friction is sufficiently large to prevent it) is obtained by noting that the sum of the external moments on the robot, computed either at its GCoM or at any stationary reference point, is equal to the sum of the rates of change of angular momentum of the individual segments about the same point. Taking moments at origin O , we have

$$M + OP \times R + \sum OG_i \times m_i g = \sum \dot{H}_{Gi} + \sum OG_i \times m_i a_i \quad (3.6)$$

where m_i is the mass, G_i is the CoM location, a_i is the CoM linear acceleration, and H_{Gi} is the angular momentum about CoM, of the i-th segment.

An important aspect of our approach is to treat the stance foot as the focus of attention of our analysis. Indeed, as the only robot segment interacting with the ground, the stance foot is a “special” segment subjected to joint forces, gravity forces, and the ground-reaction forces. Viewed from the stance foot, the dynamics of the rest of the robot may be completely represented by the ankle force/torque $-R_1$ and $-\tau_1$ (negative signs are for convention). Figure 3.18 (right) artificially disconnects the support foot from the shank to clearly show the forces in action at that joint. The dynamic equilibrium equation of the foot (segment 1) is

$$M + OP \times R + OG_1 \times m_1 g - \tau_1 - OO_1 \times R_1 = \dot{H}_{G1} + OG_1 \times m_1 a_1 \quad (3.7)$$

The equations for *static* equilibrium of the foot are obtained by setting the dynamic terms (in the right-hand side) in eq. 3.7 to zero:

$$M + OP \times R + OG_1 \times m_1 g - \tau_1 - OO_1 \times R_1 = 0 \quad (3.8)$$

Recall that to derive eq. 3.8 we could compute the moments at any other stationary reference point. Out of these, the CoP represents a special point where eq. 3.8 reduces to a simpler form,

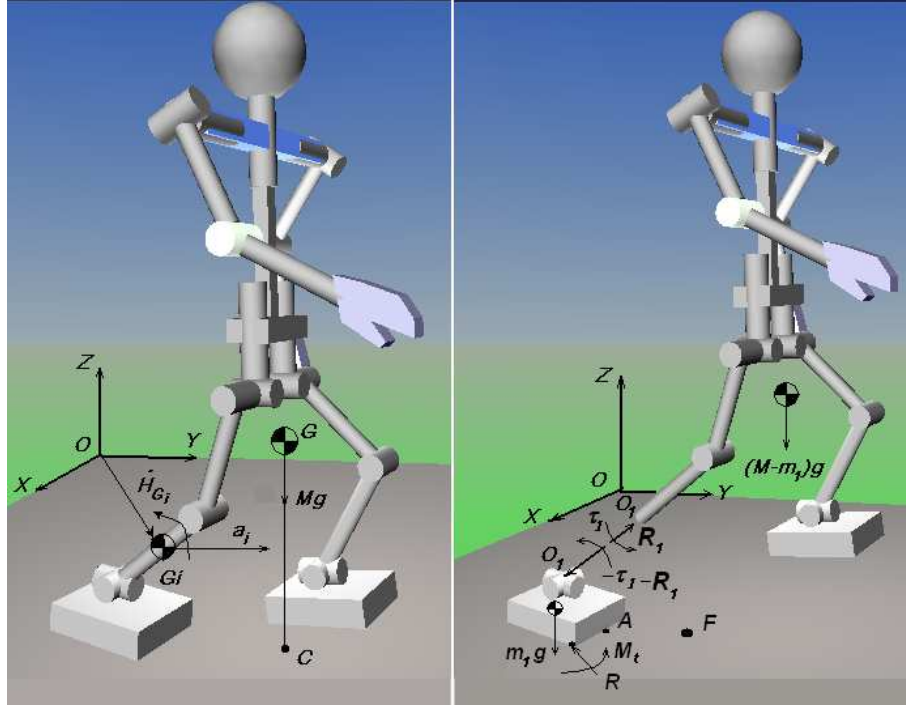


Figure 3.18: The sketch of a 3-D extended rigid-body biped robot (left), and a view with its support foot artificially disconnected from the shank to show the intervening forces (right). The CoP, GCoM, and the FRI point are denoted by P , C , and F , respectively, [51].

$$M + PG_1 \times m_1g - \tau_1 - PO_1 \times R_1 = 0 \quad (3.9)$$

Considering only the tangential (XY) vector components of eq. 3.9, we may write

$$(\tau_1 + PO_1 \times R_1 - PG_1 \times m_1g)_t = 0 \quad (3.10)$$

where the subscript t implies the tangential components. Since M is tangential to the foot/ground surface, its vector direction is normal to that surface and does not contribute to this equation (we ignore foot rotation about the normal ground, as it does not contribute to a loss of balance). In the presence of an unbalanced torque on the foot, eq. 3.10 is not satisfied for any point within the support polygon. One may, however, still find a point F outside the support boundary that satisfies eq. 3.9; i.e.,

$$(\tau_1 + FO_1 \times R_1 - FG_1 \times m_1g)_t = 0 \quad (3.11)$$

Point F is called the FRI point, and is defined as *the point on the foot/ground contact surface, within or outside the convex hull of the foot-support area, at which the resultant moment of the force/torque impressed on the foot is normal to the surface*. By “impressed force/torque”, we mean the force and torque

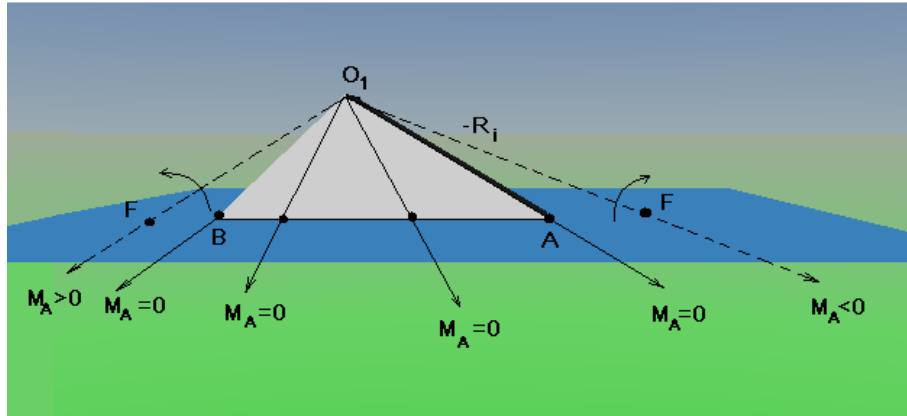


Figure 3.19: Condition for foot rotation when $\tau_1 = 0$. The figure sketches different lines of action of the force R_1 applied on the robot foot by the rest of the robot at ankle joint O_1 . If the line of action of a force intersects the ground beyond the footprint, there is a net moment applied on the foot and the foot rotates. Otherwise, the ankle joint forces may be supported by the foot/ground interaction forces, and the foot maintains static equilibrium in its stationary upright configuration, [51].

at the ankle joint, other external forces, plus the weight of the foot, and not the ground-reaction forces. Following the work of Banach (1951), [26], we may identify the impressed forces as the *acting forces*, in contrast to the reaction forces from the ground, which are the *constraint forces*.

An intuitive understanding of the FRI point is obtained by setting $\tau_1=0$, $m_1=0$ in eq. 3.11. In this case, F is simply the point on the ground where the line of action of R_1 penetrates, as shown in Figure 3.19. The case of the unactuated ankle joint was considered by Lee and Raibert (1991) [79] to analyze the hoof rotation in a monopod.

It is important to note that the location of the ankle joint and the geometry of the support-polygon boundary are the only important features of the foot that are relevant in our discussion. The actual physical shape of the foot is not important. See Figure 3.20 for a graphical illustration of this fact.

Explicit expressions for the coordinates of F , OF (OF_x , OF_y , $OF_z=0$), are obtained by computing the dynamics of the robot *minus the foot* at F ,

$$\tau_1 + FO_1 \times R_1 + \sum_{i=2}^n FG_i \times m_i g = \sum_2^n \dot{H}_{Gi} + \sum_2^n FG_i \times m_i a_i \quad (3.12)$$

Using eq. 3.11 and considering only the tangential components,

$$\left(FG_1 \times m_1 g + \sum_{i=2}^n FG_i \times m_i (g - a_i) \right)_t = \left(\sum_2^n \dot{H}_{Gi} \right)_t \quad (3.13)$$

Noting $FG_i = FO + OG_i$ and $OF = -FO$, eq. 3.13 may be rewritten as

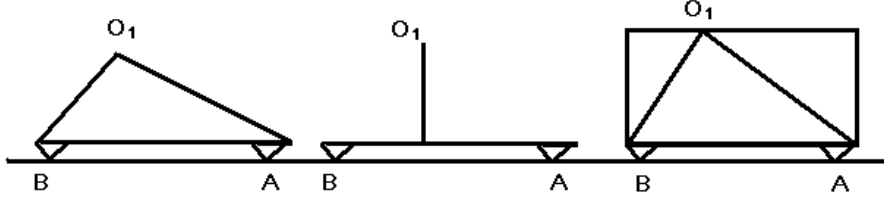


Figure 3.20: The locations of key points the ankle-joint location (O_1) and the support-polygon boundary (A and B), not its overall geometry are relevant for the behavior of the foot. The three examples of the robot foot shown in the figure have identical behavior, although their geometries are very different, [51].

$$\left(\sum_{i=2}^n OF \times m_i (a_i - g) - OF \times m_1 g \right)_t = \left(-OG_1 \times m_1 g + \sum_{i=2}^n \dot{H}_{Gi} + \sum_{i=2}^n OG_i \times m_i (a_i - g) \right)_t \quad (3.14)$$

Carrying out the operation, we may finally obtain

$$OF_x = \frac{m_1 OG_{1y} g + \sum_{i=2}^n m_i OG_{iy} (a_{iz} + g)}{m_1 g + \sum_{i=2}^n m_i (a_{iz} + g)} - \frac{\sum_{i=2}^n m_i OG_{iz} a_{iy} + \sum_{i=2}^n \dot{H}_{Gix}}{m_1 g + \sum_{i=2}^n m_i (a_{iz} + g)} \quad (3.15)$$

$$OF_y = \frac{m_1 OG_{1x} g + \sum_{i=2}^n m_i OG_{ix} (a_{iz} + g)}{m_1 g + \sum_{i=2}^n m_i (a_{iz} + g)} - \frac{\sum_{i=2}^n m_i OG_{iz} a_{ix} + \sum_{i=2}^n \dot{H}_{Giy}}{m_1 g + \sum_{i=2}^n m_i (a_{iz} + g)} \quad (3.16)$$

Properties of the FRI Point

Some useful properties of the FRI point which may be exploited in gait planning include the following:

1. The FRI point indicates the “occurrence” of foot rotation, as already described.
2. The location of the FRI point indicates the “magnitude” of the unbalanced moment on the foot. The total moment M_A^I due to the impressed forces about a point A on the support-polygon boundary (Fig. 3.18, right) is

$$M_A^I = AF \times (m_1 g - R_1) \quad (3.17)$$

which is proportional to the distance between A and F. If F is situated inside the support polygon, M_A^I is counteracted by the moment due to R and is precisely compensated; see Figure 3.21 (left) for a planar example. Otherwise, M_A^I is the uncompensated moment that causes the foot to rotate; see Figure 3.21 (right).

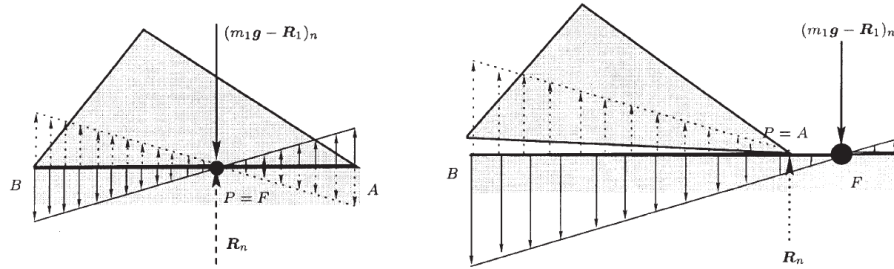


Figure 3.21: The magnitude of the moment experienced by a point on the support boundary is linearly proportional to the distance of this point from the FRI point. The magnitudes of the moments at different points are shown by the length of the arrows. Clockwise (i.e., negative) moments are shown by upward-pointing arrows, and counterclockwise (i.e., positive) moments are shown by downward-pointing arrows. In the image, of the left the moments are precisely compensated, whereas in the image on the right they are not. The subscript n denotes the normal component of a force, © A. Goswami, [51].

3. The FRI point indicates the “direction” of foot rotation. This we derive from eq. 3.17, assuming that $m_1g - R_1$ is directed downward.
4. The FRI point indicates the “stability margin” of the robot. The stability margin of a robot against foot rotation may be quantified by the minimum distance of the support-polygon boundary from the current location of the FRI point within the footprint. Conversely, when the FRI point is outside the footprint, this minimum distance is a measure of instability of the robot. An imminent foot rotation will be indicated by a motion of the FRI point toward the support-polygon boundary.

3.2.3 Universal stability criterion of the foot contact of legged robots: Contact Wrench Cone (CWC)

In this section, Dr. Hirukawa and coworkers of the AIST outline a universal stability criterion of the foot contact of legged robots [56], as following: the proposed method checks whether the sum of the gravity and the inertia wrench applied to the COG of the robot, which is proposed to be the stability criterion, is inside the polyhedral convex cone of the contact wrench between the feet of a robot and its environment, (see Fig. 3.22). The criterion can be used to determine the strong stability of the foot contact when a robot walks on an arbitrary terrain and/or when the hands of the robot are in contact with it under the sufficient friction assumption. The determination is equivalent to check whether the ZMP is inside the support polygon of the feet when the robot walks on a horizontal plane with sufficient friction. The criterion can also be used to determine whether the foot contact is sufficiently weakly stable when the friction follows a physical law. Therefore, the proposed criterion can be used to judge what the ZMP can do, and it can be used in more universal cases.

Stability Criterion of the foot contact

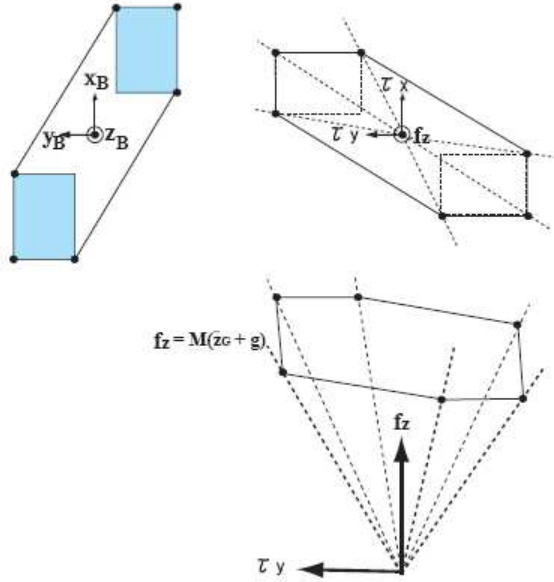


Figure 3.22: Support polygon and an intersection of the polyhedral convex cone
©Hirukawa et. al., [56].

1. Definitions

(a) Coordinates:

Figure 3.23 illustrates a legged robot whose hands may be in contact with the environment. Let \sum_R be the reference frame, \sum_B a frame fixed to the waist of the robot, and \sum_{Li} a frame fixed to the COG of the i -th link of the robot ($i = 1, \dots, N$).

Let $p_{Li} (= [x_{Li} \ y_{Li} \ z_{Li}]^T)$ be the origin \sum_{Li} and $p_B (= [x_B \ y_B \ z_B]^T)$ that of \sum_B with respect to \sum_R . In the following, the position vectors are represented with respect to \sum_R unless otherwise specified. Let p_k ($k = 1, \dots, K$) be the vertices of the support polygons of the hands and feet, and $p_G (= [x_G \ y_G \ z_G]^T)$ the position of the COG of the robot. $p_G = \sum_{i=1}^N m_i p_{Li} / \sum_{i=1}^N m_i$, where m_i is the mass of the i -th link.

Let f_k be the force applied to the robot at p_k , and n_k the unit normal vector at p_k pointed to the robot. I_i and ω_i denote the inertia tensor and the angular velocity of the i -th link with respect to \sum_R respectively.

(b) Gravity and the force of inertia and torque on the robot:

Let the sum of the gravity and the force of inertia applied to the robot be f_G and the sum of the moments about the COG of the robot τ_G with respect to \sum_R , which can be given by

$$f_G = M(g - \ddot{p}_G) \quad (3.18)$$

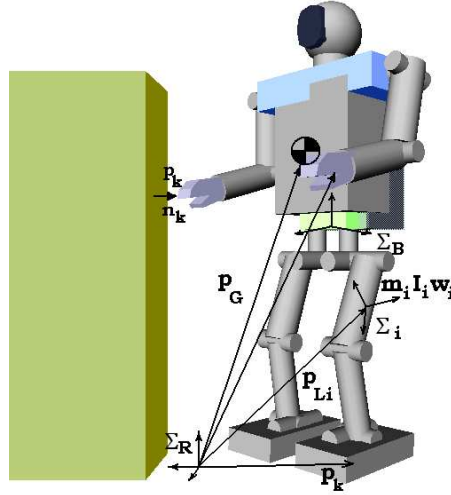


Figure 3.23: Model of the system, [56].

$$\tau_G = p_G \times M(g - \ddot{p}_G) - \dot{L} \quad (3.19)$$

where $M = \sum_{i=1}^N m_i$ is the total mass of the robot, $g = [0 \ 0 \ -g]^T$ the gravity vector, and $L = [L_x \ L_y \ L_z]^T$ the angular momentum of the robot with respect to the COG defined by

$$L = \sum_{i=1}^N \{m_i (p_{Li} - p_G) \times \dot{p}_{Li} + I_i \omega_i\} \quad (3.20)$$

- (c) Set of the contact force and torque from the environment:

Let f_C be the contact force which can be applied from the environment to the robot with respect to Σ_R and τ_C the corresponding moment. The set of (f_C, τ_C) can be given by

$$f_C = \sum_{k=1}^N \sum_{l=1}^L \epsilon_k^l (n_k + \mu_k t_k^l) \quad (3.21)$$

$$\tau_C = \sum_{k=1}^N \sum_{l=1}^L \epsilon_k^l p_k \times (n_k + \mu_k t_k^l) \quad (3.22)$$

where the friction cone at p_k is approximated by an L-polyhedral cone, t_k^l is a unit tangent vector to make $n_k + \mu_k t_k^l$ be the l -th edge of the polyhedral cone, μ_k the friction coefficient at p_k , and ϵ_k^l a nonnegative scalar. ϵ_k^l gives the magnitude of the force of the l -th edge of the approximated friction cone at the k -th contact point.

The set of (f_C, τ_C) forms a polyhedral convex cone in the space of the contact force and torque, and is called *a polyhedral convex cone of the contact wrench here*.

- (d) Strong stability and weak stability: The definitions of strong stability and weak stability can be applied to our problem as follows.

Definition 1: The contact between the robot and the environment is *strongly stable* when it is guaranteed that the contact is stable to (f_G, τ_G) . The contact is *weakly stable* when it is possible that the contact is stable to (f_G, τ_G) . The contact is *strongly unstable* when it is not weakly stable.

Strong stability cannot always be determined since the contact force is indeterminate in general. The contact is always weakly stable in our problem when the motion of the robot is feasible as we discuss in the following.

2. Strong stability determination

Let us assume that sufficient friction exists at the contact. The assumption implies that an arbitrary friction force can be generated at every contact point independent of the normal force at the point, and it can be written by

$$f_C = \sum_{k=1}^K \left(\epsilon_k^0 n_k + \sum_{l=1}^4 \epsilon_k^l t_k^l \right) \quad (3.23)$$

$$\tau_C = \sum_{k=1}^K p_k \times \left(\epsilon_k^0 n_k + \sum_{l=1}^4 \epsilon_k^l t_k^l \right) \quad (3.24)$$

where $t_k^l (l = 1, \dots, 4)$ are the unit tangent vectors at p_k whose nonnegative linear combination spans the tangent plane.

Example: (Biped robot walking on a horizontal plane with sufficient friction) Let us consider the case in which a biped robot walks on a horizontal plane as shown in Fig. 3.24. Then the horizontal elements of f_G and τ_G about z-axis

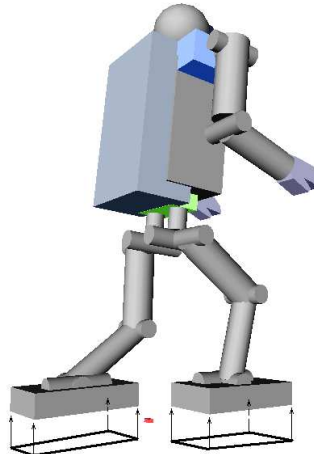


Figure 3.24: Two feet on a horizontal plane, [56].

should always balance with the contact force and torque as

$$M\ddot{x}_G = \sum_{k=1}^K (\epsilon_k^1 - \epsilon_k^2) \quad (3.25)$$

$$M\ddot{y}_G = \sum_{k=1}^K (\epsilon_k^3 - \epsilon_k^4) \quad (3.26)$$

$$Mx_G\ddot{y}_G - My_G\ddot{x}_G + \dot{L}_z = \sum_{k=1}^K \{ (\epsilon_k^3 - \epsilon_k^4) x_k - (\epsilon_k^1 - \epsilon_k^2) y_k \} \quad (3.27)$$

The polyhedral convex cone of the contact wrench is the direct product of the linear subspace given by the right-hand side of Eqs. 3.25, 3.26 and 3.27 and a polyhedral convex cone in the complement of the subspace, and therefore strong stability can be determined by checking if (f_G, τ_G) is inside the polyhedral convex cone in the complement subspace. The relationship in the complement subspace can be written by

$$M(\ddot{z}_G + g) = \sum_{k=1}^K \epsilon_k^0 \quad (3.28)$$

$$M(\ddot{z}_G + g)y_G - M\ddot{y}_G z_G + \dot{L}_x = \sum_{k=1}^K \epsilon_k^0 y_k - z_0 \sum_{k=1}^K (\epsilon_k^3 - \epsilon_k^4) \quad (3.29)$$

$$-M(\ddot{z}_G + g)x_G - M\ddot{x}_G z_G + \dot{L}_y = - \sum_{k=1}^K \epsilon_k^0 x_k - z_0 \sum_{k=1}^K (\epsilon_k^1 - \epsilon_k^2) \quad (3.30)$$

where z_0 is the height of the horizontal floor. Note that the second terms of the right-hand sides in Eqs. 3.29 and 3.30 are independent of the positions of the contact points, since the z coordinate of all the contact points is z_0 . Then we can set $z_0 = 0$ without loss of the generality, and we obtain

$$M(\ddot{z}_G + g)y_G - M\ddot{y}_G z_G + \dot{L}_x = \sum_{k=1}^K \epsilon_k^0 y_k \quad (3.31)$$

$$-M(\ddot{z}_G + g)x_G - M\ddot{x}_G z_G + \dot{L}_y = - \sum_{k=1}^K \epsilon_k^0 x_k \quad (3.32)$$

From Eqs. 3.28, 3.31 and 3.32, $(-f_G, -\tau_G)$ is an internal element of the polyhedral convex cone of the contact wrench given by Eqs. 3.21 and 3.22 if Eqs. 3.31 and 3.32 hold for at least three of positive ϵ_k^0 , and then the contact is strongly stable from Theorem 1.

Fig. 3.22 illustrates the support polygon of the robot and the corresponding intersection of the polyhedral convex cone given by the right-hand sides of Eqs. 3.21, 3.31 and 3.32 with plane $f_z = M(\ddot{z}_G + g)$. The set of $((\tau_C)_x, (\tau_C)_y)$ is the dual polygon of the support polygon, since x_k and y_k are exchanged in the right-hand sides of Eqs. 3.31 and 3.32 with the minus sign in Eq. 3.32.

Let us consider the same contact stability using the ZMP. The ZMP = (x_0, y_0) can be given by

$$\begin{aligned} x_0 &= \frac{Mx_G(\ddot{z}_G+g)-M(z_G-z_0)\ddot{x}_G-\dot{L}_y}{M(\ddot{z}_G+g)} \\ y_0 &= \frac{My_G(\ddot{z}_G+g)-M(z_G-z_0)\ddot{y}_G+\dot{L}_x}{M(\ddot{z}_G+g)} \end{aligned} \quad (3.33)$$

The ZMP is an internal point of the support polygon of the feet if

$$\begin{aligned} x_0 &= \sum_{k=1}^K \lambda_k x_k \\ y_0 &= \sum_{k=1}^K \lambda_k y_k \end{aligned} \quad (3.34)$$

$$\sum_{k=1}^K \lambda_k = 1, \lambda_k \geq 0 \quad (3.35)$$

and at least three of λ_k are positive. Let $z_0 = 0$, and from Eqs. 3.33, 3.34 we obtain

$$\begin{aligned} \frac{Mx_G(\ddot{z}_G+g)-M(z_G-z_0)\ddot{x}_G-\dot{L}_y}{M(\ddot{z}_G+g)} &= \sum_{k=1}^K \lambda_k x_k \\ \frac{My_G(\ddot{z}_G+g)-M(z_G-z_0)\ddot{y}_G+\dot{L}_x}{M(\ddot{z}_G+g)} &= \sum_{k=1}^K \lambda_k y_k \end{aligned} \quad (3.36)$$

Now we can prove that the proposed criterion is equivalent to the ZMP in the case of Example 1. Let $\epsilon = \sum_{k=1}^K \epsilon_k^0$.

Substituting Eq. 3.28 into Eqs. 3.31 and 3.32, we get

$$\begin{aligned} \frac{Mx_G(\ddot{z}_G+g)-Mz_G\ddot{x}_G-\dot{L}_y}{M(\ddot{z}_G+g)} &= \sum_{k=1}^K \frac{\epsilon_k^0}{\epsilon} x_k \\ \frac{My_G(\ddot{z}_G+g)-Mz_G\ddot{y}_G+\dot{L}_x}{M(\ddot{z}_G+g)} &= \sum_{k=1}^K \frac{\epsilon_k^0}{\epsilon} y_k \end{aligned} \quad (3.37)$$

It is trivial that Eq. 3.37 should be identical with Eq. 3.36, since $\sum_{k=1}^K \epsilon_k^0 = 1$. This proved that the proposed criterion is equivalent to the ZMP when a legged robot walks on a horizontal plane with sufficient friction.

The proposed criterion is more universal than the ZMP as described below. A question is whether the criterion has any merit or demerit compared to the ZMP in the specific case of example 1. The proposed criterion does not need the division to find the ZMP in Eq. 3.33 and therefore its computation is more numerically stable especially when the vertical

contact force is small. The trajectory of the ZMP can be plotted more comprehensively since it is a point on a plane. The proposed criterion should require an intersection plane of f_z to be plotted on a plane. See Fig. 3.22.

3.2.4 Comparison between the biped locomotion stability criteria

There were outlined three locomotion stability criteria in the previous sections, since the classical ZMP criterion to the current CWC one. In order to improve the biped locomotion of humanoid robots at uneven environment, the research is focused on strong stability criteria. The next table (3.2) summarize stability capabilities of the criteria.

	ZMP/FRI	CWC
Flat plane Foot contact Sufficient friction	Strong Stability	Strong Stability
Arbitrary terrain Hand/Foot contact Sufficient friction	N/A	Strong Stability

Table 3.2: ZMP/FRI vs. CWC

It is conclude that the “CWC” is the strongest stability criteria at least in theory, and it is better for critical cases at uneven terrain with or without multi-contact points (for example: two feet and one hand). In the case of humanoid walking on flat surface it is demonstrated from the last thirty years, that the ZMP criterion is robust enough, theoretically and experimentally. That is our case where successful results have been obtained (see Chapter 5, Appendix A).

That is the reason for using the ZMP criterion in this research, which is focused in humanoid robot locomotion.

Conclusions

Normal bipedal gait is achieved with a complex combination of automatic and volitional postural components. Normal walking requires stability to provide anti-gravity support of body weight, mobility of body segments and motor control to sequence multiple segments while transferring body weight from one limb to another. The result is energy-efficient forward progression. Human “gait cycle” has been analyzed in order to understand biped walking motion its main phases, single support and double support phases and their properties: force reaction, cycle time, foot, knee, hip and body motion trajectories. So humanoid robot trajectories could be created on the order of the human ones. It is demonstrated that the COG human motion follows the inverted pendulum laws at normal walking velocity, which is an important fact for maintaining stability while walking. The stability criteria for obtaining stable biped walking have been outlined, especially the “Zero Moment Point (ZMP)” criterion, which is the most popular and most often applied to humanoid robots in the world. The concept of ZMP has and will have an essential role in both theoretical considerations and the practical development of humanoid robots and biped locomotion. The farther away the FRI point is from the support boundary, the larger the unbalanced moment on the foot, and the greater is the instability. The distance between the FRI point and the nearest point on the polygon boundary is a useful indicator of the static stability margin of the foot. It is concluded that the dynamic stable “biped gait” should take into account the whole body dynamics to make any motion on any surface. It could be simplified as a single mass dynamics motion on specific cases, such as walking on a flat surface with straight arms and torso upright. Further research related to humanoid-human cooperation should be made in order to handle ordinary tasks in human environments. This research is oriented to maintaining stability with multi-contact points, on any terrain, and while carrying objects; such as the CWC, which checks if the sum of the gravity and the inertia wrench applied to the COG of the robot, is inside the polyhedral convex cone of the contact wrench between the feet of a robot and its environment. This criterion can be used to determine the strong stability of the foot contact even when a robot walks on an arbitrary terrain, other than a horizontal plane and/or when the hands of the robot are in contact with the terrain, under the assumption that sufficient friction should exist at the point of contact. That could be detailed in other works, whose are not the objective of the current one.

Chapter 4

Study of humanoid robot gaits

The superior man is modest in his speech, but exceeds in his actions.
(Confucius)

Biped robot “gait generation” is not a closed problem, there are many proposals for solving it. One of them is motion without active joints (passive walking), where the field of gravity is the force which actuates on the robot, making it walk. Passive walking starts with an impulse and the biped robot walks on a slope terrain. Many results have been obtained, but the problem with this kind of legged robots is that it is not possible to control the walking direction or stopping; it may be possible by changing the terrain slope. However, those are not suitable for human environments, and the passive bipeds can't do any task. Another proposal deals with active joints; that is all the joints have their own control. That way, a predefined pattern could be introduced, followed and corrected so that the robot walks stably in any direction, on any terrain, over any step length and perform any task (within mechanical and physical limits). The Rh-1 prototype has been developed for working in human environments; thus, it should be developed with “active walking”. Some pattern generation models such as Joint space, Virtual forces (which doesn't take into account biped dynamics), mass distributed and mass concentrated models (which take into account biped dynamics) will be outlined. Due the necessity of generating stable walking patterns in real-time, the mass concentrated models are used. As such, the Inverted pendulum and Cart-table models are detailed as suitable choices for obtaining stable and natural walking humanoid robot motion. The ZMP based criteria are taken into account to obtain stable biped walking.

4.1 Passive and active walking

In this section at first, the passive and active walking motion, of biped robots will be outlined in order to focus the framework of our research in the field of humanoid robots, that is the active walking with mass concentrated model.

4.1.1 Passive walking

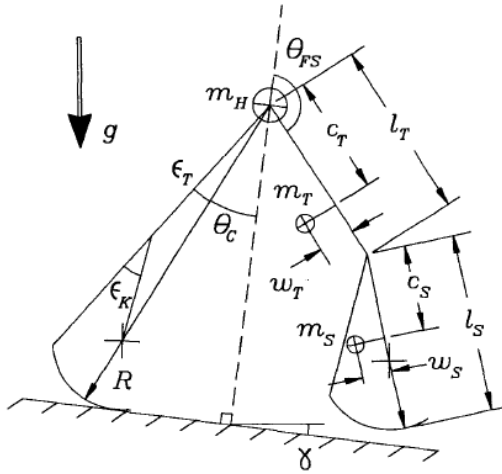


Figure 4.1: A chain of four rigid, inanimate links will walk by themselves down a shallow incline, ©T. McGeer, [84].

Some authors call it cyclic walking. These theories uses the potential field of gravity to produce walking. Normally, it is implemented on underactuated and semi underactuated legged robots.

One approach that was first pioneered by McGeer resembles the kind of mechanical solution found in walking toys. He demonstrated that a four bar mechanism in the shape of the skeleton of the lower half of the human body could walk unaided down a slight incline. As long as the lengths and masses of the various components were correctly tuned, a simple pendulum motion is enough to produce very fluid and human-like walking. Curved feet complete the control by self-correcting for any mild perturbations.

This approach is now known as McGeer's theory of passive dynamic bipedal locomotion, where the gait is simply a 'natural repetitive motion of a dynamical system'. The advantage of this system is that it consumes minimal energy and requires no computer control for normal walking on a flat surface. The disadvantage of the plain skeleton is that it is good for nothing else. As is so often the case in robotics, what is needed is a way of reconciling both a passive and a dynamic aspect to the same system.

Passive dynamic walking, a phenomenon originally described for bipeds having straight legs, also works with knees. Thus given only a downhill slope as a source of energy, a human-like pair of legs will settle into a natural gait generated by passive interaction of gravity and inertia. No muscular input is required. The physics is much the same as in straight-legged walking, but the knee-jointed

form has two advantages (i.e. Fig. 4.1). First, it offers a simple solution to the problem of foot clearance during the recovery phase. Second, in some cases it is more stable [84].



Figure 4.2: Active biped walking.

4.1.2 Active walking

When each joint is actuated by a motor and a servo-driver, the walking motion is called active. One of the main differences between passive and active walking is that the swing leg does not fall on landing motion, that way the impact force is reduced considerably, so stable motion is obtained. The Rh-1 walking motion is developed under these theories.

For generating active walking motion of biped robots, suitable patterns should be developed taking into account the dynamics and stability during the step. In order to generate the motion patterns, many models will be used such as the mass distributed model and the mass concentrated model; some cases of both of them will be described in the following sections.

The well-known mass concentrated model based on the “Inverted pendulum” and the “Cart-table”, will be described at length, because both models have been successfully used on the Rh-1 humanoid robot to obtain stable walking motion. The first method is based on the motion of a free ball on a plane in space which follows the inverted pendulum laws; similar performance is observed in human COG motion during the act of walking. This motion drives the humanoid COG in order to get a smooth, natural and stable walking motion. The second method deals with controlling of a cart motion on a flat table by optimizing its jerk. The performance is similar to the inverted pendulum motion, but this method reflects the dynamics of non-linearity during the act of walking. Furthermore, the ZMP reference pattern could be estimated in advance.

In the active walking motion, the reference patterns are the COG and the swing foot patterns, which are the spatial and the orientation trajectories at

the local axis. After that, the inverse kinematics must be computed based on the reference patterns in order to obtain the joint trajectories, which are the humanoid joint reference patterns. Furthermore, some models use the ZMP (Kawada-AIST robots, [70]), joint torque (Johnnie, [80]) and reaction force from the surface references as input for the humanoid control system (Honda robots [53]).

Active walking motion is still an open area of research, and many proposals have been made, some of them at simulation level and others on humanoid robot platforms of any size, (from toy scale to human-size scale). Successful results have been obtained mainly in Japanese research centers and universities.

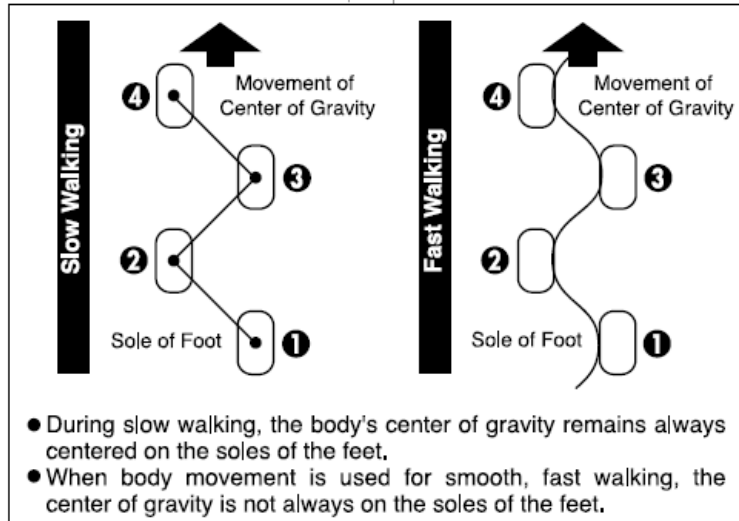


Figure 4.3: Static and dynamic gait, [10].

4.2 Static and dynamic gait

When the walking motion is done at a slow speed, the gait is called “static gait”, when the walking motion is made at current human walking or higher speeds, the gait is called “dynamic gait”. (Fig. 4.3)

4.2.1 Static gait

The center of mass must be inside the support foot while the robot is taking a step. It is called slow walking.

In static gait, the whole body dynamics of the humanoid robot does not help the stability during the walking motion, because the COG must always stay close to the middle of the support polygon (SP). Therefore, the motion of the COG on the frontal plane is increased considerably compared to the normal walking motion and static torques (due to gravity) have a stronger effect during the act of walking compared to dynamic torques (due to the inertia). In this case, the joint evolution is easily computed between the range limits to create a step with low order polynomials. In some cases, it is not necessary to compute

the inverse kinematics, so it is possible to work at the joint space level. This kind of gait is commonly used on humanoid robots of reduced scale (height < 0.50m), which move many times with pre-planned patterns without whole body control, because the inertial and structural effects do not cause considerable disturbances during motion. In this case, the ZMP is almost the same as the COG projection on the walking surface.

4.2.2 Dynamic gait

The center of mass should not be inside the support foot while the robot is taking a step, but the ZMP must be inside. It is called fast walking.

When the motion is faster, the COG could be closer or outside the boundary of the SP, thus it is human-like motion. Smooth patterns must be generated in order to reduce the inertial effects, which are higher with respect to the static gait. Paradoxically, the inertial effects help to maintain biped stability during the step, because the COG acceleration locates the ZMP closer to the middle of the SP. In this case, the COG acceleration must be controlled so that the ZMP does not overcome the SP. Some techniques reduce the jerk with high-order polynomials, but the disadvantage of high computation time doesn't allow real-time applications of gait generation, so the gait is pre-planned and the on-line biped control cancel the external disturbance. Other techniques optimize the jerk, which reduces the computation time and it is possible to develop real-time walking patterns. The on-line control reduces external disturbances, such as gravity, terrain and structural imperfections.

In this research, as explained in the previous section, the dynamic gait generation methods are focused on the “inverted pendulum” and the “cart-table” models (Kajita et. al., [64], [63]). Those models allow the COG to generate smooth and natural motion patterns by concentrating the overall humanoid robot mass on this point. The next chapter will detail the proposed walking pattern generation method which includes the “Local Axis Gait” algorithm (Arbulu et. al. [12]), when the local motion planning of the COG is computed by the previous models.

Currently, the more advanced and human-size humanoid robots have implemented “Dynamic gait” algorithms, after many years of arduous research. (i.e., WABIAN R2, ASIMO, HRP-2)

The reliability of the dynamic gait was demonstrated and it is a challenge for humanoid robot research.

4.3 Gait generation models

Many generation gait models have been proposed to obtain a walking motion. When the height of a humanoid robot is under 0.50m, the joint space method could be used, because normally it is possible to do a trial and error on the actual humanoid. Furthermore, the walking speed is not so high and the dynamics effects are not so critical as for a human-size humanoid robot. However, the initial tests on human-size humanoid robots could be approached with this method.

Another kind of gait generation model is the mass distributed model, which takes into account the whole or partial body inertia and masses of the humanoid

robot. In this case, the walking motion could only be generated off-line, because of the high computation time. Finally, the common well-known mass concentrated model based on the inverted pendulum, the cart-table and the fly wheel, are employed to obtain a stable walking motion in realtime.

In the following subsections, each model will be detailed. This research is based on the mass concentrated model.

4.3.1 Joint space method

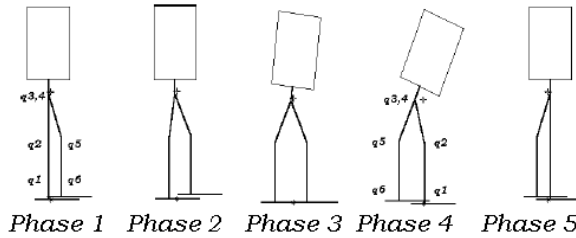


Figure 4.4: Five steps phases, [42].

This method consists of working in the joint space to generate walking patterns. It consists of computing suitable temporal trajectories between the preset joint limits of the walking motion. For example, the LEROI biped, developed at the University Carlos III of Madrid, (De la Guia et. al. [42]), proposes a simple way to calculate the temporary evolution of the joint angles of biped robot. It is based on the division of the robot step into five phases. In Fig. 4.4, the disposition of the robot in each of the mentioned phases is shown. To be able to solve the joint patterns of each phase, we need only three parameters: the desired length of the step (L), the desired speed of the step (ω) and the type of movement (walking on flat a surface or going up stairs). From these three parameters the developed software derives the trajectories of each robots joints by means of a simple geometric calculation consisting of obtaining initial and final angles of each joint for every phase.

For example, the joint motion interpolators for obtaining a walking motion for phases 1, 2 and 3 could be computed as follows:

$$\phi = \frac{a}{2} \cdot t^2 \dots \text{acceleration...zone...} (0 \leq t \leq \tau) \quad (4.1)$$

$$\phi = -\frac{a}{2} \cdot t^2 + a \cdot T \cdot t - \frac{a}{2} \cdot T^2 + \frac{\theta}{2} \dots \text{deceleration...zone...} (\tau \leq t \leq T) \quad (4.2)$$

When the joint patterns are:

$$q_4 = \phi, q_5 = -\phi \dots \text{(phase...1)} \quad (4.3)$$

$$q_2 = -\phi, q_3 = \phi \dots \text{(phase...2)} \quad (4.4)$$

$$q_3 = \frac{\theta}{2} - \phi, q_4 = \frac{\theta}{2} + \phi \dots \text{(phase...3)} \quad (4.5)$$

From the boundary conditions:

$$a = \frac{\theta}{2\tau^2}, \dots \tau = \frac{T}{2} \dots \text{and...} T = 2\sqrt{\frac{\theta}{2a}} = f(\omega) \quad (4.6)$$

4.3.2 Virtual forces model

Proposed by Jerry Pratt and co-workers, (from the Leg lab of MIT, [97]) the virtual forces model is an intuitive biped walking motion control based on the force reaction by joint torque control, which is applied to a biped planar robot (see Fig. 4.5). Virtual model control is a motion control framework that uses virtual components to create virtual forces generated when the virtual components interact with a robot system. An algorithm based on the virtual model control framework is applied to a physical planar bipedal robot. It uses a simple set of virtual components that allows the robot to walk successfully over level terrain. This model also describes how the algorithm can be augmented for rough terrain walking based on geometric consideration. The resulting algorithm is very simple and does not require the biped to have an extensive sensory system. The robot does not know the slope gradients and transition locations in advance.

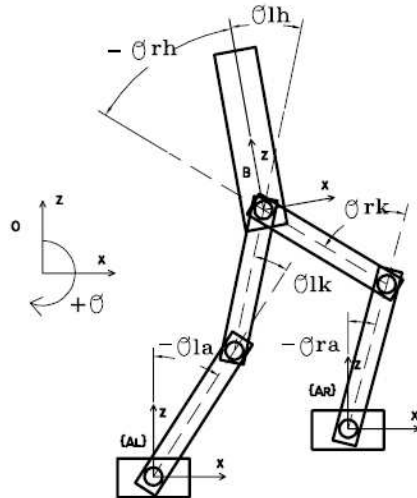


Figure 4.5: Dual-leg example. Reaction frames A_l and A_r are assumed to be in the same orientation as reference frame O so that $\overset{O}{A}_l R = \overset{O}{A}_r R = I$. ©Pratt et al. [97]

The ground is detected using foot contact switches. Using the algorithm, it has successfully compelled a simulated seven-link planar biped to walk blindly up and down slopes and over rolling terrain. Only successful planar results have been detailed.

The control equations during the walking motion have the “Virtual Forces” as input (F_l and F_r , on left and right feet) and “Leg joint torques” (τ_l and τ_r , on the left and right legs) as output, which are detailed as following:

$$\begin{bmatrix} \vec{\tau}_l \\ \vec{\tau}_r \end{bmatrix} = \begin{bmatrix} \frac{A_l}{B} J^T & 0 \\ 0 & \frac{A_r}{B} J^T \end{bmatrix} \begin{bmatrix} \vec{F}_l \\ \vec{F}_r \end{bmatrix} \quad (4.7)$$

By developing the equation 4.7:

$$\begin{bmatrix} \tau_{lk} \\ \tau_{lh} \\ \tau_{rk} \\ \tau_{rh} \end{bmatrix} = \begin{bmatrix} \frac{CV}{E} & \frac{DV}{E} & -\frac{V+QD+RC}{2E} - \frac{1}{2} \\ 0 & 0 & -\frac{1}{2} \\ -\frac{AW}{E} & -\frac{BW}{E} & \frac{W+SB-TA}{2E} - \frac{1}{2} \\ 0 & 0 & -\frac{1}{2} \end{bmatrix} \begin{bmatrix} f_x \\ f_z \\ f_\theta \end{bmatrix} \quad (4.8)$$

And each matrix value (eq. 4.8) is described as:

$$\begin{aligned} A &= -L_1 \sin(\theta_{la}) - L_2 \cos(\theta_{la} + \theta_{lk}) \\ B &= -L_1 \sin(\theta_{la}) - L_2 \sin(\theta_{la} + \theta_{lk}) \\ C &= -L_1 \cos(\theta_{ra}) - L_2 \cos(\theta_{ra} + \theta_{rk}) \\ D &= -L_1 \sin(\theta_{ra}) - L_2 \sin(\theta_{ra} + \theta_{rk}) \\ Q &= -L_2 \cos(\theta_{la} + \theta_{lk}), R = -L_2 \sin(\theta_{la} + \theta_{lk}) \\ S &= -L_2 \cos(\theta_{ra} + \theta_{rk}), T = -L_2 \sin(\theta_{ra} + \theta_{rk}) \\ E &= CB - AD \\ V &= -L_1 L_2 \sin(\theta_{lk}) \\ W &= -L_1 L_2 \sin(\theta_{rk}) \end{aligned}$$

It is stressed here that the natural dynamics of the robot is augmented with simple virtual components rather than by attempting to cancel the natural dynamics. In no case linear dynamics is assumed. The extension of this algorithm to 3D biped walking will be useful for increasing the motion in any direction and for other abilities.

4.3.3 Mass distributed models

Mass distributed models have many approaches such as whole-body motion while the robot is walking (Hirohisa et. al. [57]), taking into account as strong stability criteria that the sum of contact wrench should be inside the contact wrench cone; it is a more accurate model but the high computation cost and the iterative solution does not make it possible for the patterns to be generated in real time. Successful simulation experiments have been shown but no natural motion is obtained. Another example is the methods proposed by Albert et. al., [9], the Two Masses Inverted Pendulum Mode (TMIPM) and the The Multiple Masses Inverted Pendulum Mode (MMIPM), which consist of simulating the performance of the biped walking motion by adding pendular motions on each biped link. It accurate modelling with more pendulums with respect to a single one is demonstrated, but no real-time walking patterns are realized due to the increased computation time. From the point of view of highly redundant robots, dividing in tasks the whole-body motion, taking into account the external forces acting on the robot, Khatib et. al. [75], Sentis et. al. [104], Mansard et. al. [82]; these works divide the whole-body motion into tasks and create a hierarchy. Thus different hypotheses are taken into account, like projecting the

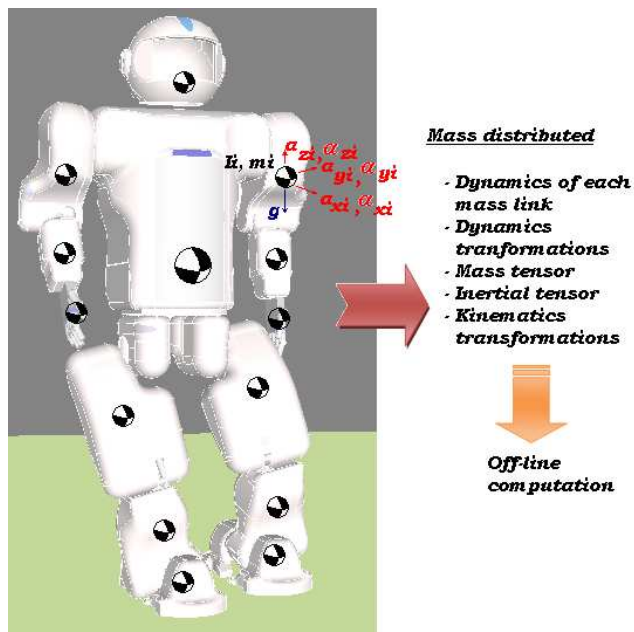


Figure 4.6: Distributed mass model. The computation cost is increased by the transformations of the whole-body dynamics model.

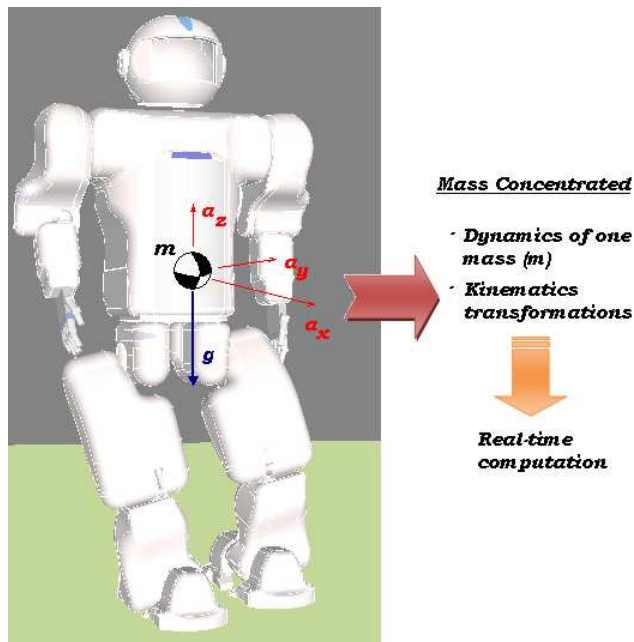


Figure 4.7: Concentrated mass model. The computations could be done in real-time.

secondary tasks into the operational space of the prior ones, and they have

achieved successful results.

Experimentally is demonstrated that, it is not necessary to obtain a walking patterns with a complex dynamic model, the complex model could be used for approaching all the inertial effects of the real robot. So the mass concentrated model is a suitable approach for computing stable walking patterns in real-time.

In order to outline the gait generation by distributed mass models, Hirukawa et. al. and Albert et. al. proposals will be described in the following sections.

4.3.4 Pattern generator of a humanoid robot, taking into account the Contact Wrench Cone (CWC)

H. Hirukawa et. al. [57], have developed a complex but accurately walking generator method taking into account the “Contact Wrench Cone” stability criteria proposed previously by them [56]. The whole body dynamics are taken into account with a multi-contact wrench. Therefore, a walking pattern generator using the CWC as the strong stability criterion, which is able to plan motion patterns of a humanoid robot that walks on an arbitrary terrain possibly with a contact between a hand and the terrain.

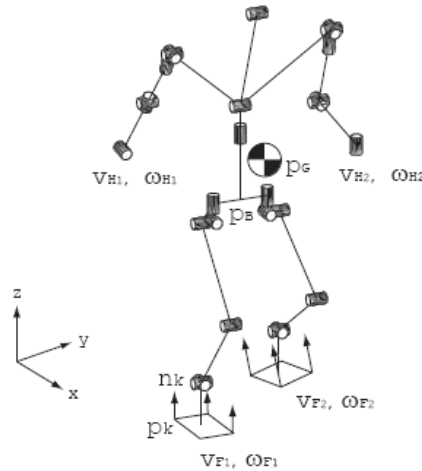


Figure 4.8: Definitions of the coordinates ©Hirukawa et. al., [57].

The main motion equations are described as follows (based on the coordinate frames of Fig. 4.8):

$$\begin{bmatrix} P \\ L \end{bmatrix} = \begin{bmatrix} ME & -M\hat{r}_{B \rightarrow G} & M_{\dot{\theta}} \\ 0 & \tilde{I} & H_{\dot{\theta}} \end{bmatrix} \begin{bmatrix} v_B \\ \omega_B \\ \dot{\theta} \end{bmatrix} \quad (4.9)$$

When:

P and L are the linear and angular momentum around the center of gravity.

p_B, v_B, ω_B are the position, velocity and the angular velocity of the coordinates on the waist link of a humanoid robot, respectively, which is supposed to

have six degrees of freedom in space with respect to the reference coordinates.

n is the number of the joints connected to the link.

$\dot{\theta}$ is the $n \times 1$ angular velocity of the joints.

M is the total mass of the robot.

E is the 3×3 unit matrix.

$r_{B \rightarrow G}$ is the position vector from the origin of the waist coordinates to the COG of the robot.

\tilde{I} is the 3×3 inertia matrix about the COG.

$M_{\dot{\theta}}$ is the $3 \times n$ inertia matrix which relates the joint velocities into the linear momentum of the robot.

$H_{\dot{\theta}}$ is the $3 \times n$ inertia matrix which relates the joint velocities into the angular momentum of the robot.

$\hat{\cdot}$ is the operator converting a 3×1 vector into a 3×3 skew-symmetric matrix whose multiplication from the left makes a vector product.

$$\dot{\theta}_{leg_i} = J_{leg_i}^{-1} \begin{bmatrix} v_{F_i} \\ \omega_{F_i} \end{bmatrix} - J_{leg_i}^{-1} \begin{bmatrix} E & -\hat{r}_{B \rightarrow F_i} \\ 0 & E \end{bmatrix} \begin{bmatrix} v_B \\ \omega_B \end{bmatrix} \quad (4.10)$$

$$\dot{\theta}_{arm_i} = J_{arm_i}^{-1} \begin{bmatrix} v_{H_i} \\ \omega_{H_i} \end{bmatrix} - J_{arm_i}^{-1} \begin{bmatrix} E & -\hat{r}_{B \rightarrow H_i} \\ 0 & E \end{bmatrix} \begin{bmatrix} v_B \\ \omega_B \end{bmatrix} \quad (4.11)$$

$$\begin{aligned} & M(\ddot{z}_G + g)(y_G - y_C) - M\ddot{y}_G(z_G - z_C) + \dot{L}_x \\ &= \sum_{k=1}^K \in_k (y_k n_{kz} - z_k n_{ky}) \equiv \tau'_{Cx} \end{aligned} \quad (4.12)$$

$$\begin{aligned} & -M(\ddot{z}_G + g)(x_G - x_C) + M\ddot{x}_G(z_G - z_C) + \dot{L}_y \\ &= -\sum_{k=1}^K \in_k (x_k n_{kz} - z_k n_{kx}) \equiv \tau'_{Cy} \end{aligned} \quad (4.13)$$

$$P_x^{ref} = M\dot{x}_G^{ref} \quad (4.14)$$

$$P_y^{ref} = M\dot{y}_G^{ref} \quad (4.15)$$

$$P_z^{ref} = M\dot{z}_G^{ref} \quad (4.16)$$

$$\xi_B = A^{-1}y \quad (4.17)$$

$$y = \begin{bmatrix} P^{ref} \\ L^{ref} \end{bmatrix} - \sum_{i=1}^2 \begin{bmatrix} M_{F_i}^* \\ H_{F_i}^* \end{bmatrix} \xi_{F_i}^{ref} - \sum_{i=1}^2 \begin{bmatrix} M_{H_i}^* \\ H_{H_i}^* \end{bmatrix} \xi_{H_i}^{ref} \quad (4.18)$$

$$A = \begin{bmatrix} M_B^* \\ H_B^* \end{bmatrix} \quad (4.19)$$

In summary a motion pattern generator of humanoid robots that walk on a flat plane, steps and a rough terrain is presented. It is guaranteed rigorously that the desired contact between a humanoid robot and terrain should be maintained by keeping the contact wrench sum between them inside the contact wrench cone under the sufficient friction assumption.

A walking pattern is generated by solving the contact wrench equations and by applying the resolved momentum control (see Fig. 4.9).

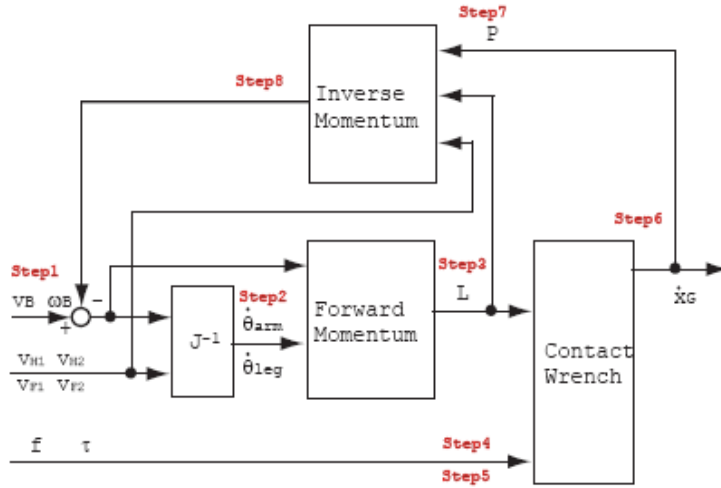


Figure 4.9: Block diagram of the pattern generator, ©Hirukawa et. al. [57].

The algorithm could be summarized in the following steps:

1. Step 1: Give $(v_{Fi}^{ref}, \omega_{Fi}^{ref})$, $(v_{Hi}^{ref}, \omega_{Hi}^{ref})$ and $(v_B^{ref}, \omega_B^{ref})$
2. Step 2: Find $(\dot{\theta}_{leg_1}^{ref}, \dot{\theta}_{leg_2}^{ref})$ by Eq. 4.10 and $(\dot{\theta}_{arm_1}^{ref}, \dot{\theta}_{arm_2}^{ref})$ by Eq. 4.11 respectively.
3. Step 3: Find L^{ref} by Eq. 4.9 and \dot{L}^{ref} by differentiation.
4. Step 4: Give \ddot{z}_G^{ref}
5. Step 5: Give λ_k^{ref}
6. Step 6: Find $\ddot{x}_G^{ref}, \ddot{y}_G^{ref}$ by solving Eqs. 4.12 and 4.13.
7. Step 7: Find P^{ref} by Eqs. 4.14, 4.15 and 4.16.
8. Step 8: Find ξ_B^{ref} by Eq. 4.17.
9. Step 9: If v_B^{ref} found in the previous step is close enough to v_B^{ref} given in the first step, go to the next ones otherwise, let v_B^{ref} be that found in the previous step and return to the first one.
10. Step 10: Find $(\dot{\theta}_{leg_1}^{ref}, \dot{\theta}_{leg_2}^{ref})$ by Eq. 4.10 and $(\dot{\theta}_{arm_1}^{ref}, \dot{\theta}_{arm_2}^{ref})$ by Eq. 4.11, and terminate the algorithm.

This algorithm proved that a strongly stable motion pattern of a humanoid robot walking on a rough terrain should exist if the friction force equations have a solution. This is the first rigorous proof that a strongly stable motion of a humanoid robot walking on a rough terrain should exist under the sufficient friction assumption if the friction force equations have a solution.

4.3.5 Two Masses Inverted Pendulum Mode (TMIPM)

From Hannover University, Albert, A. et. al., [9] developed an interesting approach for generating biped walking patterns in 2003. It is based on inverted pendulum mode, (proposed by Kajita and Tani in 1991, [67]), which has an addition of one or more pendulums, to simulate the swing leg motion. Two path planning algorithms are presented in order to increase the accuracy of the dynamic robot model, namely:

- The Two Masses Inverted Pendulum Mode (TMIPM), which consists of a robot model with two masses. One mass characterizes the torso, the second mass the swinging leg. The swing leg motion is almost arbitrary and the torso motion is calculated analytically.
- The Multiple Masses Inverted Pendulum Mode (MMIPM) is based on a model with several masses. One mass models the torso and an arbitrary number of masses is used to model the swinging leg. The foot motion of the swinging leg can be selected, e.g., in accordance to the particular situation. The remaining trajectories of the robot are then calculated iteratively.

Both methods will be outlined in order to understand the main ideas. In this sub-section the first method TMIPM will be explained and the MMIPM will be explained in the next sub-section.

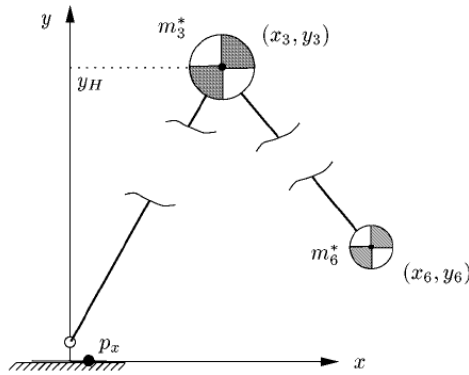


Figure 4.10: Mechanical model of the robot with two masses, where mass m_6^* represents the swinging leg and mass m_3^* represents the remaining masses of the robot ©A. Albert et. al., [57].

In order to increase the gait stability, it is desirable to develop the motion of the supporting leg (respectively torso) in respect of the dynamic reaction of the

swinging leg. For this purpose, first a system made of two masses as depicted in Figure 4.10 is considered.

The mass m_6^* represents the swinging leg and is assumed to reside at the foot of the swinging leg. The mass m_3^* represents the remaining masses of the robot and is assumed to reside at the torso.

With respect to Figure 4.10, a torque equation around the ZMP is carried out:

$$\begin{bmatrix} 0 \\ M_y \\ 0 \end{bmatrix} + \begin{bmatrix} x_3 - p_x \\ y_3 \\ 0 \end{bmatrix} \times \begin{bmatrix} 0 \\ -m_3^*g \\ 0 \end{bmatrix} + \begin{bmatrix} x_6 - p_x \\ y_6 \\ 0 \end{bmatrix} \times \begin{bmatrix} 0 \\ -m_6^*g \\ 0 \end{bmatrix} = \begin{bmatrix} x_3 - p_x \\ y_3 \\ 0 \end{bmatrix} \times \begin{bmatrix} m_3^*\ddot{x}_3 \\ m_3^*\dot{y}_3 \\ 0 \end{bmatrix} + \begin{bmatrix} x_6 - p_x \\ y_6 \\ 0 \end{bmatrix} \times \begin{bmatrix} m_6^*\ddot{x}_6 \\ m_6^*\dot{y}_6 \\ 0 \end{bmatrix} \quad (4.20)$$

The evaluation of (4.20) around the $z-axis$ (under the consideration of $y_3(t)=y_H, \dot{y}_3(t)=0$) yields

$$\begin{aligned} & \ddot{x}_3(t) - \frac{g}{y_H} (x_3(t) - p_x(t)) \\ &= \frac{m_6^*}{m_3^*y_H} ((x_6(t) - p_x(t))(\ddot{y}_6(t) + g) - \ddot{x}_6(t)y_6(t)) \end{aligned} \quad (4.21)$$

Since the foot motion of the swinging leg ($x_6(t), y_6(t)$) and the ZMP motion $p_x(t)$ are prescribed, Equation (4.21) represents an ordinary, linear, inhomogeneous differential equation for the torso motion $x_3(t)$. Theoretically, the highest gait stability is achieved for $p_x(t)=0$. For this adjustment the ZMP resides in any time instance exactly in the middle of the foot and the distance to the stability margin has a maximum value. Unfortunately, this quite restrictive constraint requires a hard discontinuity of the ZMP during the stride exchange which tends to excite oscillations. In addition, from data captured from human motion, it is known that the human foot exhibits a rolling-like motion (Dasgupta and Nakamura, 1999, [41], Gorce et al., 2001, [50]).

Thus, from the biological point of view, the adjustment $p_x(t)=0$ seems not to be very proper. Nevertheless, in the following, the ideal situation $p_x(t)=0 \forall t$ is assumed, which simplify matters but does not represent a limitation of the algorithm. Setting $p_x(t)=0$ in (4.21) leads to the differential equation

$$\ddot{x}_3(t) - \frac{g}{y_H} x_3(t) = f(t) \quad (4.22)$$

with

$$f(t) = \frac{m_6^*}{m_3^*y_H} (gx_6(t) + x_6(t)\ddot{y}_6(t) - \ddot{x}_6(t)y_6(t)) \quad (4.23)$$

The motion of the torso now depends on the trajectory of the swinging leg. The functions $x_6(t)$ and $y_6(t)$, which describe the motion of the foot of the swinging leg, are real analytic. Thus, the inhomogeneous excitation $f(t)$ on the right-hand side of Equation (4.22) itself is real analytic and the differential Equation (4.22) can be calculated with standard mathematics.

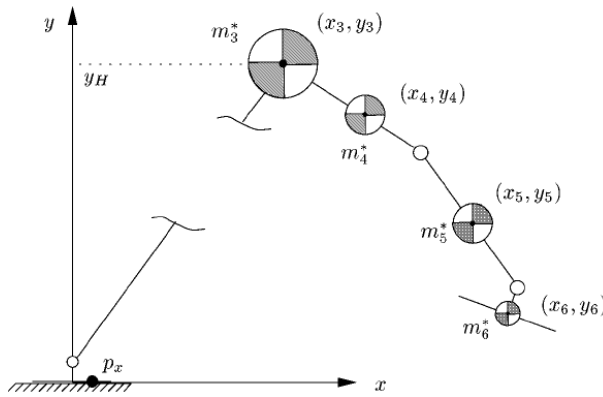


Figure 4.11: Mechanical model of the robot with multiple masses in order to respect the dynamic influence of the thigh, the shank and the foot of the swinging leg ©A. Albert et. al, [57].

4.3.6 The Multiple Masses Inverted Pendulum Mode (MMIPM)

Now the mechanical model in Figure 4.11 is considered. Here three masses are used for the modeling of the swinging leg, which is not a limitation but serves to simplify matters. Similar to the previous model (TMIPM), the inhomogeneous differential equation for the horizontal motion of the torso now becomes

$$\ddot{x}_3(t) - \frac{g}{y_H} x_3(t) = f(t) \quad (4.24)$$

When:

$$f(t) = \sum_{i=4}^k \frac{m_i^*}{m_3^*} (gx_i(t) + x_i(t)\ddot{y}_i(t) - \ddot{x}_i(t)y_i(t)) \quad (4.25)$$

A direct solution as in TMIPM is not feasible, since the individual motions of the $k - 3$ masses m_i^* now depend on each other through the kinematic linkage. Contrarily, in TMIPM, the exogenous trajectory of the swinging foot $(x_6(t), y_6(t))$ determined the inhomogeneous excitation $f(t)$ and thus the motion $x_3(t)$ of the torso mass as well. For the case of multiple masses, an iterative algorithm is used, which is sketched in 4.12. For the case of three masses (model of the swinging leg) the algorithm takes the following shape.

At first, the foot trajectory of the swinging leg $(x_6(t), y_6(t))$ is chosen and the calculation of the corresponding initial trajectory $x_3(t)$ by the TMIPM method as shown previously is carried out. Afterwards, the following iteration process is initiated:

1. Calculation of the joint trajectories $q_1(t)$ to $q_6(t)$ with the aid of the inverse kinematics (annotation: $q_1(t)$ to $q_6(t)$ represent the joint angles of the six active degrees of freedom of the robot).
2. Calculation of the trajectories of the centers of gravity $(x_4(t), y_4(t))$, $(x_5(t), y_5(t))$ and $(x_6(t), y_6(t))$ for the masses of the swinging leg by the direct kinematics.

3. Determination of the inhomogeneous excitation $f(t)$ through Equation (4.25) and generation of a set of interpolation points.
4. Interpolation with a polynomial $f^*(t)$. In contrast to what was mentioned in TMIPM, the function $f(t)$ is no longer an odd function in general. Therefore, the interpolating polynomial $f^*(t)$ has to consider all powers up to the order N :

$$f^*(t) = \sum_{i=1}^N a_i t^i \dots N \in \mathbb{N}^+ \quad (4.26)$$

5. Solution of the differential Equation (4.24) with the inhomogeneous excitation $f^*(t)$.
6. Check for terminal condition. Here the condition

$$\int_{t_B}^{t_E} (x_3^{new}(t) - x_3^{old}(t))^2 dt < e, \dots e \in \mathbb{R}^+ \quad (4.27)$$

has proven itself in experiments. The time instances t_B und t_E mark the beginning and the end of a stride. The trajectory $x_3^{new}(t)$ is the result of the current iteration and $x_3^{old}(t)$ is the trajectory of the last iteration. The iteration is stopped if both trajectories differ only marginally, i.e., the value of the integral (4.27) is below a certain limit $e \in \mathbb{R}^+$. Otherwise, the algorithm restarts on the first step with the new torso trajectory $x_3^{new}(t)$.

Throughout the experiments, a sufficient convergence appeared after three or four iterations.

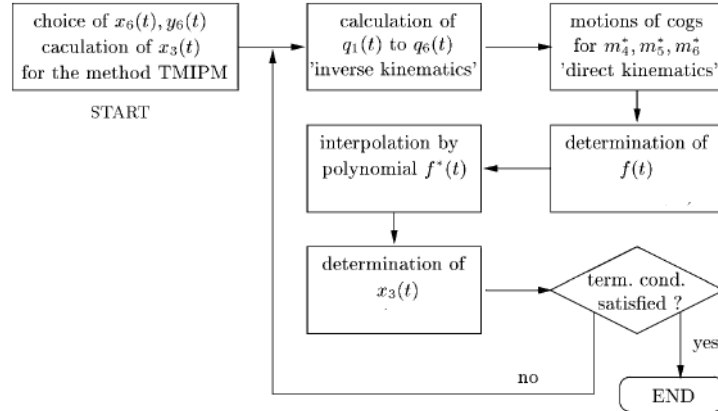


Figure 4.12: Iterative algorithm for the calculation of the torso trajectory $x_3(t)$ when using a model for the swinging leg with three concentrated masses m_4^* , m_5^* and m_6^* , © A. Albert et. al, [57]

4.3.7 Mass concentrated models

The well-known mass concentrated model simplifies the whole body dynamics to the center of gravity motion, by concentrating the whole-body mass in that point. As explained in the previous sub-sections, the mass distributed models taken into account the full or partial whole-body dynamics, so additional transformations such: dynamics of each link, dynamic transformations, mass and inertial tensors, and iterative computations increase the computation time. This computation time is not possible to operate in real-time. At this point, the mass concentrated model, which only include the dynamic motion of one mass and the kinematics computations, is the suitable model for real-time applications; that is, the walking motion could be computed in real-time, for example, the humanoid robot step length or direction could be updated, while it is walking. Furthermore, in the Appendix A is demonstrated, that the mass concentrated model could be used, for obtaining stable walking, because the human center of gravity motion looks like the inverted pendulum motion.

In the literature, there are a few approaches about the mass concentrated models, that is: the inverted pendulum model [47], [64], [80], the cart-table model [63], the flywheel model [96]. This research deals with the mass concentrated model, for generating stable walking of the humanoid robot Rh-1, which has been developed in the Roboticslab of the University Carlos III of Madrid.

Two kinds of mass concentrated models have been used for getting stable walking: the Three dimensional inverted pendulum model and the Cart-table model proposed by Kajita et. al. [64], [63]. Those models will be described in detail in the next sections.

4.3.8 The 2D Inverted pendulum model

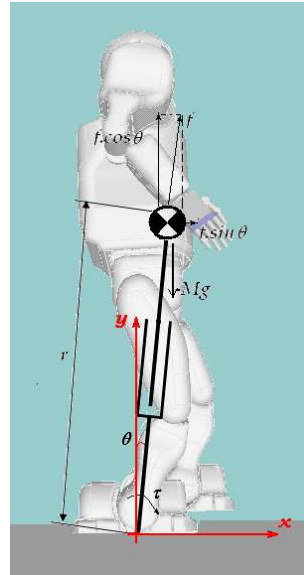


Figure 4.13: The 2D Inverted Pendulum Model with motion in x-z plane.

The gait pattern generation for a humanoid robot could be simplified as:

studying the motion in a sagittal plane and concentrating all body mass in a COG. In that way, it is possible to use the 2D Inverted pendulum model, in order to obtain stable and smooth walking motion. The 2D inverted pendulum model is composed by a mass and a telescopic leg without mass (Fig. 4.13)

The model is described in the following state variables:

r : Radius of mass position

θ : Pitch angle

f : Reaction force on pendulum base

τ : External pitch torque

From the free body diagram of the pendulum ball, the dynamics equations should be written as following:

$$F_x = f \cdot \sin \theta + \frac{\tau}{r} \cdot \cos \theta \quad (4.28)$$

$$F_z = f \cdot \cos \theta - M \cdot g - \frac{\tau}{r} \cdot \sin \theta \quad (4.29)$$

It is known that $p=(x, z)$, so the dynamics equations of pendulum ball motion are:

$$F_x = M \cdot \ddot{x} = f \cdot \sin \theta + \frac{\tau}{r} \cdot \cos \theta \quad (4.30)$$

$$F_z = M \cdot \ddot{z} = f \cdot \cos \theta - M \cdot g - \frac{\tau}{r} \cdot \sin \theta \quad (4.31)$$

There are many solutions for ball pendulum motion from this complex dynamic model. In order to simplify the dynamic problem, some constraints could be taken:

1) Motion at constraint height:

$$z = z_c \quad (4.32)$$

$$\ddot{z} = 0 \quad (4.33)$$

2) If we consider natural pendulum ball motion, the input torque turns to zero:

$$\tau = 0 \quad (4.34)$$

From these constraints the dynamic equations (4.30) and (4.31) reduce the dynamic motion to a linear one:

$$F_x = M \cdot \ddot{x} = f \cdot \sin \theta \quad (4.35)$$

$$F_z = 0 = f \cdot \cos \theta - M \cdot g \quad (4.36)$$

By combining the equations (4.35) and (4.36), the dynamic pendulum ball motion is obtained as:

$$\ddot{x} = g \cdot \frac{x}{z_c} \quad (4.37)$$

The natural motion of a pendulum ball depends on the potential gravity field (g), the position (x, z) and the level from the pendulum base (z_c). Therefore, no linear dynamic motion equations are converted to a linear one. This way, a single solution could be found and this kind of trajectory is applicable in real time applications of walking locomotion. In order to design walking patterns and to know the spatial geometry of trajectories, the orbital energy concept is introduced. The orbital energy evaluates the pendulum ball energy on a level of motion plane. It is composed by the potential and kinetic energy of pendulum ball. Therefore it is possible to know if the pendulum motion is in a state of equilibrium, going forward or never passing the zero position. The mathematical expression of orbital energy could be developed by multiplying equation (4.48) by \dot{x} and integrating it.

$$\dot{x} \left(\ddot{x} - g \frac{x}{z_c} \right) = 0 \quad (4.38)$$

$$\int \left(\ddot{x} \dot{x} - g \frac{x}{z_c} \dot{x} \right) dt = \text{constant} \quad (4.39)$$

$$\frac{1}{2} \dot{x}^2 - \frac{1}{2} \frac{g}{z_c} x^2 = E \quad (4.40)$$

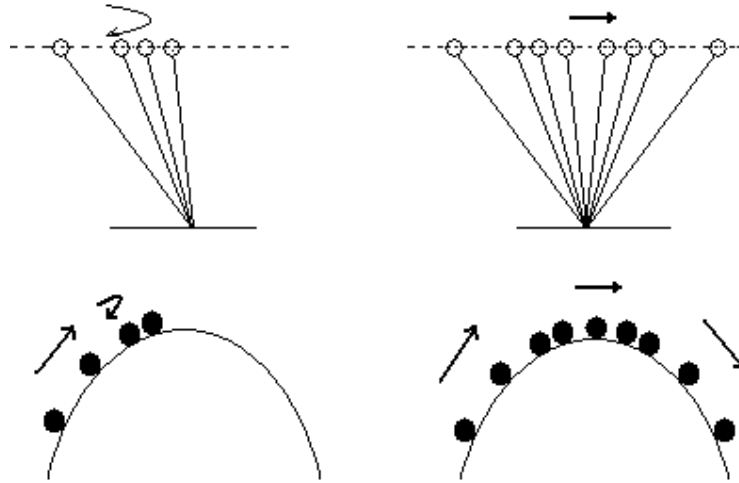


Figure 4.14: Pendulum ball rolling in potentials.

Equation (4.40) shows that a kind of energy is conserved and it is called *orbital energy*. The first term represents the kinetic energy per unit mass of the body, the second one is the virtual energy caused by a force field that generates a force " $(g/z_c)x$ " on the unit mass located at x . Furthermore (Fig. 4.14), $E>0$ means that the pendulum mass swings forward; $E=0$ represents the equilibrium state, the pendulum mass swing toward the equilibrium point or the pendulum mass swing out of the equilibrium point. Finally, $E<0$ means that the body never passes the point $x=0$.

At this point, it is possible to generate two-dimensional stable and natural walking patterns. This study is the basis for reaching the solution of three dimensional walking patterns, suitable in any humanoid robot. A human-like walking motion could be obtained, because biomechanical studies demonstrate that human COG motion in a walking cycle could approach an inverted pendulum motion [125]. The next section focused on the three-dimensional pendulum motion.

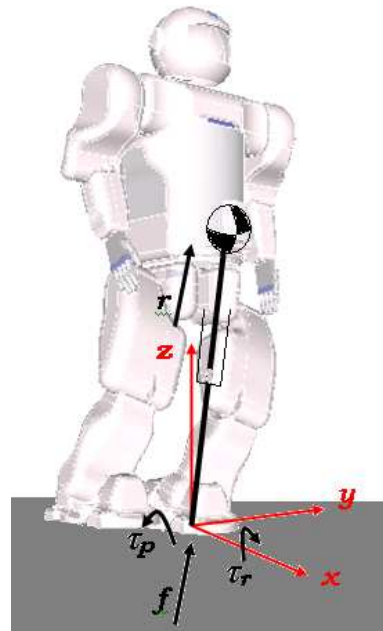


Figure 4.15: Three-dimensional Inverted Pendulum Model.

4.3.9 Laws of motion of a 3D Inverted pendulum model

In this sub-section, the inverted pendulum model will be expanded to three dimensions, because the humanoid robot motion will move in human environments. So, it is necessary to introduce the motion in the frontal plane. Furthermore, the frontal motion contributes to the humanoid robot stability while it is walking; that is, the frontal motion changes the ZMP to the support polygon during the single support phase.

Thus the 3D-LIPM makes a model of the humanoid robot COG motion, by the computation of a smooth trajectory of a single mass, which follows the inverted pendulum laws under the gravity field; the constraint is to maintain the ZMP on the support polygon during walking, in order to avoid the humanoid fall down.

Inverted Pendulum Model

In Fig. (4.15), the three-dimensional Inverted pendulum model consists of a point mass (p) and a massless telescopic leg. Let the position of the mass M : $p=(x,y,z)$. It is uniquely specified by variables $q = (\theta_r, \theta_p, r)$, so:

$$x = r \cdot \sin(\theta_p) \quad (4.41)$$

$$y = -r \cdot \sin(\theta_r) \quad (4.42)$$

$$z = r \cdot \sqrt{1 - \sin(\theta_r)^2 - \sin(\theta_p)^2} \quad (4.43)$$

The motion equation of the inverted pendulum in Cartesian coordinates is:

$$\begin{pmatrix} \tau_r \\ \tau_p \\ f \end{pmatrix} = m \begin{pmatrix} 0 & -r \cdot \cos(\theta_r) & -\frac{r \cdot \cos(\theta_r) \cdot \sin(\theta_r)}{\sqrt{1 - \sin(\theta_r)^2 - \sin(\theta_p)^2}} \\ r \cdot \cos(\theta_p) & 0 & -\frac{r \cdot \cos(\theta_p) \cdot \sin(\theta_p)}{\sqrt{1 - \sin(\theta_r)^2 - \sin(\theta_p)^2}} \\ \sin(\theta_p) & -\sin(\theta_r) & \sqrt{1 - \sin(\theta_r)^2 - \sin(\theta_p)^2} \end{pmatrix} \begin{pmatrix} \ddot{x} \\ \ddot{y} \\ \ddot{z} \end{pmatrix} + mg \begin{pmatrix} -\frac{r \cdot \cos(\theta_r) \cdot \sin(\theta_r)}{\sqrt{1 - \sin(\theta_r)^2 - \sin(\theta_p)^2}} \\ -\frac{r \cdot \cos(\theta_p) \cdot \sin(\theta_p)}{\sqrt{1 - \sin(\theta_r)^2 - \sin(\theta_p)^2}} \\ \sqrt{1 - \sin(\theta_r)^2 - \sin(\theta_p)^2} \end{pmatrix} \quad (4.44)$$

The dynamics along the x-axis is given:

$$m(z\ddot{x} - x\ddot{z}) = \frac{\sqrt{1 - \sin(\theta_r)^2 - \sin(\theta_p)^2}}{\cos(\theta_p)} \tau_p + mgx \quad (4.45)$$

And the equation for the dynamics along the y-axis is given:

$$m(-z\ddot{y} + y\ddot{z}) = \frac{\sqrt{1 - \sin(\theta_r)^2 - \sin(\theta_p)^2}}{\cos(\theta_r)} \tau_r - mgy \quad (4.46)$$

Natural three-dimensional Linear Inverted Pendulum Model

In order to reduce the motion possibilities of the pendulum, we introduce some constraints to limit this motion. One constraint limits the motion in a plane, so:

$$z = k_x x + k_y y + z_c \quad (4.47)$$

Where z_c is the distance from the xy -plane to the pendulum mass. Replacing (4.47) and its second derivative into (4.45) and (4.46), we get:

$$\ddot{x} = \frac{g}{z_c} x + \frac{k_y}{z_c} (x\ddot{y} - \ddot{x}y) + \frac{1}{mz_c} \frac{\sqrt{1 - \sin(\theta_r)^2 - \sin(\theta_p)^2}}{\cos(\theta_p)} \tau_p \quad (4.48)$$

$$\ddot{y} = \frac{g}{z_c} y - \frac{k_x}{z_c} (x\ddot{y} - \ddot{x}y) - \frac{1}{mz_c} \frac{\sqrt{1 - \sin(\theta_r)^2 - \sin(\theta_p)^2}}{\cos(\theta_r)} \tau_r \quad (4.49)$$

The above equations allow pendulum motion in any plane and slope if the motion is constrained to a flat plane ($k_x = 0$ and $k_y = 0$), so:

$$\ddot{x} = \frac{g}{z_c} x + \frac{1}{mz_c} \frac{\sqrt{1 - \sin(\theta_r)^2 - \sin(\theta_p)^2}}{\cos(\theta_p)} \tau_p \quad (4.50)$$

$$\ddot{y} = \frac{g}{z_c} y - \frac{1}{mz_c} \frac{\sqrt{1 - \sin(\theta_r)^2 - \sin(\theta_p)^2}}{\cos(\theta_r)} \tau_r \quad (4.51)$$

Note that equations (4.50) and (4.51) are independent equations and no linear dynamics is simplified to a linear one. The natural 3D-LIPM takes in to account the trajectories of Inverted Pendulum Model without input torques. Therefore, equations (4.50) and (4.51) are simplified to:

$$\ddot{x} = \frac{g}{z_c} x \quad (4.52)$$

$$\ddot{y} = \frac{g}{z_c} y \quad (4.53)$$

Solving those equations (4.52) and (4.53) three-dimensional pendulum ball motion is obtained in the field of gravity. Fig. 4.16 shows an example of the pendulum motion for a different support foot, i.e. a blue pendulum motion for the left support foot at its local frame and a red pendulum motion for the right support foot at its local frame.

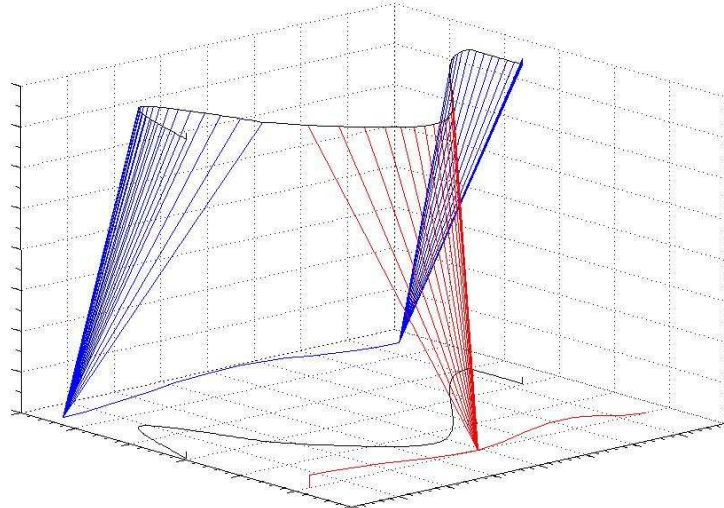


Figure 4.16: Three-dimensional Inverted Pendulum Model.

Geometry of trajectory

The spatial motion of a pendulum in the field of gravity should be studied and analyzed in order to predict stability and suitable three-dimensional local motion. Therefore, describing the local motion (Fig. 4.17) on any rotating axis, it is possible to study the effects of gravity on natural pendulum motion. It is like potential energy acting on a space shuttle.

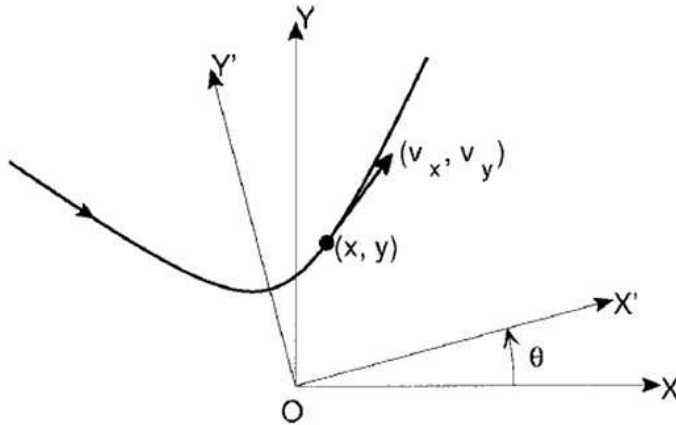


Figure 4.17: 3D-LIPM projected onto the XY plane on the local axis.

Orbital energy on each axis being:

$$E_x = \frac{1}{2}\dot{x}^2 - \frac{1}{2}\frac{g}{z_c}x^2 \quad (4.54)$$

$$E_y = \frac{1}{2}\dot{y}^2 - \frac{1}{2}\frac{g}{z_c}y^2 \quad (4.55)$$

The orbital energy on the $X'Y'$ axis is obtained as follows:

$$E'_x = \frac{1}{2}(\cos\theta.\dot{x} + \sin\theta.\dot{y})^2 - \frac{1}{2}\frac{g}{z_c}(\cos\theta.x + \sin\theta.y)^2 \quad (4.56)$$

$$E'_y = \frac{1}{2}(-\sin\theta.\dot{x} + \cos\theta.\dot{y})^2 - \frac{1}{2}\frac{g}{z_c}(-\sin\theta.x + \cos\theta.y)^2 \quad (4.57)$$

We can calculate the axis of symmetry by solving the variation of orbital energy with respect to the rotation angle; this way the maximum is founded. The mathematical expression is developed as following;

$$\frac{\partial E'_x}{\partial \theta} = A.[(\sin\theta)^2 - (\cos\theta)^2] + B.\sin\theta.\cos\theta = 0 \quad (4.58)$$

$$A = \left(\frac{g}{z_c}\right).xy - \dot{x}\dot{y} \quad (4.59)$$

$$B = \left(\frac{g}{z_c}\right).(x^2 - y^2) - (\dot{x}^2 - \dot{y}^2) \quad (4.60)$$

Finding the symmetry axis form equation (4.58), by trigonometric identities:

$$\frac{A}{B} = -\frac{\sin \theta \cdot \cos \theta}{(\sin \theta)^2 - (\cos \theta)^2} \quad (4.61)$$

$$\theta = \frac{1}{2} \tan^{-1} \left(\frac{2A}{B} \right) \quad (4.62)$$

It is well known that the *Y-axis* is the axis of symmetry for $\theta = 0$, so:

$$A = \left(\frac{g}{z_c} \right) \cdot xy - \dot{x}\dot{y} = 0 \quad (4.63)$$

$$\left(\frac{g}{z_c} \right) \cdot xy = \dot{x}\dot{y} \quad (4.64)$$

Eq. (4.64) could be used for computing the 3D-LIMP geometric shape with the mathematical orbital energy expressions from eqs. (4.54) and (4.55).

By simplifying the last equation, an interesting expression is found describing the shape of the pendulum's mass trajectory in the field of gravity (eq. 39):

$$\frac{g}{2z_c E_x} x^2 + \frac{g}{2z_c E_y} y^2 = -1 \quad (4.65)$$

It is possible to deduce that $E_x > 0$, because the *x-axis* pendulum passes by zero of the local frame and $E_y < 0$, because the *y-axis* pendulum does not pass θ of the local frame (Fig. 4.14). These facts show us that the shape of the pendulum's mass trajectory is a hyperbolic curve described by eq. (4.65). Furthermore, the natural pendulum mass motion in three dimensions give us information about the motion range for several initial conditions, which could be applied in the single support phase of humanoid body motion.

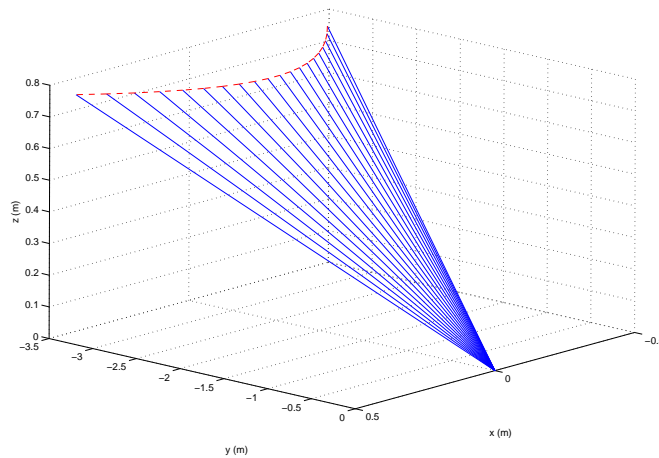


Figure 4.18: The laws of mass motion under inverted pendulum in the field of gravity.

Temporal equations

With initial conditions (x_i, \dot{x}_i) and (y_i, \dot{y}_i) at time t_i , the mass trajectory is calculated by solving differential equations (25) and (26):

$$x(t) = x_i \cosh\left(\frac{t - t_i}{T_c}\right) + T_c \dot{x}_i \sinh\left(\frac{t - t_i}{T_c}\right) \quad (4.66)$$

$$\dot{x}(t) = \frac{x_i}{T_c} \sinh\left(\frac{t - t_i}{T_c}\right) + \dot{x}_i \cosh\left(\frac{t - t_i}{T_c}\right) \quad (4.67)$$

$$y(t) = y_i \cosh\left(\frac{t - t_i}{T_c}\right) + T_c \dot{y}_i \sinh\left(\frac{t - t_i}{T_c}\right) \quad (4.68)$$

$$\dot{y}(t) = \frac{y_i}{T_c} \sinh\left(\frac{t - t_i}{T_c}\right) + \dot{y}_i \cosh\left(\frac{t - t_i}{T_c}\right) \quad (4.69)$$

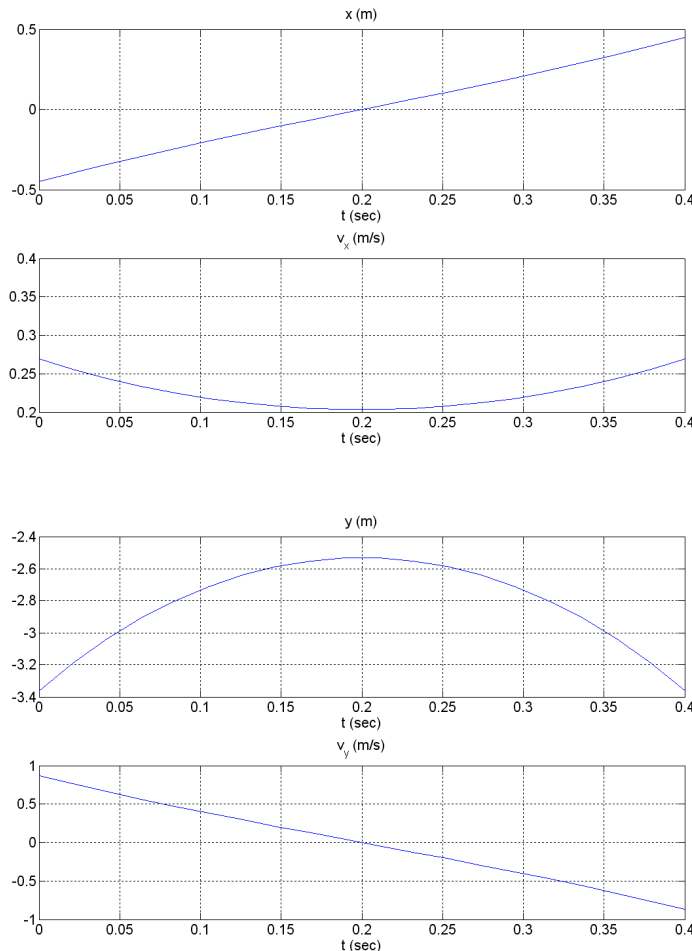


Figure 4.19: Temporal mass pendulum motion in x and y direction.

The mass trajectory of the pendulum is shown in Fig. 4.18; temporal motion in each direction (x and y) is shown in Fig. 4.19. Smooth and natural motion is obtained, and it looks like human COG motion, as we will discuss the experimental results obtained. That is, the COG is concentrated near the foot-sole (support polygon) in the single support phase, so the ZMP is inside the stable zone.

The double support phase could be modeled by a single spline. So, at this point, is necessary to clarify, that the inverted pendulum model only drives the COG motion during the single support phase, such as the COG human motion.

Furthermore, in this model, the ZMP is always on the base of the pendulum, but it is not the current ZMP multi-body position, due to the multi-body dynamics. Therefore, it is better to find a mass concentrated model whose dynamic performance is closer to the multi-body one. The Cart-table model is presented in the next section in order to bring the mass concentrated dynamic closer to the mass distributed one.

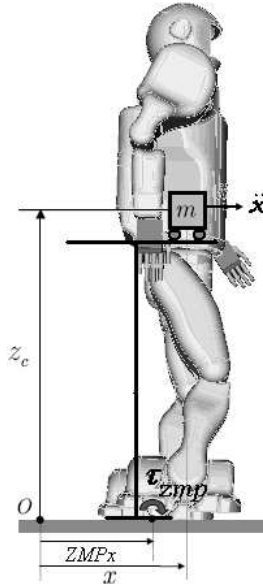


Figure 4.20: A Cart-table model, on the x -axis, ($ZMP_x = p_x$).

4.3.10 Cart-table model

COG planning by ZMP Preview Control

Selecting a point from the footprints zone, like ZMP input, we should generate COG motion as follows. At first, the COG is considered a cart-table model (Fig. 4.20). If the cart accelerates with a proper rate, the table can stay upright for a while. At this moment, the ZMP exists inside the table foot. The moment around the ZMP must be zero, so:

$$\tau_{zmp} = mg(x - p_x) - m\ddot{x}z_c \quad (4.70)$$

when

$$0 = mg(x - p_x) - m\ddot{x}z_c$$

$$p_x = x - \frac{z_c}{g}\ddot{x} \quad (4.71)$$

The same equation could be developed for the y -axis due to, planar motion at z_c , and the x and y motions are uncoupled. If the ZMP control is taken into account as a servo control problem, it is possible to put eq. (4.71) in the form of a variable state, including the time derivative of acceleration as input as shown in eq. (4.72):

$$\begin{aligned} \frac{d}{dt} \begin{pmatrix} x \\ \dot{x} \\ \ddot{x} \end{pmatrix} &= \begin{pmatrix} 0 & 1 & 0 \\ 0 & 0 & 1 \\ 0 & 0 & 0 \end{pmatrix} \begin{pmatrix} x \\ \dot{x} \\ \ddot{x} \end{pmatrix} + \begin{pmatrix} 0 \\ 0 \\ 1 \end{pmatrix} u_x \\ p_x &= \left(1 \ 0 \ \frac{z_c}{g} \right) \begin{pmatrix} x \\ \dot{x} \\ \ddot{x} \end{pmatrix} \end{aligned} \quad (4.72)$$

By using the optimal preview servo control technique, proposed by Katayama et. al. [71], it is possible to obtain the COG pattern which tracks the ZMP reference. At first, eq. (4.73) is transformed in a discrete form with sampling time T as follows:

$$\begin{aligned} x(k+1) &= Ax(k) + Bu(k) \\ p(k) &= Cx(k) \end{aligned} \quad (4.73)$$

when

$$x(k) = (x(kT) \ \dot{x}(kT) \ \ddot{x}(kT))^T,$$

$$u(k) = u_x(kT),$$

$$p(k) = p_x(kT),$$

$$A = \begin{pmatrix} 1 & T & T^2/2 \\ 0 & 1 & T \\ 0 & 0 & 1 \end{pmatrix},$$

$$B = \begin{pmatrix} T^3/6 \\ T^2/2 \\ T \end{pmatrix},$$

$$C = (1 \ 0 \ -z_c/g).$$

The performance index is as follows (for any $p^{ref}(k)$). In order to design the optimal servo control, this performance index is as follows:

$$J = \sum_{i=k}^{\infty} \left\{ Q_e e(i)^2 + \Delta x^T(i) Q_x \Delta x(i) + R \Delta u^2 \right\} \quad (4.74)$$

where

$$\begin{aligned} e(i) &= p(i) - p^{ref}(i) \text{ is a servo error} \\ Q_e, R > 0, Q_x &\text{ is a symmetric non-negative definite matrix} \\ \Delta x(k) &= x(k) - x(k-1) \text{ is the incremental state vector} \\ \Delta u(k) &= u(k) - u(k-1) \text{ is the incremental input} \end{aligned}$$

As the incremental state vector and incremental state input are used for designing the servo controller, the augmented system became as follows:

$$\begin{aligned} x^*(k+1) &= \tilde{A}x^*(k) + \tilde{B}\Delta u(k) \\ p(k) &= \tilde{C}x^*(k) \end{aligned} \quad (4.75)$$

When the augmented state vector and system matrices become as follows:

$$\begin{aligned} x^*(k) &= \begin{pmatrix} p(k) \\ \Delta x(k) \end{pmatrix}, \\ \tilde{A} &= \begin{pmatrix} 1 & C.A \\ 0 & A \end{pmatrix}, \\ \tilde{B} &= \begin{pmatrix} C.B \\ B \end{pmatrix}, \\ \tilde{C} &= \begin{pmatrix} 1 & 0 & 0 & 0 \end{pmatrix} \end{aligned}$$

The ZMP reference could be previewed for N_L step future, at every sampling time, so the optimal controller which minimizes the performance index (4.74) is described as following:

$$u(k) = -G_i \sum_{i=0}^k e(k) - G_x x(k) - \sum_{j=1}^{N_L} G_p(j) p^{ref}(k+j) \quad (4.76)$$

The gains G_i , G_x and $G_p(j)$ are calculated from the weights Q_e , Q_x , R and the system matrices eq. (4.73). In the Annexes, the gains computation will be detailed. Three terms are included in the preview controls, the integral action on the tracking error, the state feedback and the preview action on the future reference. In Fig. 4.21, when the COG is in a lower position, the maximum value of the preview gain is higher with respect to the other ones; so the $u(k)$ value increases for walking at a lower COG height. This way the humanoid increases its bending motion while it is walking in a lower position. In order to test the proposed COG dynamic motion, many simulations have been made, i.e., Fig. 4.22 to Fig. 4.25, consecutive transitions as a walking pattern are generated for a previewing period of 0.8 sec. Thus, it takes 0.1 seconds for the

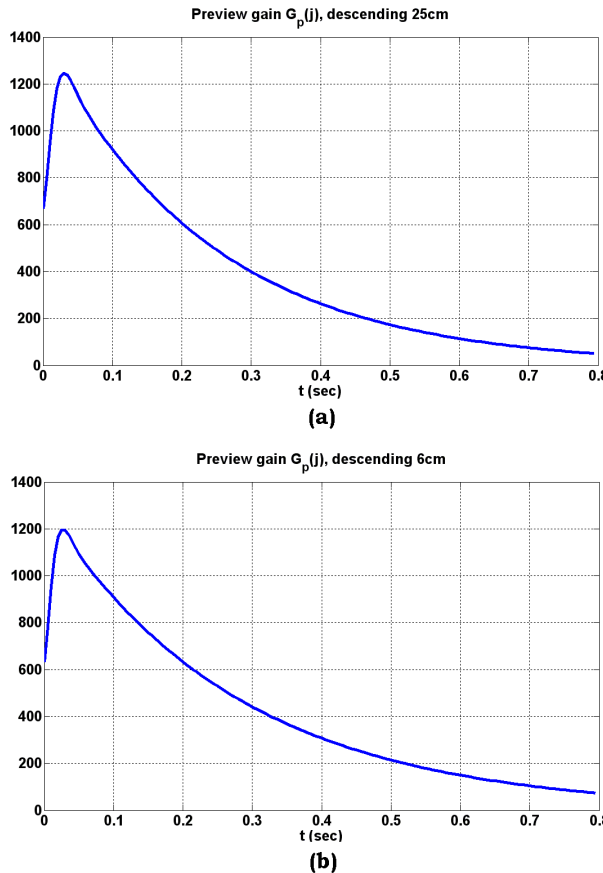


Figure 4.21: Preview gain $G_p(j)$: (a) $Z_c=0.614\text{m}$, (b) $Z_c=0.814\text{m}$ ($T=5\text{ ms}$, $Q_e=1.0$, $Q_x=0_{3x3}$, $R=1.0 \times 10^{-6}$).

double support phase, whose ZMP reference transition is made with splines, and 0.7 seconds for doing the single support phase, when the ZMP reference is maintained at a fix point. If we observe the ZMP tracking at the start of single support phase, in x direction (sagittal), the trajectory is undershooting and overshooting in y direction (frontal). That is because the previewing period is too short, but enough to maintain the stability, because the ZMP is always inside the support polygon.

As described in the preview figures, when in sagittal motion, that is, when the motion is going ahead in time, the actual ZMP has a little undershoot (Fig. 4.22 and Fig. 4.23), due to the short preview time, but next, we will show that it is enough to maintain the humanoid's stability during the walking motion or when it is taking a step. The following figures will show the frontal motion of the COG, by the preview control of ZMP.

The patterns generated in frontal direction allows the dynamic motion of the COG smoothly. It is noticed that the reference patterns finished in *NL* state more than the generated one, because the preview control takes into account the future states of the reference in order to track that. That way optimizes the

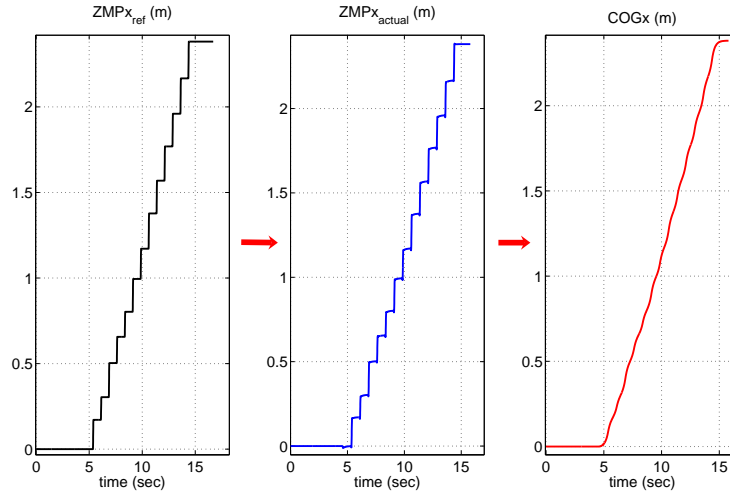


Figure 4.22: Pattern generated reference ZMP_x (black line), actual ZMP_x (blue line) and COG_x (red line).

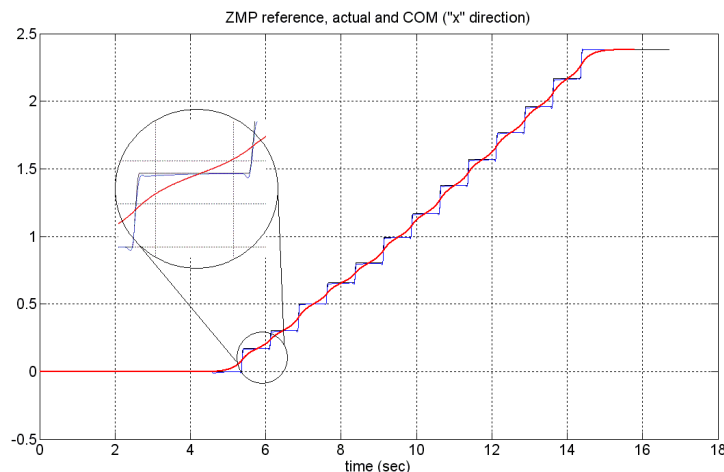


Figure 4.23: Overlapping the patterns generated. It is observed and undershoot in the actual ZMP, due to the short preview time.

COG state because the future horizon has been previewed.

4.3.11 Discussion about inverted pendulum and cart-table models

In this paragraph, some observations are made with respect to the generation methods of walking patterns, in particular, about the one described above. The inverted pendulum model simplifies the humanoid motion dynamics and a natural COG motion is obtained; but there is no direct relationship with the ZMP reference. Furthermore, there is a discontinuity in the change from the

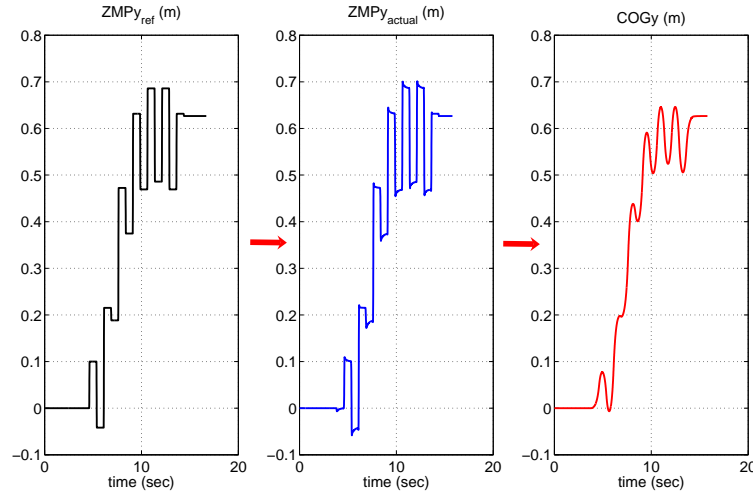


Figure 4.24: Pattern generated reference ZMP_y (black line), actual ZMP_y (blue line) and COG_y (red line).

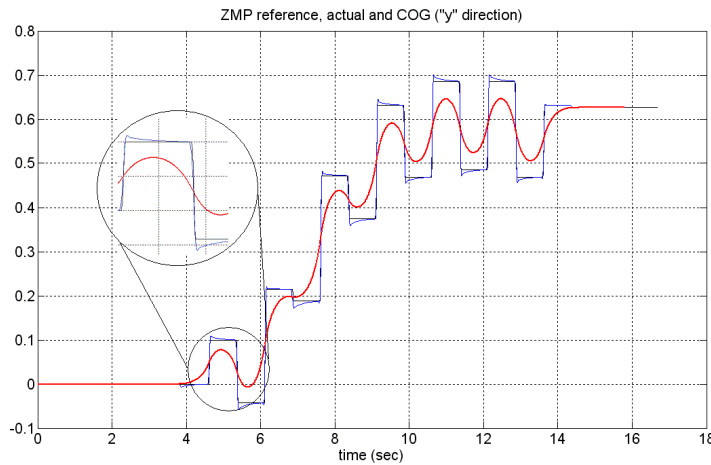


Figure 4.25: Overlapping the patterns generated. It is observed an overshoot in the actual ZMP, due to the short preview time.

single support phase to the double one, so at high walking velocity, the jerk is an important fact. It could be improved, by using high-order splines. Thus, the preview control of the cart-table model optimizes the jerk and the continuity is maintained all the time, no matter the change of phase. This way, high walking speed is possible. Finally there is a unique relationship between the ZMP and COG motion (see Fig. 4.26).

Both methods could be used indistinctly for generating stable walking patterns, but the Cart-table have the next advantages over the 3D-LIMP:

- The jerk is optimized, by the cost function, which is used for computing

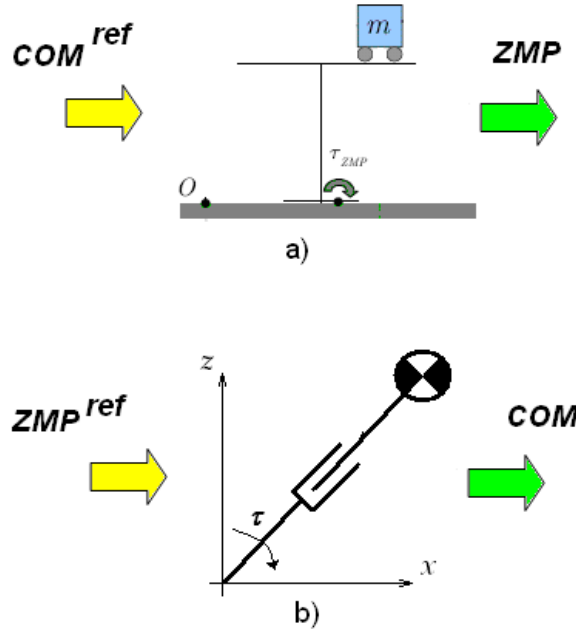


Figure 4.26: Comparison between Cart-table and 3D-LIPM.

the preview gain. So, smooth patterns could be obtained.

- The ZMP motion is modelled better than 3D-LIPM, because non-linear dynamics of the Cart is taken into account.
- By the Preview control of the ZMP, the COG motion for future NL states is optimized. So, the trajectory of the COG is computed taking into account the ZMP performance in the future step.
- The motion of the COG in the single support phase does not need other interpolator such as splines; so, smoothest COG trajectory is obtained with respect to 3D-LIPM. Furthermore, COG highest speed motion could be developed.

The advantages of this methods could be summarized in the next table (see Table 4.1):

About the Cart-table model, a few solutions have been proposed for its ZMP preview control, such as: Katayama et. al., [71] in 1985, which has been used in this research. There are other solutions by Choi et. al., [38] in 2004 and Kim et. al., [76] in 2007. The last solution reduce considerably the error of the tracked ZMP respect to the preview two solutions; so at high velocities it is a more stable walking pattern generator. In this research, the first solution is used, because the Rh-1 humanoid robot does not walk at high velocities and the walking patterns are enough stable too.

It is clear that, the Cart-table model is better for generating stable walking patterns of humanoid robots, because a single mass motion driven by the cart, could maintain the stability while the humanoid robot is walking.

Feature	3D-LIPM	Cart-table
Stable and smooth patterns	OK	OK
Real-time computation	OK	OK
Modelling SS* phase COG motion	OK	OK
Modelling DS** phase COG motion	-	OK
Modelling ZMP motion	-	OK
Previewing future ZMP states	-	OK
Reflects the non-linear dynamics	-	OK

Table 4.1: 3D-LIPM vs. Cart-table. (*SS: Single Support; **DS: Double Support)

Conclusions

The concepts of passive and active walking have been explained in order to give a background of biped robot gait generation models. The static gait, useful for low scale biped/humanoid robots and the dynamic gait used in the human-size biped/humanoid robots, are outlined and discussed. Some well-known gait generation models have been detailed in this chapter and have been tested on some biped and humanoid robots. At first, some methods do not take into account biped dynamics such as the Joint space method, which is an intuitive choice suitable for static gait cases it generates straightforward joint patterns without inverse kinematics or direct dynamics. This method interpolates trajectories between the joint boundary conditions, limited by the step length, height, orientation, velocity and accelerations depending on the interpolators; this method is not suitable for three-dimensional dynamic biped walking patterns, because the coordination between the sagittal and the frontal (or coronal) plane is not easy to obtain. The virtual force model outlines an interesting approach on uneven terrain, but only in the planar case. Furthermore it is not clear what biped walking stability criteria is being used. Other methods which take into account biped dynamics, such as mass distributed models are outlined. The sufficient friction of multi-contact point method is explained in order to illustrate the strong stability criteria in a multi-body walking pattern generator. The high computation time doesn't allow applying the walking pattern calculations in real-time, because the whole body dynamics need an iterative process with many variables to get the solution. Another approach models the swing foot like many inverted pendulums with successful results, but with preplanned walking patterns, because the iterative solution. In this case the real-time applications is not possible either. Under the dynamics modelling of walking pattern generation, the mass concentrated model is a good choice for real-time application. The objectives of the mass concentrated models for developing a stable gait of a biped robot are to obtain suitable COG and ZMP reference trajectories. They should perform like the multi-body robot dynamics and the trajectories can be computed in real-time. The preview controller of the ZMP is one method for generating a stable biped walking patterns and satisfies successfully the objectives. This thesis has used the last models, because it is demonstrated in this chapter that humanoid robot performance during the walking motion could be developed stably by controlling a single mass motion on a plane, in space, by following the ZMP constraint.

Chapter 5

Gait generation method

We are what we repeatedly do. Excellence, then, is not an act, but a habit.
(Aristotle)

Some approaches for achieving stable biped walking motion give the joint torques and surface reaction forces as references of the control system; other approaches use the joint patterns, body attitude and ZMP as references in order to achieve stable walking motion. The second approach is used in this research. The methodology proposed for computing the joint patterns is divided into several layers, which will be described in detail. The proposed layers are global motion planning, which could be computed by any classical path planning method; local motion planning with an innovative method called “Local Axis Gait” algorithm, based on foothold configurations; the COG and ZMP reference patterns computed by mass concentrated models and the swing foot motion computed by suitable splines; the next layer computes the inverse kinematics and dynamics by “screw theory”; and finally, the off-line control method is proposed, by a single rotational spring. Additionally, as an extension of walking pattern generation method, the “Acyclic gait” method will be detailed. This method deals with the gait generation of humanoid robot, which could do a generic step from any configuration to other one. This chapter describes the layers for generating the stable walking patterns of humanoid robots, which has been successfully tested on two human-size humanoid robots platforms: the Rh-1 (developed at the Universidad Carlos III de Madrid, Spain) and HRP-2 (developed by Kawada Ind. Inc. and AIST, Japan; the most advanced in the world). Finally, the “Acyclic gait” has been tested in the HRP-2 humanoid robot.

5.1 Outline

The proposed gait generation methods in the literature deal with computing the joint torque (i.e. [35], [80]) or joint angle patterns (i.e. [53], [63], [126]), the body attitude, the force surface reaction and the ZMP patterns as the input references of the humanoid robot control system. Many proposals for obtaining those references deal with algorithms which obtain stable walking patterns, reduce energy consumption, avoid singularities, optimize cost computation time, analytic and closed solutions. In this chapter, the computation of the joint angle and ZMP patterns is divided into five layers, which will be detailed in the next sections. As an example, the gait generation method should perform the humanoid walking motion as shown in Figure 5.1.

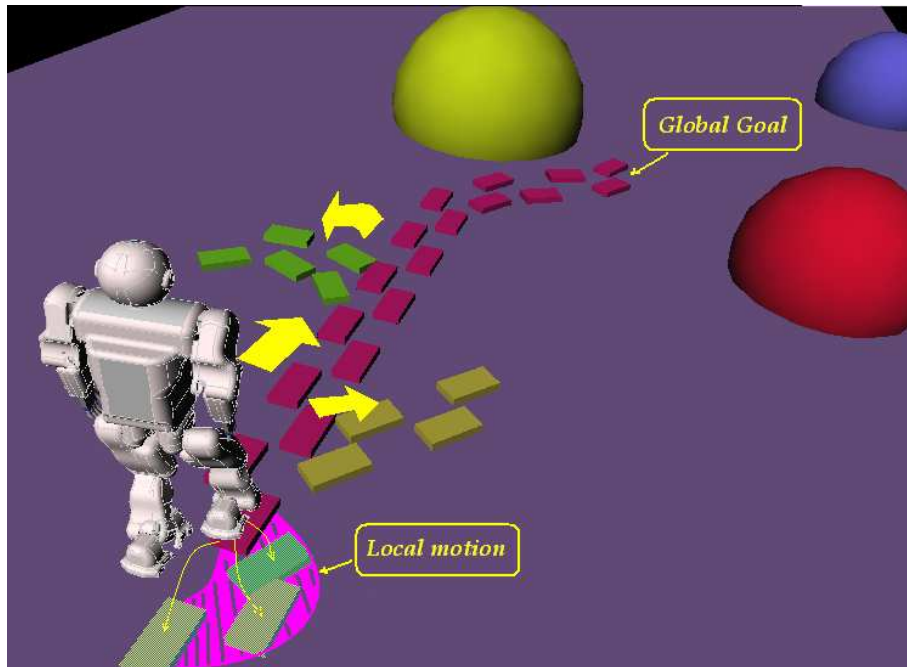


Figure 5.1: Concept of gait generation method. For reaching the “Global goal”, a set of “Local motions” must be generated. Thus the local motion decide the better foot location for going ahead, go back, turn left, turn right, doing lateral step, climbing a stair or ramp.

5.2 Layers of the “Gait generation” method

Walking pattern strategies will be described and simulation and experimental results will be shown. Overall layers for computing the walking patterns are shown in Fig. 5.2

The layers could be described as follows: Layer 1, global motion, deals with finding the global way in order the global goal of the humanoid robot; layer 2, local motion, deals with finding the local feet, ZMP and COG goals; layer 3 computes the reference patterns between previously computed local goals. In

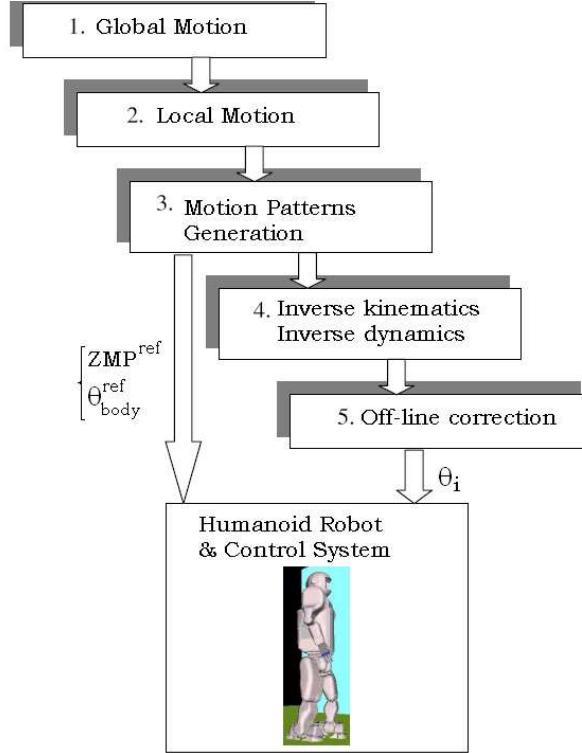


Figure 5.2: Layers for humanoid gait motion generation.

layer 4, the inverse kinematics and inverse dynamics are computed in order to obtain the articular robot motion from the Cartesian one and verify the constraints as joint angles, angular velocities, and torque limits. Finally, in layer 5, an off-line joint angles correction is made to send to the robot and its control system.

5.3 Layer 1: Global motion

Normally, the humanoid robot will walk and inter-actuate in human environments which have obstacles (for example, furniture, machines, devices). However, these obstacles must be avoided while the robot is walking so it can reach the global goal configuration. Global motion could be obtained by any well-known path planning algorithms used in robotics. In this case, the humanoid robot is taken a one solid, when the boundaries are its width, depth and height. This solid must avoid collisions in the walking environment. Many approaches have been developed, such as Kuffner et. al. [78], Pardos, J. M. (PhD. thesis, [93]) and so on. The choice of the adequate algorithm depends on the application; it is better than a real-time application algorithm, because the humanoid robot will be interact in current environments with humans. The objective of this layer is to find the global path of the humanoid robot to reach its global goal. This layer will not be developed in this thesis, but it is outlined in order to be taken into account in the gait generation method (for example, Fig. 5.3

shows the global humanoid motion).

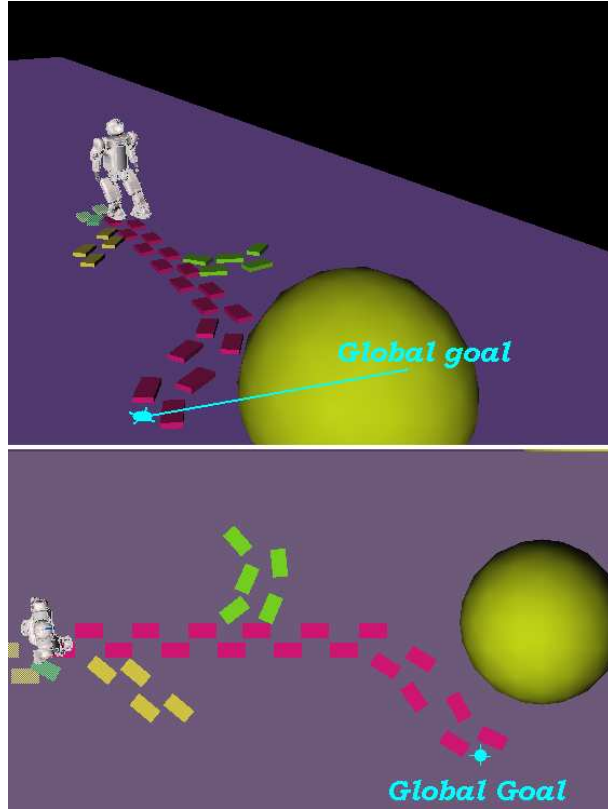


Figure 5.3: Layer 1: Global motion of the humanoid robot.

5.4 Layer 2: Local motion - “Local Axis Gait” algorithm

It is the layer when the swing foot spatial patterns and footholds are computed. The swing foot patterns are computed by single splines of fifth order, which allows for controlling the foot acceleration; the spatial boundaries are the footholds, which are the configurations (position and orientation) of the swing foot. The detail of this layer will be shown in this section (Arbulu et. al., [12], [15]).

5.4.1 Swing foot motion

In order to change the global position of the humanoid robot, the swing foot should change its configuration from initial position and orientation to the goal position and orientation. The goal configuration is limited by the physical constraint of the robot as like angular joint limits, angular joint velocities, angular accelerations, singularities and joint torques. The 3D foot motion planning for

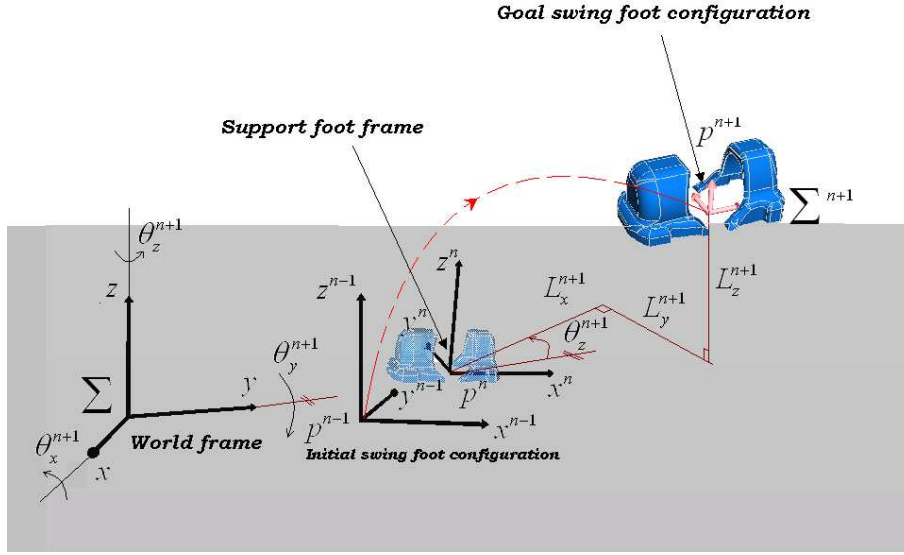


Figure 5.4: Swing foot and reference frames for 3D planning motion in each step. In this case, the n^{th} step planning is shown.

taking the n^{th} step should be modeled as shown in Fig. 5.4. The swing foot moves from the initial configuration (position and orientation $(n - 1)^{th}$ frame) to the goal configuration (position and orientation $(n + 1)^{th}$ frame). The input parameters are the swing foot goal configuration (position and orientation), defined in the appropriate local axis as: $(L_x, L_y, L_z, \theta_x, \theta_y, \theta_z)^{n+1}$.

Polynomials have been used for approximation because they can be evaluated, differentiated, and integrated easily and infinitely using just basic arithmetic operations of addition, subtraction and multiplication. A polynomial of order n or degree n is a function of the form:

$$\phi(t) = w_1 + w_2.t + \dots + w_n.t^{n-1} = \sum_{k=1}^n w_k.t^{k-1} \quad (5.1)$$

Where $\phi(t) \in \mathbb{Q}^n$, \mathbb{Q}^n being the set or linear space of all polynomials (5.1) of order n . The swing foot motion is planned by two fifth-order interpolators, (5.2) one for raising the foot ($\phi_1(t)$, (5.3)) and one for landing the foot ($\phi_2(t)$, (5.4)), on each axis motion and orientation motion.

$$\phi(t) = \begin{cases} \phi_1 \left(t, x_i^1, \dot{x}_i^1, \ddot{x}_i^1, x_f^1, \dot{x}_f^1, \ddot{x}_f^1 \right) \\ \phi_2 \left(t, x_i^2, \dot{x}_i^2, \ddot{x}_i^2, x_f^2, \dot{x}_f^2, \ddot{x}_f^2 \right) \end{cases} \quad (5.2)$$

They allow us to control the foot position, velocity and acceleration, so they are minimized. The foot landing reacting force, the angular knee velocity. Smooth and natural joints motion is obtained.

$$\phi_1(t) = w_6^1 t^5 + w_5^1 t^4 + w_4^1 t^3 + w_3^1 t^2 + w_2^1 t + w_1^1 \quad \forall [0, T/2] \quad (5.3)$$

$$\phi_2(t) = w_6^2 t^5 + w_5^2 t^4 + w_4^2 t^3 + w_3^2 t^2 + w_2^2 t + w_1^2 \quad \forall [T/2, T] \quad (5.4)$$

Where the fifth-order polynomial is characterized by the following boundary conditions in each zone; i.e., for j -th zone ($j=1$ for climbing, $j=2$ for landing) on the x -axis:

- T : Step time
- x_i^j : Initial position of j -th zone
- \dot{x}_i^j : Initial velocity of j -th zone
- \ddot{x}_i^j : Initial acceleration of j -th zone
- x_f^j : Final position of j -th zone
- \dot{x}_f^j : Final velocity of j -th zone
- \ddot{x}_f^j : Final acceleration of j -th zone

The polynomial coefficients (eqs. (5.5) to (5.10)) could be developed as follows from the boundary conditions described above:

$$w_1^j = x_i^j \quad (5.5)$$

$$w_2^j = \dot{x}_i^j \quad (5.6)$$

$$w_3^j = \frac{\ddot{x}_i^j}{2} \quad (5.7)$$

$$w_4^j = 10 \left(\frac{x_f^j - x_i^j}{T^3} - \frac{\dot{x}_i^j}{T^2} - \frac{\ddot{x}_i^j}{2T} \right) - 4 \left(\frac{\dot{x}_f^j - \dot{x}_i^j}{T^2} - \frac{\ddot{x}_i^j}{T} \right) + \frac{1}{2} \left(\frac{\ddot{x}_f^j - \ddot{x}_i^j}{T} \right) \quad (5.8)$$

$$w_5^j = -15 \left(\frac{x_f^j - x_i^j}{T^4} - \frac{\dot{x}_i^j}{T^3} - \frac{\ddot{x}_i^j}{2T^2} \right) + 7 \left(\frac{\dot{x}_f^j - \dot{x}_i^j}{T^3} - \frac{\ddot{x}_i^j}{T^2} \right) - \left(\frac{\ddot{x}_f^j - \ddot{x}_i^j}{T^2} \right) \quad (5.9)$$

$$w_6^j = 6 \left(\frac{x_f^j - x_i^j}{T^5} - \frac{\dot{x}_i^j}{T^4} - \frac{\ddot{x}_i^j}{T^3} \right) - 3 \left(\frac{\dot{x}_f^j - \dot{x}_i^j}{T^4} - \frac{\ddot{x}_i^j}{T^3} \right) + \frac{1}{2} \left(\frac{\ddot{x}_f^j - \ddot{x}_i^j}{T^3} \right) \quad (5.10)$$

The continuity at the end of the rising zone and at the start of the landing one should satisfy the next conditions:

$$\phi_1(T/2) = \phi_2(T/2) \quad (5.11)$$

$$\dot{\phi}_1(T/2) = \dot{\phi}_2(T/2) \quad (5.12)$$

$$\ddot{\phi}_1(T/2) = \ddot{\phi}_2(T/2) \quad (5.13)$$

As we will see in (5.20), goal foot configuration depends on support foot position, because the support foot is the local axis of gait input parameters. By applying the fifth-order splines developed above between the local axes $n-1$ -th

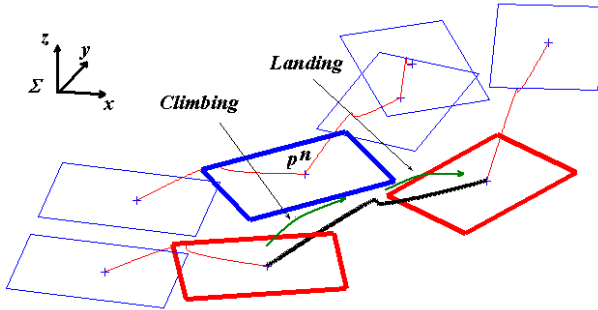


Figure 5.5: Swing foot motion planning changing walking direction in real time. The n -th step trajectory is represented by the bold black line, which has two zones: climbing and landing. The swing foot is represented by the bold red rectangles, while the support foot is represented by the bold blue rectangle.

to $n+1$ -th (from the n -1 swing foot configuration to the $n+1$ one) a smooth natural foot motion is obtained. Some simulation results are shown in Fig. 5.5. It is possible to change the walk direction and step length in real time by using the proposed algorithm. Any configuration motion could be obtained, but it is limited by the physical humanoid constraints like angular joint motion, angular velocities and joint torques. Thus, a set of splines (3 couples for changing position, and 3 couples for changing direction) are developed in order to get the foot motion, as seen in eqs. (5.14) to (5.19).

$$\phi_x(t) = \{\phi_{1x}(t) \wedge \phi_{2x}(t)\} \quad (5.14)$$

$$\phi_y(t) = \{\phi_{1y}(t) \wedge \phi_{2y}(t)\} \quad (5.15)$$

$$\phi_z(t) = \{\phi_{1z}(t) \wedge \phi_{2z}(t)\} \quad (5.16)$$

$$\phi_{\theta x}(t) = \{\phi_{\theta 1x}(t) \wedge \phi_{\theta 2x}(t)\} \quad (5.17)$$

$$\phi_{\theta y}(t) = \{\phi_{\theta 1y}(t) \wedge \phi_{\theta 2y}(t)\} \quad (5.18)$$

$$\phi_{\theta z}(t) = \{\phi_{\theta 1z}(t) \wedge \phi_{\theta 2z}(t)\} \quad (5.19)$$

5.4.2 Local axis gait algorithm

As you can see in Fig. 5.4, it is possible to identify the parameters and frames as for the n th step as follows:

- Σ : World frame
- \sum^n : n th local configuration frame, support foot
- \sum^{n-1} : $(n-1)$ th local configuration frame, swing foot
- \sum^{n+1} : $(n+1)$ th local configuration frame, swing foot
- P^n : n th position of support foot local frame

- P^{n-1} : $(n - 1)^{th}$ position of swing foot local frame
- P^{n+1} : $(n + 1)^{th}$ position of swing foot local frame
- L_x^{n+1} : $(n + 1)^{th}$ lateral swing foot displacement (x)
- L_y^{n+1} : $(n + 1)^{th}$ frontal swing foot displacement (y)
- L_z^{n+1} : $(n + 1)^{th}$ vertical swing foot displacement (z)
- θ_x^{n+1} : $(n + 1)^{th}$ rotation in X axis world
- θ_y^{n+1} : $(n + 1)^{th}$ rotation in Y axis world
- θ_z^{n+1} : $(n + 1)^{th}$ rotation in Z axis world

The goal foot configuration (position, P^{n+1} , and orientation, θ^{n+1}) is the input parameter for taking the next step. It could be obtained by humanoid sensors or external command. Those input parameters could be generalized in order to compute the $n - th$ step in real time as:

$$P^n = P^{n-1} + R(\theta_z^n)^T \cdot L^n \quad (5.20)$$

where

$$P^n = \begin{pmatrix} p_x^n \\ p_y^n \\ p_z^n \end{pmatrix}, \quad P^{n-1} = \begin{pmatrix} p_x^{n-1} \\ p_y^{n-1} \\ p_z^{n-1} \end{pmatrix},$$

$$R(\theta_z^n)^T = \begin{pmatrix} \cos(\theta_z^n) & -\sin(\theta_z^n) & 0 \\ \sin(\theta_z^n) & \cos(\theta_z^n) & 0 \\ 0 & 0 & 1 \end{pmatrix}, \quad L^n = \begin{pmatrix} L_x^n \\ -(-1)^n L_y^n \\ L_z^n \end{pmatrix}$$

As seen in eq. 5.20, goal foot configuration depends on support foot position, because the support foot is the local axis of gait input parameters. By applying the fifth-order splines developed above between local axes $n-1-th$ to $n+1-th$ (from $n-1$ swing foot configuration to $n+1$ one), a smooth and naturally foot motion is obtained.

5.5 Layer 3: Motion Patterns Generation- “COG and ZMP” references

As explained in Chapter 4, two concentrated mass models will be used in this research. Experimentally, it is obtained that the mass concentrated model, (Kajita et. al. 2002, 2003, [63], [64], Loeffler et. al. 2004, [80], Arbulu et. al 2006 [16], Choi et. al. 2004 [38]) gives a suitable approach for generating walking patterns in real time, because computation time is reduced considerably by concentrating the whole body mass in the center of gravity (COG). Therefore, the walking patterns only must generate the motion of one mass in space.

The ZMP reference computation will be made by the Cart-table model proposed by Kajita et. al. [63]. This method allows us to predict the COG motion from a ZMP future reference. A second loop of the ZMP preview control allows us to include the whole body humanoid dynamics and correct the mass concentrated assumptions.

The well-known criteria is the ZMP-based criteria (Vukobratovic et. al . 2004 [118]) and it has achieved a successful result in current humanoid robots;

the single idea of the ZMP is the point on the walking surface where the moment due to inertial and gravitational effects acting on the biped robot is zero. Thus, the walking motion is stable if this point is inside the convex hull (Fig. 5.6).

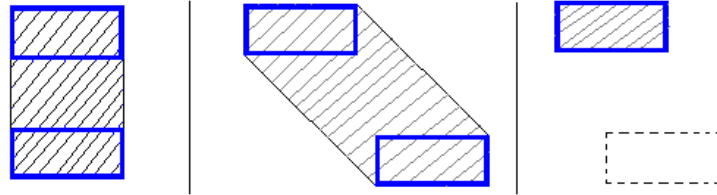


Figure 5.6: Convex hull (polygon with diagonal lines) between the feet (blue rectangles). The first and second ones are double support, the third one is a single support case. In any case, the ZMP must be inside to achieve stable walking.

At this stage, the constraint of the walking pattern is to maintain the ZMP inside the convex hull during the act of walking.

In our case, to produce walking, the humanoid robot references are the joint states, attitude and the ZMP. Other cases like the Honda robots [108] furthermore introduce the force reaction as reference. The humanoid robot control system should follow the references in order to achieve stable walking.

5.6 Cases of applying layers 1 to 3

The “Local axis gait” algorithm could be used with any mass-concentrated walking pattern generation model. In this work, two cases will be described, the inverted pendulum model and the cart-table model.

With the inverted pendulum model, it could be described as follows:

We define two change foot points, starting at the n -th step and finishing at one (i.e., Fig. 5.7). These points will be defined as median ZMP ($\overline{ZMP}^{(n)}$). It is possible to generalize the configuration as follows (as you can see in equation (5.21)):

$$\begin{bmatrix} \bar{Z}\bar{M}\bar{P}_x^{(n)} \\ \bar{Z}\bar{M}\bar{P}_y^{(n)} \end{bmatrix} = \begin{bmatrix} \cos(\theta_z^{(n+1)}) & -\sin(\theta_z^{(n+1)}) \\ \sin(\theta_z^{(n+1)}) & \cos(\theta_z^{(n+1)}) \end{bmatrix} \cdot \begin{bmatrix} L_x^{(n+1)} / 2 \\ (-1)^{(n)} \cdot L_y^{(n+1)} / 2 \end{bmatrix} \quad (5.21)$$

In order to define the COG reference trajectory, the inverted pendulum model has been used by generating the COG trajectory between the median ZMP.

Some examples of global motion are shown in Figs. 5.8 and 5.9.

As discussed previously, there is no relationship between the ZMP and COG references, because external dynamics are not considered in the inverted pendulum model, and it is supposed that the ZMP is always inside the support foot in the pendulum base while the robot is taking the n -th step.

Therefore, in order to get that relationship and plan the ZMP reference, the cart-table model and the ZMP preview control are used as a walking pattern

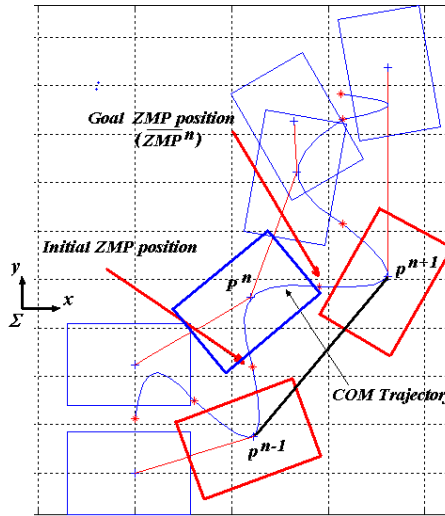


Figure 5.7: ZMP and COG motion planning in the n -th step, Inverted pendulum model walking pattern.

model. In this case, the ZMP planning has a little change, as you can see in Fig. 5.10.

In this case, it is possible to get a dynamical relationship between the COG motion and the ZMP reference; furthermore, an important characteristic is that we decide when the ZMP will stay (i.e., in a P^n foot print or around that), and the COG trajectory is computed by controlling the jerk of the cart on the table. As a result, a smoother motion is obtained compared to the motion of the inverted pendulum (i.e., while changing from single to double support phase).

As will be shown in the experimental results, is it possible to preview the ZMP motion and assure stable walking or any motion while the robot is taking a step. It is one of the main contributions of this work, because the acyclic gait could be generated.

An example of walking patterns generated is shown in Fig. 5.11. In this case, it is possible to decide when the ZMP should stay during the single support phase. That is, while the swing foot is in the air, the ZMP must be in the predefined footprint. The actual ZMP (red line) gives us an idea of the dynamical behaviour of the humanoid robot while it is walking. It does not track the ZMP reference (black line), because the preview time is not long enough to track the reference, but the motion is stable because the actual ZMP is inside the convex hull. This way, it is possible to define a stability zone of the foot print. The COG dynamic pattern is generated (blue line) with the restriction to drive the ZMP inside the convex hull. It is possible to observe that the COG pattern is not always inside the convex hull during the single support phase, but the ZMP keeps its position. In the experimental results, the dynamic COG pattern would be validated successfully.

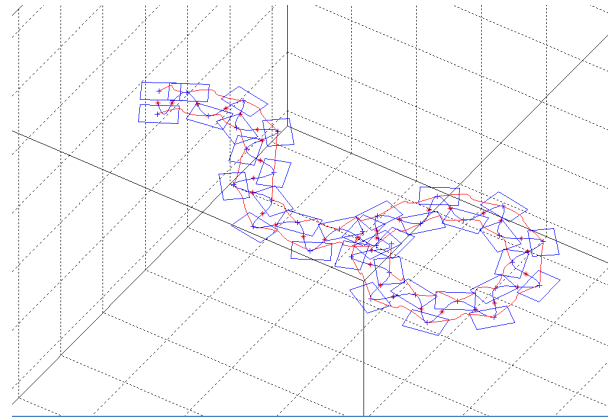


Figure 5.8: Global motion with 3D-LIPM. Projection of COG motion planning (blue trajectory), foot motion (red trajectories); each rectangle is the feet.

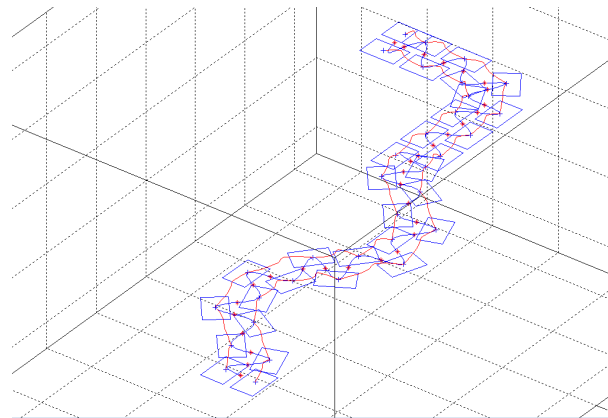


Figure 5.9: Global motion with 3D-LIPM. Projection of COG motion planning (blue trajectory), foot motion (red trajectories); each rectangle is the feet.

5.7 Layer 4: Kinematics and dynamics modelling

At this time, the spatial motion of the humanoid robot is obtained by the three layers explained above. Therefore, as the input references are the joint angle patterns for each humanoid actuator, it is necessary to compute them by suitable kinematics and dynamics models. The computation of the joint patterns have been made on each local COG and swing foot motion, which is on the “ $k - th$ ” step.

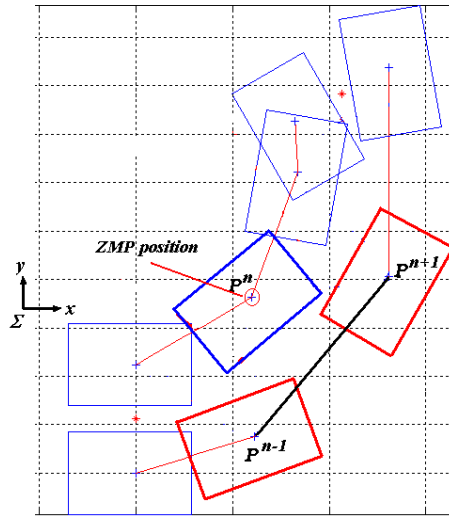


Figure 5.10: ZMP and COG motion planning in the n -th step, Cart-table model.

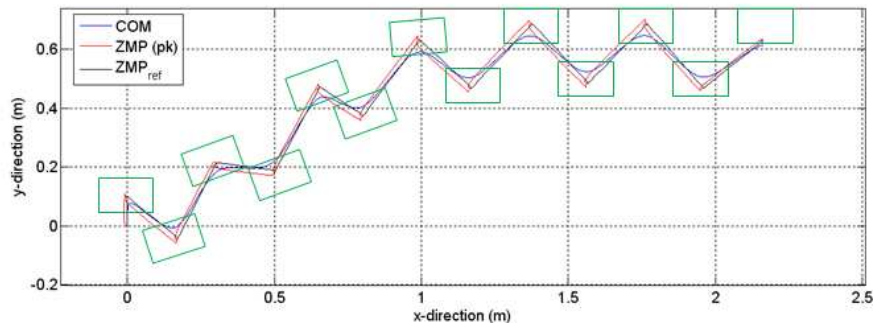


Figure 5.11: Global motion with Cart-table. Reference ZMP (black line), actual ZMP (red line) and COG (blue line) trajectories in a plane parallel to the walking surface.

5.7.1 Background of screw theory, Paden-Kahan subproblems and lie groups

There are many choices of method for the kinematics and dynamic study of humanoid robots, such as Denavit-Hartenberg parameters, quaternions, euler angles, screw theory-based study and others. The selection of the adequate method depends on the analytical complexity (highly redundant robots), computational cost and intrinsic problems of the mathematical and physical modelling (i.e., singularities, analytical and closed solutions).

Murray et. al. [86] espouse the elegance of the “product of exponential” (POE, a sequence of screw product) formula over the Denavit-Hartenberg parameterization for robot kinematics (Barrientos et. al. [27]). It is this author’s opinion that the power of POE formulation lies in its geometric foundation.

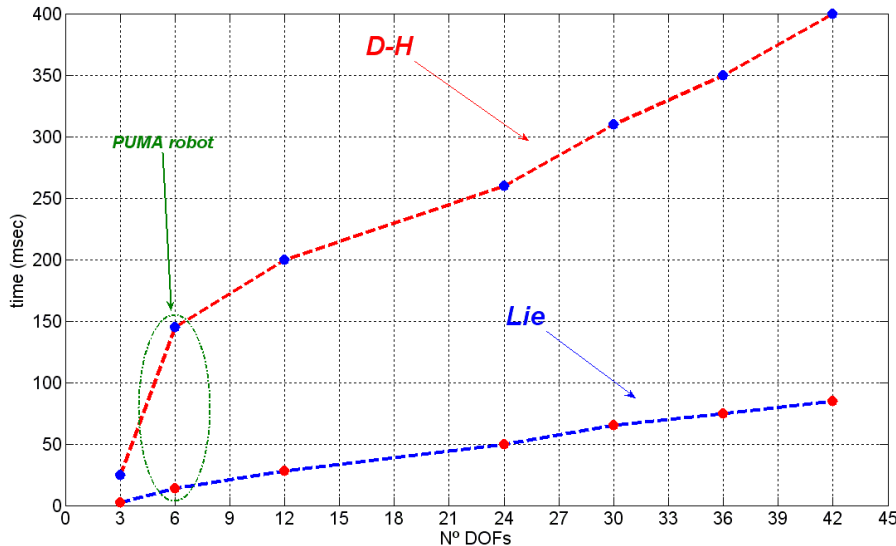


Figure 5.12: Time computation of inverse kinematics using D-H parameters and inverse Jacobian vs. POE

As such, it allows more freedom in reduction of the complexity of the transformation matrices. The POE construction is straightforward since the user does not have to remember a set of rules relating consecutive joint parameters. The directions of the axis rotations or displacements are simply taken in accordance with the spatial station frame. Also, the user works with physical link lengths rather than distances between coordinate axes. The biggest practical advantage is that the POE formulation uses only two frames to describe the forward kinematics as opposed to n frames for the Denavit-Hartenberg parameterization, so the POE does not suffer from singularities due to the use of local coordinates. Finally, the POE approach likely provides a better platform for determining an analytical solution for the inverse kinematics, because the screws describe the rigid body motion in a geometric way. Beyond that, many similarities exist between the two approaches. In each case, the user must work with a set of 4×4 matrices. From a calibration standpoint, characteristics that affect the accuracy of the Denavit-Hartenberg (D-H) parameterization enter into the POE formulation in similar ways. Ultimately, both methods provide the same information with similar amounts of computational complexity. The Denavit-Hartenberg parameterization has been the standard in robotics for many years, and it appears the switch to the POE formulation is slow in coming.

In many cases, the inverse kinematics computation of the redundant robots could be solved by dividing them into manipulators robots so that redundancy is avoided. For 24 DOFs robot (as a humanoid robot, Fig. 5.12), the computation time by POE is about 50 msec, while by D-H parameters it is 200 msec more (running Matlab in PC: AMD Athlon(tm) 64 Processor 3200+, 2.02 GHz, 1.00 GB RAM). Finally, it is observed that the slope of the above curve “Time computation vs. N^o DOFs” increases faster for the inverse kinematics computation with D-H compared to POE; thus, it is demonstrated that for the humanoid

robot application, it is better to use the inverse kinematics computation by POE than by to D-H parameters with the Jacobian method.

In order to compute the joint torques, (for selecting the actuators and checking the torque limits) and test the control system, a multi-body dynamic model should be developed, so the Lagrangian method under screw theory is proposed (Fig. 5.13), Ploen, PhD. [95]. The Lagrange equations can be computed in closed form, allowing detailed analysis of the properties of the system.

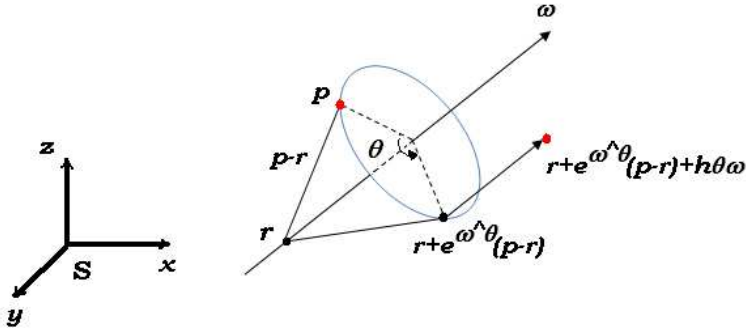


Figure 5.13: Screw motion of "p".

The Chasles theorem says that every rigid body motion can be made by a rotation about an axis combined with a translation parallel to that axis. This is a “**screw motion**”. The infinitesimal version of a screw motion is the Lie algebra $\text{se}(3)$; this is a TWIST ξ .

The screw theory has the following advantages:

- It allows a global description without singularities due to the use of local coordinates (e.g., Euler angles, Denavit-Hartenberg). It is possible to use only two coordinate frames, the base “S” and the tool “H” ones.
- A truly geometric description of rigid motion to facilitate the kinematics analysis. A very natural and explicit description of the “Jacobian Manipulator” which has none of the drawbacks of the local representation of the traditional Jacobian.
- The same mathematical treatment for the different robot joints: revolute and prismatic.

For the above reasons, the “Screw theory” is used for kinematics and dynamics modelling.

The Lie groups are very important for the mathematical analysis and the geometry, because they serve to describe the symmetry of analytical structures [94]. A Lie group is an analytical manifold that is also a group. A Lie algebra is a vectorial space over a field that completely captures the structure of the corresponding Lie group. The homogeneous representation of a rigid motion belongs to the special Euclidean Lie group (**SE(3)**), [86]. The Lie algebra of **SE(3)**, denoted $\text{se}(3)$, can be identified with the matrices called twists (ξ^\wedge), (eq. 5.22), where the skew symmetric matrix (ω^\wedge), (eq. 5.23) is the Lie algebra **so(3)** of the orthogonal special Lie group (**SO(3)**), which represents all

rotations in three-dimensional space. A twist can be geometrically interpreted using the screw theory, as Charles's theorem proved that any rigid body motion could be produced by a translation along a line followed by a rotation around the same line. This is a screw motion, and the infinitesimal version of a screw motion is a twist.

$$\xi^\wedge = \begin{pmatrix} \omega^\wedge & v \\ 0 & 0 \end{pmatrix} \in se(3) /$$

$$se(3) = \{(v, \omega^\wedge) : v \in \mathbb{R}^3, \omega^\wedge \in so(3)\} \in \mathbb{R}^{4 \times 4} \quad (5.22)$$

$$\omega^\wedge = \begin{pmatrix} 0 & -\omega_3 & \omega_2 \\ \omega_3 & 0 & -\omega_1 \\ -\omega_2 & \omega_1 & 0 \end{pmatrix} / \forall$$

$$\omega = \begin{pmatrix} \omega_1 \\ \omega_2 \\ \omega_3 \end{pmatrix} \wedge v = \begin{pmatrix} v_1 \\ v_2 \\ v_3 \end{pmatrix}$$

$$\Rightarrow \omega \times v = \omega^\wedge \cdot v \quad (5.23)$$

The main connection between **SE(3)** and **se(3)** is the exponential transformation (eq. 5.24), (eq. 5.25). It is possible to generalize the forward kinematics map for an arbitrary open-chain manipulator with **n** DOF of magnitude θ , through the product of those exponentials, expressed as POE (eq. 5.26), where **g(0)** is the reference position for the coordinate system.

$$e^{\xi^\wedge \theta} = \begin{pmatrix} e^{\omega^\wedge \theta} & E(\theta) \\ 0 & 1 \end{pmatrix} \in SE(3); \omega \neq 0$$

$$E(\theta) = (I - e^{\omega^\wedge \theta})(\omega \times v) + \omega \omega^T v \theta \quad (5.24)$$

$$e^{\xi^\wedge \theta} = \begin{pmatrix} I & v\theta \\ 0 & 1 \end{pmatrix} \in SE(3); \omega = 0$$

$$e^{\xi^\wedge \theta} = I + \omega^\wedge \cdot \sin \theta + \omega^\wedge \cdot \omega^\wedge \cdot (1 - \cos \theta) \quad (5.25)$$

$$g(\theta) = \prod_{i=1}^n e^{\xi_i^\wedge \cdot \theta_i} \cdot g(0) \quad (5.26)$$

A very important payoff for the POE formalism is that it provides an elegant formulation of a set of canonical problems, the Paden and Kahan [86] sub-problems, among others, which have a geometric solution for theirs inverse kinematics. It is possible to obtain a close-form solution for the inverse kinematics problem of complex mechanical systems by reducing them into the appropriate canonical sub-problems.

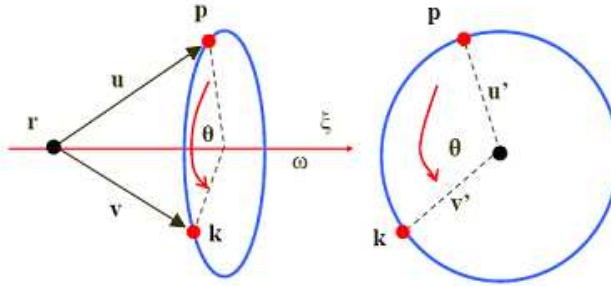


Figure 5.14: Rotation on single axis " ω " from point "p" to point "k"

Paden-Kahan Subproblems

The Paden-Kahan subproblems, which divide the inverse kinematics problem, are described as follows:

Paden-Kahan 1: Rotation about a single axis

Finding the rotation angle using “screw theory” and Lie groups, at first, the point rotation expression from “p” to “k” is expressed by:

$$e^{\xi \wedge \theta} \cdot p = k \quad (5.27)$$

The twist and projection vectors on the rotation plane are as follows:

$$\xi = \begin{pmatrix} v \\ \omega \end{pmatrix},$$

$$\xi = \begin{pmatrix} -\omega \times r \\ \omega \end{pmatrix} \quad (5.28)$$

$$u' = u - \omega \omega^T u \quad (5.29)$$

$$v' = v - \omega \omega^T v \quad (5.30)$$

Finally, the rotation angle is calculated with the following expression:

$$\theta = \text{atan2} [\omega^T (u' \times v'), u'^T \cdot v'] \quad (5.31)$$

Paden-Kahan 2: Rotation about two subsequent axes

The rotation expression is the following (Fig. 5.15):

$$e^{\xi_1 \wedge \theta_1} \cdot e^{\xi_2 \wedge \theta_2} \cdot p = e^{\xi_1 \wedge \theta_1} \cdot c = k \quad (5.32)$$

The respective twists are described as follows:

$$\xi_1 = \begin{pmatrix} -\omega_1 \times r \\ \omega_1 \end{pmatrix} \quad (5.33)$$

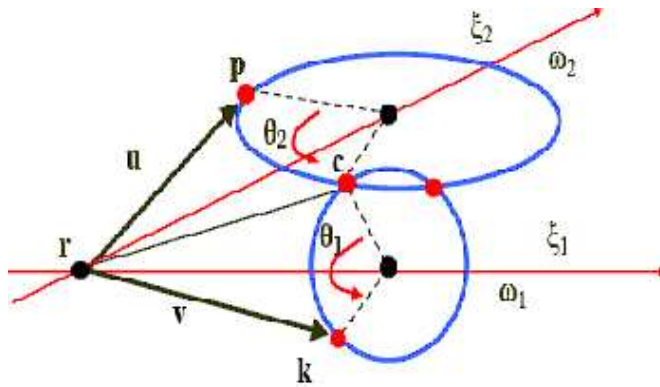


Figure 5.15: Rotation on two subsequent axes “ w_1 ” and “ w_2 ” from “ p ” to “ c ” and from “ c ” to “ k ”

$$\xi_2 = \begin{pmatrix} -\omega_2 \times r \\ \omega_2 \end{pmatrix} \quad (5.34)$$

Some values are computed in order to obtain the point “ c ” with the following expressions:

$$\alpha = \frac{(\omega_1^T \omega_2) \omega_2^T u - \omega_1^T v}{(\omega_1^T \omega_2)^2 - 1} \quad (5.35)$$

$$\beta = \frac{(\omega_1^T \omega_2) \omega_1^T v - \omega_2^T u}{(\omega_1^T \omega_2)^2 - 1} \quad (5.36)$$

$$\gamma^2 = \frac{\|u\|^2 - \alpha^2 - \beta^2 - 2\alpha\beta\omega_1^T \omega_2}{\|\omega_1 \times \omega_2\|^2} \quad (5.37)$$

Obtaining the point “ c ” :

$$c = r + \alpha\omega_1 + \beta\omega_2 \pm \gamma(\omega_1 \times \omega_2) \quad (5.38)$$

Once we get “ c ” for the second sub-problem, we can apply the first Paden-Kahan sub-problem to get the solutions for θ_1 and θ_2 . Beware that there might be two solutions for “ c ”, each of them gives a different solution for θ_1 and θ_2 .

Paden-Kahan 3: Rotation to a given distance

The distance “ δ ” is shown as follows:

$$\left\| e^{\xi \wedge \theta} - q \right\| = \delta \quad (5.39)$$

The associate twist and vectors projection in the perpendicular plane of rotation axis could be computed as:

$$\xi = \begin{pmatrix} -\omega \times r \\ \omega \end{pmatrix} \quad (5.40)$$

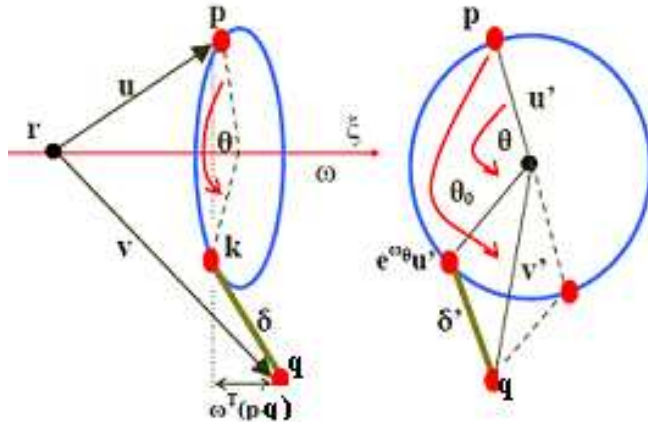


Figure 5.16: Rotation of point “p” to “k” which is a distance “ δ ” from “q”

$$u' = u - \omega\omega^T u \quad (5.41)$$

$$v' = v - \omega\omega^T v \quad (5.42)$$

Projecting “ δ ” in “ ω ” direction:

$$\delta'^2 = \delta^2 - |\omega^T (p - q)|^2 \quad (5.43)$$

If we let “ θ_0 ” be the angle between the vectors “u” and “v”, we have:

$$\theta_0 = \text{atan}2 [\omega^T (u' \times v'), u'^T \cdot v'] \quad (5.44)$$

Finally, we obtain the rotation angle by:

$$\theta = \theta_0 \pm \cos^{-1} \left(\frac{\|u'\|^2 + \|v'\|^2 - \delta'^2}{2 \|u'\| \|v'\|} \right) \quad (5.45)$$

5.7.2 Whole-body humanoid kinematics model

In order to control the motion of humanoid arms, it is necessary to complete the kinematic model developed in previous work Pardos, PhD [93] with a slight modification in order to control the COG attitude. The Rh-1 kinematics configuration is shown in Fig. 5.17. This section describes the four manipulator kinematics model, proposed as a contribution of this work (see Fig. 5.18). The constraints are to follow the backbone motion and to choose the appropriate hierarchy in maintaining the common shoulder DOF motion, when the arms are going to reach a goal. Furthermore, the arm motion should be controlled only in a combination of five non-physical degrees of freedom (θ_x^{rh} to θ_z^{rh} , for right hand and θ_x^{lh} to θ_z^{lh} for left hand), because the arm has five degrees of freedom

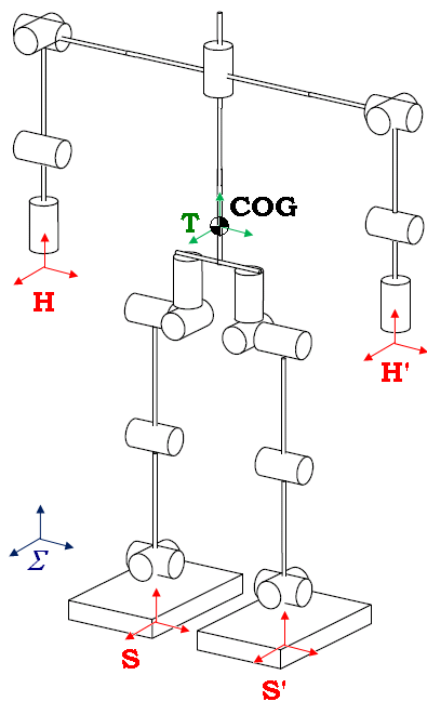


Figure 5.17: Rh-1 kinematics configuration.

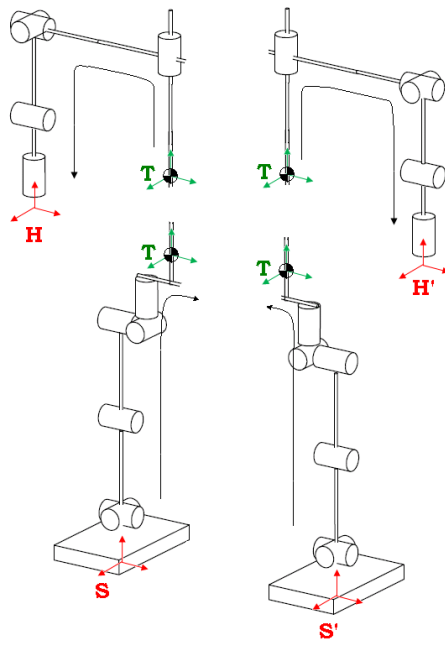


Figure 5.18: Four manipulator kinematics model.

including the shoulder. We will call the foot, COG or hands position and orientation the non-physical degrees of freedom, because they could be treated like any DOF in the product of exponential formulation.

As you can see in Fig. 5.17, it is necessary to define the frames as follows: the world frame (Σ), the frames attached on each foot (S, S'), the frame of the center of gravity (T), and the frames attached to the hands (H, H'). After that, the four manipulator kinematics division is made in order to treat each leg and arms and independent manipulators and apply the conventional robotics manipulator solutions, taking into account the effects of a mobile base. It is noticed that in Fig. 5.18, the kinematic model for the legs starts from the foot to the COG, and for the arms it starts from the COG to the hands.

5.7.3 Forward kinematics

The screw theory, Lie groups, product of exponentials (POE) and Paden-Kahan sub-problems are used to compute forward and inverse kinematics [86].

Now, let us define the configurations, twists, parameters and variables that should be used for solving the robot kinematics. The right leg and arm kinematics are solved; the left ones should be solved in the same way, as follows (Fig. 5.19):

- $g_{st}(0)$: Initial manipulator configuration (right leg)
- $g_{st}(\theta)$: Goal manipulator configuration (right leg)
- $g_{th}(0)$: Initial manipulator configuration (right hand)
- $g_{th}(\theta)$: Goal manipulator configuration (right hand)
- θ_1 to θ_{21} : Degrees of freedom
- $\theta_{\theta_x}^{rh}$ to $\theta_{\theta_z}^{rh}$: Right hand orientation
- $\theta_x^a, \theta_y^a, \theta_z^a, \theta_{\theta_x}^a, \theta_{\theta_y}^a$,
- $\theta_{\theta_z}^a$: COG position and orientation
- θ_x^r to $\theta_{\theta_z}^r$: Right foot position and orientation
- ξ_1 to ξ_{21} : Twists of degrees of freedom
- ξ_x^{rh} to $\xi_{\theta_z}^{rh}$: Twists of non-physical degrees of freedom (right hand)
- ξ_x^a to $\xi_{\theta_z}^a$: Twists of non-physical degrees of freedom (COG)
- ξ_x^r to $\xi_{\theta_z}^r$: Twists of non-physical degrees of freedom (right foot)
- ω_1 to ω_{21} : Direction of degrees of freedom
- v_x^{rh} to $\omega_{\theta_z}^{rh}$: Direction of non-physical degrees of freedom (right hand)
- v_x^a to $\omega_{\theta_z}^a$: Direction of non-physical degrees of freedom (COG)
- v_x^r to $\omega_{\theta_z}^r$: Direction of non-physical degrees of freedom (right foot)
- k, r, p, m, q, c, n : Points for analysis

The forward kinematics for the right leg, eq. (6.95) and the right arm, eq. (6.96) is obtained with the product of exponentials as a sequence of screw motions applied to the initial configurations.

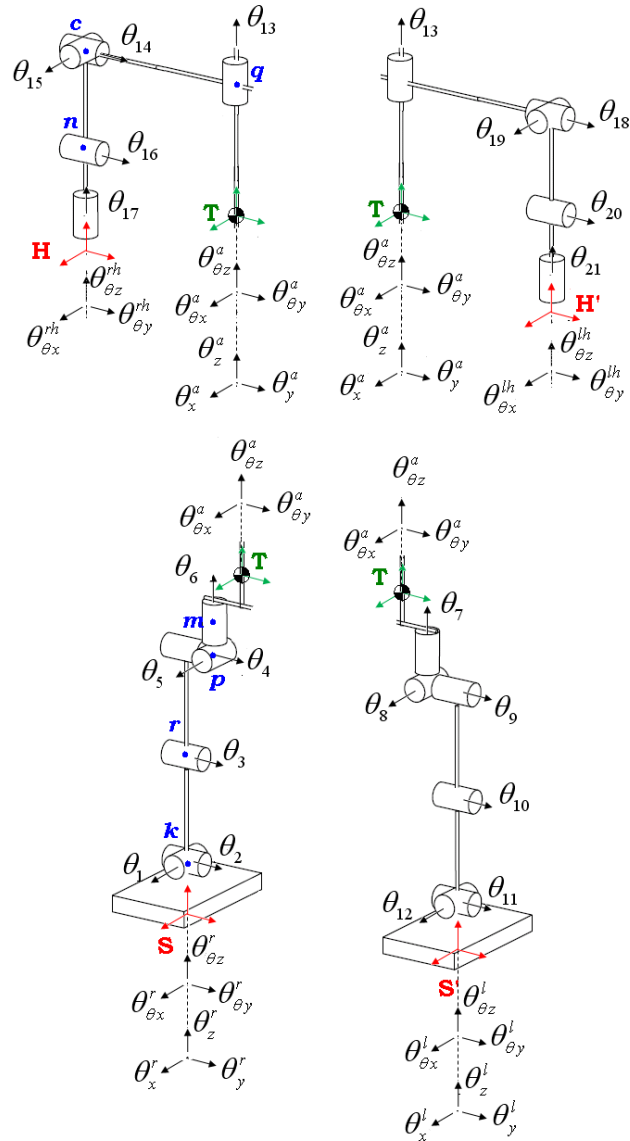


Figure 5.19: Degrees of freedom (θ_1 to θ_{21}), position and orientation of hands ($\theta_{\theta_x}^r$ to $\theta_{\theta_z}^r$, $\theta_{\theta_x}^{lh}$ to $\theta_{\theta_z}^{lh}$), COG (θ_x^a , θ_y^a , θ_z^a , $\theta_{\theta_x}^a$, $\theta_{\theta_y}^a$, $\theta_{\theta_z}^a$) and feet (θ_x^r to $\theta_{\theta_z}^r$, θ_x^l to $\theta_{\theta_z}^l$).

$$g_{st}(\theta) = e^{\xi_x^r \wedge \theta_x^r} \cdot e^{\xi_y^r \wedge \theta_y^r} \cdot e^{\xi_z^r \wedge \theta_z^r} \cdot e^{\xi_{\theta_x}^r \wedge \theta_{\theta_x}^r} \cdot e^{\xi_{\theta_y}^r \wedge \theta_{\theta_y}^r} \cdot e^{\xi_{\theta_z}^r \wedge \theta_{\theta_z}^r} \cdot e^{\xi_1 \wedge \theta_1} \dots e^{\xi_{\theta_z}^a \wedge \theta_{\theta_z}^a} \cdot g_{st}(0) \quad (5.46)$$

$$g_{th}(\theta) = e^{\xi_x^a \wedge \theta_x^a} \cdot e^{\xi_y^a \wedge \theta_y^a} \cdot e^{\xi_z^a \wedge \theta_z^a} \cdot e^{\xi_{\theta_x}^a \wedge \theta_{\theta_x}^a} \cdot e^{\xi_{\theta_y}^a \wedge \theta_{\theta_y}^a} \cdot e^{\xi_{\theta_z}^a \wedge \theta_{\theta_z}^a} \cdot e^{\xi_{13} \wedge \theta_{13}} \dots e^{\xi_{\theta_z}^{rh} \wedge \theta_{\theta_z}^{rh}} \cdot g_{th}(0) \quad (5.47)$$

5.7.4 Inverse kinematics

The inverse kinematics problem deals with the computation of the joint angles (θ_1 to θ_{21}), from any time COG, hands and feet configuration. The Paden-Kahan subproblems [86] are used for carrying out that computation. At first, the reference configuration eq. (5.48) and twists are computed (i.e., right leg):

$$g_{st}(0) = \begin{bmatrix} 1 & 0 & 0 & T_x - S_x \\ 0 & 1 & 0 & T_y - S_y \\ 0 & 0 & 1 & T_z - S_z \\ 0 & 0 & 0 & 1 \end{bmatrix} \quad (5.48)$$

Where the axis directions are expressed by:

$$\begin{aligned} v_x^r &= \begin{bmatrix} 1 \\ 0 \\ 0 \end{bmatrix}; v_y^r = \begin{bmatrix} 0 \\ 1 \\ 0 \end{bmatrix}; v_z^r = \begin{bmatrix} 0 \\ 0 \\ 1 \end{bmatrix}; \omega_{\theta x}^r = \begin{bmatrix} 1 \\ 0 \\ 0 \end{bmatrix}; \omega_{\theta y}^r = \begin{bmatrix} 0 \\ 1 \\ 0 \end{bmatrix}; \omega_{\theta z}^r = \begin{bmatrix} 0 \\ 0 \\ 1 \end{bmatrix} \\ \omega_1 &= \begin{bmatrix} 1 \\ 0 \\ 0 \end{bmatrix}; \omega_2 = \begin{bmatrix} 0 \\ 1 \\ 0 \end{bmatrix}; \omega_3 = \begin{bmatrix} 0 \\ 1 \\ 0 \end{bmatrix}; \omega_4 = \begin{bmatrix} 0 \\ 1 \\ 0 \end{bmatrix}; \omega_5 = \begin{bmatrix} 1 \\ 0 \\ 0 \end{bmatrix}; \omega_6 = \begin{bmatrix} 0 \\ 0 \\ 1 \end{bmatrix} \\ v_x^a &= \begin{bmatrix} 1 \\ 0 \\ 0 \end{bmatrix}; v_y^a = \begin{bmatrix} 0 \\ 1 \\ 0 \end{bmatrix}; v_z^a = \begin{bmatrix} 0 \\ 0 \\ 1 \end{bmatrix}; \omega_{\theta x}^a = \begin{bmatrix} 1 \\ 0 \\ 0 \end{bmatrix}; \omega_{\theta y}^a = \begin{bmatrix} 0 \\ 1 \\ 0 \end{bmatrix}; \omega_{\theta z}^a = \begin{bmatrix} 0 \\ 0 \\ 1 \end{bmatrix} \end{aligned}$$

Thus the twists are computed as follows:

$$\begin{aligned} \xi_x^r &= \begin{bmatrix} v_x^r \\ 0 \end{bmatrix}; \quad \xi_y^r = \begin{bmatrix} v_y^r \\ 0 \end{bmatrix}; \quad \xi_z^r = \begin{bmatrix} v_z^r \\ 0 \end{bmatrix}; \\ \xi_{\theta x}^r &= \begin{bmatrix} -\omega_{\theta x}^r \times S \\ \omega_{\theta x}^r \end{bmatrix}; \xi_{\theta y}^r = \begin{bmatrix} -\omega_{\theta y}^r \times S \\ \omega_{\theta y}^r \end{bmatrix}; \xi_{\theta z}^r = \begin{bmatrix} -\omega_{\theta z}^r \times S \\ \omega_{\theta z}^r \end{bmatrix} \\ \xi_1 &= \begin{bmatrix} -\omega_1 \times k \\ \omega_1 \end{bmatrix}; \quad \xi_2 = \begin{bmatrix} -\omega_2 \times k \\ \omega_2 \end{bmatrix}; \quad \xi_3 = \begin{bmatrix} -\omega_3 \times r \\ \omega_3 \end{bmatrix} \\ \xi_4 &= \begin{bmatrix} -\omega_4 \times p \\ \omega_4 \end{bmatrix}; \quad \xi_5 = \begin{bmatrix} -\omega_5 \times p \\ \omega_5 \end{bmatrix}; \quad \xi_6 = \begin{bmatrix} -\omega_6 \times p \\ \omega_6 \end{bmatrix} \\ \xi_{\theta x}^a &= \begin{bmatrix} -\omega_{\theta x}^a \times T \\ \omega_{\theta x}^a \end{bmatrix}; \xi_{\theta y}^a = \begin{bmatrix} -\omega_{\theta y}^a \times T \\ \omega_{\theta y}^a \end{bmatrix}; \xi_{\theta z}^a = \begin{bmatrix} -\omega_{\theta z}^a \times T \\ \omega_{\theta z}^a \end{bmatrix} \end{aligned}$$

We should review a previous work Pardos, PhD [93] to compute the inverse kinematics (i.e., right leg). The slight variation is the control of COG orientation

(attitude) by the non-physical DOF ($\theta_{\theta_x}^a$, $\theta_{\theta_y}^a$, $\theta_{\theta_z}^a$). However, to find the θ_3 angle, the Paden-Kahan 3 sub-problem is used:

$$\left\| e^{-\xi_{\theta_z}^r \wedge \theta_{\theta_z}^r} \cdots e^{-\xi_x^r \wedge \theta_x^r} \cdot g_{st}(\theta) \cdot g_{st}(0)^{-1} \cdot e^{-\xi_{\theta_z}^a \wedge \theta_{\theta_z}^a} \cdots e^{-\xi_{\theta_x}^a \wedge \theta_{\theta_x}^a} \cdot p - k \right\| = \\ \left\| e^{\xi_1^\wedge \theta_1} \cdots e^{\xi_6^\wedge \theta_6} \cdot p - k \right\| \quad (5.49)$$

$$\delta = \left\| e^{\xi_3^\wedge \theta_3} \cdot p - k \right\| \xrightarrow{P-K-3} \theta_3 \quad (5.50)$$

After that, it is possible to compute the angles θ_1 and θ_2 by the Paden Kahan 2 sub-problem, because their axis direction crosses at point “k”. Thus, we compute those angles as following:

$$e^{-\xi_{\theta_z}^r \wedge \theta_{\theta_z}^r} \cdots e^{-\xi_x^r \wedge \theta_x^r} \cdot g_{st}(\theta) \cdot g_{st}(0)^{-1} \cdot e^{-\xi_{\theta_z}^a \wedge \theta_{\theta_z}^a} \cdots e^{-\xi_{\theta_x}^a \wedge \theta_{\theta_x}^a} \cdot p = \\ e^{\xi_1^\wedge \theta_1} \cdots e^{\xi_6^\wedge \theta_6} \cdot p \quad (5.51)$$

$$a = e^{\xi_1^\wedge \theta_1} \cdot e^{\xi_2^\wedge \theta_2} \cdot p' \xrightarrow{P-K-2} \theta_1, \theta_2 \quad (5.52)$$

Next, the rotation axis of joint angles θ_4 and θ_5 cross at point “p”, so the Paden Kahan 2 sub-problem could be used to compute them.

$$e^{-\xi_3^\wedge \theta_3} \cdot e^{-\xi_2^\wedge \theta_2} \cdot e^{-\xi_1^\wedge \theta_1} \cdots e^{-\xi_x^r \wedge \theta_x^r} \cdot g_{st}(\theta) \cdot g_{st}(0)^{-1} \cdot e^{-\xi_{\theta_z}^a \wedge \theta_{\theta_z}^a} \cdots e^{-\xi_{\theta_x}^a \wedge \theta_{\theta_x}^a} \cdot m = \\ e^{\xi_4^\wedge \theta_4} \cdots e^{\xi_6^\wedge \theta_6} \cdot m \quad (5.53)$$

$$b = e^{\xi_4^\wedge \theta_4} \cdot e^{\xi_5^\wedge \theta_5} \cdot m' \xrightarrow{P-K-2} \theta_4, \theta_5 \quad (5.54)$$

Finally, as we have done before, all the known terms are passed to the left side of the equation 5.56 and using the Paden Kahan 1 sub-problem, the θ_6 angle is computed by rotating the origin of the “S” axis around axis 6:

$$e^{-\xi_5^\wedge \theta_5} \cdot e^{-\xi_4^\wedge \theta_4} \cdot e^{-\xi_3^\wedge \theta_3} \cdots e^{-\xi_x^r \wedge \theta_x^r} \cdot g_{st}(\theta) \cdot g_{st}(0)^{-1} \cdot e^{-\xi_{\theta_z}^a \wedge \theta_{\theta_z}^a} \cdots e^{-\xi_{\theta_x}^a \wedge \theta_{\theta_x}^a} \cdot S = \\ e^{\xi_6^\wedge \theta_6} \cdot S \quad (5.55)$$

$$h = e^{\xi_6^\wedge \theta_6} \cdot S \xrightarrow{P-K-1} \theta_6 \quad (5.56)$$

In the same way the left leg inverse kinematics could be computed. Now, we propose the computation of the right arm inverse kinematics as follows.

First, from Fig. 5.19, we should define the initial configuration as:

$$g_{th}(0) = \begin{bmatrix} 1 & 0 & 0 & H_x - T_x \\ 0 & 1 & 0 & H_y - T_y \\ 0 & 0 & 1 & H_z - T_z \\ 0 & 0 & 0 & 1 \end{bmatrix} \quad (5.57)$$

so the axis directions are expressed by:

$$v_x^a = \begin{bmatrix} 1 \\ 0 \\ 0 \end{bmatrix}; v_y^a = \begin{bmatrix} 0 \\ 1 \\ 0 \end{bmatrix}; v_z^a = \begin{bmatrix} 0 \\ 0 \\ 1 \end{bmatrix}; \omega_{\theta_x}^a = \begin{bmatrix} 1 \\ 0 \\ 0 \end{bmatrix}; \omega_{\theta_y}^a = \begin{bmatrix} 0 \\ 1 \\ 0 \end{bmatrix}; \omega_{\theta_z}^a = \begin{bmatrix} 0 \\ 0 \\ 1 \end{bmatrix}$$

$$\omega_{13} = \begin{bmatrix} 0 \\ 0 \\ 1 \end{bmatrix}; \omega_{14} = \begin{bmatrix} 0 \\ 1 \\ 0 \end{bmatrix}; \omega_{15} = \begin{bmatrix} 1 \\ 0 \\ 0 \end{bmatrix}; \omega_{16} = \begin{bmatrix} 0 \\ 1 \\ 0 \end{bmatrix}; \omega_{17} = \begin{bmatrix} 0 \\ 0 \\ 1 \end{bmatrix}$$

$$\omega_{\theta x}^{rh} = \begin{bmatrix} 1 \\ 0 \\ 0 \end{bmatrix}; \omega_{\theta y}^{rh} = \begin{bmatrix} 0 \\ 1 \\ 0 \end{bmatrix}; \omega_{\theta z}^{rh} = \begin{bmatrix} 0 \\ 0 \\ 1 \end{bmatrix}$$

Thus the twists are computed as follows:

$$\xi_x^a = \begin{bmatrix} v_x^a \\ 0 \end{bmatrix}; \quad \xi_y^a = \begin{bmatrix} v_y^a \\ 0 \end{bmatrix}; \quad \xi_z^a = \begin{bmatrix} v_z^a \\ 0 \end{bmatrix};$$

$$\xi_{\theta x}^a = \begin{bmatrix} -\omega_{\theta x}^a \times T \\ \omega_{\theta x}^a \end{bmatrix}; \xi_{\theta y}^a = \begin{bmatrix} -\omega_{\theta y}^a \times T \\ \omega_{\theta y}^a \end{bmatrix}; \xi_{\theta z}^a = \begin{bmatrix} -\omega_{\theta z}^a \times T \\ \omega_{\theta z}^a \end{bmatrix}$$

$$\xi_{13} = \begin{bmatrix} -\omega_{13}^a \times q \\ \omega_{13}^a \end{bmatrix}; \quad \xi_{14} = \begin{bmatrix} -\omega_{14}^a \times c \\ \omega_{14}^a \end{bmatrix}; \quad \xi_{15} = \begin{bmatrix} -\omega_{15}^a \times c \\ \omega_{15}^a \end{bmatrix}$$

$$\xi_{16} = \begin{bmatrix} -\omega_{16}^a \times n \\ \omega_{16}^a \end{bmatrix}; \quad \xi_{17} = \begin{bmatrix} -\omega_{17}^a \times H \\ \omega_{17}^a \end{bmatrix};$$

$$\xi_{\theta x}^{rh} = \begin{bmatrix} -\omega_{\theta x}^{rh} \times H \\ \omega_{\theta x}^{rh} \end{bmatrix}; \xi_{\theta y}^{rh} = \begin{bmatrix} -\omega_{\theta y}^{rh} \times H \\ \omega_{\theta y}^{rh} \end{bmatrix}; \xi_{\theta z}^{rh} = \begin{bmatrix} -\omega_{\theta z}^{rh} \times H \\ \omega_{\theta z}^{rh} \end{bmatrix}$$

By using the Paden Kahan sub-problems the inverse kinematics should be computed. However, we could rotate point “n” around the axis θ_{13} to θ_{17} and compute the norm up to point “q”. This way, the rotation of θ_{16} and θ_{17} does not cause any effect, because their directions are cross at “n”. Furthermore, the norm until “q” is not affected by θ_{13} and θ_{14} , because, their directions have point “q” as common one. This way, by the Paden Kahan 3 sub-problem the θ_{15} angle is computed. We use the equation 5.59, which correspond to the right arm:

$$\left\| e^{-\xi_{\theta z}^a \wedge \theta_{\theta z}^a} \dots e^{-\xi_x^a \wedge \theta_x^a} \cdot g_{th}(\theta) \cdot g_{th}(0)^{-1} \cdot e^{-\xi_{\theta z}^{rh} \wedge \theta_{\theta z}^{rh}} \dots e^{-\xi_{\theta x}^{rh} \wedge \theta_{\theta x}^{rh}} \cdot n - q \right\| =$$

$$\left\| e^{\xi_{13}^\wedge \theta_{13}} \dots e^{\xi_{17}^\wedge \theta_{17}} \cdot n - q \right\| \quad (5.58)$$

$$\delta' = \left\| e^{\xi_{15}^\wedge \theta_{15}} \cdot n - q \right\| \xrightarrow{P-K-3} \theta_{15} \quad (5.59)$$

Angle θ_{15} is known and the rotation axis of θ_{13} and θ_{14} crosses at “q”, so, by rotating “n” around those axes, the canonical Paden Kahan 2 sub-problem is obtained in order to compute both angles:

$$e^{-\xi_{\theta z}^a \wedge \theta_{\theta z}^a} \dots e^{-\xi_x^a \wedge \theta_x^a} \cdot g_{th}(\theta) \cdot g_{th}(0)^{-1} \cdot e^{-\xi_{\theta z}^{rh} \wedge \theta_{\theta z}^{rh}} \dots e^{-\xi_{\theta x}^{rh} \wedge \theta_{\theta x}^{rh}} \cdot n =$$

$$e^{\xi_{13}^\wedge \theta_{13}} \dots e^{\xi_{17}^\wedge \theta_{17}} \cdot n \quad (5.60)$$

$$a' = e^{\xi_{13}^\wedge \theta_{13}} e^{\xi_{14}^\wedge \theta_{14}} \cdot n' \xrightarrow{P-K-2} \theta_{13}, \theta_{14} \quad (5.61)$$

Finally, by rotating “q” around the axis of the angles θ_{16} and θ_{17} , the Paden Kahan 2 sub-problem is obtained again, so those angles are obtained:

$$e^{-\xi_{15}^\wedge \theta_{15}} \dots e^{-\xi_{13}^\wedge \theta_{13}} e^{-\xi_{\theta_z}^a \wedge \theta_{\theta_z}^a} \dots e^{-\xi_x^a \wedge \theta_x^a} \cdot g_{th}(\theta) \cdot g_{th}(0)^{-1} \cdot e^{-\xi_{\theta_z}^{rh} \wedge \theta_{\theta_z}^{rh}} \dots e^{-\xi_{\theta_x}^{rh} \wedge \theta_{\theta_x}^{rh}} \cdot q =$$

$$e^{\xi_{16}^\wedge \theta_{16}} \cdot e^{\xi_{17}^\wedge \theta_{17}} \cdot q \quad (5.62)$$

$$b' = e^{\xi_{16}^\wedge \theta_{16}} e^{\xi_{17}^\wedge \theta_{17}} \cdot q \xrightarrow{P-K-2} \theta_{16}, \theta_{17} \quad (5.63)$$

The same steps should be made to compute the inverse kinematics of the left arm. At this time, the whole body kinematics of the humanoid robot Rh-1 is obtained. We must take into account that the arms have 5 DOF, so it is not possible to reach any goal in space. That fact will be clarified in the simulation results, when the arm is making a gesture. That motion is limited, because the objective of this humanoid prototype is to walk, the arm motion is not the main research fact.

It is necessary to clarify the relationship between the spatial patterns (COG, hands and feet references) and the inverse kinematics in order to compute the joint angles. Each point of the spatial patterns, at any time, is the input of the inverse kinematics algorithm. These algorithm, should be executed in each step, in the current local axis.

5.7.5 Inverse dynamics

In order to compute the joint torques and dynamics constraints, a dynamic model should be proposed (Arbulu et. al., [14]). Thus the Lagrange formulation (Lagrangian) under the lie groups and screw theory has been developed, because it gives us a natural description of a Jacobian manipulator and accurate dynamic computation. The Lagrange formulation could be expressed as follows:

$$L(\theta, \dot{\theta}) = K(\theta, \dot{\theta}) - V(\theta) \quad (5.64)$$

where $K(\theta, \dot{\theta})$ is the overall links kinetics energy contribution and $V(\theta)$ the potential one:

$$K(\theta, \dot{\theta}) = \sum_{i=1}^n K_i(\theta, \dot{\theta}) = \frac{1}{2} \dot{\theta}^T M m(\theta) \dot{\theta} \quad (5.65)$$

$$V(\theta) = \sum_{i=1}^n V_i(\theta) = \sum_{i=1}^n m_i g h_i(\theta) \quad (5.66)$$

with the motion equation by Γ torques being the following:

$$\frac{d}{dt} \left(\frac{\partial L}{\partial \dot{\theta}} \right) - \frac{\partial L}{\partial \theta} = \Gamma, \quad (5.67)$$

which could be expressed as the follows:

$$M.m(\theta) \cdot \ddot{\theta} + N(\theta, \dot{\theta}) = \Gamma \quad (5.68)$$

Thus, $M.m(\theta) \in \Re^{n \times n}$ is the inertial manipulator matrix and it is defined by the operational Jacobian manipulator J_{tli} and the inertial generalized matrix M_i as:

$$M.m(\theta) = \sum_{i=1}^n J_{tli}^T(\theta) \cdot M_i \cdot J_{tli}(\theta) \quad (5.69)$$

The humanoid robot platform Rh-1 has 21 DOF's, Cabas et. al. 2006 [36] and the HRP-2 Kaneko et. al. 2004 [70] has 28 degrees of freedom, and consequently $M.m(\theta) \in \Re^{21 \times 21}$ and $M.m(\theta) \in \Re^{28 \times 28}$ respectively. The angular acceleration vector is defined by $\ddot{\theta}$, (which has the angular acceleration of each joint). Thus the joints torque without potential forces has been made by $M.m(\theta) \cdot \ddot{\theta}$. For each link, we define the frame attached to its COG (L_i); so, from the floating base T (i.e, for the right leg, see Fig. 5.19, the treatment for the upper body is the same. In order to generalize, external forces are taken into account, such as ground friction and ground reaction). The Jacobian manipulator is computed as follows:

$$J_{tli}^T(\theta) = [\xi_1^\dagger \dots \xi_i^\dagger \dots 0 \dots 0] \quad (5.70)$$

where:

$$\xi_j^\dagger = Ad_{\left(e^{\xi_j^\wedge \cdot \theta_j} \dots e^{\xi_i^\wedge \cdot \theta_i} \cdot g_{tli}(0)\right)}^{-1} \xi_j \quad \forall \quad j \geq i \quad (5.71)$$

The Ad_g is composed by the translation vector “ p ” and “ R ”, which is the trochoid of extreme point (“ l_i ”) turning around base (“ t ”), such as the 6×6 matrix:

$$Ad_g = \begin{bmatrix} R & \hat{p}R \\ 0 & R \end{bmatrix} \quad (5.72)$$

The “g” transformation being as following:

$$g_{tli}(\theta) = e^{\xi_1^\wedge \theta_{12}} \cdot e^{\xi_1^\wedge \theta_{11}} \dots e^{\xi_i^\wedge \theta_i} \cdot g_{tli}(0) \quad (5.73)$$

When the generalized inertia matrix is expressed by:

$$M_i = \begin{bmatrix} m_i \cdot Id & 0 & I_{xzi} & I_{xzi} \\ 0 & I_{xi} & I_{xyi} & I_{xzi} \\ & & I_{yi} & I_{yzi} \\ & & & I_{zi} \end{bmatrix} \quad (5.74)$$

The kinetic energy of each link could be detailed as follows. When the velocity is compared to the mobile body “t” (COG):

$$\begin{aligned} K_i(\theta, \dot{\theta}) &= \frac{1}{2} (V_{tli}^t)^T \cdot M_i \cdot V_{tli}^t \\ K_i(\theta, \dot{\theta}) &= \frac{1}{2} \dot{\theta}^T \cdot J_{tli}^T \cdot M_i \cdot J_{tli} \cdot \dot{\theta} \end{aligned} \quad (5.75)$$

When m_i is the mass, I_{xi} , I_{yi} and I_{zi} are the inertia moments and I_{xyi} , I_{xzi} and I_{yzi} the inertia products of the link “i”. The matrix “Id” is the identity matrix.

The $N(\theta, \dot{\theta})$ term gives us the joints torque due to the potential forces, and is defined as (5.76):

$$N(\theta, \dot{\theta}) = \frac{\partial V}{\partial \theta} \quad (5.76)$$

From (5.66):

$$V(\theta) = \sum_{i=1}^n m_i g h_i(\theta) \quad (5.77)$$

Where m_i is the mass of the i -th link, g is the gravity acceleration and $h_i(\theta)$ the COG height of the i -th link. More details of the forward/inverse kinematic and forward/inverse dynamic modelling will be shown in a journal paper.

As an example, a 3 DOF manipulator inverse dynamic should be detailed in order to illustrate the algorithm (Fig. 5.20)

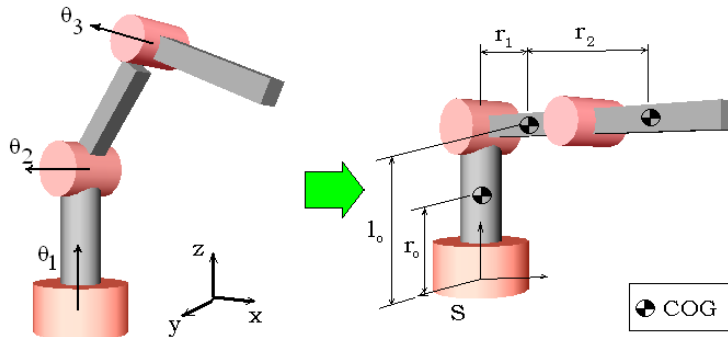


Figure 5.20: Manipulator with three degrees of freedom.

By the frame attached to the COG of the link “i”, we define the coordinates with respect to the “S” frame as:

$$C_1 = \begin{pmatrix} 0 \\ 0 \\ r_O \end{pmatrix}, C_2 = \begin{pmatrix} r_1 \\ 0 \\ l_O \end{pmatrix}, C_3 = \begin{pmatrix} r_1 + r_2 \\ 0 \\ l_O \end{pmatrix} \quad (5.78)$$

After that, the system for analysis is as follows:

$$\begin{aligned} g_{sC_1}(0) &= \begin{bmatrix} Id & C_1 \\ 0 & 1 \end{bmatrix} \\ g_{sC_2}(0) &= \begin{bmatrix} Id & C_2 \\ 0 & 1 \end{bmatrix} \\ g_{sC_3}(0) &= \begin{bmatrix} Id & C_3 \\ 0 & 1 \end{bmatrix} \end{aligned} \quad (5.79)$$

And the generalized inertia matrix:

$$M_i = \begin{bmatrix} m_i.Id & 0 & 0 \\ 0 & I_{xi} & 0 \\ 0 & 0 & I_{yi} \\ 0 & 0 & I_{zi} \end{bmatrix} \quad (5.80)$$

Next the Jacobian body manipulator is expressed by:

$$J_1 = J_{sC_1}^b(0), J_2 = J_{sC_2}^b(0), J_3 = J_{sC_3}^b(0) \quad (5.81)$$

The inertia matrix of the manipulator could be computed as:

$$Mm(\theta) = J_1^T \cdot M_1 \cdot J_1 + J_2^T \cdot M_2 \cdot J_2 + J_3^T \cdot M_3 \cdot J_3 = \begin{bmatrix} M_{11} & M_{12} & M_{13} \\ M_{21} & M_{22} & M_{23} \\ M_{31} & M_{32} & M_{33} \end{bmatrix} \quad (5.82)$$

With the last computations, it is possible to compute the inertial generalized torque vector (Γ'') as:

$$Mm(\theta) \cdot \ddot{\theta} = \Gamma'' \quad (5.83)$$

Finally, the potential effect could be computed by:

$$V(\theta) = m_1.g.h_1(\theta) + m_2.g.h_2(\theta) + m_3.g.h_3(\theta) \quad (5.84)$$

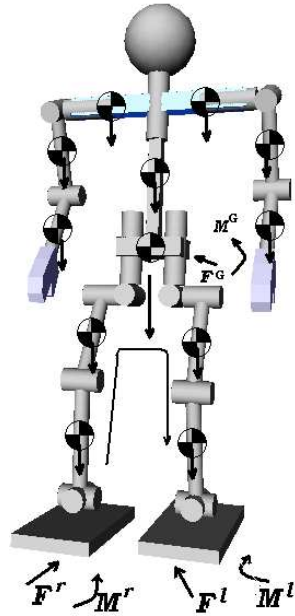


Figure 5.21: Rh-1 mass distribution for dynamics modelling.

Where:

$$\begin{aligned} h_1(\theta) &= r_0 \\ h_2(\theta) &= l_0 - r_1 \cdot \sin \theta_2 \\ h_3(\theta) &= l_0 - (r_1 + r_2) \cdot \sin \theta_2 - r_2 \cdot \sin(\theta_2 + \theta_3) \end{aligned}$$

And the potential generalized torque (Γ') for all the joints is expressed by:

$$N(\theta, \dot{\theta}) = \frac{\partial V}{\partial \theta} = \begin{bmatrix} 0 \\ -(m_2.g.r_1 + m_3.g.(r_1 + r_2)) . \cos \theta_2 - m_3.g.r_2 . \cos(\theta_2 + \theta_3) \\ -m_3.g.r_2 . \cos(\theta_2 + \theta_3) \end{bmatrix} = \Gamma' \quad (5.85)$$

The same idea is applied to the Rh-1 humanoid robot platform (Fig. 5.21).

5.8 Layer 5: Off-line control

In order to cover the mechanics, terrain imperfections and dynamical simplifications, the gait control is necessary to achieve like stable walking. It is very important that the humanoid robot performs like its dynamic model. In our case, as we have constrained the dynamics to a concentrated mass model, the whole body dynamic and potential effects should be compensated by the controller. In order to compensate the dynamics effects off-line, it is possible to feedback the multibody ZMP as a second loop in the preview control [63] another way is by forward dynamics, Siciliano et. al. 2008 [105]. Another contribution of this thesis is the off-line control by compensation of the dynamics and effect of gravity from the motion capture walking motion. A suitable single dynamic model is proposed in this case, based on the inverted pendulum with spring model. The on-line gait control proposed by Honda Mo. Co., [53] takes into account three loops: the reaction force control, the ZMP control and the landing foot control. That is a guide for achieve stable walking. Another proposal is to combine the off-line walking patterns with real-time modification, it is an interesting approach for achieving stable walking and saving computation time of the on-line patterns, Huang et. al. 2000 [59]. Although it is not implemented yet in the Rh-1 humanoid robot, it will be explained for future works. This chapter is divided as following: Off-line control models are described and the proposal is detailed. The next section deals with on-line control.

Experimentally, the off-line control gait allows for walking around four dynamic steps, because the dynamical robot model has many simplifications constrained to the mass concentrated model. It is demonstrated that similar results are obtained with multibody dynamics modelling. That is, because the joint flexion structure is not taken into account (rigid dynamics), the vertical moment, impact force and friction are not accurately modeled. Any way, it is possible to reduce the online control ranges by off-line control.

State-of-the-art off-line control

This kind of control takes into account the whole body dynamics of the robot. One approach [105] deals with the forward dynamics modelling. In this case, the whole body dynamics is taken into account all the time. The high computation time cannot be implemented in real time pattern generation. Another one deals with the feedback of the ZMP multi-body as another preview control loop [63]. The second one concentrates the mass in a point; that way, it is possible to be

implemented as an online pattern generation.

Off-line control proposition

In this work, the innovative off-line compensation is proposed by compensating the gravity, dynamic effects and mechanical flexion on each joint (i.e. ankle and hip joints). The considerable deviations are in the single support phase; thus, this model is only used in that phase. The methodology is as follows: the robot is going to walk without any compensation. Next, the hip motion on a real robot is captured (Fig. 5.22). After that, this motion is modelled as an inverted pendulum with spring, which could be used in sagittal and frontal planes, as shown in Fig. 5.23.

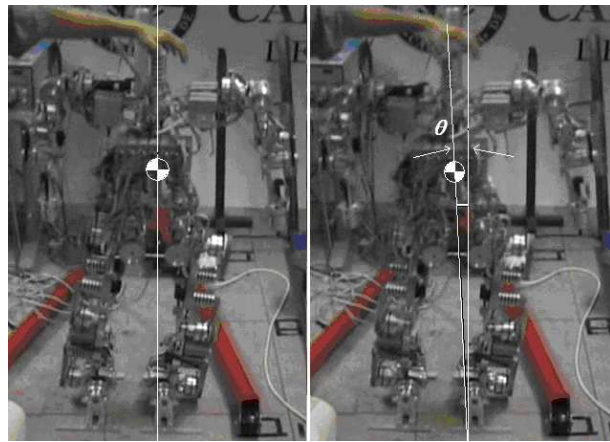


Figure 5.22: Flexion frontal angle “ θ ” due to the dynamics and effects of gravity.

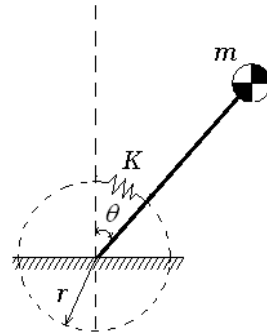


Figure 5.23: Inverted pendulum with spring.

This model could be described as the following equations (Fig. 5.24):

$$F_K = K \cdot r \cdot \theta \quad (5.86)$$

$$x = l \cdot \sin \theta \quad (5.87)$$

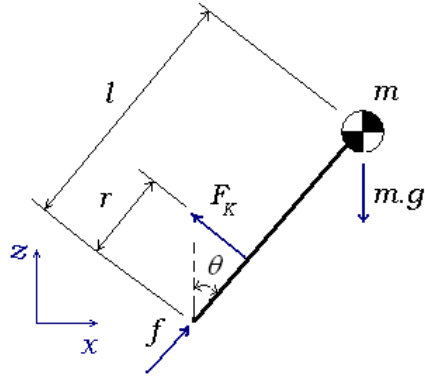


Figure 5.24: Inverted pendulum with spring-free body diagram.

$$z = l \cdot \cos \theta \quad (5.88)$$

The dynamic equation is as follows:

$$-F_K \cdot \cos \theta = m \cdot \ddot{x} \quad (5.89)$$

$$F_K \cdot \sin \theta - m \cdot g = m \cdot \ddot{z} \quad (5.90)$$

We are interested in compensating the “ θ ” angle each time, so for each little angle, we should apply the above physical equations. This way eq. 5.89 with eqs. 5.87 and 5.86 give us the next relationship:

$$K \cdot r \cdot \theta = m \cdot l \cdot \ddot{\theta} \quad (5.91)$$

Where:

$$\ddot{\theta} = \frac{K \cdot r}{m \cdot l} \theta \quad (5.92)$$

Experimentally, we notice that the horizontal displacement causes the robot to fall down, so the “x” direction is analyzed. The vertical one is not affected by the dynamics, only by the gravity as a constant.

An interesting relationship is found when the angle does not depend on the gravity, only the spring constant (K), spring force position (r), mass (m) and COG (l) position, where “K” and “r” could be computed heuristically.

By solving equation 5.92, the θ temporal equation obtained is:

$$\theta(t) = \theta_i \cosh\left(\frac{t - t_i}{T_\theta}\right) + T_\theta \dot{\theta}_i \sinh\left(\frac{t - t_i}{T_\theta}\right) \quad (5.93)$$

$$\dot{\theta}(t) = \frac{\theta_i}{T_\theta} \sinh\left(\frac{t - t_i}{T_\theta}\right) + \dot{\theta}_i \cosh\left(\frac{t - t_i}{T_\theta}\right) \quad (5.94)$$

And the time constant is:

$$T_\theta = \sqrt{\frac{m.l}{K.r}}$$

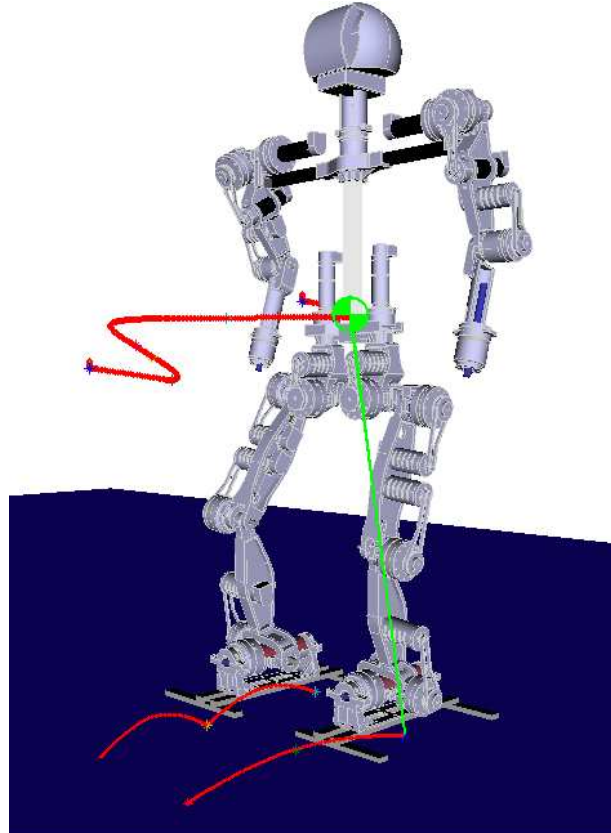


Figure 5.25: Humanoid robot walking as a rigid body. The COG (green) follows the 3D-LIPM reference (red). The feet follow the splines references, too.

While the humanoid robot is walking as a rigid body, the spatial COG motion follows the 3D-LIPM, Cart-table or any other pattern as a COG reference (Fig. 5.25), but experimentally the robot joints and terrain imperfections do not allow following that reference.

The pattern generated by any concentrated mass model is corrected at the start of single support phase.

As shown in Fig. 5.22, on starting the single support phase, the robot rotates around the support foot to the middle; this rotation is due to the ankle and hip frontal joint which do not support the inertial and gravitational forces of the robot mid in air, because these joints are not rigid.

Those effects must be compensated in order to achieve stable walking. This compensation corrects the robot's attitude and the ZMP position.

We divide the robot joint patterns into the single and double support phases, so on starting the single support phase, the compensation must start by maintaining the position and velocity continuity. For example, to compensate the

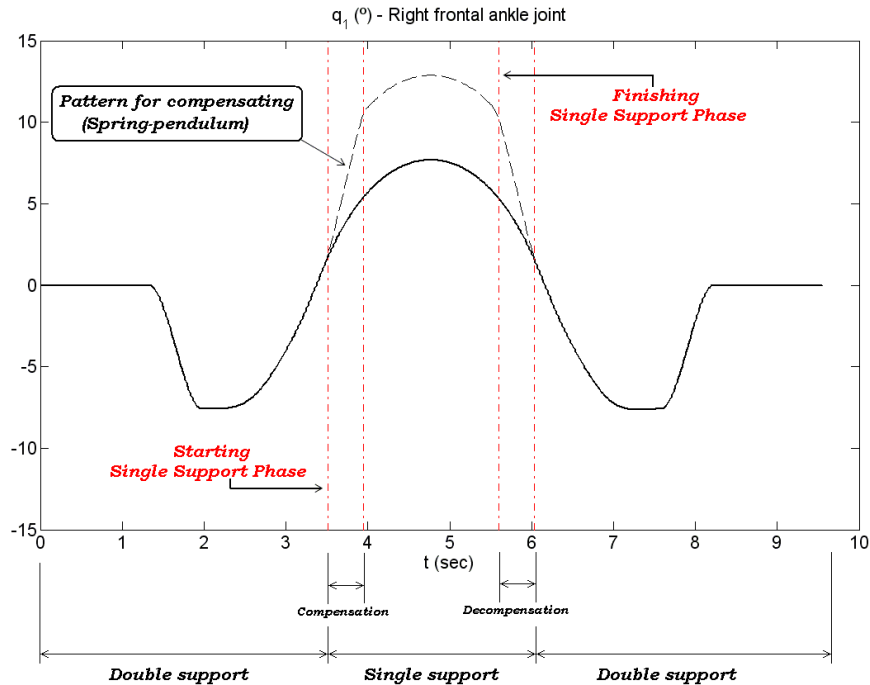


Figure 5.26: The theoretical pattern (bold black line) and the compensated pattern (dashed black line) of the right frontal ankle joint: q_1 . In the single support phase, the COG follows the 3D-LIPM, cart-table or another one, with combination of the pendulum with spring to compensate the defects of inertia, gravity, mechanics and terrain.

frontal motion, the frontal ankle joints could be used as shown in Fig. 5.26 and Fig. 5.27. The pattern for compensating is computed by the dynamics of the spring pendulum model described above (Fig. 5.23).

After the single support phase, we should decompensate the joint patterns because in the double support phase, the robot performs as theoretical reference patterns. In order to have an idea of the spatial displacement of the robot by the compensation, we compute the forward kinematics to measure the spatial COG and feet displacement with the compensation patterns (i.e., Fig. 5.28). This additional COG displacement is necessary in order to compensate for the dynamics, gravity, structural and terrain imperfections to achieve stable walking motion, because it allows us to perform the ZMP in the support polygon and the attitude in the right position.

The real robot follows close to the theoretical COG pattern by applying the compensation. That way, the pendulum with spring model is validated, because the additional joint rotation is canceled by the structural flexion.

As it is shown in the experimental results in Fig. 5.29, the Rh-0 humanoid robot could walk with the compensation proposed above. In the chapter of results, it will be detailed that at least four steps can be taken. After that, the actual humanoid dynamics makes the humanoid fall down. More factors as

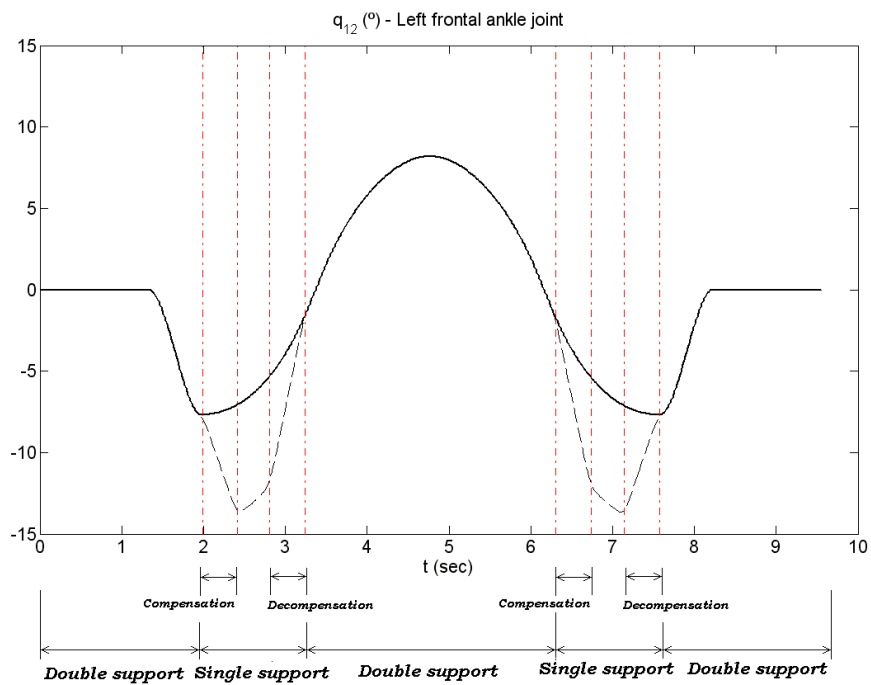


Figure 5.27: The theoretical pattern (bold black line) and the compensated pattern (dashed black line) of the left frontal ankle joint: q_{12} .

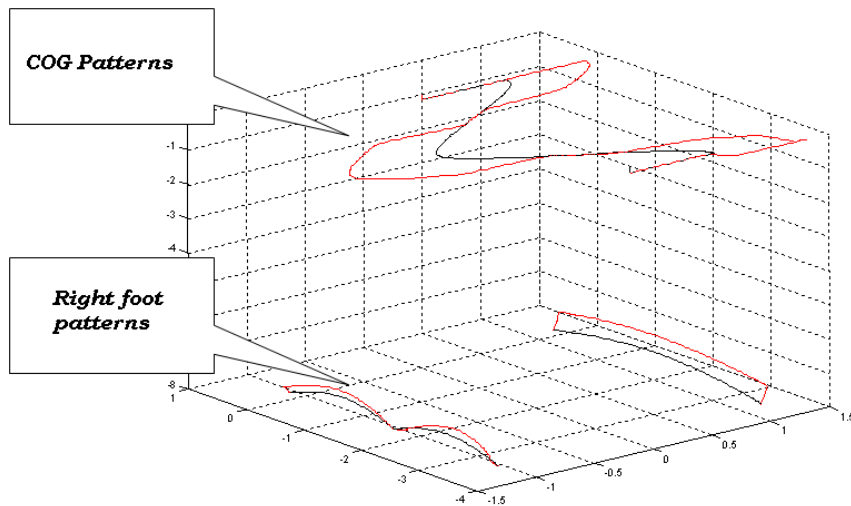


Figure 5.28: The theoretical COG spatial pattern (black line) and the compensated pattern (red line). Feet patterns are shown, too.

the synchronization sensors, terrain imperfections, friction, non rigid mechanics, and a little slide of the ankle joints do not allow the robot to move in a stable

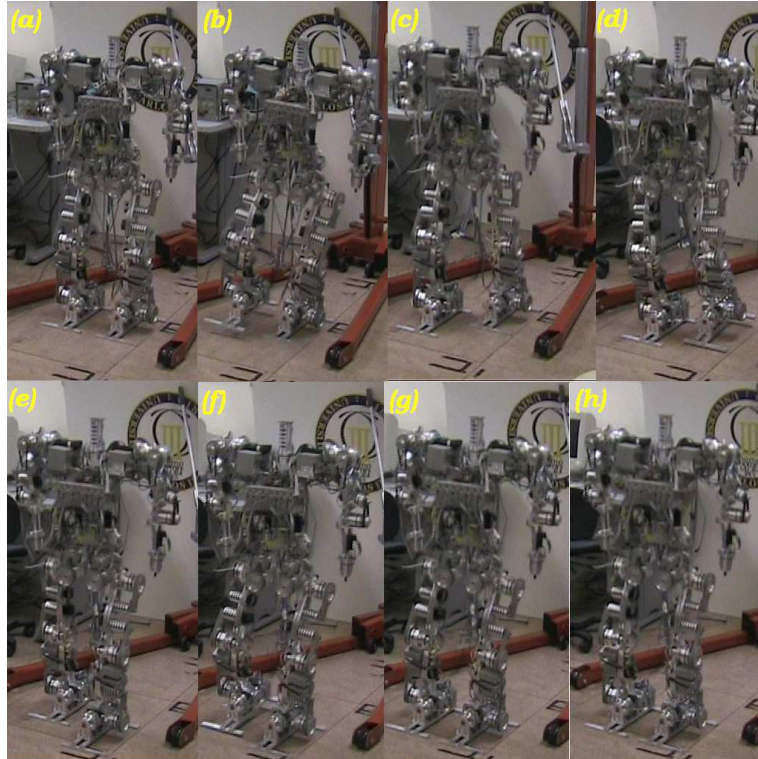


Figure 5.29: Rh-0 humanoid robot walking with the proposed compensation.

motion.

So, the compensation method is validated for taking few steps.

That way, it is not enough to compensate for the off-line control, so on-line control is necessary. It will be described in other work.

5.9 Acyclic Gait

This section presents, the main contribution of this thesis in the humanoid robot field; some gait should be developed for the humanoid robot (see Arbulu et. al., 2008 [19]). The preview control of the ZMP method is used, and will be demonstrate successful results. In this study, the preview gain for each dynamic transition, from any stage to another, should be taken into account; because the COG of the robot could change its vertical position (Z_c) during the transition. Whole-body humanoid dynamics must be taken into account in this case, because the humanoid links will change their configuration in space at any time. As such the inertial and gravitational effects could cause the humanoid to fall down, due to the acyclic motion. As a strategy, it is possible to take those effects to compensate the acyclic motion, like increasing the swing foot velocity, compensating each arm motion, yawing, tilting and rolling the body to compensate the total momentum of the humanoid motion. This is one way that acyclic motion is different from standard walking motion when the COG is moving in a plane. It will be shown that the preview gains for two different

vertical positions of the COG are quite similar to each other; thus, it is possible to consider the medium vertical position value of the preview gain (the value for \bar{Z}_c) in order to generate the dynamically stable transition. That one is between two generic stages; that is why, one asynchronous step should be generated.

5.9.1 Related work

The gait motion planning for a humanoid robot to walk on any surface has many solutions; many take into account the concentrated mass model [64] and others the distributed mass model, furthermore considering friction [57]. The first work does not deal with the effect of whole-body motion while the humanoid is walking, because when the robot is walking, it is always upright and its arms are stretched vertically, so the arm motion doesn't disturb the walking motion considerably. Anyway, it is a cyclic motion, and the motion pattern could be generated in real-time, but the dynamic effect of the whole-body inertial forces and gravity are compensated by the controller. The second work deals with the whole-body motion while the robot is walking, taking into account as strong stability criteria that the sum of the contact wrench should be inside the contact wrench cone. It is a more accurate model but the high computation cost and the iterative solution do not make it possible to generate the patterns in real time; successful simulation experiments have been shown but no natural motion is obtained. To go from any posture to another by a step (which we call "acyclic gait"), the whole-body motion should be taken into account in order to maintain the dynamic stability. Many works about humanoid robot whole-body motion have been carried out, some dealing with the control of linear and angular momentum [65],[66],[46]. This approach used in spatial robotics, Yoji et. al. 1989 [116] gives us an interesting whole-body motion control by controlling the linear and angular momentum, so it is a 6x1 vector which shows us the macroscopic performance of the robot, no matter how complicated it is. From the point of view of a highly redundant robot dividing the whole-body motion in tasks, and taking into account the external forces acting on the robot, see Khatib et. al. [74], Sentis et. al. [104] and Mansard and Chaumette [82]. These works divide whole-body motion into tasks and create a hierarchy, thus different hypotheses are taken into account, such as projecting the secondary tasks in the operational space of the prior ones. Successful results have been obtained and it may be one of the global ways to solve our problem. The path planning methods are an alternative to generating whole body motion, Kuffner et. al. 2003 [78], Koga et. al. 1994 [77] in the case of avoiding obstacles. This is not our case. Other criteria at the kinematic level are proposed by Yoshida et. al. 2006 [129] when the hierarchy of tasks is obtained by the combination of a joint selection matrix and projection in the null-space. Dynamic stability while walking is obtained by ZMP Preview control, Kajita et. al. 2003 [63], Verrelst et. al. 2006 [117], Wieber et. al. 2006 [124], Katayama et. al. 1985 [71]. Whole-body motion is developed by the generalized inverse kinematics under the Jacobian method. Another approach, proposed by Terada et. al. 2007 [111] can treat vertical COG oscillation by using Dynamical 3D-Symmetrization. This method symmetrizes dynamic characteristics of vertical motion and horizontal motion by constraining the vertical COG motion with a differential equation. This method can solve for the equations of motion which involve vertical COG oscillation. This can allow the generation of various gaits such as running and

dancing. The validity of the proposed method is demonstrated on a simulated robot, but only simulation results are achieved with this method. We propose an approach by solving the whole-body motion in a direct and natural way with the screw theory, Murray et. al. 1994 [86], Arbulu et. al. 2005 [17]. This chapter is divided as follows: at first, we formulate the problem statement; next, the proposed solution is detailed; after that, the results are shown and discussed as an application in the HRP-2 humanoid robot, Kaneko et. al. 2004 [70], and finally, the conclusions and future works will be explained.

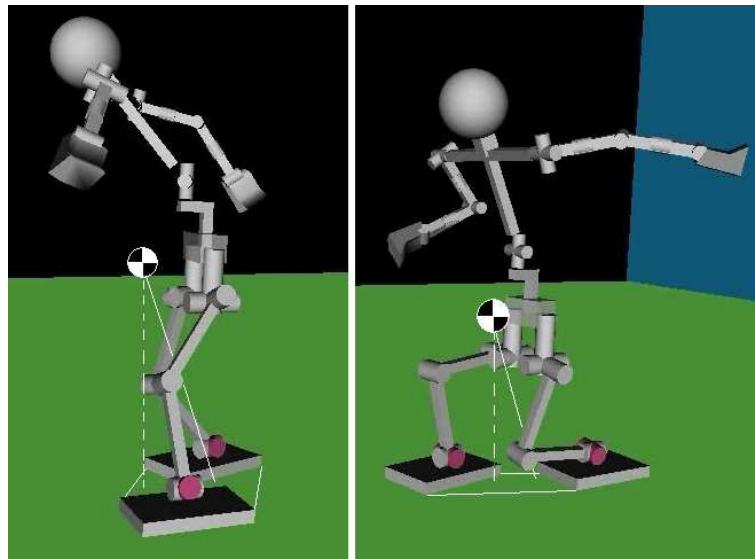


Figure 5.30: Motion from any statically stable posture to another one.

5.9.2 Problem Statement

The problem arises when it is necessary to move the humanoid robot from any statically stable position to another. In both cases, the center of gravity (COG) position is known and it is projected onto the support polygon. Furthermore, the initial and final whole-body configuration, that is, the feet, hip, hands and neck positions and orientation, is known, too (see Fig. 5.30). Thus, the ZMP, Vukobratovic et. al. 2004 [118] must be inside the support polygon while the robot is moving. It is easy to see that the boundary conditions are known but the transition from the initial state to the final one is unknown. This work proposes an approach in order to meet that requirement: solving the whole body motion with screw theory.

5.9.3 Overview of the Method

The free motion under the field of gravity should be made (because only the force of gravity is acting on the robot), from any posture to another (Fig. 5.31). The kinematics and dynamics modelling under screw theory, Paden-Kahan sub-problems and Lie groups are used [86], [17], [92]. Those theories allow us to

compute the inverse kinematics directly without internal singularities and dynamics modelling, Abraham et. al. 1987 [8] by using the natural Jacobian manipulator.

Hence, the input values are the initial and goal robot joint states. At first, we use the forward kinematics in order to compute the footprints and initial COG and goal configurations. The local axis gait algorithm is used (Arbulu et. al. 2007 [12]) for the motion planning which takes into account constraints such as joint angular limits and torque limits. Dynamic stable motion is obtained by the ZMP Preview control [63]. By using inverse kinematics, the joint legs motion are computed. Next, the inverse dynamics with the Lagrangian formulation is computed to check the joint torques of the dynamic motion.

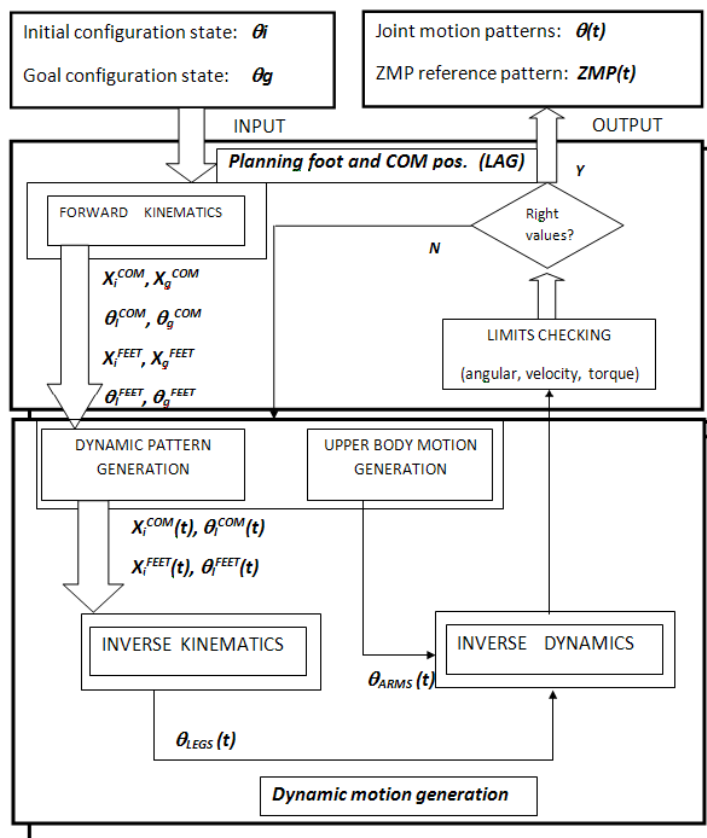


Figure 5.31: Flowchart of the method. X_i and X_g , are the initial and goal position, and θ_i and θ_g are the initial and goal orientation. Those are computed for the COG and feet by the forward kinematics.

The lower body motion has been detailed in the chapter on gait generation. Here we should detail the upper body and afterwards the whole body motion generation.

5.9.4 Upper body motion

The upper body is composed of a tree structure system, that is, the chest, neck and arms. In order to generate the respective motion and maintain dynamic stability, the multibody ZMP should be inside the support polygon. It is not so easy as the normal walking motion when the whole body could be simplified as a pendulum mass, because the whole body motion is made in symmetric way. However, it should be possible to generate the upper body motion by dynamically compensating the arm motion, taking into account their momentum: the next subsection deals with this subject. In that way, the whole body could be simplified as a pendulum, or a cart-table model. In this work, the upper body motion takes into account this fact. So, the chest, neck and arm motion are computed in order to minimize the disturbance effect, due to their asynchronous motion, while the robot is taking the step. The respective trajectories are calculated in the joint space, because it is a free motion, by using 7th order splines which allows us to directly control the joint limit restrictions like angles, angular velocities, angular accelerations and jerks. Therefore, the splines that have been used could be described by eq. 5.95 for any joint of the upper body (see Fig. 5.32).

$$\theta_i^u(t) = w_8^u t^7 + w_7^u t^6 + w_6^u t^5 + w_5^u t^4 + w_4^u t^3 + w_3^u t^2 + w_2^u t + w_1^u \quad (5.95)$$

When the boundary conditions are (i.e. for the i^{th} – link):

- T : Step time
- θ_i^u : Initial angular position
- ω_i^u : Initial angular velocity
- α_i^u : Initial angular acceleration
- j_i^u : Initial angular jerk
- θ_f^u : Final angular position
- ω_f^u : Final angular velocity
- α_f^u : Final angular acceleration
- j_f^u : Final angular jerk

Therefore, from the boundary conditions, the splines coefficients could be expressed as follows (eqs. 5.96 to 5.103):

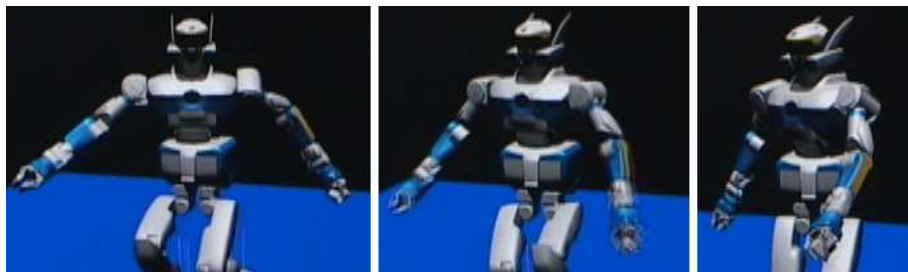


Figure 5.32: The upper body motion as an asynchronous way.

$$w_1^u = \theta_i^u \quad (5.96)$$

$$w_2^u = \omega_i^u \quad (5.97)$$

$$w_3^u = \frac{1}{2} \alpha_i^u \quad (5.98)$$

$$w_4^u = \frac{1}{6} j_i^u \quad (5.99)$$

$$\begin{aligned} w_5^u &= \frac{35}{T^4} (\theta_f^u - \theta_i^u) - \frac{1}{T^3} (15\omega_f^u + 20\omega_i^u) + \\ &\quad \frac{5}{T^2} \left(\frac{1}{2} \alpha_f^u - \alpha_i^u \right) - \frac{1}{3T} \left(\frac{1}{2} j_f^u + 2j_i^u \right) \end{aligned} \quad (5.100)$$

$$\begin{aligned} w_6^u &= -\frac{84}{T^5} (\theta_f^u - \theta_i^u) + \frac{1}{T^4} (39\omega_f^u + 45\omega_i^u) - \\ &\quad \frac{1}{T^3} (7\alpha_f^u - 10\alpha_i^u) + \frac{1}{T^2} \left(\frac{1}{2} j_f^u + j_i^u \right) \end{aligned} \quad (5.101)$$

$$\begin{aligned} w_7^u &= -\frac{70}{T^6} (\theta_f^u + \theta_i^u) - \frac{1}{T^5} (34\omega_f^u + 36\omega_i^u) + \\ &\quad \frac{1}{2T^4} (13\alpha_f^u - 15\alpha_i^u) - \frac{1}{T^3} \left(\frac{1}{2} j_f^u + \frac{2}{3} j_i^u \right) \end{aligned} \quad (5.102)$$

$$\begin{aligned} w_8^u &= -\frac{20}{T^7} (\theta_f^u - \theta_i^u) + \frac{10}{T^6} (\omega_f^u + \omega_i^u) - \\ &\quad \frac{2}{T^5} (\alpha_f^u - \alpha_i^u) + \frac{1}{6T^4} (j_f^u + j_i^u) \end{aligned} \quad (5.103)$$

5.9.5 Whole body motion

As for lower body motion, the Preview controller of the ZMP could be used. As studied before in chapter 4, the preview gain “ $G_p(j)$ ” for two different hip levels (Z_c) is computed in order to find the control variable “ $u(k)$ ”, eq. 5.104.

The values obtained are shown in Figure 5.33, which performs in a similar way with different “ Z_c ” values, so it is possible to compute the Preview gain value (“ $G_p(j)$ ”) for the median of “ Z_c ”, that is for the median hip height between the initial and final postures of the humanoid robot, which will walk the “acyclic gait”.

$$u(k) = -G_i \sum_{i=0}^k e(k) - G_x x(k) - \sum_{j=1}^{N_L} G_p(j) p^{ref}(k+j) \quad (5.104)$$

In order to compensate for the inertial effect of the upper body, an extension of LAG algorithm by including the overall humanoid body dynamics is proposed. Thus, the actual multibody ZMP is taken into account as feedback for correcting

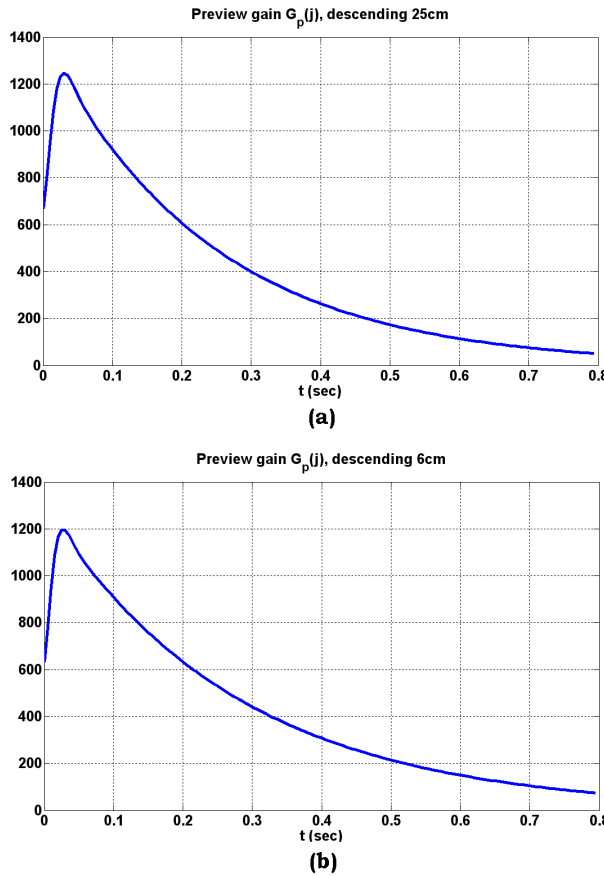


Figure 5.33: Preview gain $G_p(j)$: (a) $Z_c=0.614\text{m}$, (b) $Z_c=0.814\text{m}$ ($T=5\text{ ms}$, $Q_e=1.0$, $Q_x=0_{3 \times 3}$, $R=1.0 \times 10^{-6}$).

the COG pattern. This way, two preview controls could be used, one for tracking the error of the ZMP between the reference and the multibody ZMP, and another preview control for tracking the ZMP reference. The result is the COG pattern obtained, which is composed by the difference of the first and second loop states (Fig. 5.34).

When computing the ZMP multi body, an approximation that includes overall body dynamics is by computing the total linear and angular momentum. This kind of solution could be expressed as follows:

$$p_x^{mult} = \frac{mgx + p_z \dot{P}_x - \dot{L}_y}{mg + \dot{P}_z} \quad (5.105)$$

$$p_y^{mult} = \frac{mgy + p_z \dot{P}_y + \dot{L}_x}{mg + \dot{P}_z} \quad (5.106)$$

When:

$$P = [P_x \ P_y \ P_z]^T : \text{Total linear momentum}$$

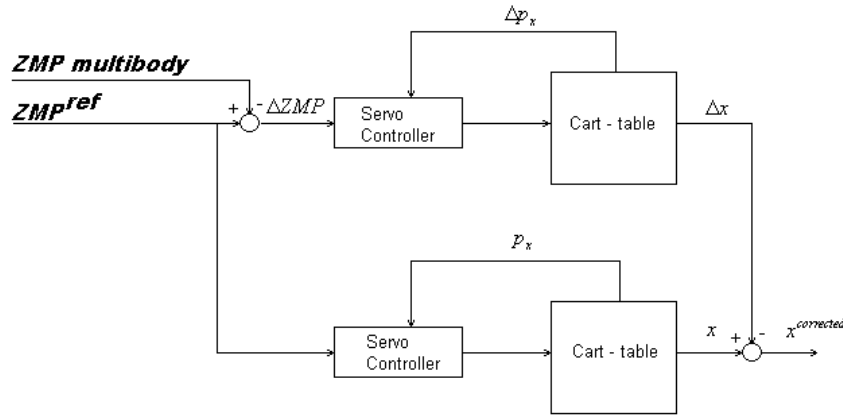


Figure 5.34: COG planning by compensating with the multi body ZMP

$$L = [L_x \ L_y \ L_z]^T : \text{Total angular momentum}$$

$$g = [0 \ 0 \ -g]^T : \text{Gravity vector}$$

$$c = [x \ y \ z]^T : \text{Center of mass position}$$

$$m : \text{total mass}$$

The ZMP multibody, eqs. (5.105), (5.106), allows us to know the real ZMP of the humanoid robot, and from the preview control implemented (Fig. 5.34), it is possible to correct the COG pattern in order to maintain stability while the robot is changing its posture.

An example of swing foot vertical motion, is shown in the Fig. 5.35, as it is seen the ZMP is always inside the support foot sole boundary, during the single support phase.

As an example, Fig. 5.36 shows two acyclic steps of the HRP-2 humanoid robot platform.

The dynamic transition, during the single support phase, is achieved by the cart-table model. This model maintain the ZMP in stable zone on each step. So, it could be used for generating acyclic steps.

Additional correction could be made by other cart-table loop, which take into account the whole-body dynamics of the humanoid robot, so the COG motion compensates that dynamics.

In the next chapter, successful results will validate the proposed method, which could be used with any humanoid robot.

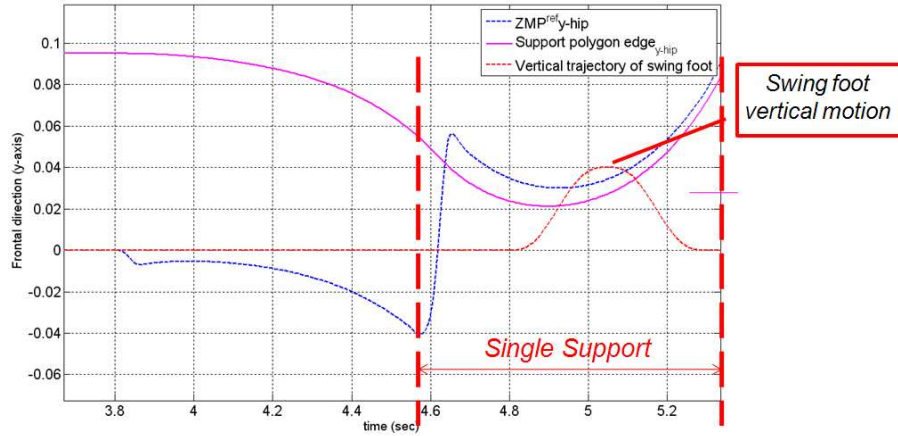


Figure 5.35: One acyclic step. The ZMP trajectory on frontal plane with respect to the COG is always inside the support foot sole boundary. The swing foot motion is made while the ZMP is inside the foot sole boundary.

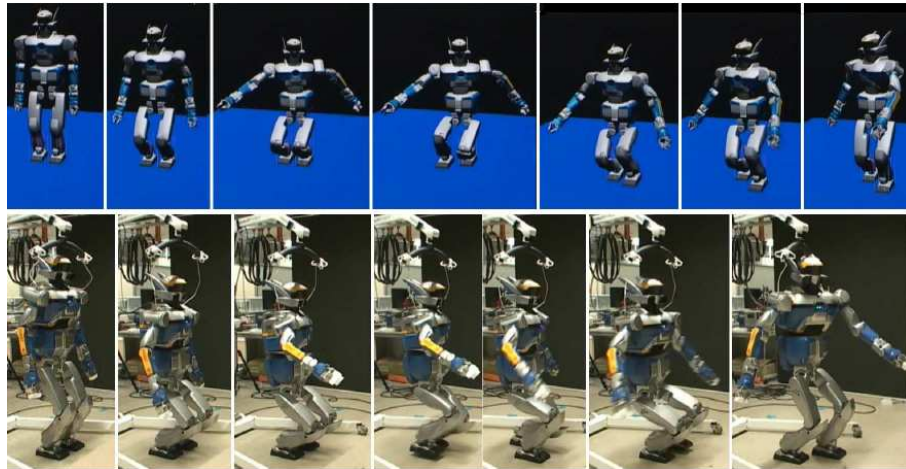


Figure 5.36: Two acyclic steps.

Conclusions

The walking pattern generation method has been detailed in this chapter, which is composed of five layers. Each of them is obtained by dividing the problem into lower ones. The main contributions of this chapter are: proposing and validating the “Local Axis Gait” algorithm (Arbulu et. al.) for generation of local motion planning. The alternative kinematics and dynamics modelling are validated in the Rh-1 and HRP-2 humanoid robot platforms. Implementing and validating the use of screws provides a very geometric description of rigid motion, so the analysis of the mechanism is greatly simplified. Furthermore, it is possible to make the same mathematical treatment for the different robot joints: revolute and prismatic. We propose and validate the kinematics modelling of hu-

manoid robots using screw theory and Paden-Kahan sub-problems, which have the following advantages:

- *Avoiding singularities because of the global description of the rigid body motion; we only need to define two frames (base and tool) and the rotation axis of each DOF to analyze the kinematics in a closed way.*
- *The Paden-Kahan sub-problems allow computing the inverse kinematics at position level.*
- *Faster computation time of the inverse kinematics with respect to the inverse jacobian method, Euler angles or D-H parameters, so it contributes to real-time applications.*

We propose and validate the dynamics modelling of humanoid robots using the screw theory and Lagrange method, which have the following advantages:

- *To compute the Jacobian is not necessary to derivate, only a set of matrix transformations is needed (including the twists).*
- *The Lagrange method allows to solve the equations in a closed form and it is possible to make detailed analyses of the systems' properties.*

With this research, the walking pattern generation method is validated with the Rh-1 humanoid robot and alternative ability is proposed in the HRP-2 humanoid robot platform. It is called “Acyclic gait”, and it is achieved by using the ZMP preview control method, it has been detailed in the last section. The “Acyclic gait motion” of humanoid robots could be a challenge of input design parameters of the robot, motion patterns and control system, because, if the humanoid robot could walk in any way, it would be easier to achieve the standard gait. Expanding the joint angle ranges, previously in the humanoid design phase could be achieved by this kind of gait. A method dealing with non-cyclic planar footstep motion with different body configuration is proposed. It is validated by several simulations and experimental results on the humanoid robot HRP-2. The kinematics proposed is also valid. Hence, the Lie groups, screw theory and Paden-Kahan sub-problems prove to be suited to the kinematics and dynamic humanoid robot modeling, which avoids internal singularities and gives us a direct analytical solution. The ZMP Preview Control method appears to be robust enough to be applied even in this case, in which the height of the COM varies in order to generate dynamically stable acyclic motion patterns. Future work is focused in complementing the method with auto-collision avoidance in order to constrain the motion to physical limits automatically and also to improve the compensation of vertical momentum on rotation motion. In summary, the main contributions of this chapter are validating the “Local Axis Gait” algorithm (Arbulu et. al. 2007) for generation of local motion planning and validating the ZMP preview control (Kajita et. al. 2003) to generate acyclic gait motion, which has the following advantages:

- *Predicts stable ZMP position based on mass concentrated model without taking into account the whole body humanoid configuration.*
- *The mass concentrated model allows generating walking patterns in real time.*

Chapter 6

Results

History will never accept difficulties as an excuse.
(J. F. Kennedy)

The proposed algortihms are validated suscessfully in two humanoid robot platforms: Rh-1 and HRP-2. The Rh-1 humanoid robot platform was developed under the direction of Prof. Carlos Balaguer, in the Robotics lab of the University Carlos III of Madrid, Spain (National Spanish Project funding by the CYCIT DPI2004-00325). The second platform, the HRP-2 humanoid robot platform was developed by Kawada Industries Inc. and the AIST, in Japan (National Japanese Project, HRP). Suscessfull results have been obtained and these will be shown in this chapter. In this chapter at first, the Rh-1 and HRP-2 humanoid robot platforms specifications will be shown. Secondly, simulations and experimental results of walking pattern generation method proposed including “the acyclic gait” will be shown and discussed.

6.1 Rh-1 specifications

The Rh-1 humanoid robot developed in the Roboticslab of the University Carlos III of Madrid (Fig. 6.1), is about 1.35m tall and weights 50 Kg. (Fig. 6.2). It has 21 degrees of freedom (see Table 6.1) distributed in its legs, arms and waist. The joint angular ranges of the Rh-1 humanoid robot are quite similar to the human, except for some range due to mobility requirements. Some angles are not possible for a human and some of them are not for the robot (see Table 6.2). Cantilever type structure is used on the hip joints to obtain wide range motion. The structure is designed with aeronautical aluminium, which is strong and light material. The mechanical transmission system is composed of a flat harmonic drive and belt transmission in order to create a compact design. It has onboard hardware, inertial sensors, a camera including batteries, and a wireless connection with the work station; its autonomy is about 30 min. and it can perform with an external supply. The software is custom-designed for integrating the hardware devices, which include communications, sensor management and control system. The cover was designed mainly to hide and protect the hardware, and also to improve aesthetics of the humanoid robot. This first prototype can walk up to 0.7 Km/h, as we will show in the experimental results. Furthermore, it can respond to voice and gesture commands by using a USB microphone and a cammera placed on its head. Its camera can compute the orientation distance of the user in order to compute the suitable motion for approaching him. The Rh-1 can speak to the user saying things, such as greetings or his name, finish any task or recognize the user by the vision system, which interacts with a face database. The gesture recognition system can speak to the user, which is the current user gesture. With the arms, the Rh-1 can make some gestures, too.

As will be demonstrated, the motion pattern algorithms proposed in this thesis have been successfully tested in this humanoid robot platform.

Link	Number of DOF	Total
Head	-	-
Waist	1 (Yaw)	1
Arm	4	4x2
Shoulder	1 (Pitch)	
	1 (Roll)	
Elbow	1 (Pitch)	
Wrist	1 (Roll)	
Leg	6	6x2
Hip	1 (Yaw)	
	1 (Roll)	
	1 (Pitch)	
Knee	1 (Pitch)	
Ankle	1 (Pitch)	
	1 (Roll)	
		21

Table 6.1: Rh-1 humanoid robot degrees of freedom.



Figure 6.1: Rh-1 humanoid robot.

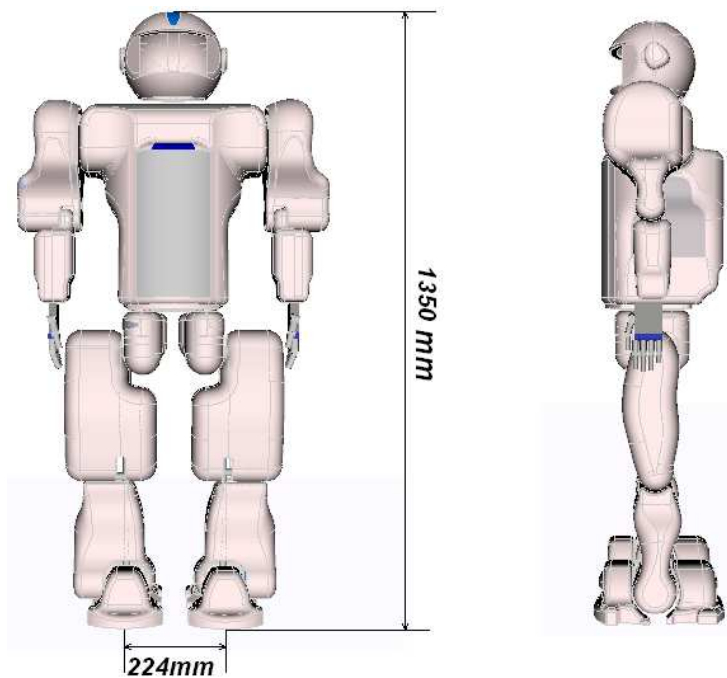


Figure 6.2: Rh-1 humanoid robot dimensions.

A simulator software was designed in order to test the walking patterns before the real robot. This simulator has a VRML environment when the joint,

Joint	Human angular range	Rh-1 angular range
Head	-50 to 50 (Roll)	-
	-50 to 60 (Pitch)	-
	-70 to 70 (Yaw)	-
Arm		
Shoulder	-90 to 0 (Roll)	-95 to 0 (Roll)
	-180 to 50 (Pitch)	-180 to 60 (Pitch)
	-90 to 90 (Yaw)	-
Elbow	-145 to 90 (Pitch)	-135 to 0 (Pitch)
	-90 to 90 (Yaw)	-
Wrist	-55 to 25 (Roll)	-90 to 90 (Roll)
	-70 to 90 (Pitch)	-
Hand	0 to 90 (Pitch)	-16 to 60 (Pitch)
Waist	-50 to 50 (Roll)	-
	-30 to 45 (Pitch)	-
	-40 to 40 (Yaw)	-45 to 45 (Yaw)
Leg		
Hip	-45 to 20 (Roll)	-20 to 20 (Roll)
	-125 to 15 (Pitch)	-80 to 80 (Pitch)
	-45 to 45 (Yaw)	-15 to 15 (Yaw)
Knee	0 to 130 (Pitch)	0 to 100 (Pitch)
Ankle	-20 to 30 (Roll)	-20 to 20 (Roll)
	-20 to 45 (Pitch)	-25 to 25 (Pitch)

Table 6.2: Rh-1 humanoid robot angular joint ranges vs human angular joint ranges.

velocity and torque limits can be verified. At first, the tests started around 2005, and “static gait” was tested with the humanoid without main control computers, batteries or cover-mounted onboard. Walking motion in many directions has been developed and successfully validated on different surfaces. However, the walking velocity was low, about 20 sec. per step. The next year, in 2006, mechanical, walking pattern generation and control improvements allow it to walk about 20 times faster than the previous year, about 0.7 Km/h (1.25 sec. per step). In 2007, more mechanical, walking patterns improvements and batteries, control computers and mounted cover increased the humanoid weight about 15 Kg., so the robot weight 48.5 kg. Successful walking motion results have been obtained when movement is in a straight direction.

6.2 HRP-2 specifications

Kaneko et. al. 2004 ([70]) describes the HRP-2 humanoid robot as following: HRP-2 is a humanoid robotics platform, which has been developed in phase two of HRP. HRP was a humanoid robotics project which was run by the Ministry of Economy, Trade and Industry (METI) of Japan from 1998FY to 2002FY for five years. The ability of the biped locomotion of the HRP-2 is improved so that the HRP-2 can cope with an uneven surface, can walk at human speed, and can

walk on a narrow path. The ability of whole body motion of the HRP-2 is also improved so that the HRP-2 can get up by itself if it tips over safely.



Figure 6.3: HRP-2 humanoid robot.

Link	Number of DOF	Total
Head	2	2
Waist	1 (Yaw)	2
	1 (Pitch)	
Arm	6	6x2
Shoulder	1 (Pitch)	
	1 (Roll)	
	1 (Yaw)	
Elbow	1 (Pitch)	
Wrist	1 (Roll)	
	1 (Pitch)	
Leg	6	6x2
Hip	1 (Yaw)	
	1 (Roll)	
	1 (Pitch)	
Knee	1 (Pitch)	
Ankle	1 (Pitch)	
	1 (Roll)	
		30

Table 6.3: HRP-2 humanoid robot degrees of freedom.

The HRP-2 humanoid robot (Fig. 6.3, Table 6.3) dimensions are: 1.539m

Joint	Human angular range (deg)	HRP-2 angular range (deg)
Head	-50 to 50 (Roll)	-
	-50 to 60 (Pitch)	-30 to 45 (Pitch)
	-70 to 70 (Yaw)	-45 to 45 (Yaw)
Arm		
Shoulder	-90 to 0 (Roll)	-95 to 10 (Roll)
	-180 to 50 (Pitch)	-180 to 60 (Pitch)
	-90 to 90 (Yaw)	-90 to 90 (Yaw)
Elbow	-145 to 90 (Pitch)	-135 to 0 (Pitch)
	-90 to 90 (Yaw)	-
	-55 to 25 (Roll)	-
Wrist	-70 to 90 (Pitch)	-90 to 90 (Pitch)
	0 to 90 (Pitch)	-16 to 60 (Pitch)
	-50 to 50 (Roll)	-
Hand	-30 to 45 (Pitch)	-
	-40 to 40 (Yaw)	-45 to 45 (Yaw)
	-	-
Leg		
Hip	-45 to 20 (Roll)	-35 to 20 (Roll)
	-125 to 15 (Pitch)	-125 to 42 (Pitch)
	-45 to 45 (Yaw)	-45 to 30 (Yaw)
Knee	0 to 130 (Pitch)	0 to 150 (Pitch)
Ankle	-20 to 30 (Roll)	-20 to 35 (Roll)
	-20 to 45 (Pitch)	-75 to 42 (Pitch)

Table 6.4: HRP-2 humanoid robot angular joint ranges vs. human angular joint ranges.

tall, 0.621m wide and 0.355m of deep. Its weight including batteries is 58 kg. It can walk up to 2.5 Km/h.

To make a human feel friendly towards an HRP-2, an external appearance for the HRP-2 was designed by Mr. Yutaka Izubuchi, who is a mechanical animation designer famous for his robots that appear in Japanese anime, including the well-known “Pat labor” (stands for Patrol Labor).

The design concepts of HRP-2 are lightness, compactness, with performance for application tasks like cooperative work in the open air. To realize the HRP-2, several distinctive mechanisms are employed.

The design policy for the movable range of each joint is the same as that employed by the HRP-2P. First, we designed that to be about the same as that of a standard human so that a humanoid robot performs human tasks as well as a human. Table 6.4 shows the data on the movable range of the head, right arm, right hand, waist, and right leg of a standard human.

HRP-2 inherits the cantilever type structure from its leg module HRP-2L, [69] and its prototype HRP-2P. The reason is that the cantilever type structure, which enables the robot to have fewer collisions between both inside upper limbs and enables it to cross its legs, brings following advantages to HRP-2. One advantage is that this structure is suitable to prevent the tipping over. By shaping the support polygon, which is made of supported legs (or a single

supported leg). The cantilever type structure enables the robot to have a wide landing point area for the swinging leg and can appropriately shape the support polygon for the phase of double-supported legs by selecting the landing point of the swing leg. Crossing legs further enables the support polygon to be on the opposite side of supported leg.

The other advantage is that this structure permits a cross-legged walk such as a walk on a balance beam. The HRP-2 would be able to pass, even if walking paths are narrow and limited.

The HRP-2 inherits the waist joint from the HRP-2L and the HRP-2P, since the waist joint also brings several advantages. One is that the HRP-2 can get up by it-self by using a waist joint with 2 D.O.F. (pitch axis and yaw axis), Kanehiro et. al. 2003 [68]. Another is that HRP-2 can be lithe in build. The lither the upper body is, the smoother its gait is. Another is that the moment generated in the yaw axis of the HRP-2 can be suppressed by using waist motion. This compensation is applied for high-speed walks. Furthermore, the waist joint extends the working space of the arms. Although the HRP-2 has 6 D.O.F. in each arm and 1 D.O.F. in each hand, waist motion gives redundancy to the arm motion.

In the electrical design for the HRP-2, several efforts for a light weight and the realization of a compact body were adopted as well as the HRP-2P. In addition, the electrical system of the HRP-2 was designed with great care to achieve reliability compared with that of the HRP-2P.

The HRP-2 has two CPU boards in the body. One of them is utilized for the real-time controller of whole body motion, while the other is utilized for non-real-time control system including the VVV software system and the sound system. Although these computer systems seem to be the same as those of HRP-2P, almost all the boards were renewed for reliability in HRP-2.

The type of bus is a PCI bus that has become the most popular bus in the field of industry. Another renewed board is a CPU board, though the exclusive CPU board was not developed for the HRP-2. It is the selected CPU board, which is based on Pentium III and has a sound function on the market. Since the sound board used in the computer system of HRP-2P became useless, a more compact-sized computer system was achieved in the HRP-2.

6.3 Simulation and Experimental results

Many simulations and experimental results could validate the gait generation algorithms proposed in Chapter 5. In order to test the algorithms before that in the humanoid robot, many simulations have been made to assure stable walking, joint angles and torque constraints.

6.3.1 Simulation results on the Rh-1 humanoid robot platform

The simulation results applying the gait generation algorithms under the “Local axis gait” that is the local planning walking pattern method are shown and validated in the actual humanoid robot, previously applying the proposed off-line control.

$L_x(m)$	$L_y(m)$	$L_z(m)$	$\theta_x(deg)$	$\theta_y(deg)$	$\theta_z(deg)$
0	0.224	0	0	0	0
0.180	0.224	0	0	0	20
0.180	0.224	0	0	0	40
0.180	0.224	0	0	0	60
0.180	0.224	0	0	0	80
0.180	0.224	0	0	0	100
0.180	0.224	0	0	0	120
0.180	0.224	0	0	0	140
0.180	0.224	0	0	0	160
0.100	0.224	0	0	0	180
0.180	0.224	0	0	0	200
0.180	0.224	0	0	0	220
0.150	0.224	0	0	0	240
0.180	0.224	0	0	0	260
0.180	0.224	0	0	0	280
0.120	0.224	0	0	0	300
0.180	0.224	0	0	0	320
0.180	0.224	0	0	0	340
0.180	0.224	0	0	0	320
0.180	0.224	0	0	0	300
0.180	0.224	0	0	0	280
0.180	0.224	0	0	0	260
0.180	0.224	0	0	0	240
0.180	0.224	0	0	0	220
0.180	0.224	0	0	0	200
0.180	0.224	0	0	0	220
0.180	0.224	0	0	0	240
0.180	0.224	0	0	0	260
0.180	0.224	0	0	0	280
0.180	0.224	0	0	0	300
0.180	0.224	0	0	0	300
0	0.224	0	0	0	300

Table 6.5: Walking parameters for taking many steps and changing direction.

As an example, the humanoid rotates around a circular path. After that, changing direction is shown in Fig. 6.4 and Fig. 6.5. The “Local axis gait” algorithm allows the robot to walk in smooth walking patterns while changing direction and swing foot configuration (i.e., step length, step width, foot landing orientation). The input parameters for taking the steps are shown in Table 6.5. That is the foot displacement in each direction (L_x , L_y , L_z) and the rotation in each direction (θ_x , θ_y , θ_z), which define the boundaries of the walking patterns (see Chapter 5, section 5.4.2). In the Table, the orientation changes on each step and some of the steps change their length. Furthermore, those boundaries must be constrained to the physical limits of the humanoid robot, such as joints ranges, angular joint velocities and joint torques.

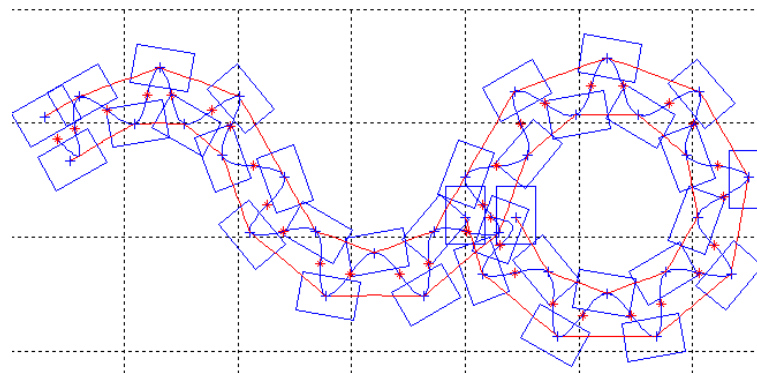


Figure 6.4: Walking patterns under the LAG algorithm. The blue rectangles are feet, the COG motion (blue patterns) and the feet motion (red patterns).

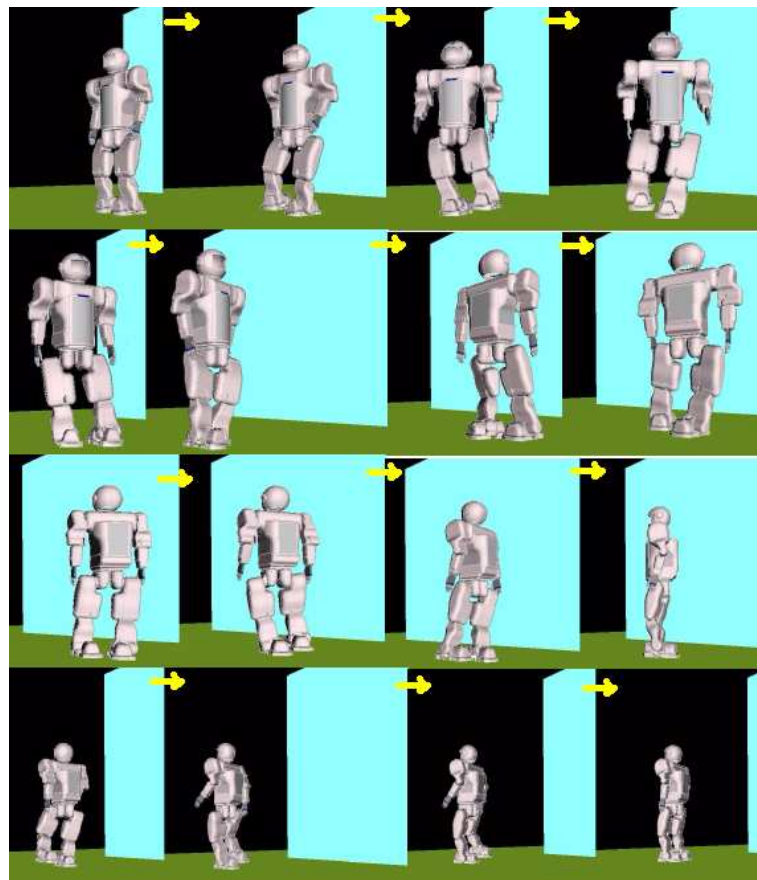


Figure 6.5: Snapshots of the Rh-1 walking under the LAG algorithm.

This simulator could compute the joint patterns, velocities and torques in order to verify the humanoid robot constraint, before applying those joint patterns to the real robot.

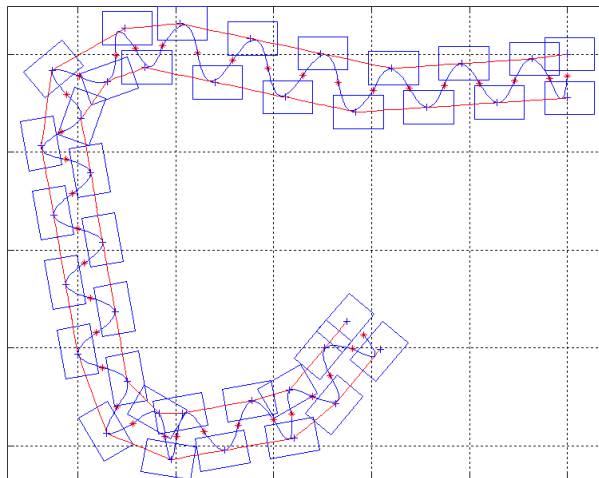


Figure 6.6: Walking patterns under the LAG algorithm.

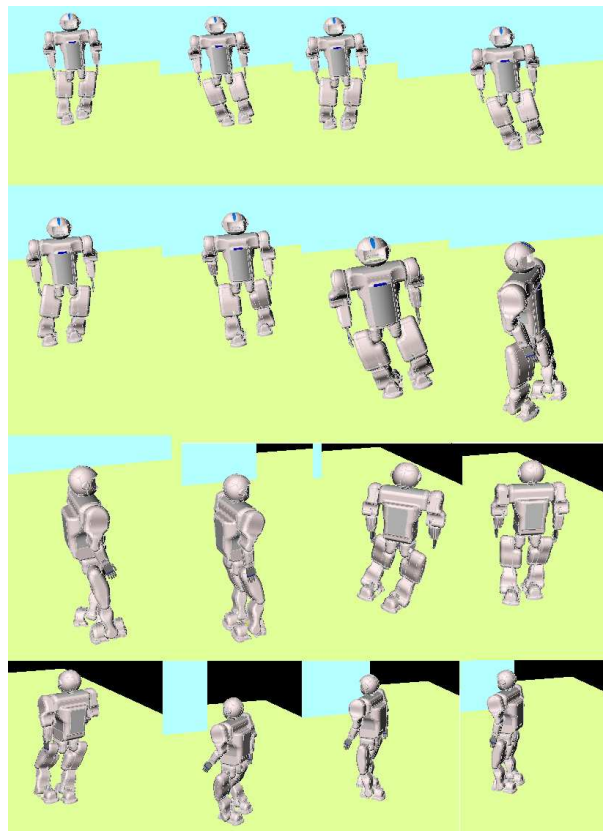


Figure 6.7: Snapshots of the Rh-1 walking under the LAG algorithm.

The self and outside collision are taken into account in order to avoid humanoid robot damages. Figs. 6.4 and 6.5 validate the algorithm proposed in

order to generate walking patterns.

Another example is shown in Figs. 6.6 and 6.7. In this case, diagonal motion is followed. After that, the diagonal direction is changed. Next, the robot turns left, walks straight, turns left again and walks straight.

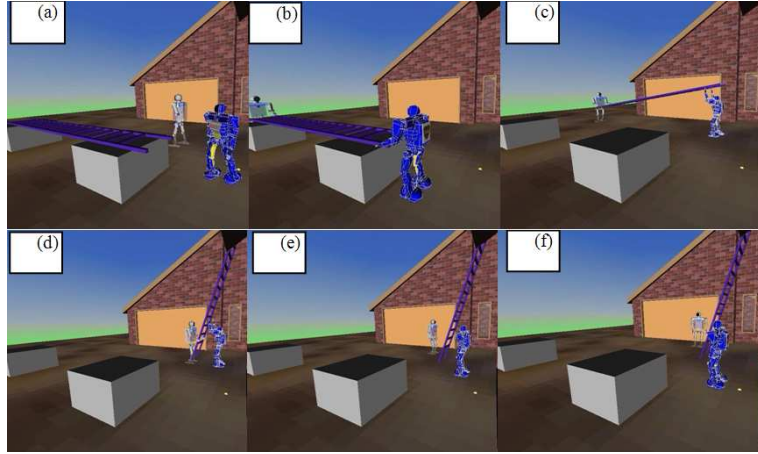


Figure 6.8: The Rh-1 working in cooperation with a human carrying a construction ladder. (a) approaching. (b) grasping. (c) giving. (d) leaving. (e) and (d) back to the rest position.

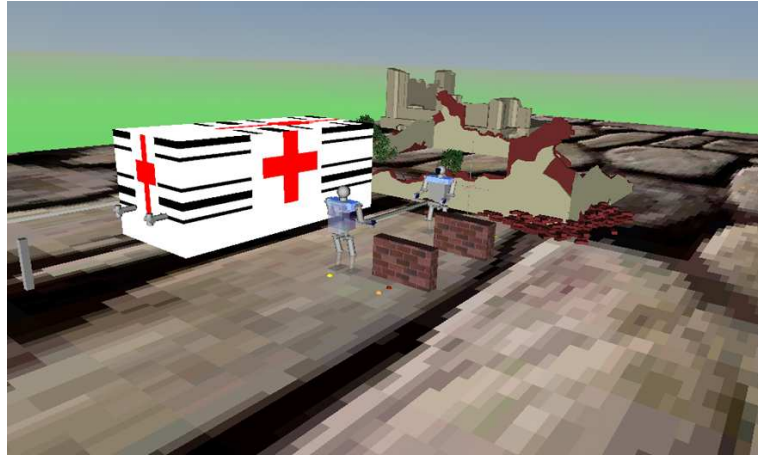


Figure 6.9: Cooperation in disaster cases. In this case, the walking pattern and control system must deal with rough terrain during working cooperation tasks. Therefore, strong stability criteria such as the CWC could be used to prevent the humanoid from tipping over.

In the Rh-1 simulator, some cooperation works have been implemented in order to project robot cooperation abilities. (Arbulu et. al. 2008, [13]). For example, the human-humanoid robot cooperation carrying a construction ladder. Some snapshots are shown in Fig. 6.8; another example is in disaster cases (Fig. 6.9).

6.3.2 Experimental results on Rh-1 humanoid robot platform

In this sub-section, many experimental results, developed in the Rh-1 humanoid robot platform will be shown, such as: static gait, dynamic gait, a gesture with arm. So, the proposed walking pattern generator method is validated successfully. Some results have been shown in the IURS 2006 Robotics Summer School on Humanoid Robots, by the Prof. Carlos Balaguer [22].

1. Static gait

Some experimental results will be discussed, whose have been obtained on the Rh-1 humanoid robot platform in 2005 by Arbulu et. al., [17]. As examples, the Rh-1 walking forward and turning left will be shown.

1.1 Walking forward

At first, the static gait is evaluated, in this case, the Rh-1 humanoid robot is walking forward with velocity about 0.0468Km/h, length of step $L_x = 0.13m$ and the results are shown (Fig. 6.10).

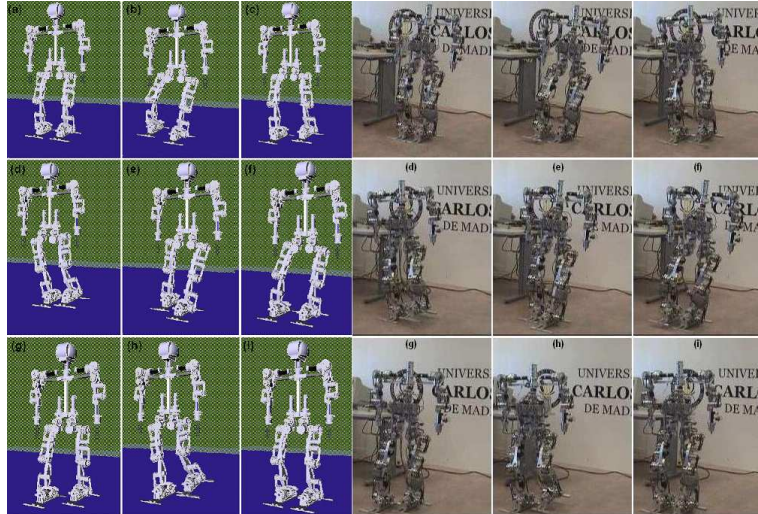


Figure 6.10: VRML simulation and the Rh-1 without cover, static gait taking four steps forward.

The swing foot overlaps with the support foot due to the elasticity of the structure. This is compensated with the roll axis of the ankle and hip before landing the swing foot. Fig. 6.11 shows measured joint trajectories, the angular velocity and the motor current (Fig. 6.12) of the right leg for three walking steps forward. They are very similar to the theoretical ones, which validate the developed kinematic algorithms based on the Lie logic, at least during the balancing phase. The difference of those joint angle plots is due mainly to the following facts: firstly, control while walking is an open loop, so we use some reference points to adjust each joint rotation; secondly, the elasticity of

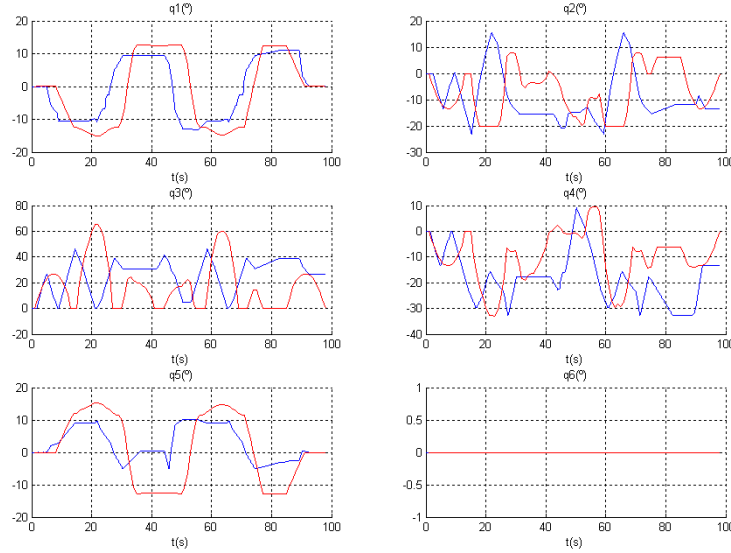


Figure 6.11: Angular patterns of overlapped right leg joints. The red are ones the measured patterns and the blue ones are the reference patterns.

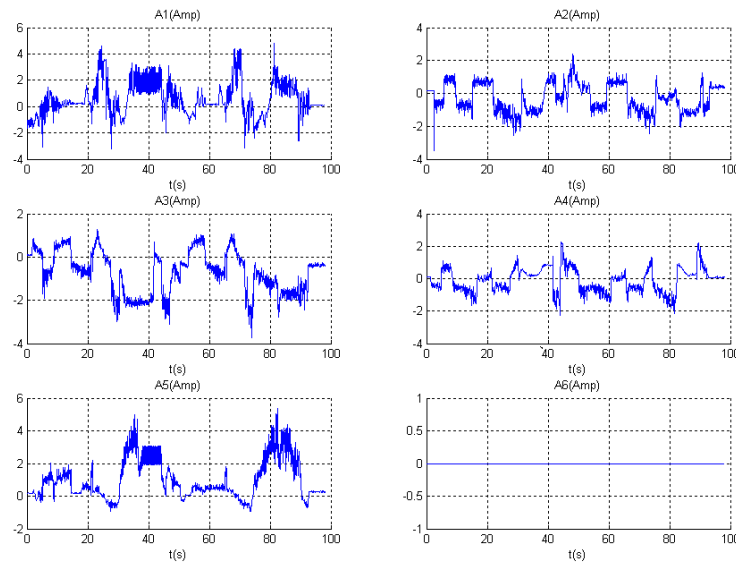


Figure 6.12: Current of the right leg joints.

the structure is not considered while computing the reference joint trajectories. The velocity plots are not smooth (Fig. 6.11), due to the angle interpolators, but the ZMP is in the right position because the robot walks slowly; one step takes about 20 seconds.

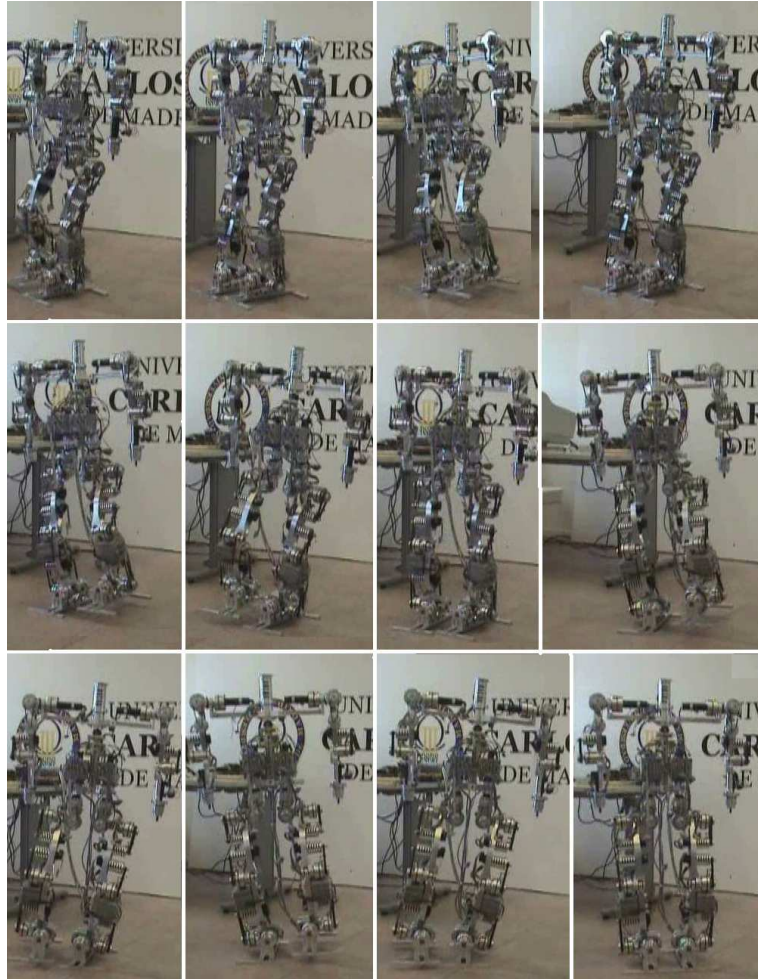


Figure 6.13: Snapshots of gait rotating on the vertical axis.

1.2 Turning left

Another example is the walking test rotating around its vertical axis, which allows the robot to change direction any time. In this case, the θ_z angle is about 15 degrees, and the velocity of rotation about 1 deg/sec. The step length about $L_x = 0.10m$ and the lateral foot motion about $L_y = 0.10m$; the maximum height of the swing foot is about 0.10m, which increases the angular velocity of the knee joint, so it should be reduced. The time for one step is about 10 sec. Successful results have been obtained in the laboratory and on open air terrain (Fig. 6.13). Until now, static patterns have been tested and validated in the Rh-1 humanoid robot platform. The advantages of the static gait is that the impact forces from the walking terrain are reduced considerably, as well as the inertial and gravitational effects on each joint, because the whole structure performs like an elastic one, so the attitude control could be exercised with open loop as a single geometric relationship. Furthermore, walking stability is controlled by positioning the COG on the support foot.

2. Dynamic gait

The dynamic walking patterns are based on ZMP stability control. Our results were obtained in 2006, (Arbulu et. al. [16]) with structural improvements allowing the humanoid to walk from 0.35 Km/h to 0.7 Km/h.

2.1 Walking at 0.35Km/h

Three steps forward obtained at 0.35Km/h with dynamic walking pattern. The inverted pendulum model, under the gravity field, drives the COG humanoid trajectory smoothly and at natural motion.

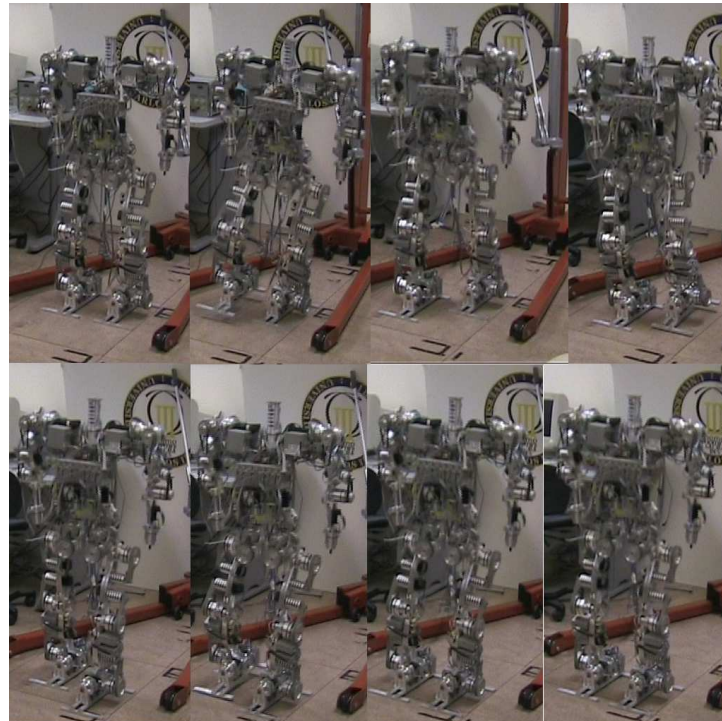


Figure 6.14: Three steps by dynamic walking patterns under the LAG algorithm, at 0.35Km/h.

The mass concentrated model is used, proposed by Kajita et. al. [64], [63], following the “Local Axis gait” algorithm [12], described in Chapter 5. The first experiment with dynamic walking patterns is shown in Fig. 6.14, when the step length is $L_x = 0.180m$, the maximum height of the swing foot is 0.04m and the walking speed is about 0.35 Km/h. The reference COG and foot patterns, shown in Fig. 6.15, allow a smooth and natural walking motion.

The reference and actual leg joint patterns, the actual angular velocities and the currents for this experimental test are shown in Figs. 6.16 to 6.19. In Fig. 6.16, the reference joint patterns are overlapped with the compensated ones. In this case, the off-line compensation is delayed (the compensation time) from the first step, because in order to follow the mass concentrated model all

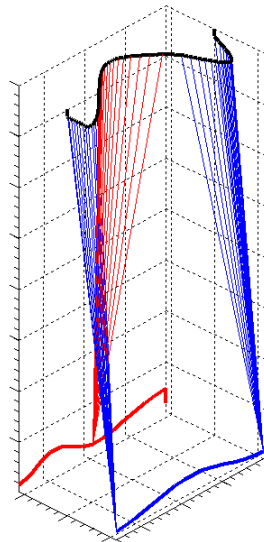


Figure 6.15: Walking reference patterns. COG pattern (black line), right foot (red line) and left foot (blue line).

the time, some joints stop during the compensation time (for about 0.5 sec). Experimentally, this compensation is not evident.

In Fig. 6.17, the compensated reference joint patterns and the actual ones are overlapped in order to check the joint controllers. As you can see, the reference joint patterns are followed with few errors due to the dynamics of the whole robot body, but it is enough to obtain stable walking.

Next, Fig. 6.18 shows the actual angular joint velocities for checking the motors velocity limits.

Finally, in the Fig. 6.19, the actual joint currents are shown. These currents give us information about the joints more loaded, because the current is proportional to the joint torques.

In summary, the more loaded joints are located in the ankles and the knees. At starting the single support phase, the ankles must to support the whole-body of the humanoid, so the torques increase until their maximum value; furthermore, during the single support phase and when the swing foot is making a stride, the higher torques are registered; but, the motor currents limits are satisfied. Sometimes the maximum current value is constant, because it is limited by the servo-driver, however the joint position is tracked successfully.

On the other hand, the highest joint velocity is carried out by the knees; because the knees must to sweep a wide angle during walking. This velocity is lower than the motor velocity limit (8000 RPM). The knee velocity could be reduced, by decreasing the swing foot height or step length. Furthermore, the knee motor should be the more powerfull, because it supports high torque and velocities.

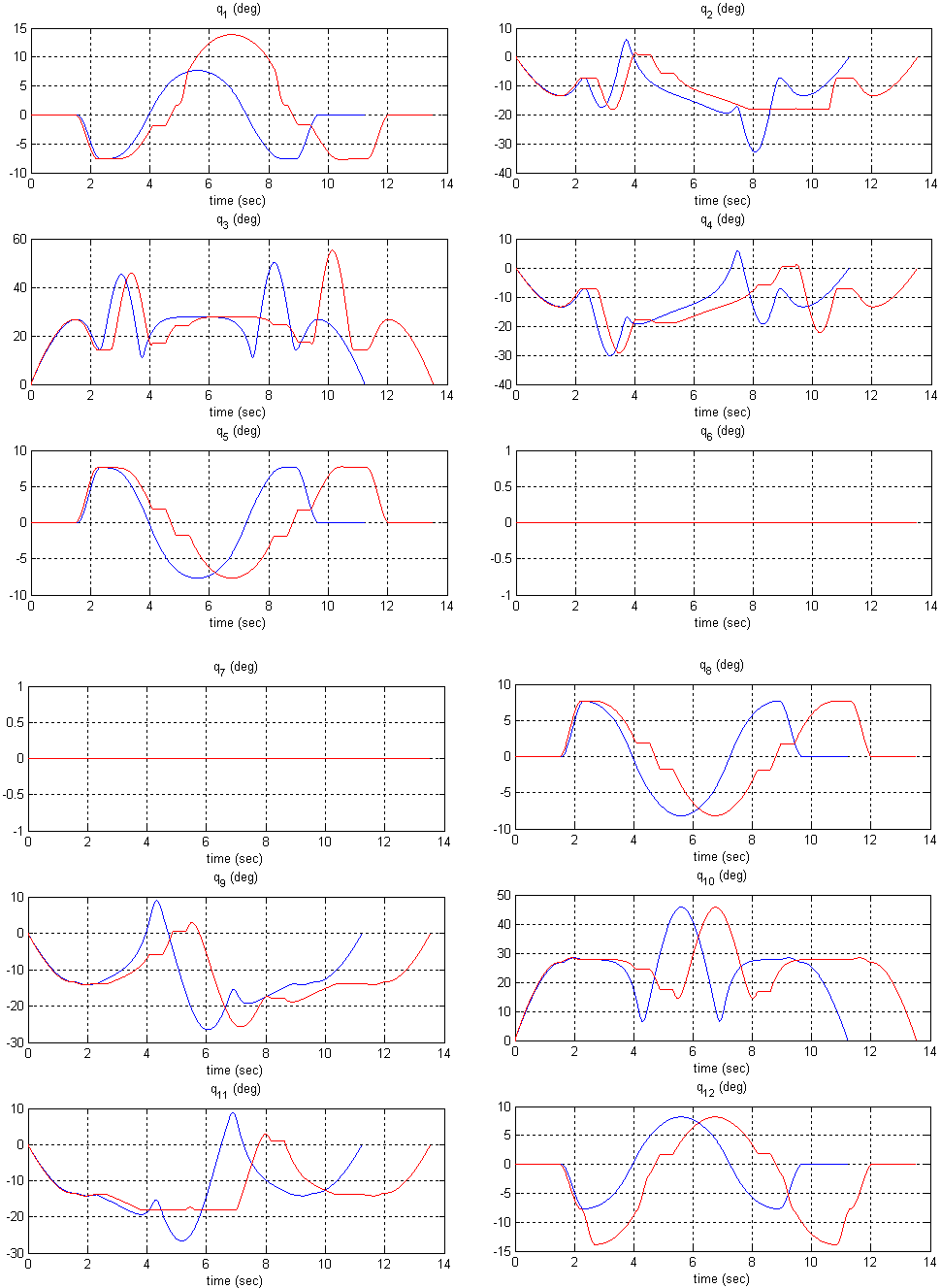


Figure 6.16: Joint patterns of each leg, which are q_1 to q_6 for the right leg and q_7 to q_{12} for the left leg. The blue patterns are the reference patterns and the red patterns include the off-line compensation with delay.

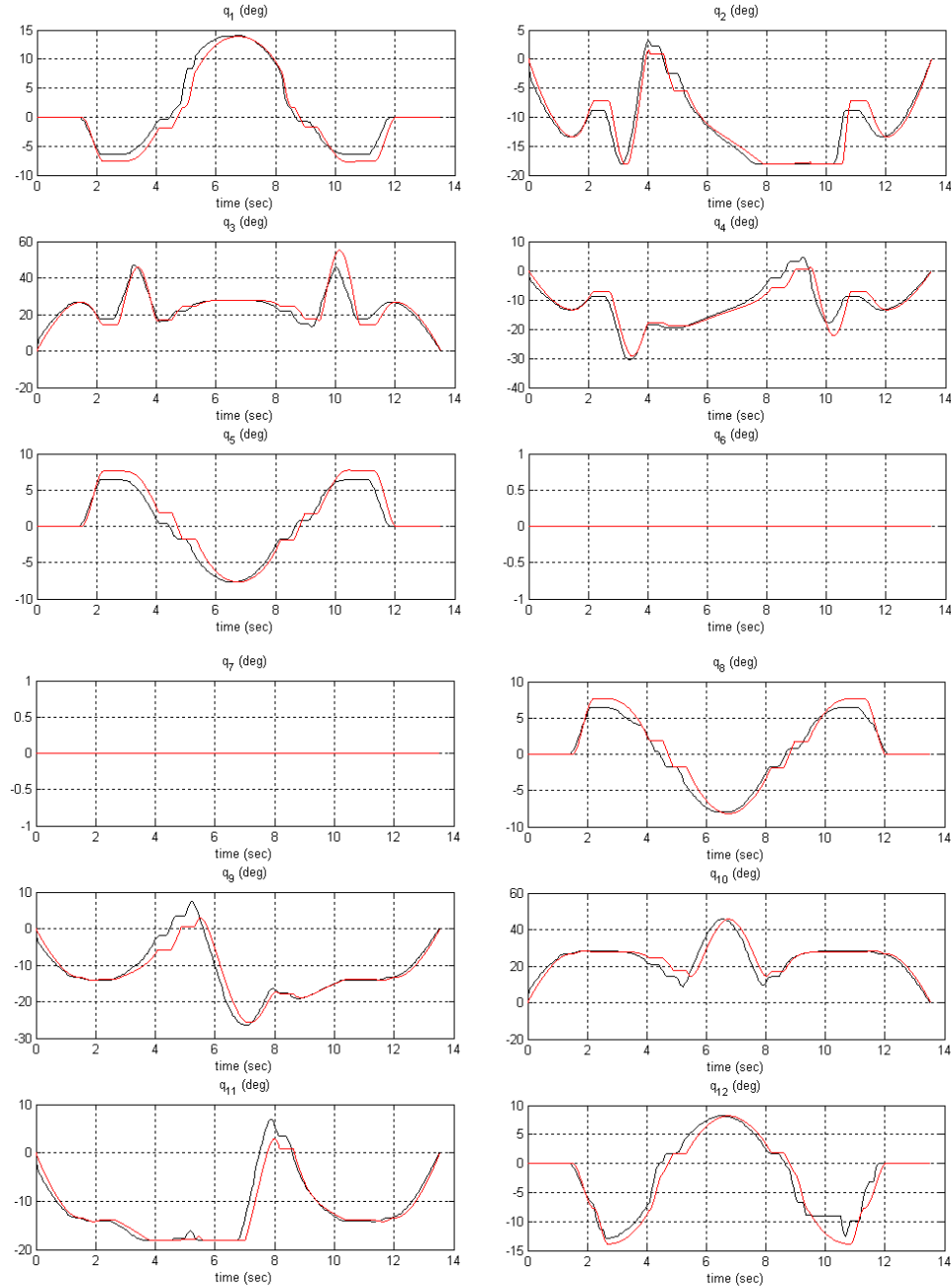


Figure 6.17: Joint patterns of each leg, which are q_1 to q_6 for the right leg and q_7 to q_{12} for the left leg. The red patterns are the compensated reference patterns and the black patterns are measured by the encoders. The joint control allows the patterns to follow with a little error, but it is enough to obtain a stable walk.

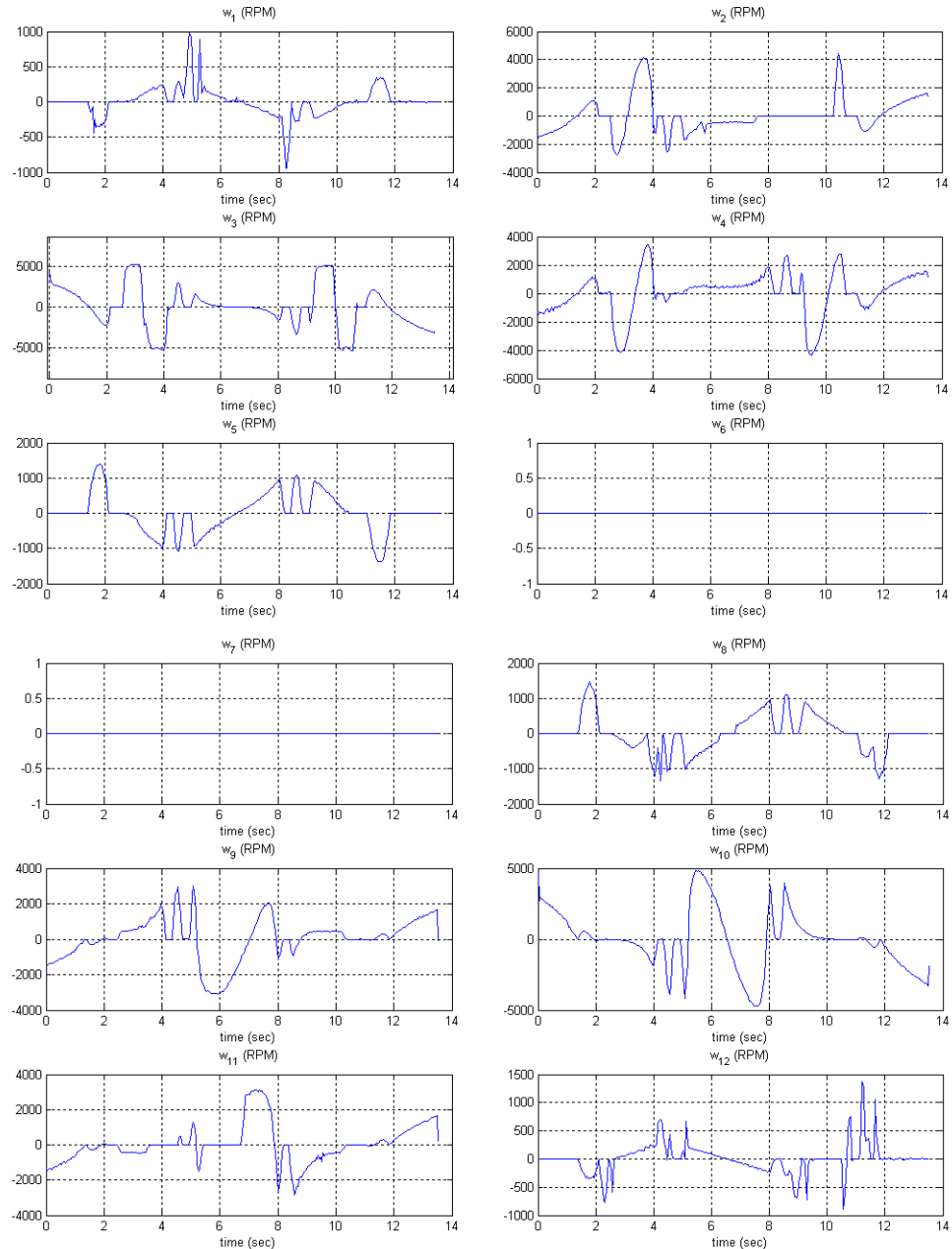


Figure 6.18: Joint angular velocities of each leg, which are w_1 to w_6 for the right leg and w_7 to w_{12} for the left leg. Velocities during walking.

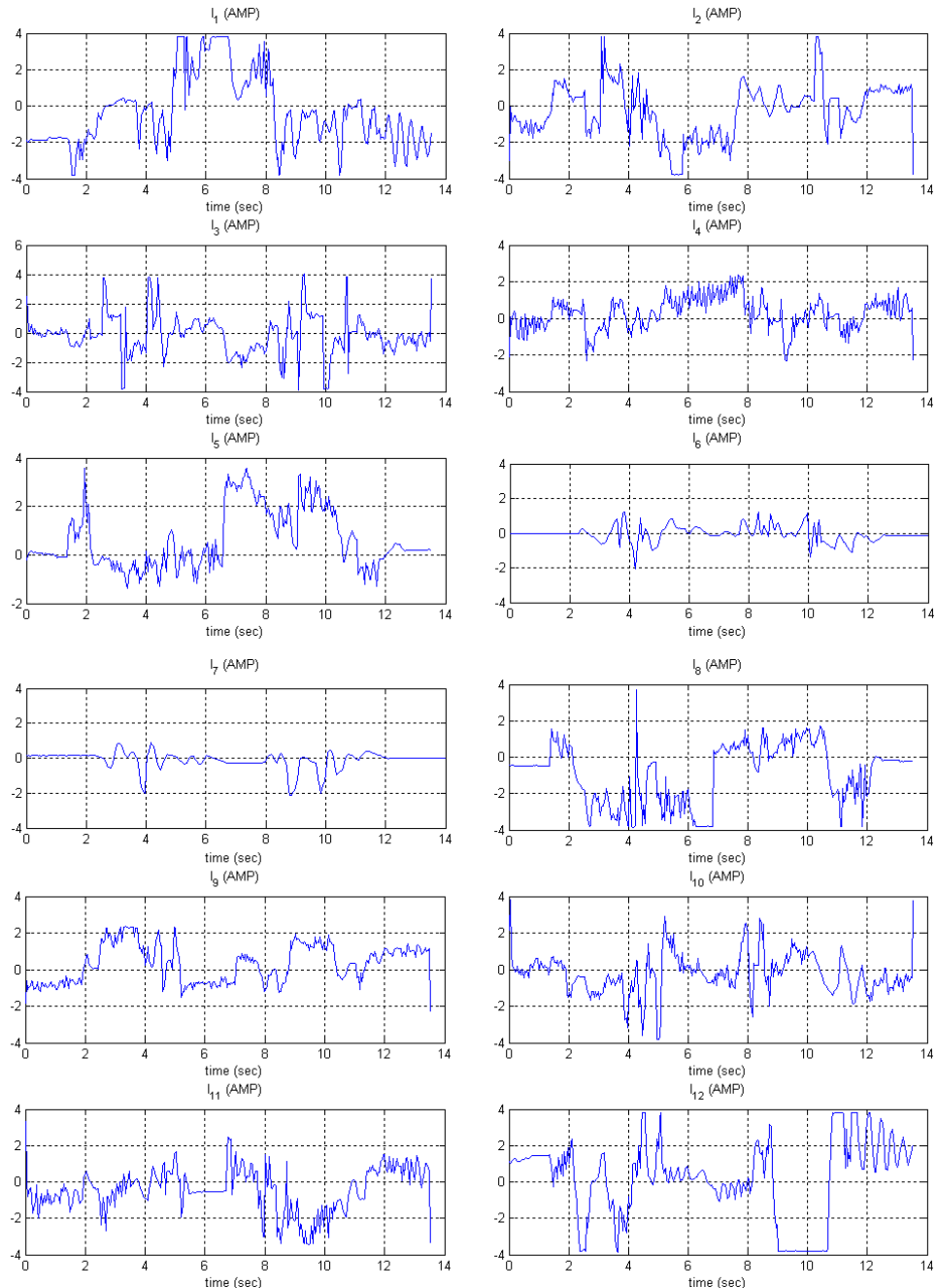


Figure 6.19: Joint currents of each leg, which are I_1 to I_6 for the right leg and I_7 to I_{12} for the left leg. Actual currents during walking motion.

2.2 Walking at 0.7Km/h

In this test, the Rh-1 humanoid robot is increasing the walking velocity while it is making four steps forward. Succesfull results are shown in the next

Figures.

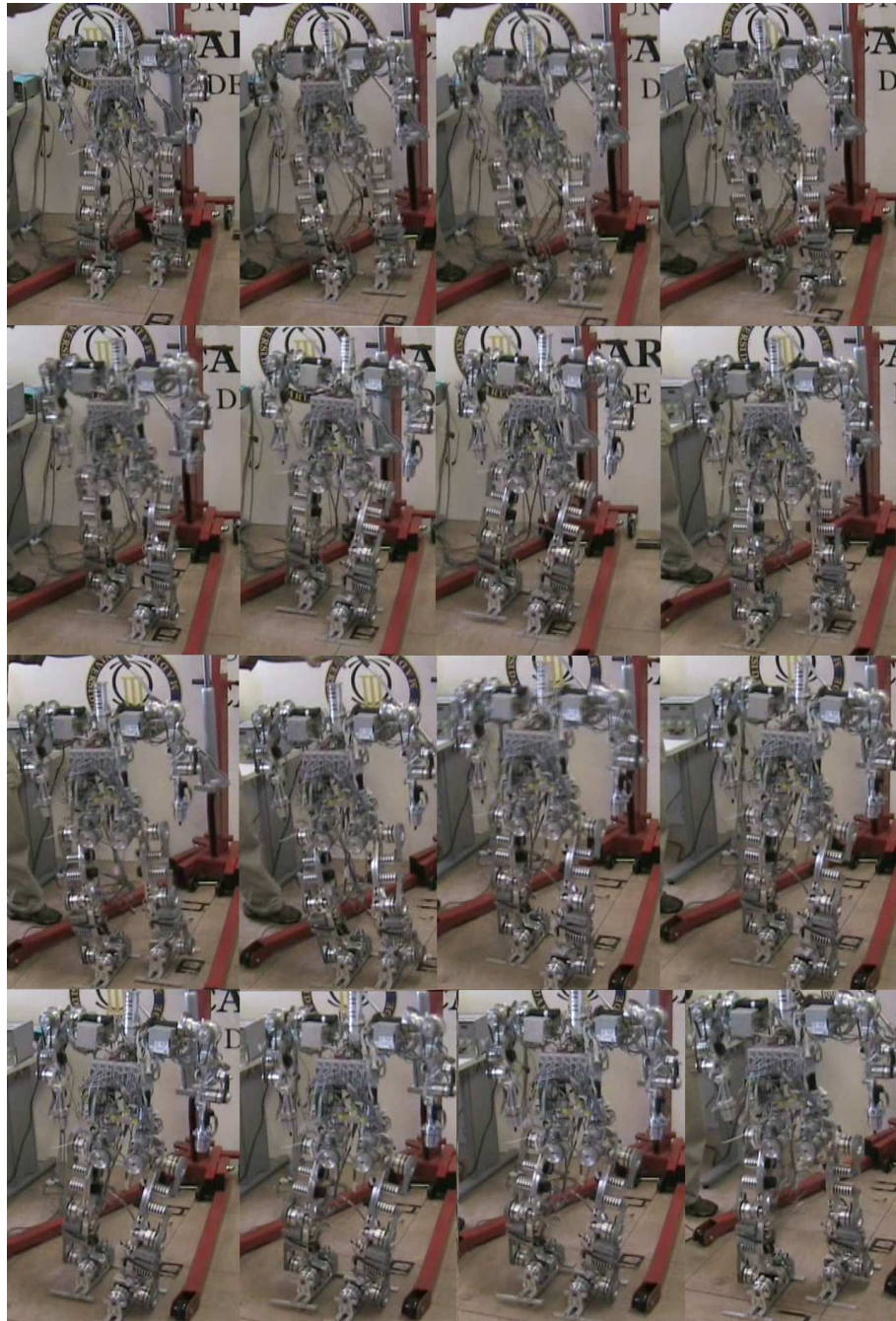


Figure 6.20: Four steps by dynamic walking patterns under the LAG algorithm, increasing velocity about 0.7Km/h. Experimentally, the dynamic walking patterns are tested successfully. Higher velocity and continuity of walking patterns could be obtained by closing the loop of the whole body control system.

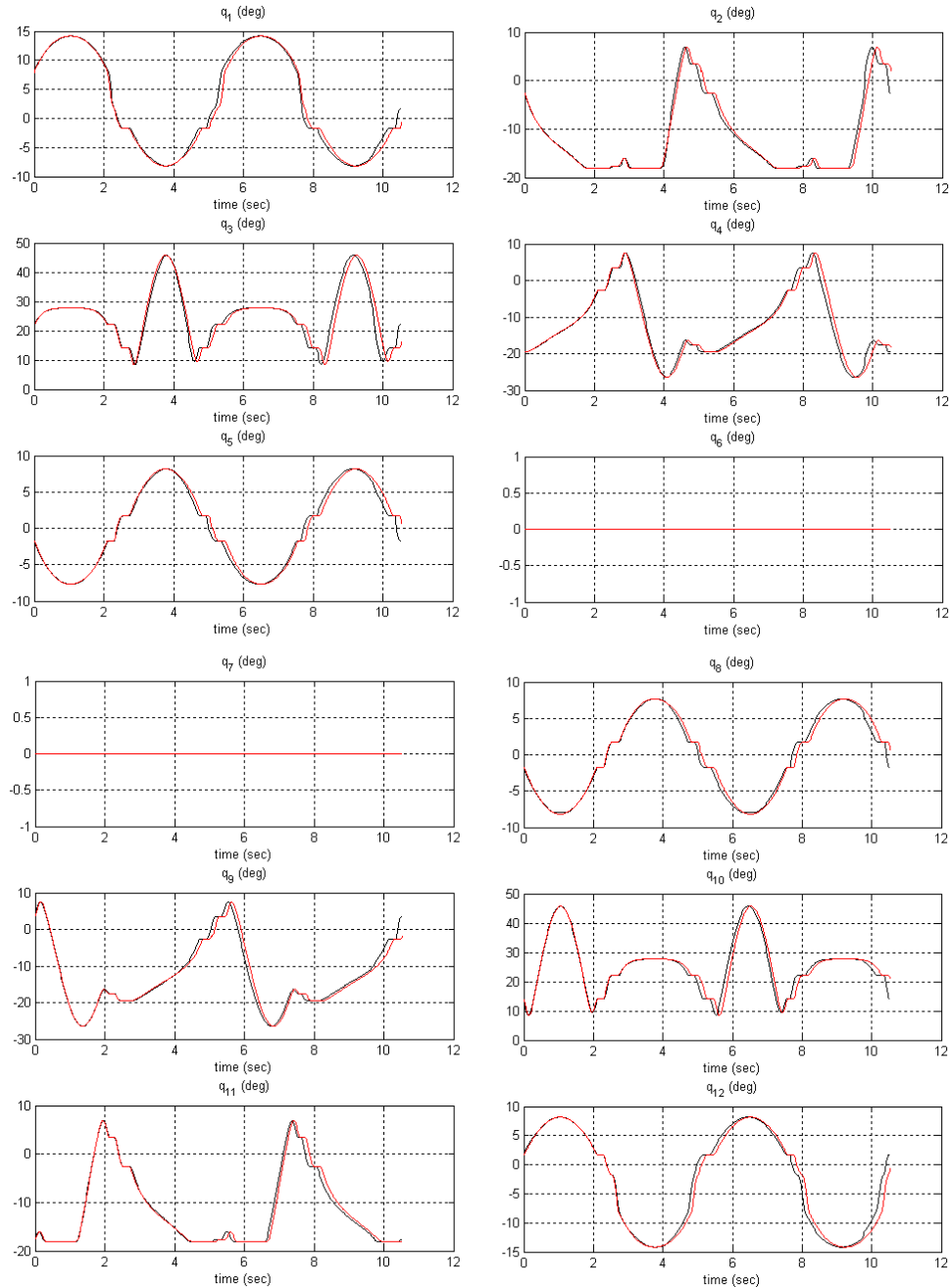


Figure 6.21: Joint patterns of each leg, which are q_1 to q_6 for the right leg and q_7 to q_{12} for the left leg. The red patterns are the compensated reference patterns and the black patterns are measured by the encoders. The joint control allows to track the patterns with a little error, but it is enough to obtain a stable walk.

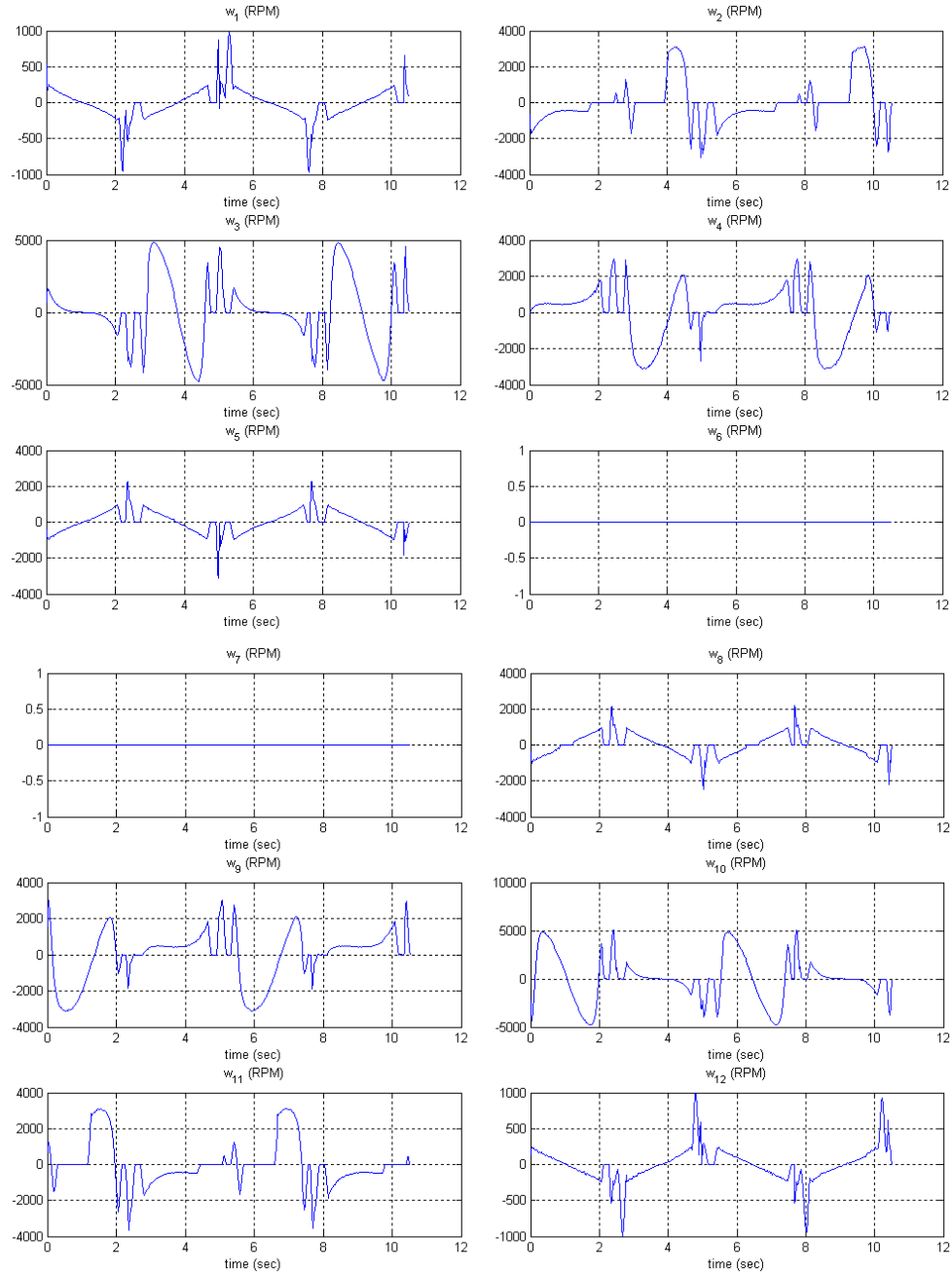


Figure 6.22: Joint angular velocities of each leg, which are w_1 to w_6 for the right leg and w_7 to w_{12} for the left leg. Actual velocities during walking.

This test describes the walking motion at 0.7 Km/h (Fig. 6.20, with $L_x=0.180\text{m}$) for four steps. In this case, the off-line compensated joint pattern references and the measured ones have almost the same performance with a little error like the

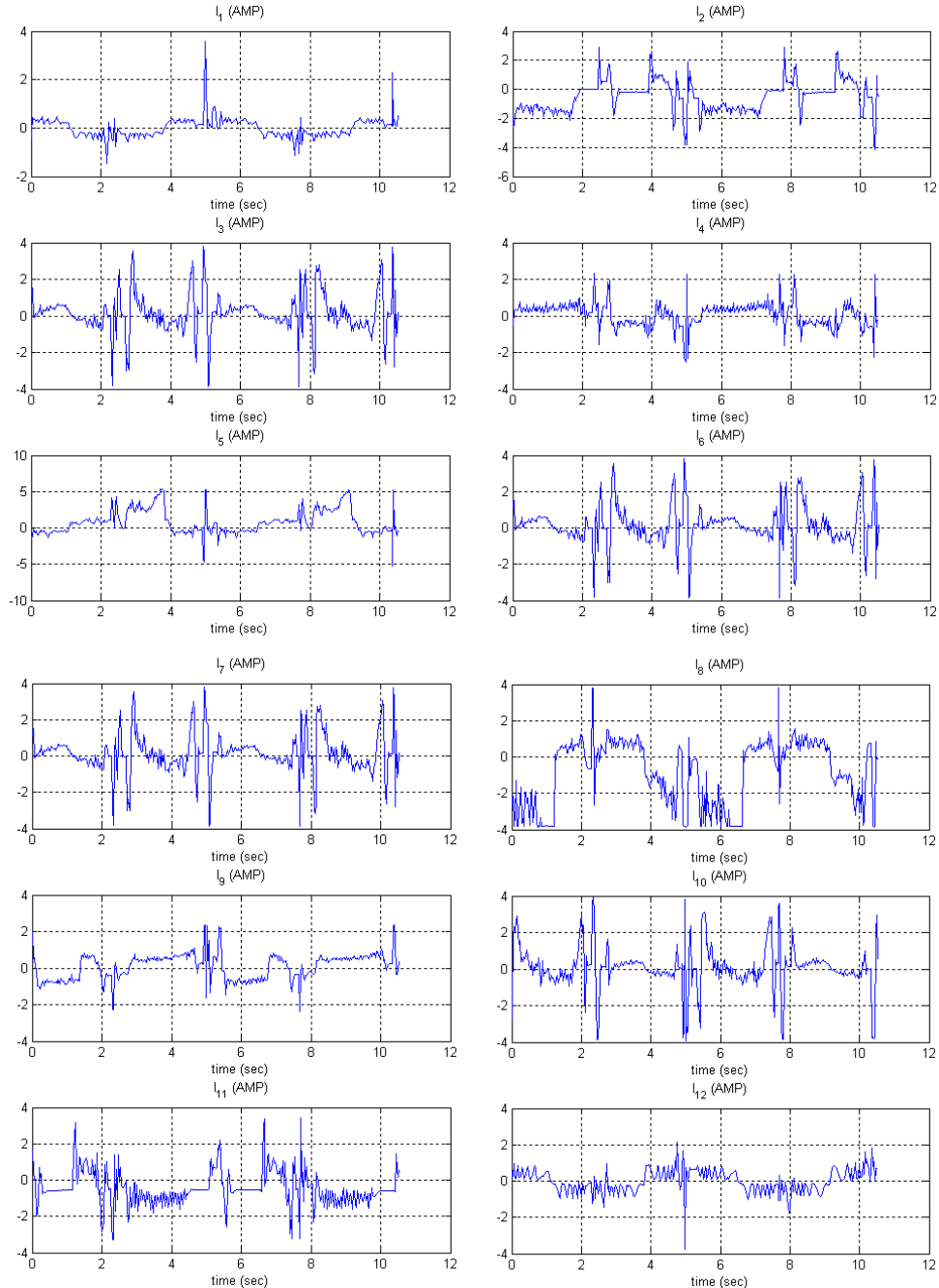


Figure 6.23: Joint currents of each leg, which are I_1 to I_6 for the right leg and I_7 to I_{12} for the left leg. Actual currents during walking motion.

previous test, but it is enough to obtain stable walking motion (Fig. 6.21 to Fig. 6.23). The current peaks are observed more times because the walking velocity

is higher compared to the previous case, so the climbing and landing motions of the swing foot are faster. While the swing foot is climbing, the inertial and gravitational effects cause higher energy consumption for following the reference joint position; otherwise, the landing impact increases the current because the reference joint position should be tracked, too. The knee joints reach the higher angular velocity (w_3 and w_{10}), because it is sensitive to the lifting of the swing foot. So, this factor should be taken into account during the gait generation patterns, in order to reduce dynamical effects. Finally, the Fig. 6.19 describes the current of each joint during the walking motion, the currents measure the energy consumption and they give us an idea of torque in each joint, so the dynamic and gravity effects are included. Furthermore, those measures allow to check the actuator current limits. The maximum values are registered in the support leg, at the single support phase (see I_1 the right frontal ankle joint, between 5 and 6 seconds, the swing foot is the left one, so, it is making a step).

2.3 Walking at 0.55Km/h with cover and hardware onboard

This test deals with the Rh-1 humanoid robot including the main control computer mounted onboard, batteries and covers (Fig. 6.24). In this case, the humanoid robot increases its weight from 35kg. to 48.5kg.

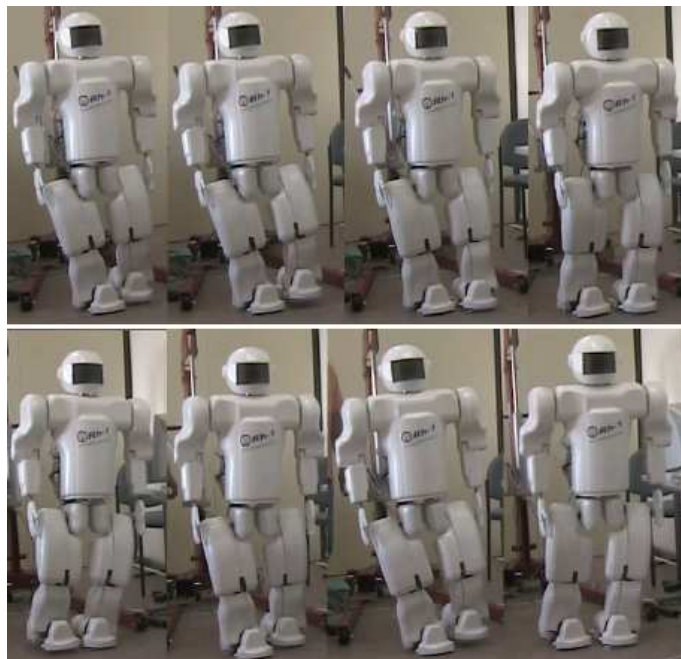


Figure 6.24: Three steps by dynamic walking patterns under the LAG algorithm, velocity about 0.55Km/h. With onboard hardware, batteries and covers, the weight the Rh-1 increases from 35kg. to 48.5kg.

The center of gravity changes position and must be taken into account in order to generate stable walking patterns.

As the walking control is at open loop, only three stable steps are obtained. If you analyze joint patterns (Fig. 6.25), the open loop compensation is made

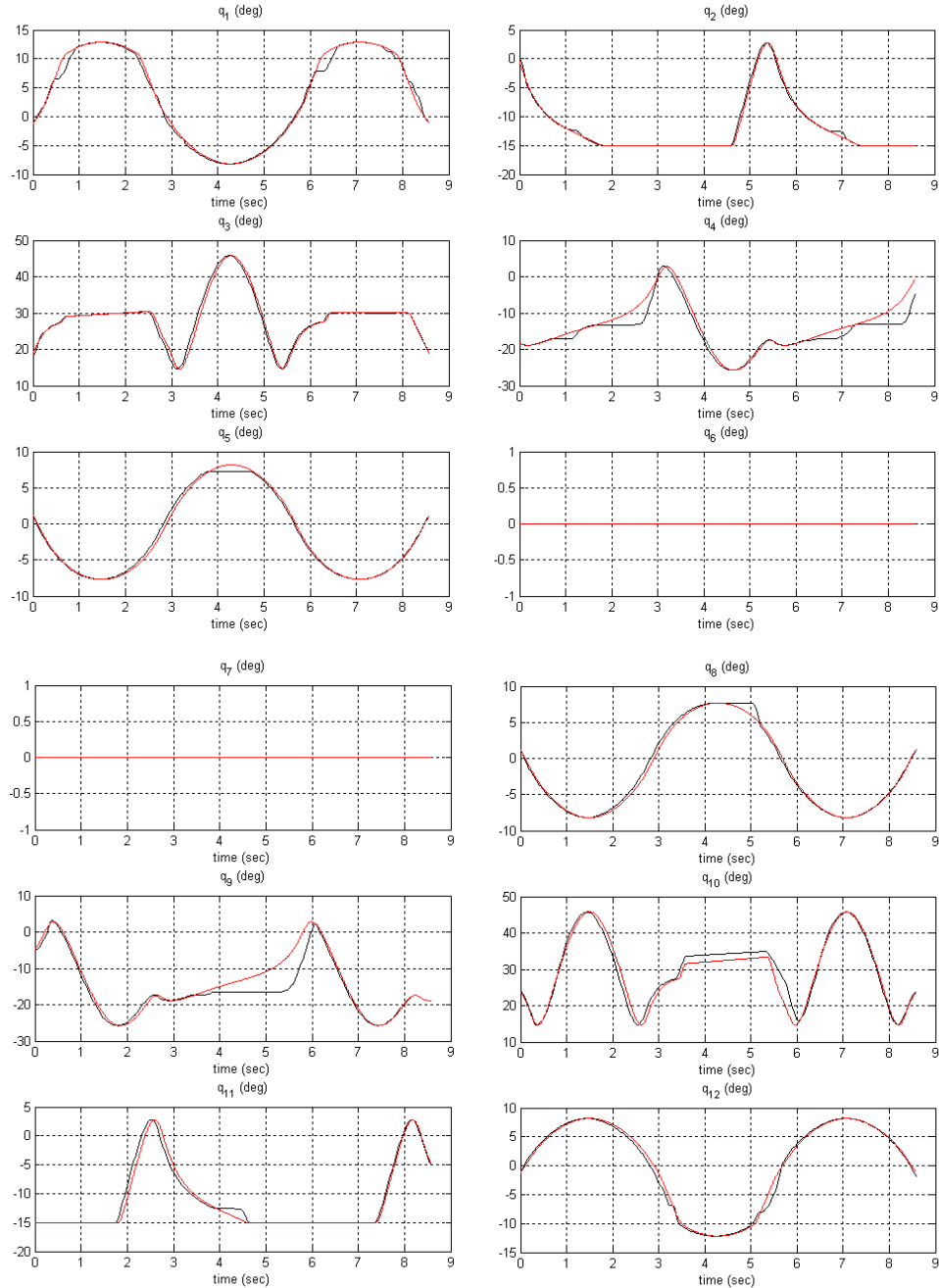


Figure 6.25: Joint patterns of each leg, which are q_1 to q_6 for the right leg and q_7 to q_{12} for the left leg. The red patterns are the compensated reference patterns and the black patterns are measured by the encoders. Joint control allows to track the patterns with a little error, but it is enough to obtain a stable walk.

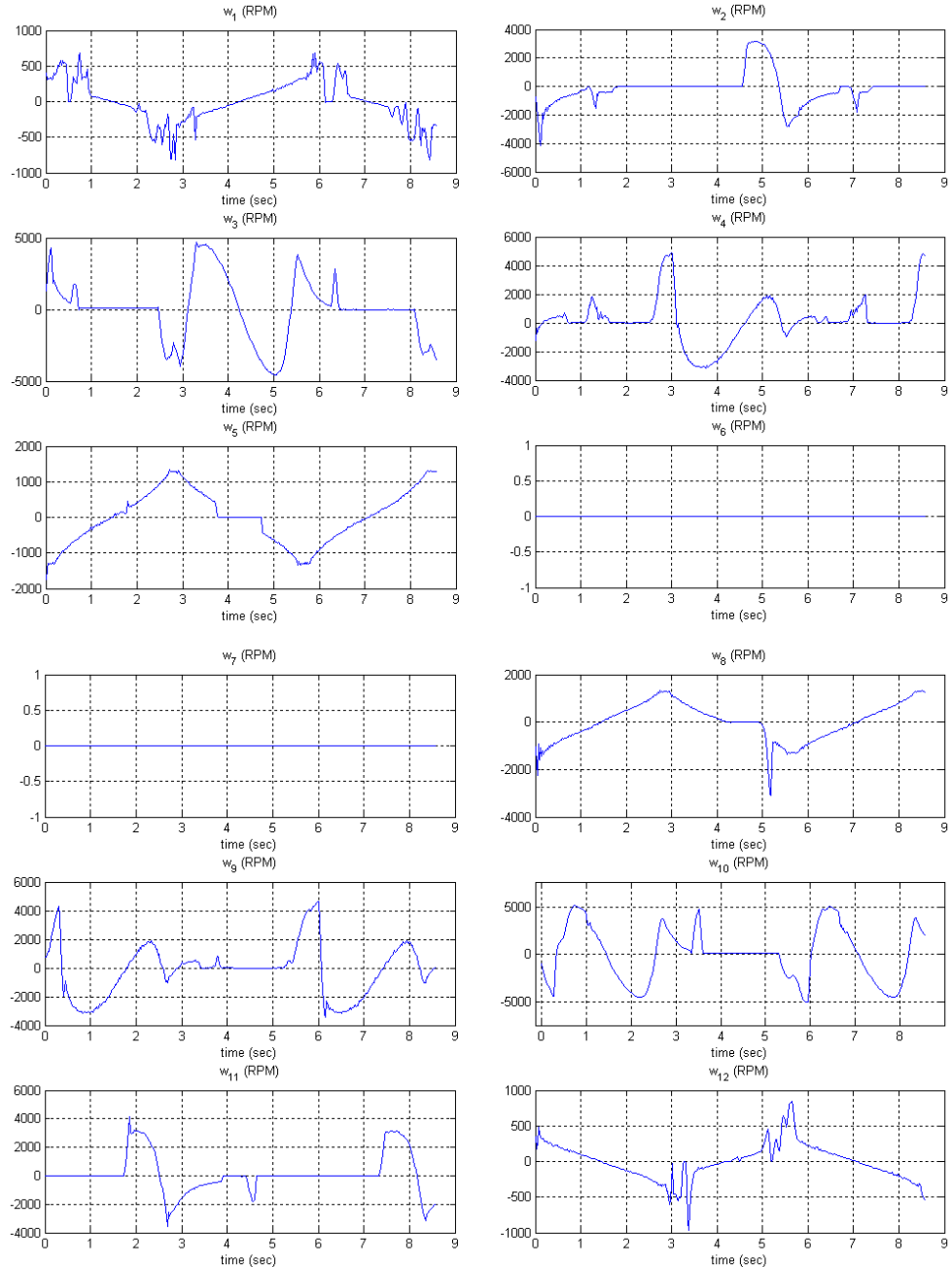


Figure 6.26: Joint angular velocities of each leg, which are w_1 to w_6 for the right leg and w_7 to w_{12} for the left leg. Actual velocities during walking.

without delay. The measured patterns (black lines), q_4 and q_9 , do not track the reference patterns, in the single support phase, because the actual weight increases the respective joint torques and the motors are overloaded (as we will see next), so, those must be changed. The angular velocities turn to zero in this

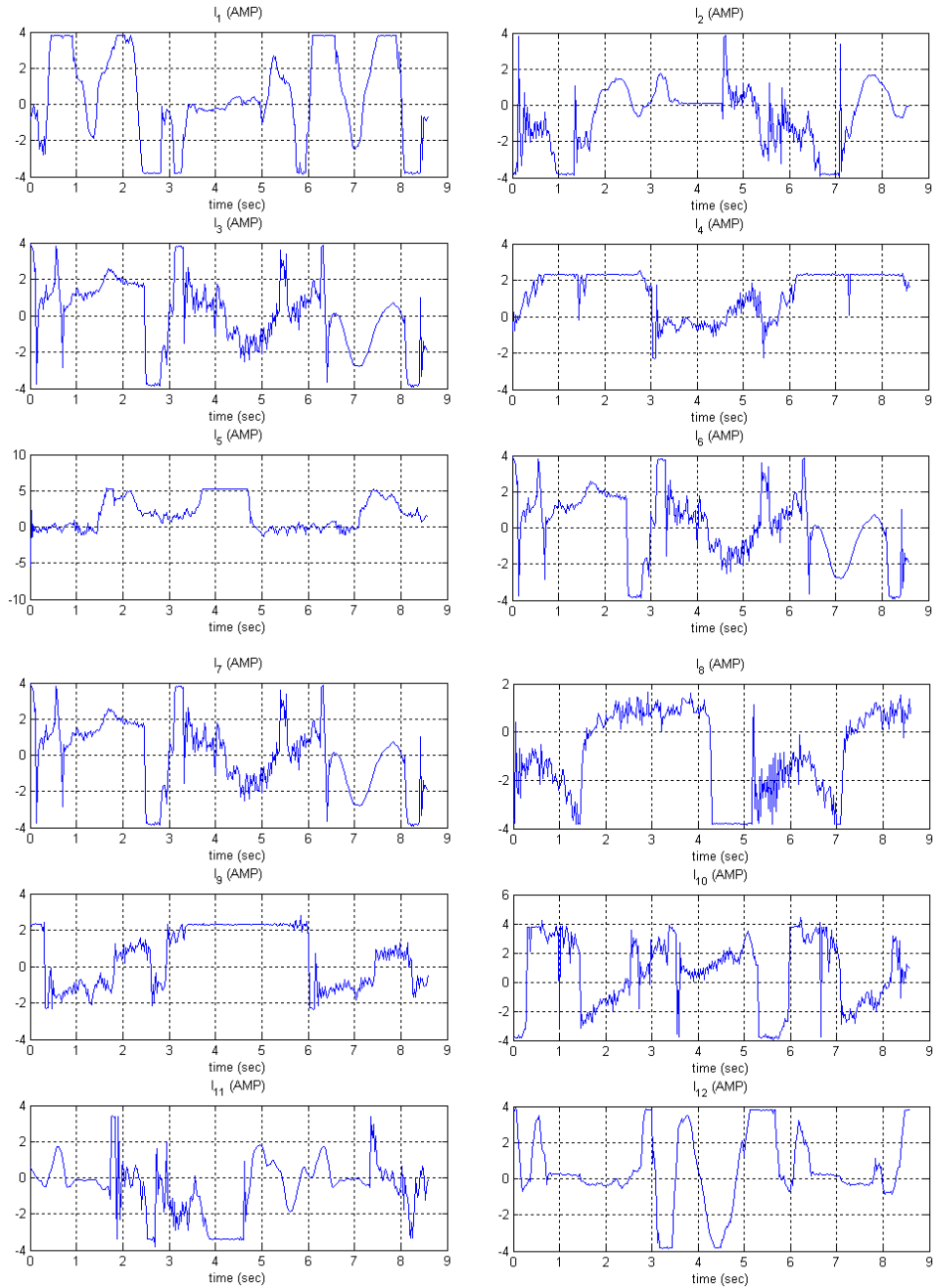


Figure 6.27: Joint currents of each leg, which are I_1 to I_6 for the right leg and I_7 to I_{12} for the left leg. Actual currents during walking motion.

case (Fig. 6.26). And the currents maintains the maximum values for a longer time (Fig. 6.27) due to the higher weight, too. However, stable walking motion can be obtained.

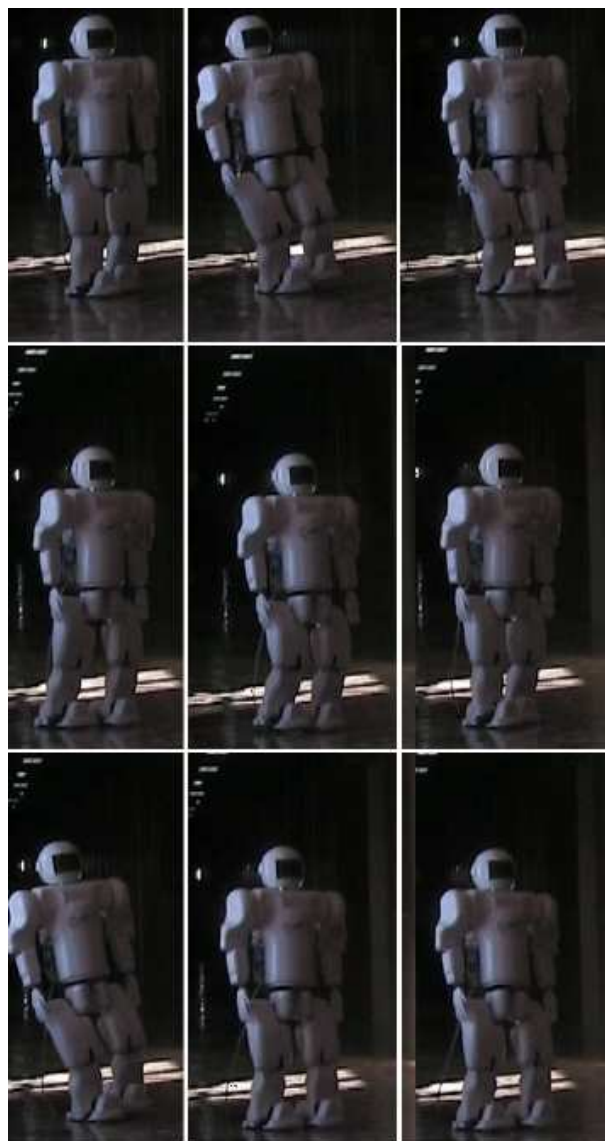


Figure 6.28: Three steps by dynamic walking patterns in the hall under the LAG algorithm, velocity about 0.55Km/h. With onboard hardware, batteries and covers, the weight of the Rh-1 increases from 35kg. to 48.5kg.

The same test in the hall is shown in Fig. 6.28. It is validated the walking motion algorithm in this case, too. In this case, the walking surface has low friction with respect to the lab floor's, so the robot control system should be tuned to maintain the stability of the humanoid. Additional improvements such as, rubber sole, foot landing compliance control, stiffness joint structure could achieve better walking motion. In this test, two stable walking steps have achieved due to the low friction surface, control and structure imperfections. However, the proposed walking pattern generator, which includes off-line control

module, could be used for these tests.

2.4 Making a gesture with left hand

AnOther test by moving the arms in order to make a gesture is shown in Fig. 6.29, where the Rh-1 humanoid robot is making a greeting.

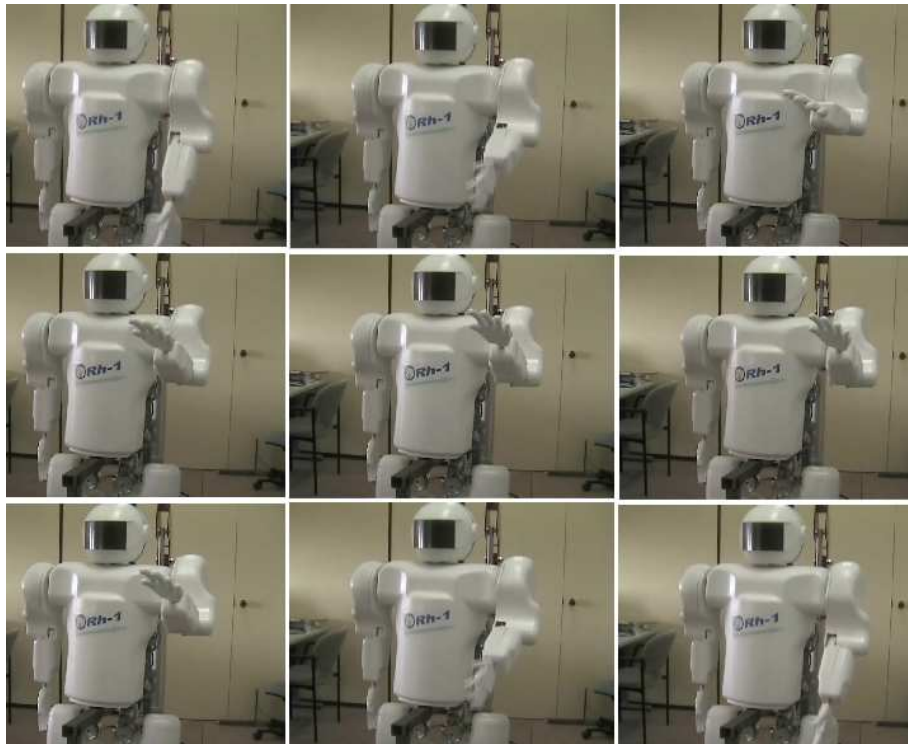


Figure 6.29: Rh-1 humanoid robot making a greeting.

The basic motion planning for making a greeting is shown in Figs. 6.30 to 6.33, when the motion is made with four degrees of freedom. This is an overconstrained inverse kinematics computation, because we can control six degrees of freedom in space with the arm of five DOF's (including the neck joint). That way, in order to plan the motion, we should control three spatial trajectories and two orientation trajectories.

In the test, we have selected five trajectories: the spatial trajectories (on each axis) and two orientation trajectories (see Fig. 6.31 and Fig. 6.32). Those are selected for controlling the arm motion and reaching the goal accurately.

The joint patterns have been obtained by the kinematics model proposed in the Chapter 5, section 5.7.2. In the Fig. 6.33 smooth joints arm trajectories are shown, therefore the kinematics modelling is validated too. However, the solution of the overconstrained kinematics problem is limited by the Paden-Kahan subproblems results; that is, the goal is not reached in this case, but the nearest solution without singularities has been obtained.

Additional improvements on the planning hand motion could be achieved

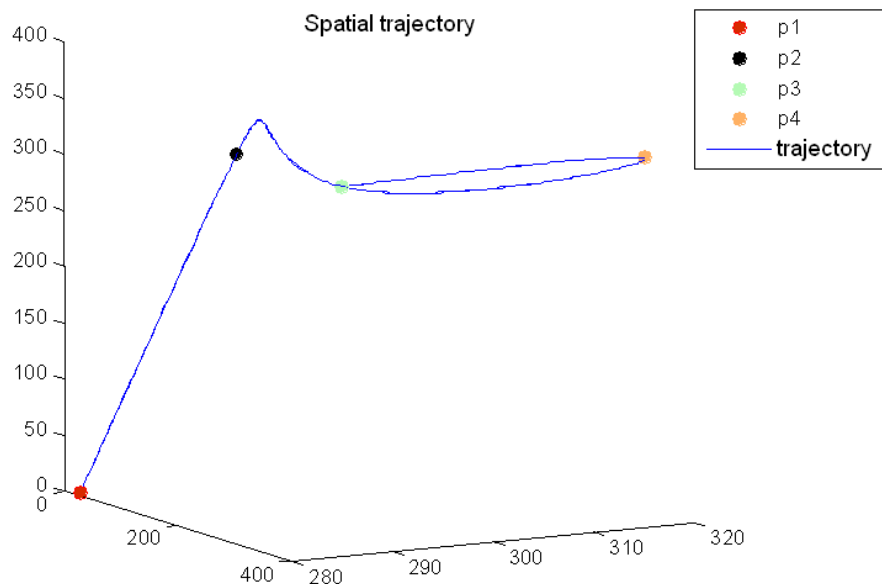


Figure 6.30: Spatial trajectory of the humanoid hand. The points p_1 , p_2 , p_3 and p_4 are the subgoals needed to make a gesture.

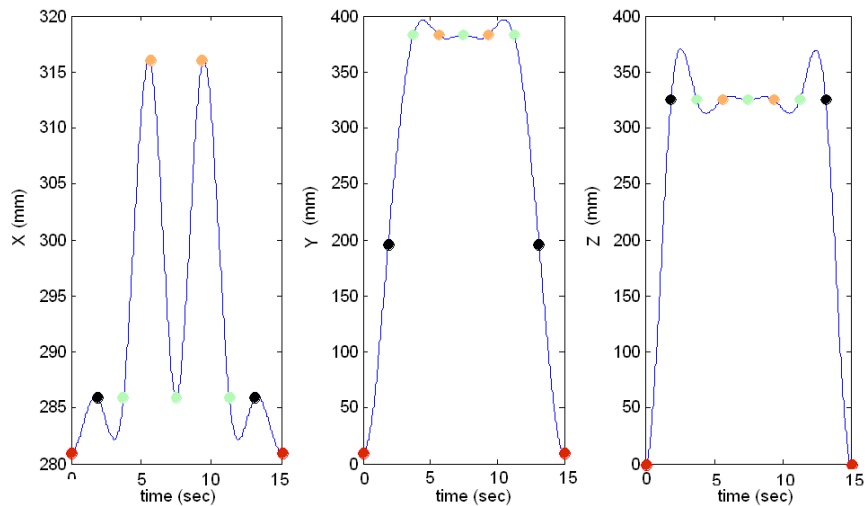


Figure 6.31: X, Y and Z temporal spatial trajectories of the humanoid hand.

with path planning methods, which allow to avoid internal or external collisions with actual environments. These methods have not been studied in this research, because it is focused on generate stable walking patterns.

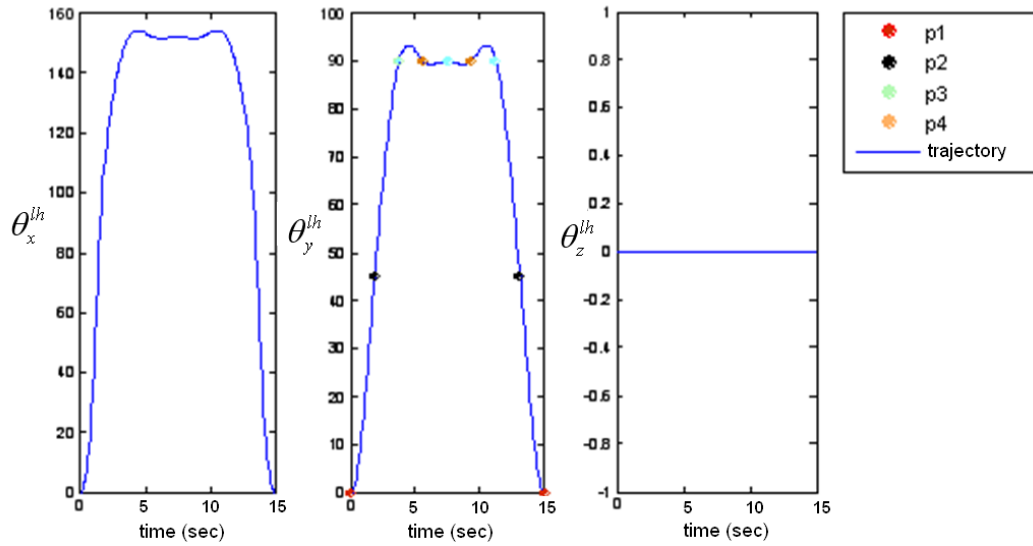


Figure 6.32: θ_x^{lh} , θ_y^{lh} and θ_z^{lh} temporal orientation trajectories of the humanoid hand.

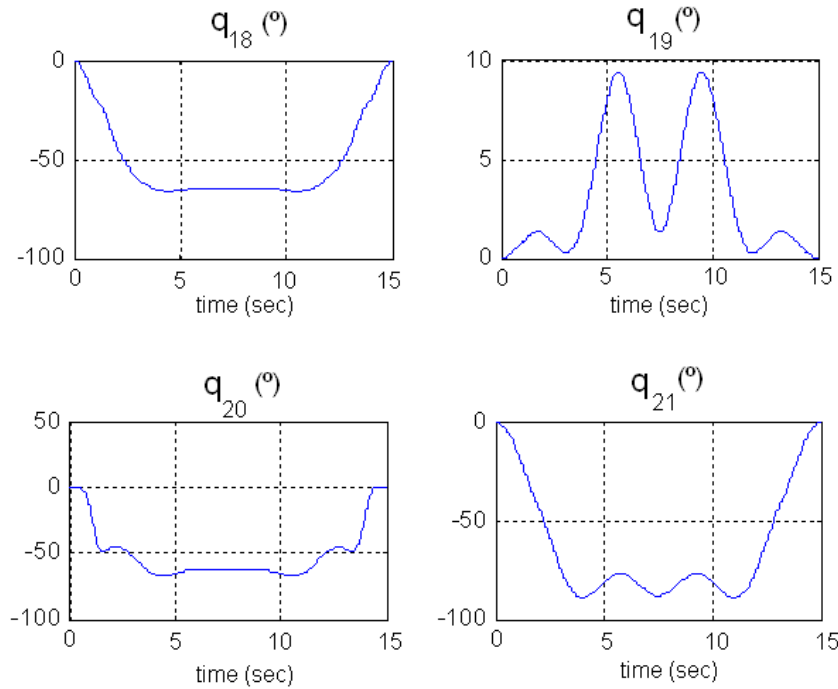


Figure 6.33: Temporal joints trajectories of the humanoid's left arm.

6.3.3 Simulation and Experimental results on HRP-2 humanoid robot platform

Many tests have been done in order to validate the proposed algorithm. Some of them will be presented as follows one acyclic step forward, one acyclic step

backward with swing foot rotation and two acyclic steps forward.

1. One acyclic step forward

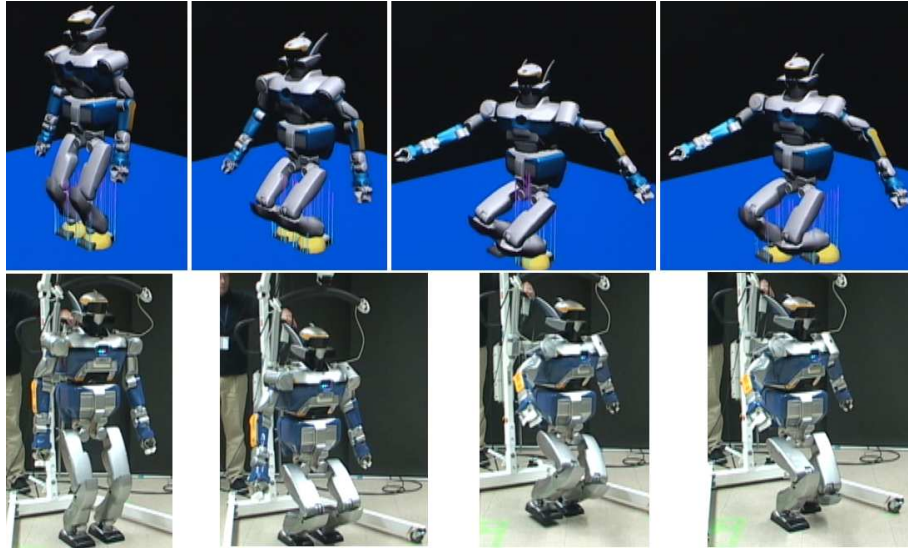


Figure 6.34: Simulation and actual acyclic step forward.

As you can see in Fig. 6.34, one asynchronous step forward is shown. The sequence of the step is next: at first, the humanoid robot gets down from the sitting position and moves its arms, chest and neck; after that, a step is taken and it continues moving its arms, chest and neck to the goal configuration.

In Fig. 6.35, many actual joint evolutions from the initial to the goal states are shown; we can see that the goal state is reached in a smooth and natural way. The simulation results show us a dynamically stable motion. It is called acyclic motion because there is no leg and arm coordination as in normal walking motion; it is the same case in the following examples. This experiment is tested and validated successfully in the HRP-2 humanoid robot platform.

It is possible to analyze the motion pattern in frontal and sagittal directions (Fig. 6.36). In the frontal motion direction, the actual ZMP (blue line) differs with respect to the reference ZMP (red line) in the single support phase by about 0.04m, but dynamic stability is maintained because it is inside the convex hull. In addition, the reaction force on each foot is analyzed in order to improve the force distribution in the motion pattern.

As seen in Fig. 6.36, during the single support phase, the maximum reaction force on the support foot is about 680 N nearest to the humanoid robot's weight, and on landing, the reaction force is practically the same on each foot. That is because the motion pattern is designed to assure equivalent force distribution on each foot.

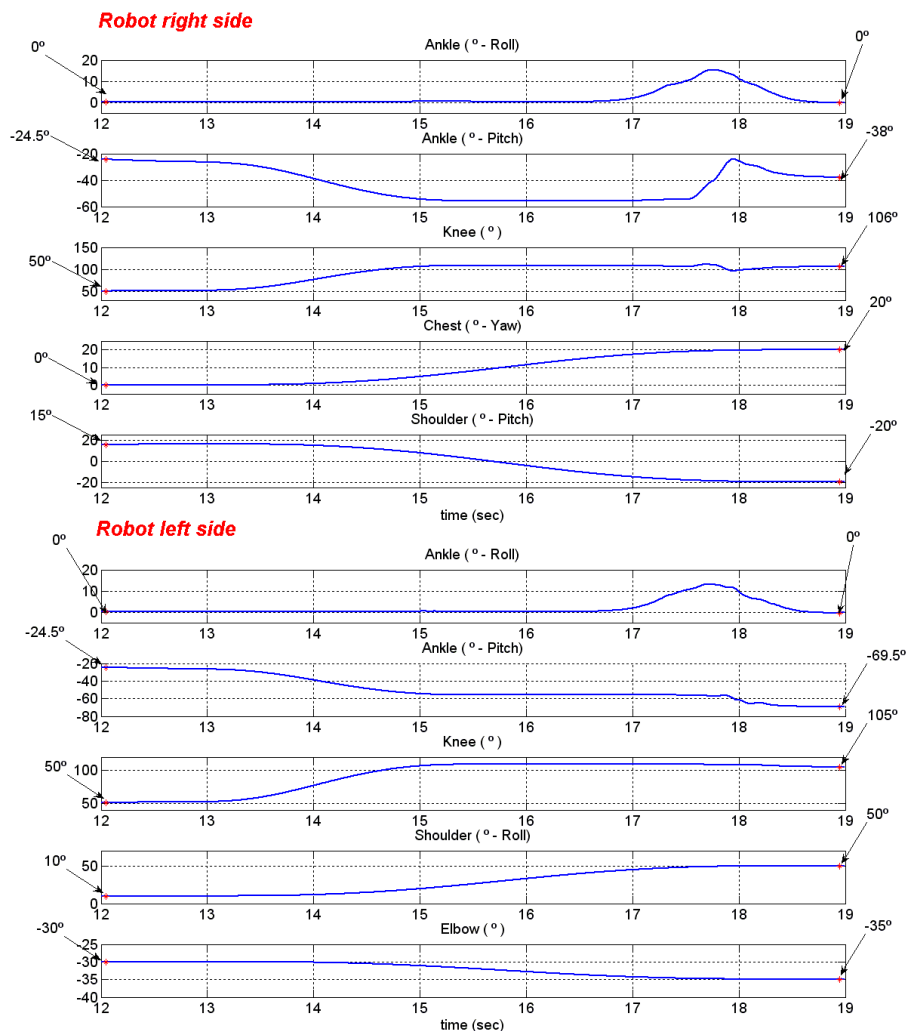


Figure 6.35: Actual results of angular joint patterns for taking one acyclic step forward, from the initial to the goal state. The right and the left side are shown. In both cases, the goal state is reached by a smooth and natural motion from the initial one (red dots).

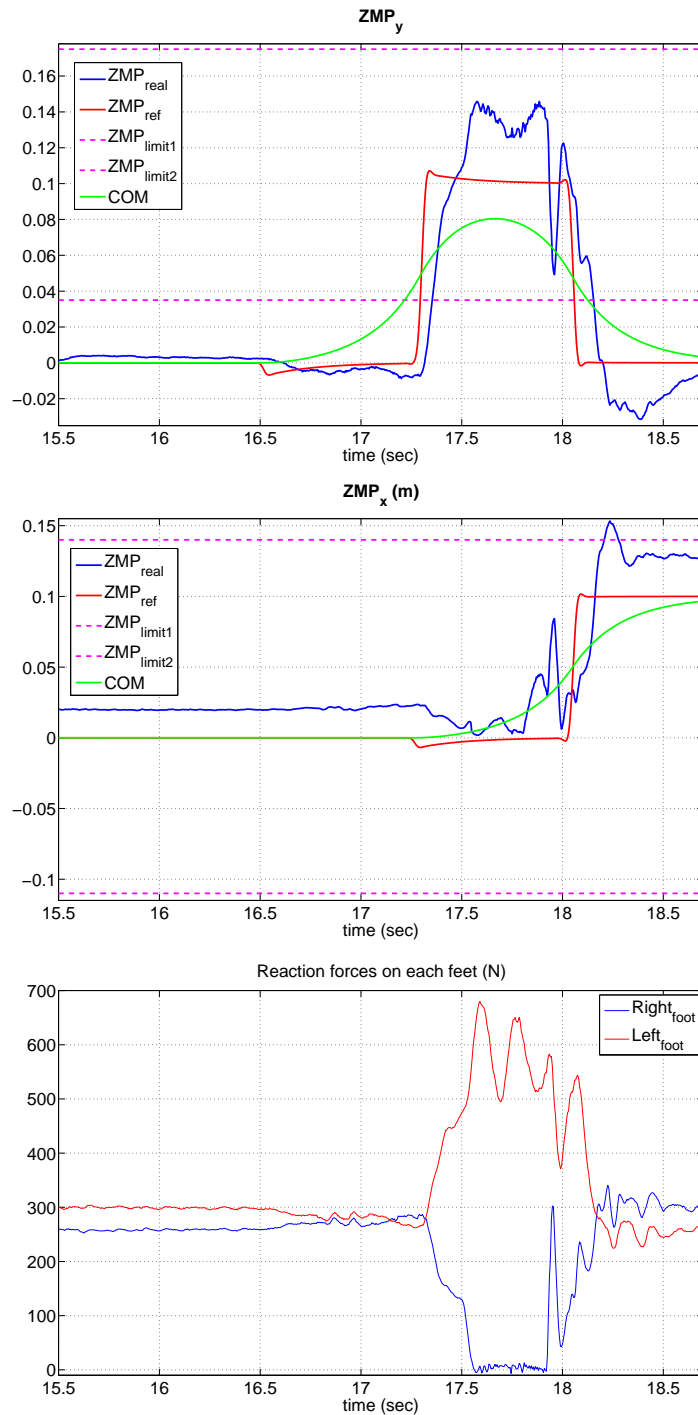


Figure 6.36: ZMP_y , ZMP_x reference and measuring. COG_y , COG_x trajectory and vertical reaction forces on each foot.

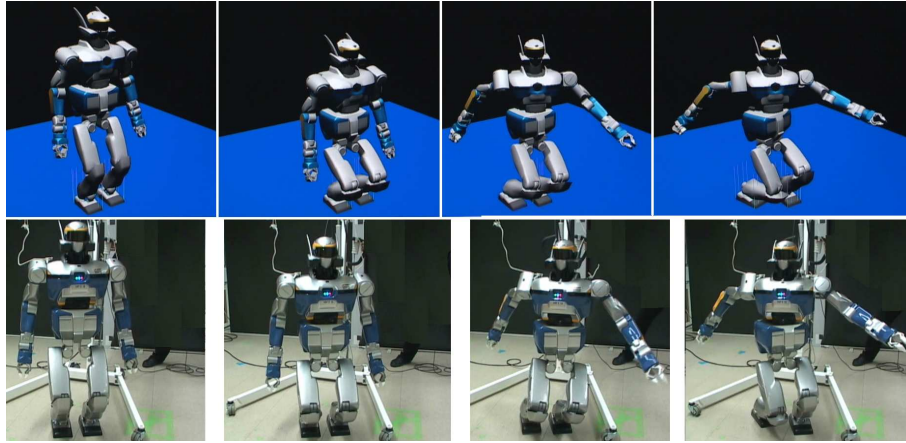


Figure 6.37: Simulation and experimental result of one acyclic step backward and rotating.

2. One acyclic step backward and turning

Let us go to the next case, when the acyclic motion is backward and with rotation. The simulation is shown in Fig. 6.37. As in the previous experiment, the continuous motion from the sitting position to open arms and down the robot body has been made when the goal configuration is statically stable, too. The joint patterns reach their respective input goal smoothly (Fig. 6.38).

The proposed motion in the HRP-2 platform (Fig. 6.37) is successfully validated.

The motion patterns and the actual measures can be analyzed, as seen in Fig. 6.39. In this case, for the single support phase, the maximum ZMP error is about 0.06m in frontal motion and 0.025m in sagittal motion. Hence, the motion is dynamically stable because the actual ZMP is inside the convex hull. It is possible to observe that the ZMP reference is not strictly followed by the actual ZMP due to the acyclic motion, as we have deduced in advance.

The second loop of preview control, which takes into account the whole-body ZMP is a good choice for tracking the ZMP reference. So more stable motion could be obtained. (see Chapter 5, section 5.9.5).

The reaction forces on each foot are shown in Fig. 6.39. Their behaviour is almost the same as in the preview experiment. And the maximum value on the support foot reaches about 700 N, which is approximately the weight of the robot. Finally, the force distribution on each foot is similar to the starting motion.

Improvements of the controller in yaw axis should be done in the future, because while the humanoid is taking the step, the support foot slides around yaw axis. That problem could be solved partially by compensating the inertial torque at yaw axis, by the angular momentum. The cause of this torque is the upper body rotation while the swing foot is on the air.

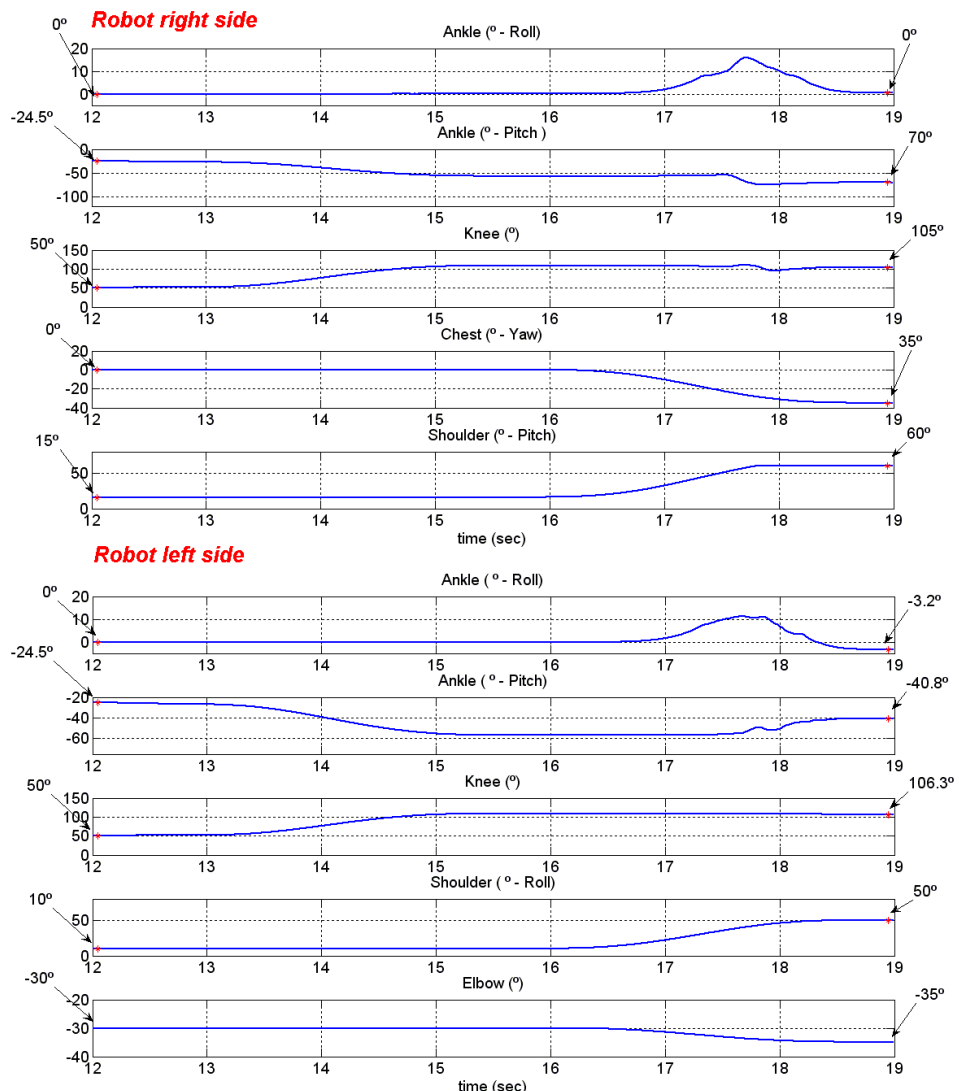


Figure 6.38: Actual results of angular joint patterns for taking one acyclic step backward from the initial to the goal state. The right side and the left side of the humanoid are shown. In both cases, the goal state is reached by a smooth and natural motion from the initial one (red dots).

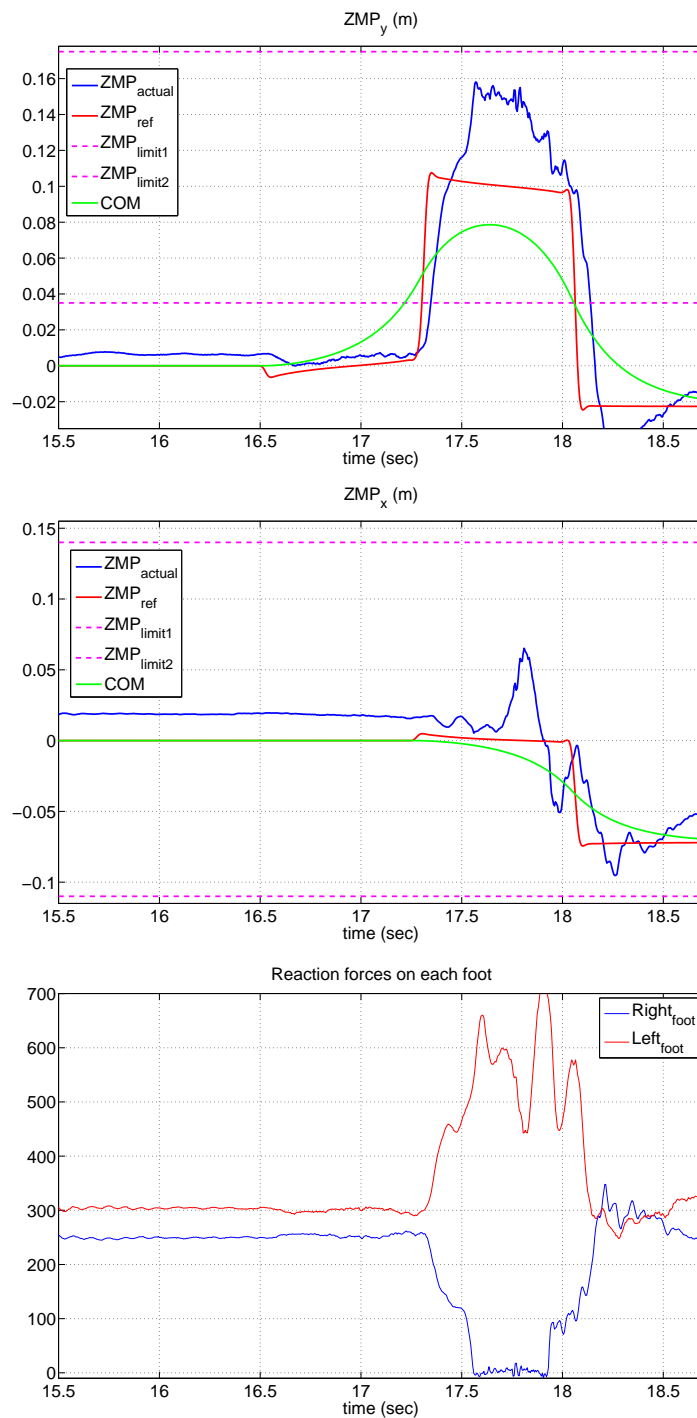


Figure 6.39: ZMP_y , ZMP_x reference and measuring. COG_y , COG_x trajectory and vertical reaction forces on each foot.

3. Two acyclic steps forward

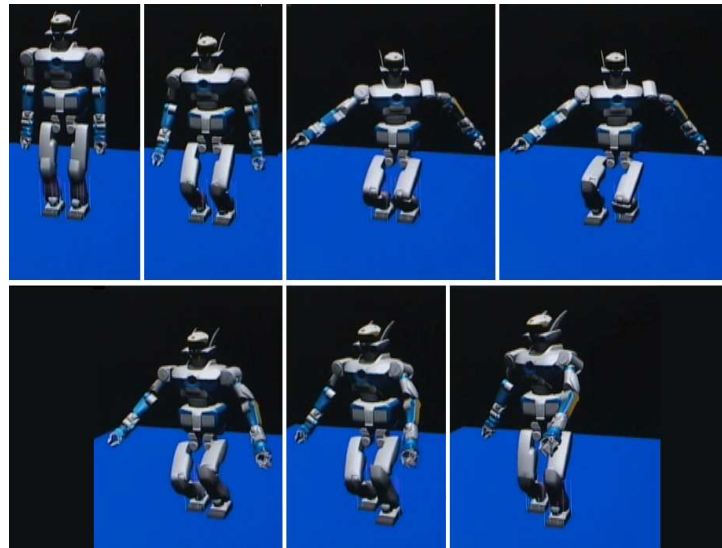


Figure 6.40: Simulation of two acyclic steps forward.

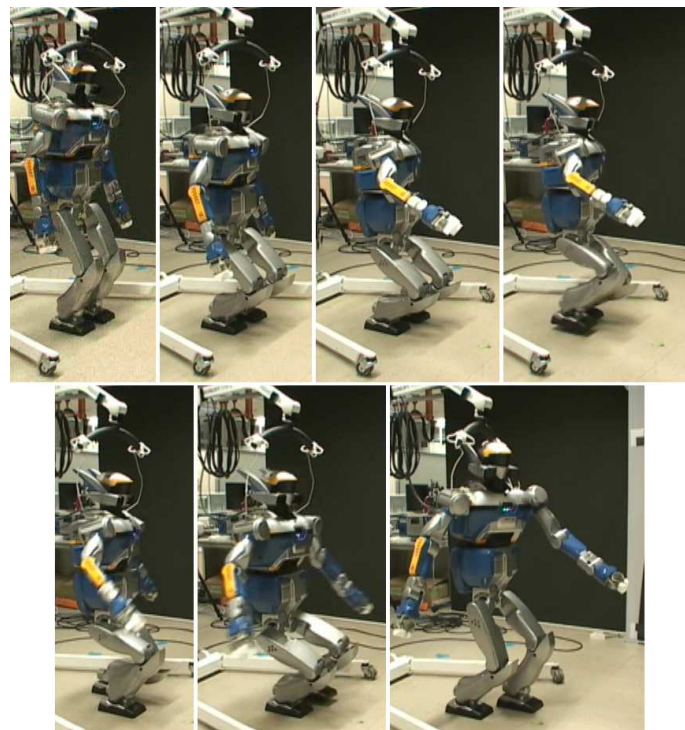


Figure 6.41: Experiment of two acyclic steps forward.

The latest case deals with a motion of two acyclic steps. Simulation results

can be seen in Fig. 6.40.

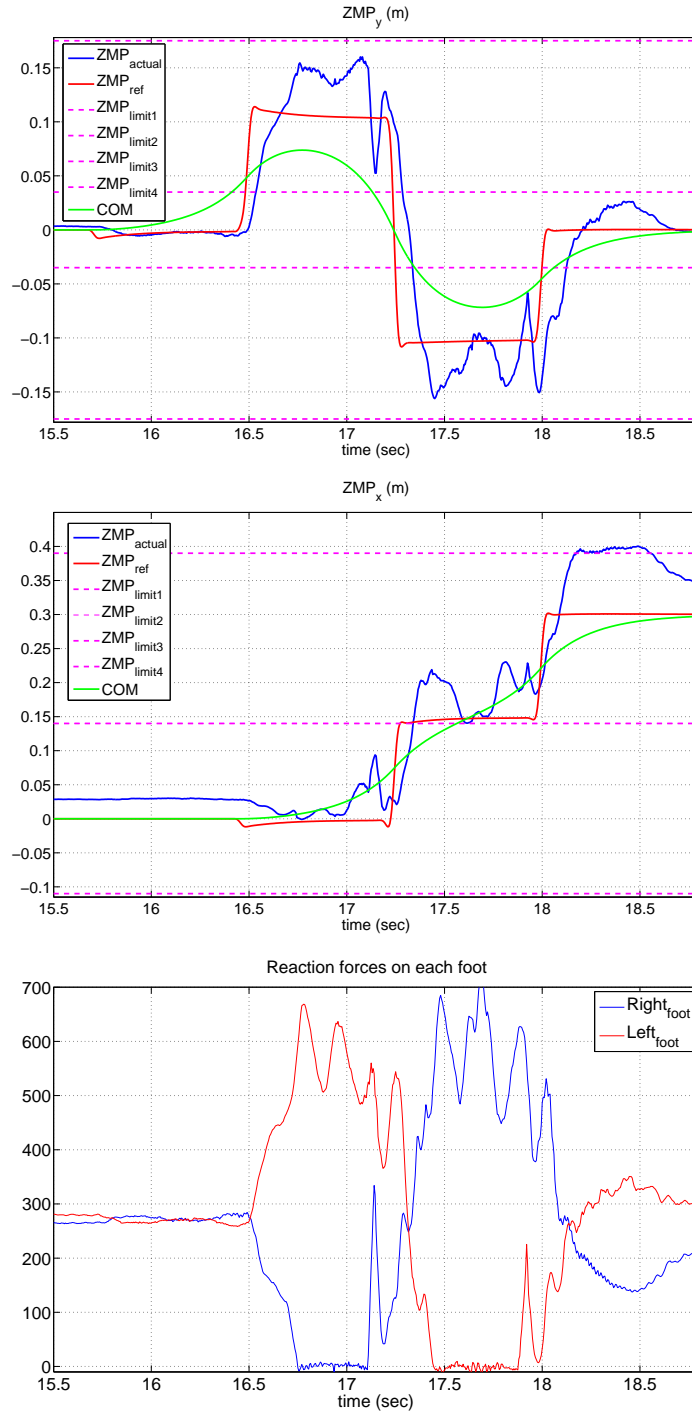


Figure 6.42: ZMP_y , ZMP_x reference and measuring. COG_y , COG_x trajectory and vertical reaction forces on each foot.

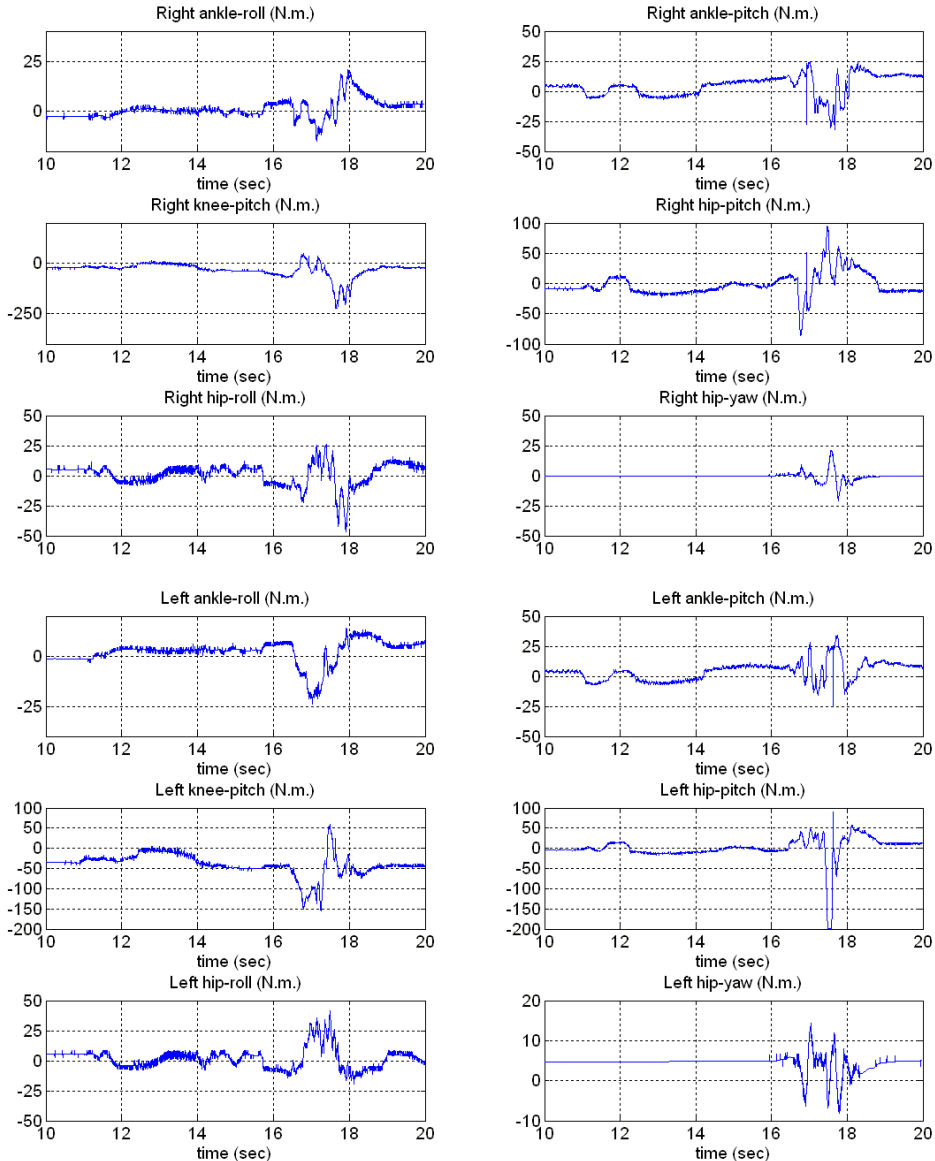


Figure 6.43: Torques on each joint of both legs while taking two acyclic steps forward.

At first, the body is going to the lower configuration while the humanoid is taking the first acyclic step. After that, the body goes to the goal configuration while the robot takes the second acyclic step. The experiment is validated in the actual humanoid robot (Fig. 6.41). The actual ZMP is constrained all the time to the support area, in the frontal and sagittal direction, as is shown in Fig. 6.42, when the maximum error is about 0.05m in both directions. This way, dynamical stability is obtained. As in the previous cases, the reaction force on the support feet remains around the weight of the humanoid robot and

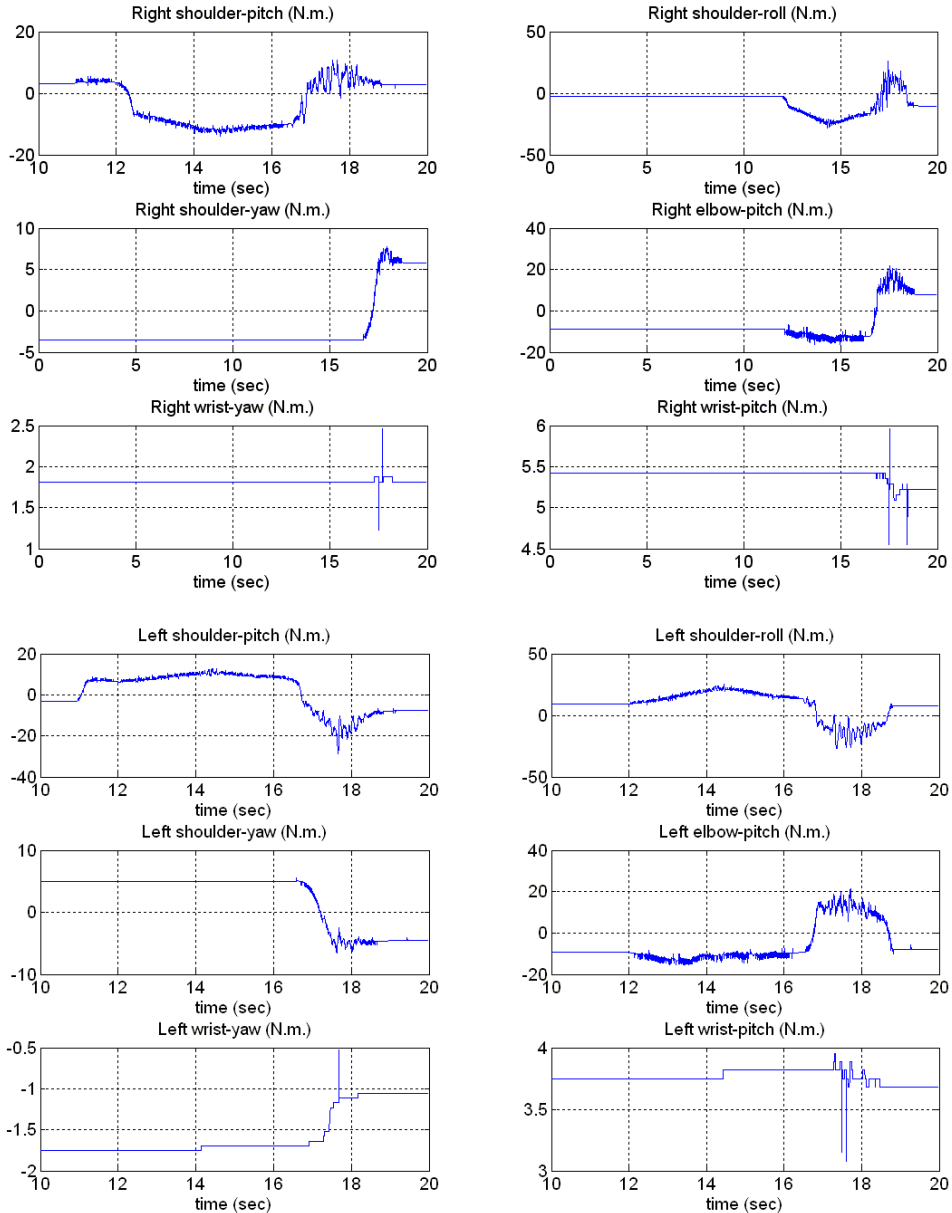


Figure 6.44: Torques on each joint of both arms while taking two acyclic steps forward.

equititative mass distribution is observed on double support. Thus the motion pattern is validated by this fact, too.

The torques on each joint should be discussed in order to improve the motion patterns (Figs. 6.43 to Fig. 6.45) and reduce the overload joints, due to the inertial and gravitational effects during the motion. As you can see, the higher torques are supported by the knees, so the motion pattern, when the robot's

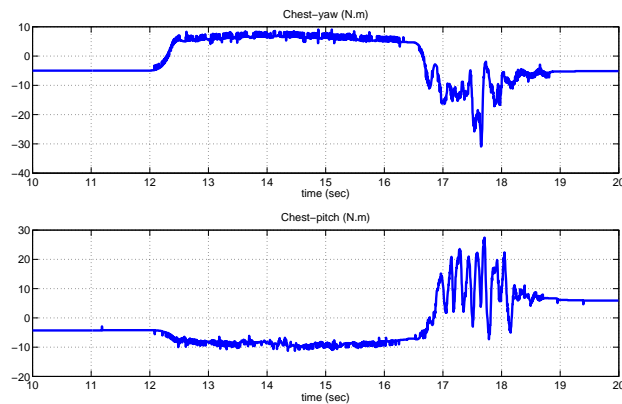


Figure 6.45: Torques on chest while taking two acyclic steps forward.

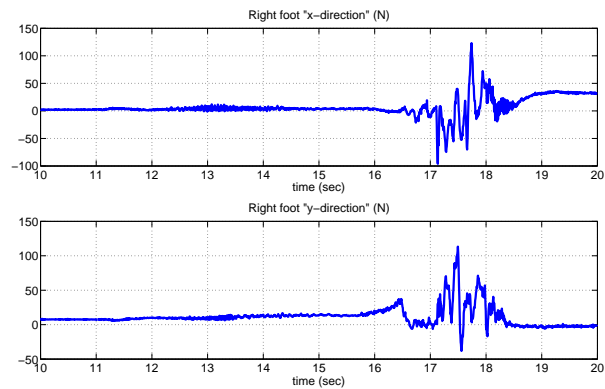


Figure 6.46: Horizontal force reactions on right foot.

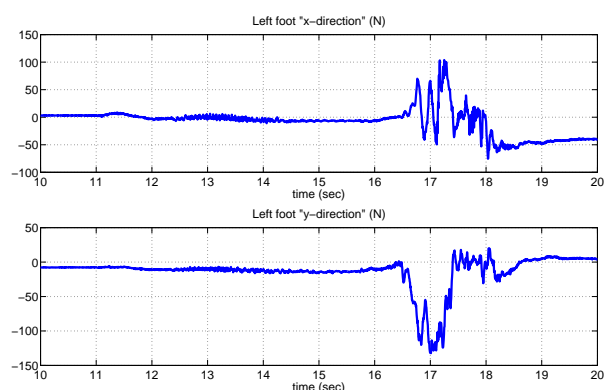


Figure 6.47: Horizontal force reactions on left foot.

weight is going down, should reduce the speed in order to reduce the dynamics effects. The torque in the left hip joint (pitch axis) supports a peak when the right foot starts the climbing motion. In this stage, the robot body is going up at high speed, so it is better to reduce it in order to improve the hip torque behaviour.

Furthermore, the reaction forces on the feet in the horizontal directions increase during the single support phase on each foot due to surface friction (Fig. 6.46 to Fig. 6.47). Therefore, in order to reduce the sliding, those forces should take into account in the humanoid robot controller to improve the acyclic gait.

Conclusions

The proposed algorithms are successful, validated by many simulations and experimental results on two humanoid robot platforms: the Rh-1 and the HRP-2. Some experiments shown in this chapter successfully validate the proposed solution to generate a dynamic acyclic humanoid robot motion. The kinematic and dynamic models proposed are also valid. Hence, the Screw theory, Paden-Kahan sub-problems and the Lie groups are an alternative solution for the kinematic and dynamic humanoid robot modelling, which avoids internal singularities and gives us a direct analytical solution. In the Rh-1 humanoid robot, the walking pattern generation method is validated on the simulator and in straightforward walking by the real robot. Due to the absence of inertial and force sensors feedback, only a few steps of dynamic gait were realized. What follows are the main improvements in the next version of the humanoid robot platform to obtain stable walking motion:

- More powerful motors must be used in the knee and hip (Pitch) to increase the walking velocity with this weight.
- More powerful servo-drivers for supplying peak currents on overloaded joints, during any motion, especially starting the single support phase.
- Improve the walking pattern generation to obtain smooth patterns and be able to increase walking velocity.
- Improve the mechanical structure on the overloaded joints (ankle and hip) in order to reduce the gravitational effect on starting the single support phase.
- Close the control loop with the inertial sensors.
- Mounting the force/torque sensors on foot and hands to close the ZMP and impedance control loops.
- Increase the degrees of freedom for the arms in order to have better manipulability, especially in cooperation tasks.

In the HRP-2 humanoid robot, the proposed walking pattern generator has been tested successfully with the improvement of “acyclic gait motion”. The ZMP Preview Control method can also be employed in this case to generate the dynamically stable acyclic motion patterns.

Chapter 7

Conclusions, contributions and future works

7.1 Conclusions

Although stable humanoid locomotion is not a closed problem, this work has proposed and validated a feasible methods for generating stable walking patterns. The conclusions of the present work are detailed as follows:

1. Trends of humanoid robots construction

Human evolution to bipedalism is an option for developing intelligent machines. That way, some progress on walking robotics was explained with the emphasis on the results in the few research groups around the world. Though walking robotics is an important and attractive research area in robotics, not enough applications have been made yet. For the future of walking robotics, considering how to improve this situation will be necessary.

This was briefly discussed and reconsideration of the goal of walking robotics research was pointed out for the improvement of the situation. As an example of the trends about humanoid size, weight and structural complexity, the evolution of HONDA robots is shown in Fig. 7.1.

From the picture above, in order to reduce power consumption and increase motion stability, the weight and height are reduced throughout the construction of humanoid robot prototypes. The degrees of freedom (DOFs) are the minimum for high dexterity by using strong, light materials, small electronic but powerful devices, high torque motors, powerful modelling and control algorithms.

Other important groups such as Kawada-AIST and Waseda have developed high dexterity humanoids robots, so the arms and body DOF increase, the height is about 1.60m and the weight is maintained around 60Kg. In these cases, the height and weight end to human measurements, (as seen in Fig. 7.2, Fig. 7.3).

From this analysis of the most important humanoid robot projects, the mechanical size and configuration of the Rh-1 and Rh-2 prototypes are

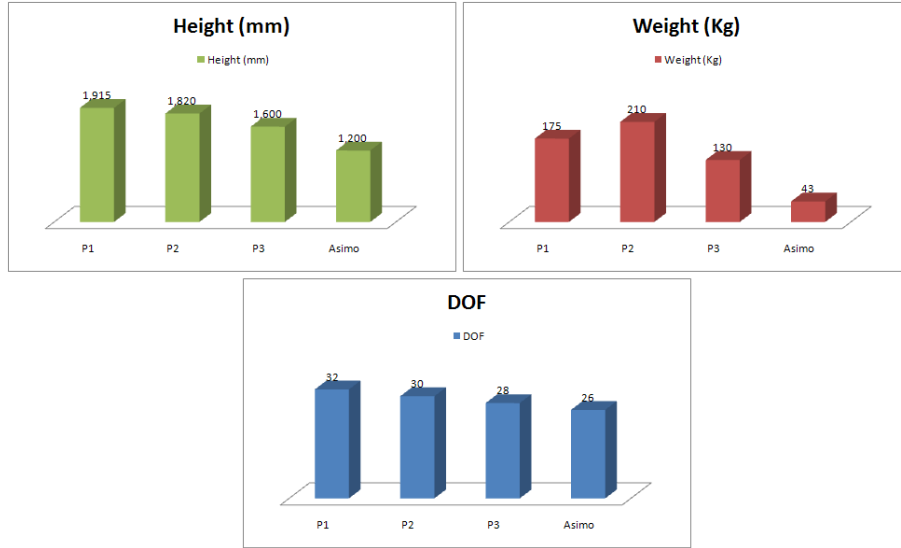


Figure 7.1: The evolution of HONDA humanoid robots.

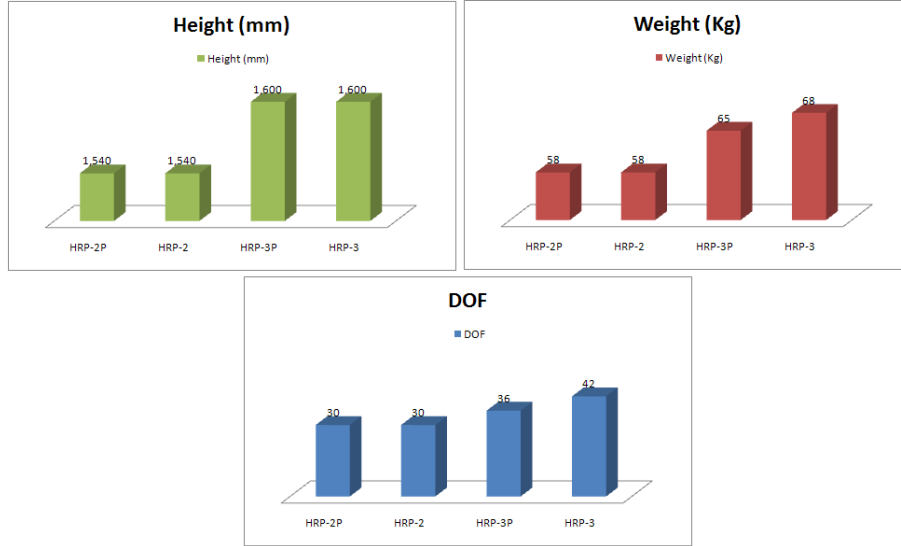


Figure 7.2: The evolution of the Kawada-AIST humanoid robots.

explained as following: the Rh-1 was developed for cooperating at indoor environments, that way the selected dimensions take as an approach the ASIMO robot ones; that is, Rh-1 could attend to a sitted person. For that, the height of 1.35m is enough. Otherwise, the current Rh-2 prototype will be designed for cooperating at outdoor environments, so the trend is to approach the HRP-2 platform; because, it was developed for working in cooperation with a stand up person. Thus, the height selected is about 1.50m and more complex kinematics will be developed, specially in the

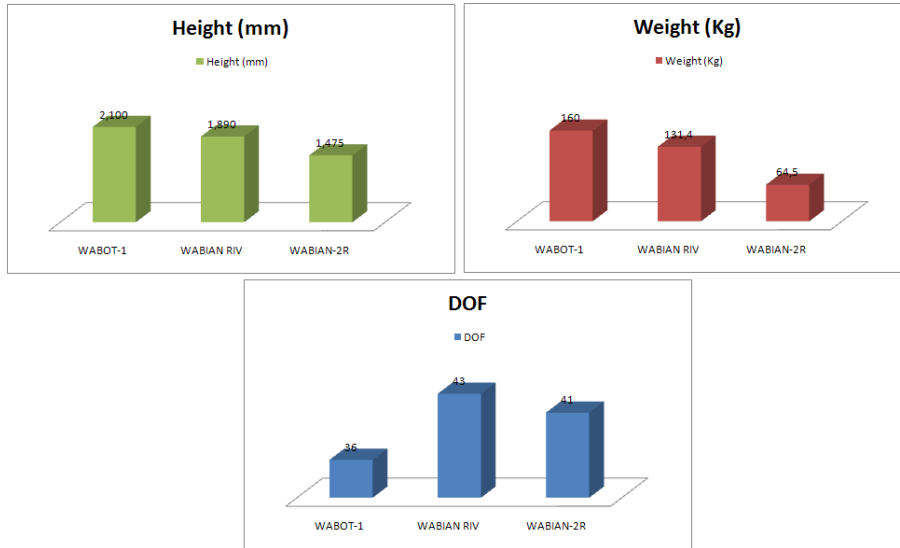


Figure 7.3: The evolution of the WASEDA humanoid robots.

arms, in order to increase its manipulability.

2. About human locomotion and humanoid robot locomotion

Normal bipedal gait is achieved with a complex combination of automatic and volitional postural components. Normal walking requires stability to provide antigravity support of body weight, mobility of body segments and motor control to sequence multiple segments while transferring body weight from one limb to another. The result is energy-efficient forward progression. Human “gait cycle” has been analyzed in order to understand biped walking motion its main phases, single support and double support phases and their properties: force reaction, cycle time, foot, knee, hip and body motion trajectories. So humanoid robot trajectories could be created on the order of the human ones. It is demonstrated that the COG human motion follows the inverted pendulum laws at normal walking velocity, which is an important fact for maintaining stability while walking. The stability criteria for obtaining stable biped walking have been outlined, especially the “Zero Moment Point (ZMP)” criterion, which is the most popular and most often applied to humanoid robots in the world. The concept of ZMP has and will have an essential role in both theoretical considerations and the practical development of humanoid robots and biped locomotion. The farther away the FRI point is from the support boundary, the larger the unbalanced moment on the foot, and the greater is the instability. The distance between the FRI point and the nearest point on the polygon boundary is a useful indicator of the static stability margin of the foot. It is concluded that the dynamic stable “biped gait” should take into account the whole body dynamics to make any motion on any surface. It could be simplified as a single mass dynamics motion on specific cases, such as walking on a flat surface with straight arms and torso

upright. Further research related to humanoid-human cooperation should be made in order to handle ordinary tasks in human environments. This research is oriented to maintaining stability with multi-contact points, on any terrain, and while carrying objects; such as the CWC, which checks if the sum of the gravity and the inertia wrench applied to the COG of the robot, is inside the polyhedral convex cone of the contact wrench between the feet of a robot and its environment. This criterion can be used to determine the strong stability of the foot contact even when a robot walks on an arbitrary terrain, other than a horizontal plane and/or when the hands of the robot are in contact with the terrain, under the assumption that sufficient friction should exist at the point of contact. That could be detailed in other works, whose are not the objective of the current one.

3. Humanoid robot locomotion

The concepts of passive and active walking have been explained in order to give a background of biped robot gait generation models. The static gait, useful for low scale biped/humanoid robots and the dynamic gait used in the human-size biped/humanoid robots, are outlined and discussed. Some well-known gait generation models have been detailed in this chapter and have been tested on some biped and humanoid robots. At first, some methods do not take into account biped dynamics such as the Joint space method, which is an intuitive choice suitable for static gait cases it generates straightforward joint patterns without inverse kinematics or direct dynamics. This method interpolates trajectories between the joint boundary conditions, limited by the step length, height, orientation, velocity and accelerations depending on the interpolators; this method is not suitable for three-dimensional dynamic biped walking patterns, because the coordination between the sagittal and the frontal (or coronal) plane is not easy to obtain. The virtual force model outlines an interesting approach on uneven terrain, but only in the planar case. Furthermore it is not clear what biped walking stability criteria is being used. Other methods which take into account biped dynamics, such as mass distributed models are outlined. The sufficient friction of multi-contact point method is explained in order to illustrate the strong stability criteria in a multi-body walking pattern generator. The high computation time doesn't allow applying the walking pattern calculations in real-time, because the whole body dynamics need an iterative process with many variables to get the solution. Another approach models the swing foot like many inverted pendulums with successful results, but with preplanned walking patterns, because the iterative solution. In this case the real-time applications is not possible either. Under the dynamics modelling of walking pattern generation, the mass concentrated model is a good choice for real-time application. The objectives of the mass concentrated models for developing a stable gait of a biped robot are to obtain suitable COG and ZMP reference trajectories. They should perform like the multi-body robot dynamics and the trajectories can be computed in real-time. The preview controller of the ZMP is one method for generating a stable biped walking patterns and satisfies successfully the objectives. This thesis has used the last models, because it is demonstrated in this chapter, that humanoid robot performance during the walking motion could be developed stably by controlling a single

mass motion on a plane, in space, by following the ZMP constraint.

4. About gait generation method

The walking pattern generation method has been detailed in the chapter 5, which is composed of five layers. Each of them is obtained by dividing the problem into lower ones. With this research, the walking pattern generation method is validated with the Rh-1 humanoid robot and alternative ability is proposed in the HRP-2 humanoid robot platform. It is called “Acyclic gait”. The “Acyclic gait motion” of humanoid robots could be a challenge of input design parameters of the robot, motion patterns and control system, because, if the humanoid robot could walk in any way, it would be easier to achieve the standard gait. Expanding the joint angle ranges, previously in the humanoid design phase could be achieved by this kind of gait. A method dealing with non-cyclic planar footstep motion with different body configuration is proposed. It is validated by several simulations and experimental results on the humanoid robot HRP-2. The kinematics proposed is also valid. Hence, the screw theory, Lie groups and Paden-Kahan sub-problems prove to be suited to the kinematics and dynamic humanoid robot modeling, which avoids internal singularities and gives us a direct analytical solution. The ZMP Preview Control method appears to be robust enough to be applied even in this case, in which the height of the COG varies in order to generate dynamically stable acyclic motion patterns. Future work is focused in complementing the method with auto-collision avoidance in order to constrain the motion to physical limits automatically and also to improve the compensation of vertical momentum on rotation motion. Other contribution of this research deal with to validate the ZMP preview control (Kajita et. al.) to generate acyclic gait motion, which has the following advantages:

- Predicts stable ZMP position based on mass concentrated model without taking into account the whole body humanoid configuration.
- The mass concentrated model allows generating walking patterns in real time.

5. About the results

- The proposed algorithms are successful validated by many simulations and experimental results on two humanoid robot platforms: the Rh-1 and the HRP-2. Some experiments have been shown in chapter 6, whose successfully validate the proposed solution to generate a dynamic acyclic humanoid robot motion.
- The kinematic and dynamic models proposed are also valid. Hence, the Screw theory, Paden-Kahan sub-problems and the Lie groups are an alternative solution for the kinematic and dynamic humanoid robot modelling, which avoids internal singularities and gives us a direct analytical solution. In the Rh-1 humanoid robot, the walking pattern generation method is validated on the simulator and in straightforward walking by the real robot. Due to the absence of

inertial and force sensors feedback, only a few steps of dynamic gait were realized.

- In the HRP-2 humanoid robot, the proposed walking pattern generator has been tested successfully with the improvement of “acyclic gait motion”. The ZMP Preview Control method can also be employed in this case to generate the dynamically stable acyclic motion patterns.
- These results show the overloaded joints, tracking the joint patterns in the control system of the Rh-1 humanoid robot, so those data could be used for improving the next version (Rh-2). Furthermore, the HRP-2 experimental tests shown more information such as force reaction, ZMP tracking and joint torques in a critical case (that is during acyclic gait). Those data could be used as reference for the next prototype (Rh-2).

7.2 Contributions

It is possible to summarize the main contributions of this thesis as following:

1. About walking patterns generation

- Proposal and validation of the “Local Axis Gait” (LAG) algorithm for generation of local motion planning (Arbulu et. al. 2007 and 2008, [12], [15]). This novel method computes generic steps, that is the step could be generated for going forward, backward, turning left or right, going to left or to right, at any flat surface with or without slope. Furthermore, it could generate walking patterns for climbing stairs. It has the next advantages:
 - The ZMP is always in the support polygon, so stable walking is obtained.
 - Intuitive foot step planning for generating stable walking patterns.
 - The use of mass concentrated model contributes to generate walking patterns in real-time.
- Proposal and validation the “Acyclic Gait” algorithm for humanoid robots. This algorithm is tested successfully on the humanoid robot HRP-2. It generates a dynamic transition between two generic stance humanoid configurations,(Arbulu et. al. 2008, [19]). Which has the next advantages:
 - The LAG algorithm is used in this method for planning the foot configuration.
 - The Preview control of the ZMP is used for generating the smooth COG motion. Furthermore, the ZMP is maintained inside the support polygon during the single support phase.
 - With the feedback of ZMP multibody in a second loop of the preview control, the stability is improved.

- Proposal and validation of a motion planning method of humanoid robots. It is composed by five layers and it computes the joint and ZMP optimized references of the humanoid robot, whose allow to Rh-1 humanoid robot (at open loop) walks until 0.7 Km/h and to the HRP-2 (at closed loop) walks until 1 Km/h .

2. About kinematics and dynamics modelling

- The alternative kinematics and dynamics modelling are validated in the Rh-1 and HRP-2 humanoid robot platforms.
- Implementation and validation of the use of screws, which provides a very geometric description of rigid motion, so the analysis of the mechanism is greatly simplified. Furthermore, it is possible to do the same mathematical treatment for the different robot joints: revolute and prismatic.
- Proposal and validation of the kinematics modelling of humanoid robots using screw theory and Paden-Kahan sub-problems, which have the following advantages:
 - Avoiding singularities because of the global description of the rigid body motion: we only need to define two frames (base and tool) and the rotation axis of each DOF to analyze the kinematics in a closed way.
 - The Paden-Kahan sub-problems allow us to compute the inverse kinematics at the position level.
 - Faster computation time of the inverse kinematics compared to the inverse Jacobian method, Euler angles or D-H parameters, so it contributes to real-time applications.
- Proposal and validation of the dynamics modelling of humanoid robots using the screw theory and Lagrange method, which have the following advantages:
 - To compute the Jacobian, it is not necessary to derivate only a set of matrix transformations is needed (including the twists).
 - The Lagrange method allows us to solve the equations in a closed form and it is possible to make detailed analyse of the system's properties.

3. About simulator environment and gait generation code

- Developing a simulator environment in order to test the proposed algorithms on the robot. This simulator has been developed with VRML format. The functions (of the humanoid model) run on MATLAB Simulink. Simulations of static and dynamic gait are developed; after that the walking patterns have been tested in the real robot. Furthermore, this simulator could be customized for any robot.

- A gait generation code for applying in realtime on humanoid robots. This code could be customized for any humanoid robot, only it is necessary to change the parameters of kinematics and dynamics.

4. About contribution on Rh-1 and Rh-2 humanoid robots

- Kinematics specifications for designing the Rh-1 humanoid robot, and specifications of the Rh-2.
- The number of DOF, body dimensions and body configuration have been proposed of Rh-1 humanoid robot.
- Introducing the Rh-1 kinematical, dynamical, control, mechanical, electrical problems for improving the new humanoid version (Rh-2).

5. About papers, journals, end-of-course projects

- Applying the static gait to the CONDO humanoid robot and receiving the First Award in Almeria, Summer 2006.
- Preparing notes for the Summer School in Benicassim in 2006. Technical notes about kinematics and dynamic walking patterns, whose have been implemented in the Rh-0 humanoid robot from 2005 until 2006.
- About 20 papers as co-author, 9 written on my own (see [12], [13], [14], [16], [17], [18], [19]), one journal article accepted, [15] and two journal articles submitted.
- About 7 end-of-course projects as tutor. Those projects deal with the kinematics and dynamics humanoid modelling, simulation environments and walking pattern generation code.

7.3 Future work

What follows are the main improvements in the next version of the humanoid robot platform to obtain stable walking motion and additional abilities:

- Walking patterns based on a complex dynamics model. This kind of model could improve the motion control of the whole-body robot, so more stable walking is obtained. Furthermore, improve the walking pattern generation to obtain smooth patterns and be able to increase walking velocity.
- To make the dynamic model similar to the actual robot. So, the dynamic model could predict closely the real humanoid behavior, that prediction contributes to tuning correctly the control parameters.
- Hardware and software improvements such better components and the real-time operating system.
- Increase the degrees of freedom for the arms in order to have better manipulability, especially in cooperation tasks (i.e. Fig. 7.4).



Figure 7.4: Cooperation tasks on construction.

- Close loop control to obtain stable walking with the inertial sensors' and the force/torque sensors on foot and hands.
- Additional friction control should be developed (see Fig. 7.5).

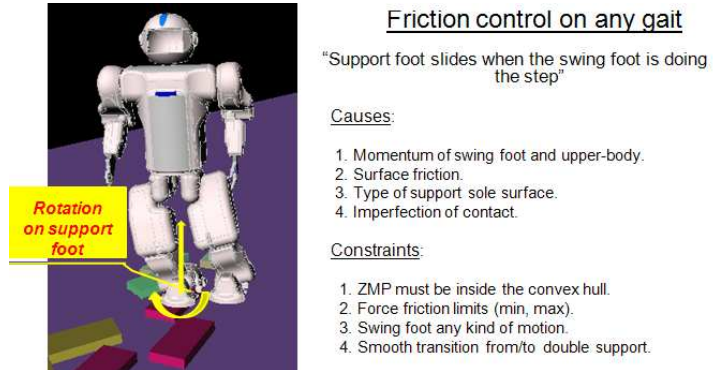


Figure 7.5: Friction control of foot rotation.

- Improve the mechanical structure on the overloaded joints (ankle and hip) in order to reduce the gravitational effect on starting the single support phase.
- More powerful servo-drivers for supplying peak currents on overloaded joints, during any motion, especially starting the single support phase (see Fig. 7.6).
- More powerful motors must be used in the knee and hip (Pitch) to increase the walking velocity with this weight (see Fig. 7.6).
- Mounting powerful interaction devices such stereo cameras, array of microphones, artificial skin, laser telemeter. With that devices it would be

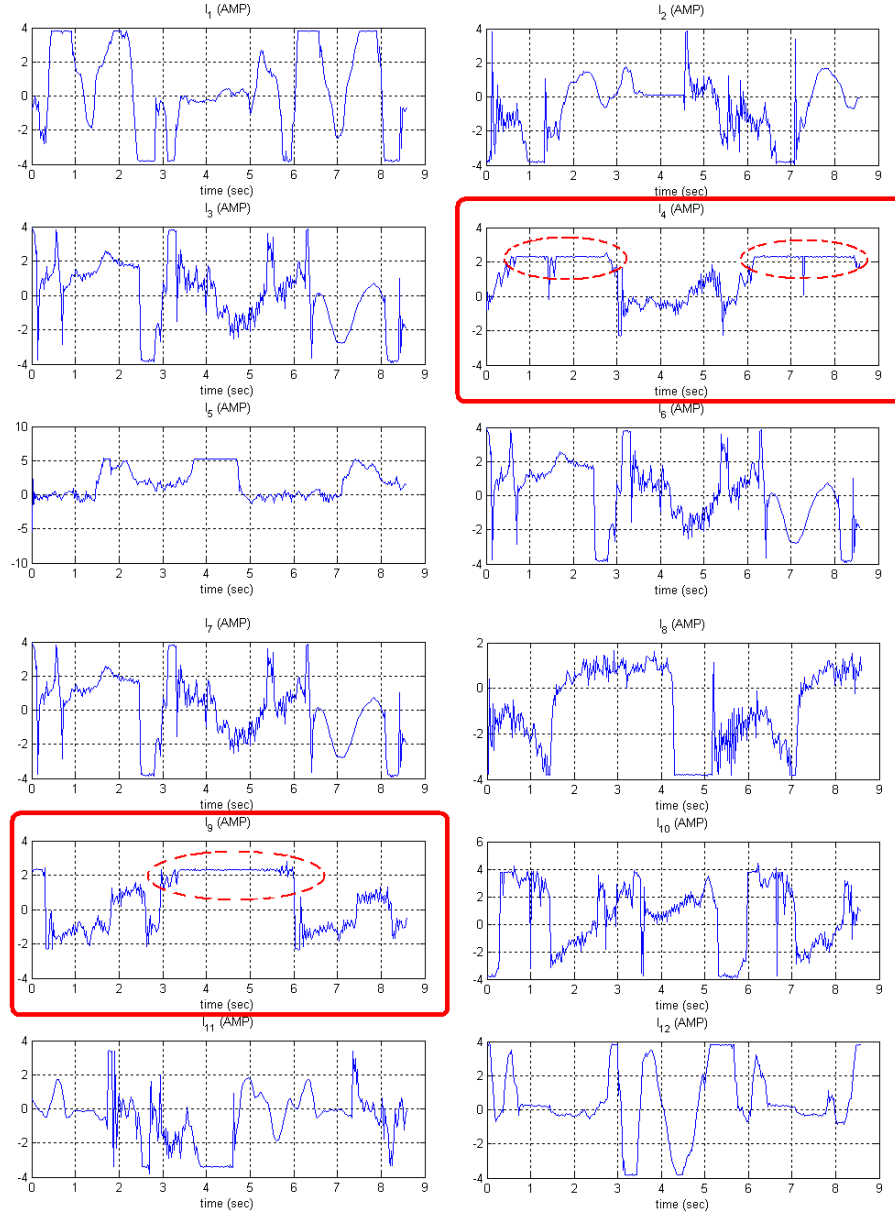


Figure 7.6: Current consumption by left (q_{10}) and right (q_4) hips (Pitch direction, red rectangles). In red rectangles the currents are constant, because the load requires the motor current limit.

possible to create an environment map, in order to get its own location and planning optimal routes.

Appendices

Appendix A

Human COG projection and ZMP Measure system

In this appendix, the COG projection on the floor (center of pressure, CoP) and ZMP measure system developed in the robotics lab are described. This section deals with the hardware, software and experimental results [18].

Hardware Architechture

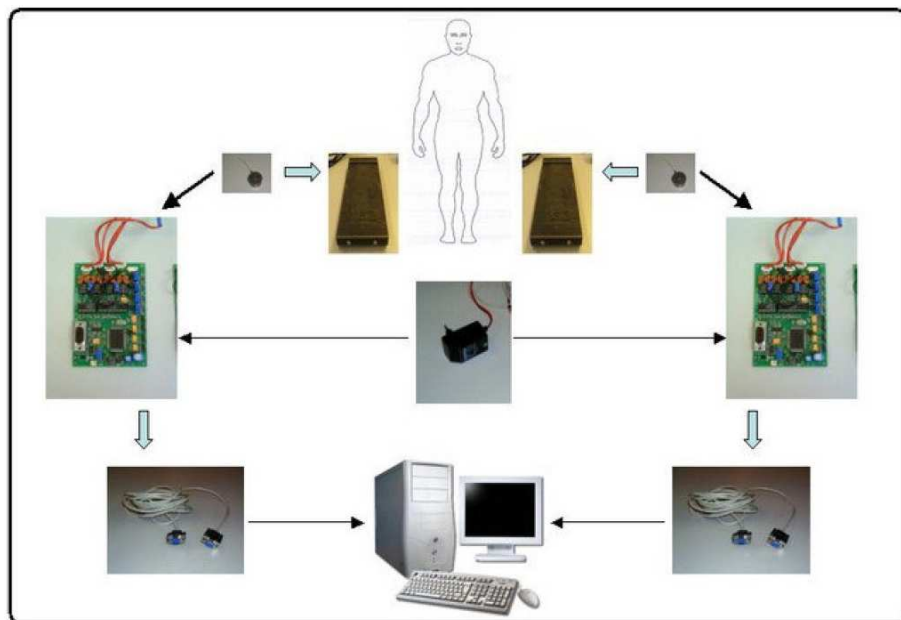


Figure A.1: ZMP hardware measure system.

The hardware architecture (see Fig. A.1) is composed by the following components: two metal platforms, eight load cells and two data acquisition cards. The metal platforms each have four load cells; both platforms act like shoes

on the human walker. The load cells take the measure of the force reaction and those take into account the mass distribution of the human body while it is walking. The data acquisition cards receive the data from the load cells and those have two functions: the first function is to compute the position of the force reaction and the other is to send the measure of each load cell with the result of the first function.

a) Two metal platforms

A human will put the metal platforms on his/her feet, and then he/she will walk with them. One platform and four load cells for one foot is shown in Fig. A.2. Rectangular platforms are used in order to minimize errors, and they were designed to have minimum friction with the floor.

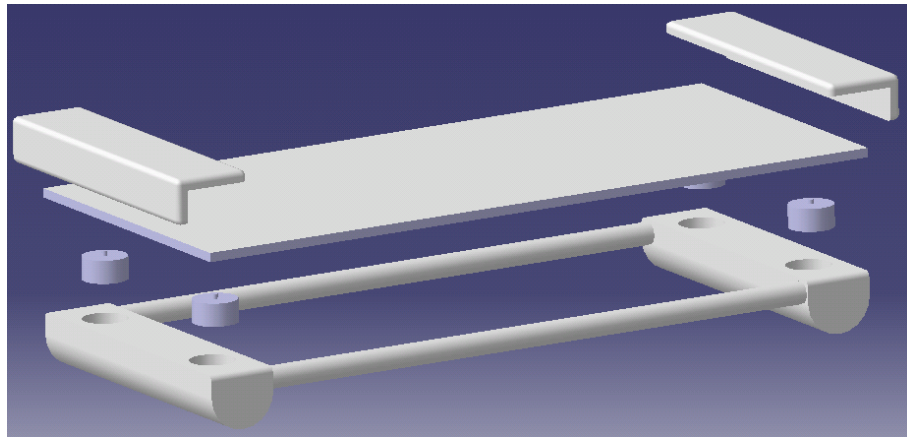


Figure A.2: CAD design of the metal platform with load cells.

b) Eight load cells

There are four load cells for each platform (eight in total), located at the corners of the platform. This layout with four contact points is enough to cover the stability area (Fig. A.2).

Kyowa LM-50KA load cells are designed to resist up to 51kg. Load cells work like a full Wheatstone bridge. This one axis sensor is quite good for achieving our first objective: to watch the On-Line trajectory of the Center of gravity projection.

c) Two data acquisition cards

The output of the load cells will go to a data acquisition cards to convert the signal into a digital one. These cards can get up to 100 samples per second coming from the load cells (see Fig.A.3).

The characteristics of each card are as follows:

- Four input for load cells.
- Supply for the cells.

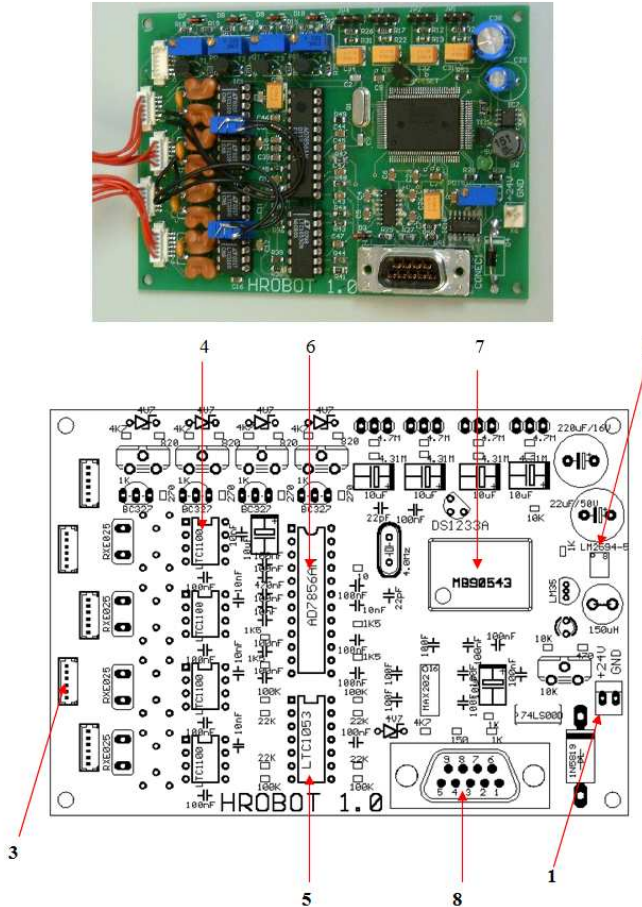


Figure A.3: Acquisition card.

- Amplifier.
- 14 bit conversor.
- Number of samples per sec.: 100.
- Power supply: 24 Vcc.
- Output RS-232 (communication with PC).
- Small dimensions: 80mm x 110mm.

Software Architecture

The load cell measures should be processed and shown in an output system like a PC. Thus, a custom software system has been developed. One of the most important advantages of this experiment is the possibility of watching the walking movement on-line. An interface has been programmed to show on the PC screen the movement of the platforms and the COG and ZMP trajectories (Fig. A.4). The MatLab GUIDE (Graphical User Interface Development Environment [4]) has been chosen for programming. The software architecture is shown in Fig. A.5. Via the serial port, the data from the acquisition cards are read

and shown on the screen of the PC. The user can view the human steps and the on-line COG evolution on the screen. After that, it is possible to analyze the COG motion off line, in two directions (frontal and sagittal), and compute the ZMP in order to verify the dynamic stability while the human is walking. The concentrated mass model has been used to compute the ZMP. Successful results have been obtained, and the mass concentrated model is validated, and can be used for planning humanoid robot walking.

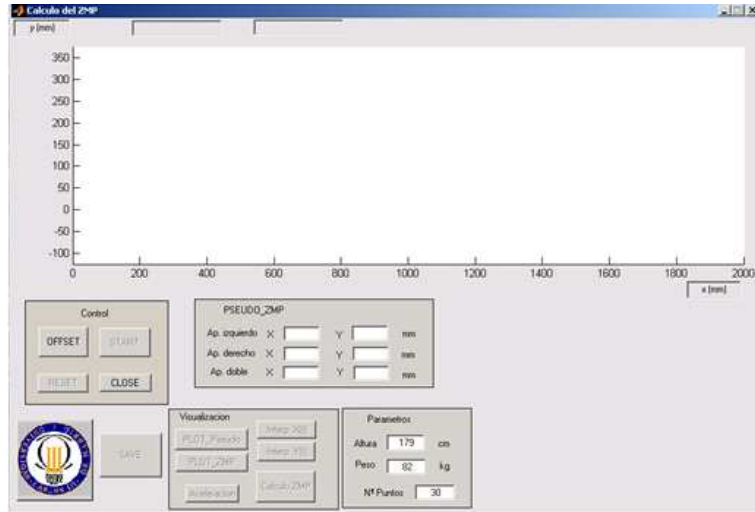


Figure A.4: ZMP guide overview.

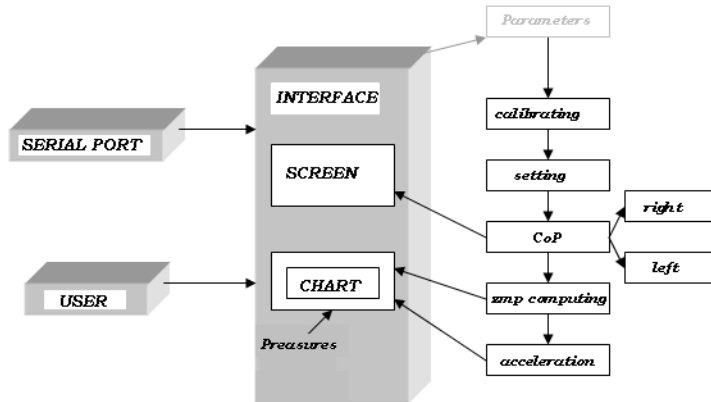


Figure A.5: ZMP software structure.

The interface (Fig. A.5) interacts with many functions like calibrating, setting, COG projection (or Center of Pressure, CoP) computation, acceleration and ZMP computing. After introducing the parameters, the calibration and setting process is done; it is ready to start the walking and take the measure of the CoP. This measure will be shown in the following section, and it is computed

as follows (Fig. A.6):

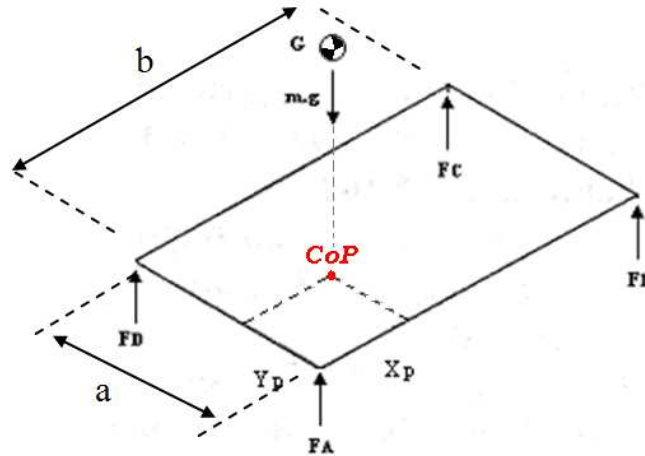


Figure A.6: Center of pressure computation, taking into account the forces of each corner on the platforms.

$$F_A + F_B + F_C + F_D = W \quad (\text{A.1})$$

$$\sum M_Y = 0 \rightarrow x_P = \frac{F_B + F_C}{W} \cdot a \quad (\text{A.2})$$

$$\sum M_X = 0 \rightarrow y_P = \frac{F_D + F_C}{W} \cdot b \quad (\text{A.3})$$

Thus the CoP is computed by the total momentum (eq. A.2, A.3). It is clear that it is possible to measure only the vertical forces on each platform corner, because the load cells can take only this measure on the vertical axis. It is enough for us in order to measure the CoP, especially in the single support phase, because it is the critical one.

Experimentally, for slow walking motion, the center of pressure must be inside the center of the support sole (static gait). However, for normal walking motion (about 1 Km/h or more, dynamic gait), the CoP should stay outside of the support sole. With this system, both cases are validated. Furthermore, the mass concentrated model (3D-LIMP, will be detailed in Chapter 5) could be used to compute the ZMP position.

Experimental results

The experimental results (Fig. A.7) can be detailed as follows. The online CoP position while the human is walking can be seen in Fig. A.9 by the black circles for the single support phase and in the red ones for the double support phase. It is clear that the CoP motion is similar to the inverted pendulum orbit under the field of gravity, as we will explain later. However, for analyze the CoP trajectory, it is possible to join the preview points after the on-line tests (see

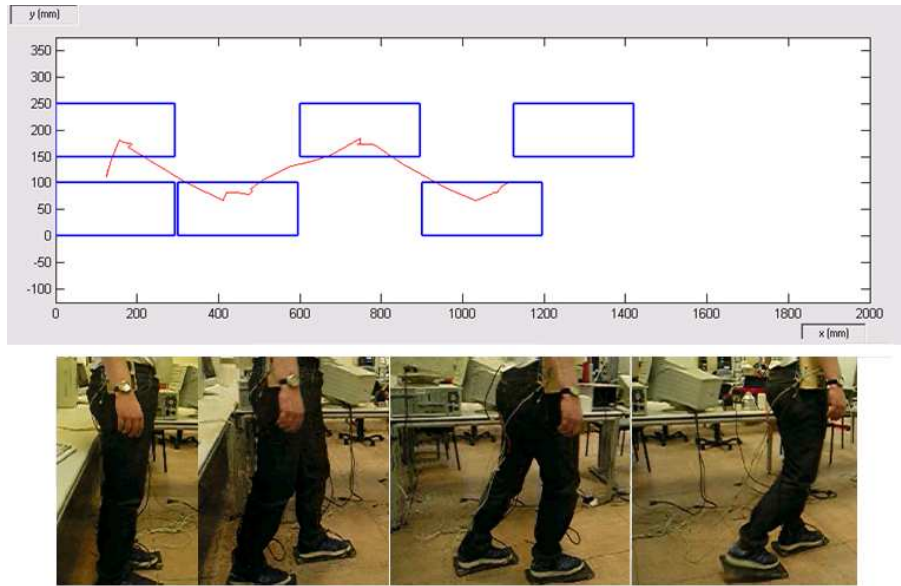


Figure A.7: Experimental walking test.

Fig. A.10). The red trajectory is not in the middle of the support foot in the single support phase, because dynamic human walking is done. Furthermore, the interface allows us to view the CoP trajectory in “x” and “y” directions (sagittal and frontal), as shown in Fig. A.11 and Fig. A.12; the performance is similar to the uncoupled COG motion under pendulum laws. Finally, the velocity change (acceleration, Fig. A.13) can be plotted in order to visualize the dynamics of the CoP. This acceleration values is used to compute the ZMP (Fig. A.14) as previously defined. During dynamic stable walking motion, the ZMP is always inside the support polygon. In conclusion, this test allows us to predefine the COG and ZMP reference trajectories in order to obtain dynamic stable walking.

To compute the ZMP, the approximate mass concentrated model is used (Fig. A.8):

$$(x - zmp_x) = \ddot{x} \cdot \frac{z_c}{g} \quad (\text{A.4})$$

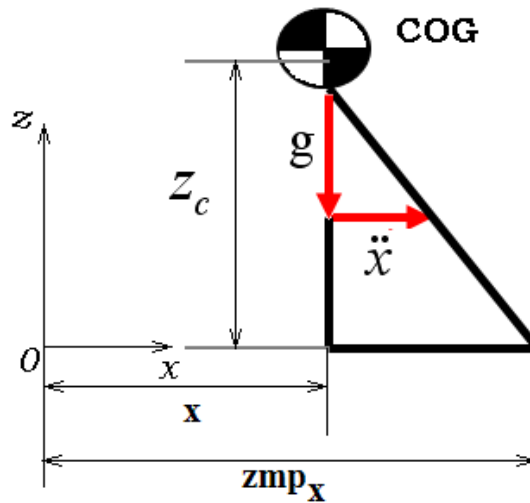


Figure A.8: ZMP_x computation, with mass concentrated model.

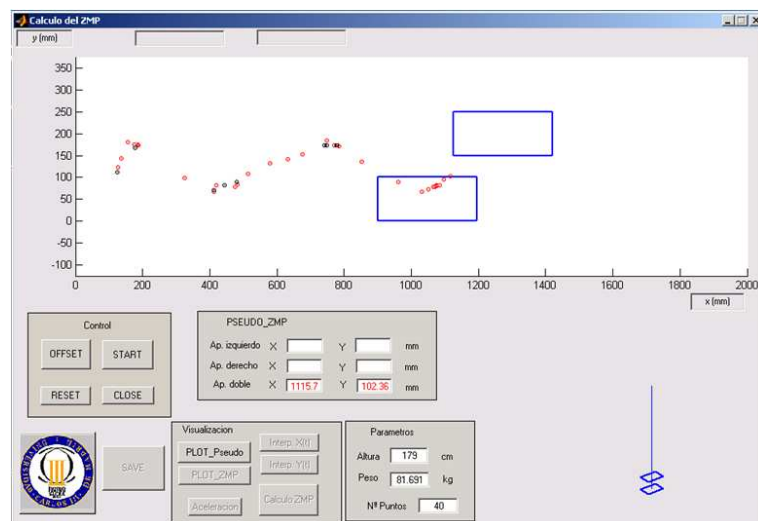


Figure A.9: On-line measure of experimental walking test.

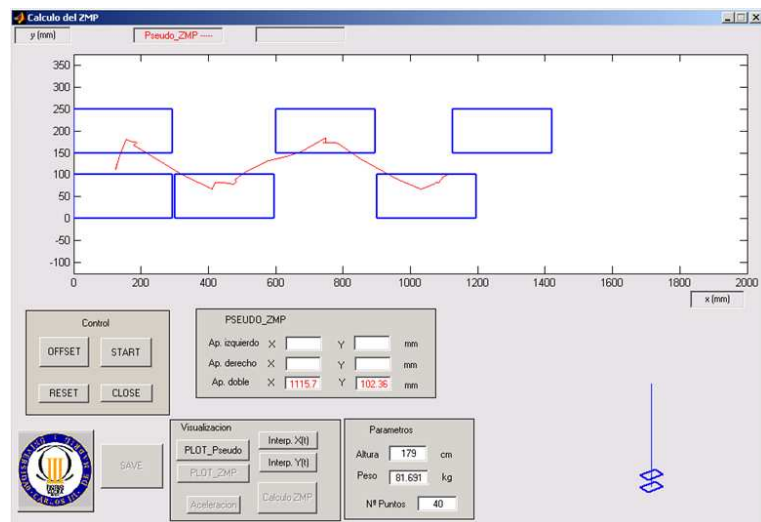


Figure A.10: Off-line chart of preview experimental walking test.

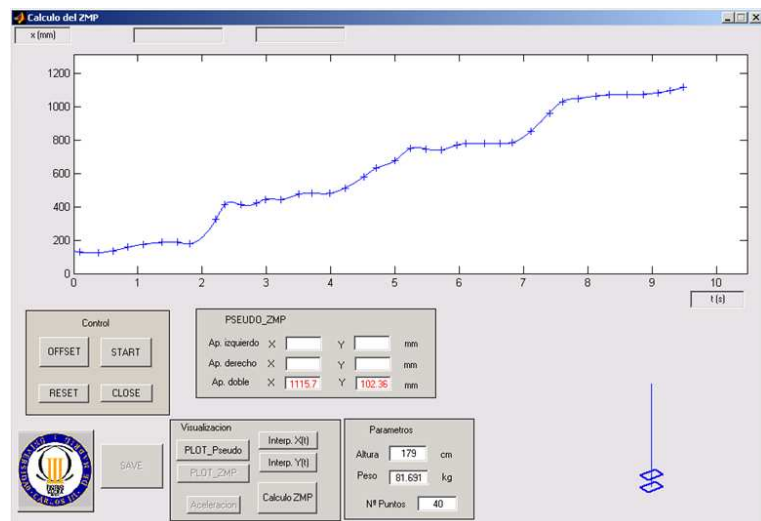


Figure A.11: Plotting sagittal CoP motion.

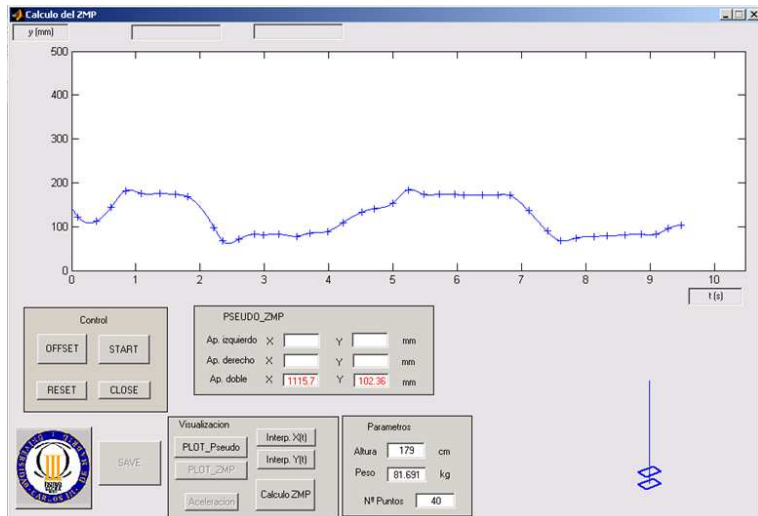


Figure A.12: Plotting frontal CoP motion.



Figure A.13: Acceleration in each direction.

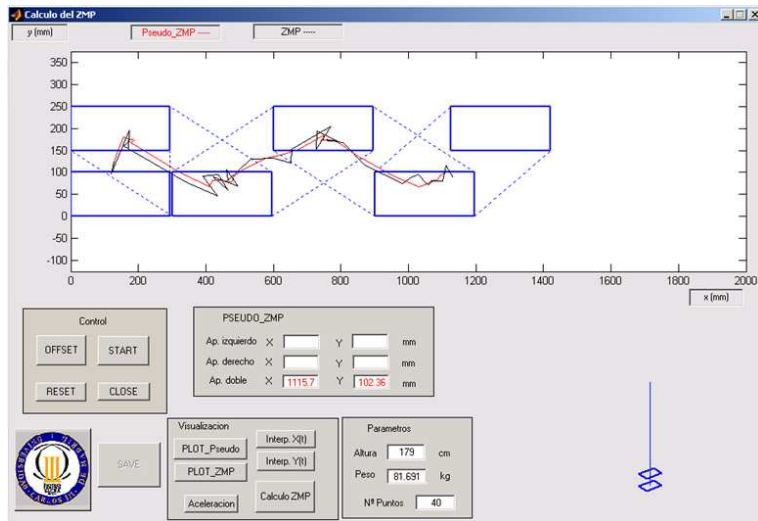


Figure A.14: ZMP evolution (black line).



Figure A.15: Experimental walking test.

Appendix B

Distribution of masses and inertias of medium human

Regarding mass distribution (*from the Naval Aerospace Medical Research Laboratory and coworkers, Vol. I: Male aviators, [20]*, which will be partially reproduced in this appendix), the following tables show the mass and inertia moment of each human link (Tables B.1 to B.11).

Body Segmentation

In order to describe its mass distribution properties, the body is segmented by planes as shown in Figure B.1. These planes relate to the body in the erect standing position and are identified as described below:

1 HEAD PLANE: A plane that passes through the right and left gonion and nuchale.

2 NECK PLANE: A compound plane in which a horizontal plane through cervicale intersects anteriorly with a second plane. The second plane passes through the lower of the two clavicle landmarks, is perpendicular to the midsagittal plane, and makes a 45 degree angle with the horizontal plane.

3 THORAX PLANE: A horizontal plane that passes through the 10th rib midspine landmark.

4 ABDOMINAL PLANE: A horizontal plane passing through the higher of the two iliocristale landmarks.

5 HIP PLANE: A plane perpendicular to the frontal plane passing through the center of the crotch and the midpoint between the anterior superior iliac spine landmark and trochanterion.

6 KNEE PLANE: A horizontal plane passing through the lateral femoral epicondyle.

7 ANKLE PLANE: A horizontal plane passing

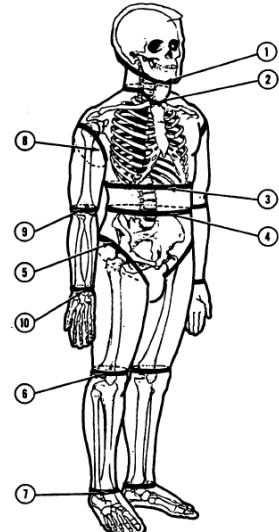


Figure B.1: Planes of body segmentation.

through the sphyriion landmark.

8 SHOULDER PLANE: A plane passing through the acromion landmark and the anterior and posterior scye point marks of the axillary folds.

9 ELBOW PLANE: A plane passing through the olecranon process and the medial and lateral humeral epicondyle landmarks.

10 WRIST PLANE: A plane perpendicular to the long axis of the forearm passing through the radial stylion landmark.

The mass distribution data were calculated from regression equations reported in McConville et al. (1980), [83]. These data are based upon a stereophotometric assessment of volume. The assumption that the distribution of volume can be substituted for the distribution of mass is supported by the data reported in Young et al. (1983), [130]. The reader is referred there for more information.

The alignment of principal axes for each segment, the mass, and principal moments of inertia (calculated with respect to the segment center of mass) are presented in Table B.1 to B.11. A general assumption of body symmetry with respect to the midsagittal plane has been made so that properties of right and left segments are identical.

For purposes of specifying the segmental principal axes directions, a whole body reference axis system (r) is defined. This reference system is based on a standing surface in which the X_r , axis points anteriorly, the Y_r , axis to the left and the Z_r axis vertically upward.

The principal axes neck, thorax, and pelvis are rotated from this reference position, as shown in Table B.1 to B.11. The principal axes for the extremity segments (with the exception of the hand and foot) are such that the Z_p axis is aligned with the long axis of the bones and the X_p and Y_p axes are perpendicular to it with no preferred direction since the X_p and Y_p principal moments are equal. The orientation of the principal axes for the hand and foot are coincident with the reference axes.

For the head, a local anatomically defined coordinate system (a) is used as the reference coordinate system. It is defined by the Y_a , axis running from the right tragon to the left tragon, the X_a , axis being the normal vector from the Y_a axis to the right infraorbitale, the Z_a axis being formed by the cross product of the X_a and Y_a axes vectors, and the origin being located on a line connecting the tragions (Y_a) at a point closest to sellion. The relative orientation of the principal axes for the head to the anatomical axes (a) is shown in Figure B.2. For the head, the X_p axis is rotated 36 degrees counterclockwise about the Y_a axis.

The segmental masses were determined from the relative proportions of segmental volumes obtained from regression equations developed by McConville et al. (1980), and total body masses of 63.3 kilograms for the small-sized man, 81.5 kilograms for the Mid-sized man and 97.7 kilograms for the large-sized man.

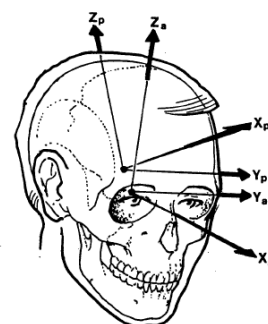


Figure B.2: Principal axis orientation for the head relative to the anatomical axis system.

	Mass	Moments		
		X	Y	Z
SMALL	4.0	193	219	144
MID-SIZE	4.2	206	235	153
LARGE	4.4	218	250	161

Table B.1: Head properties. The principal axes are rotated -36 degrees on the Y_a axis.

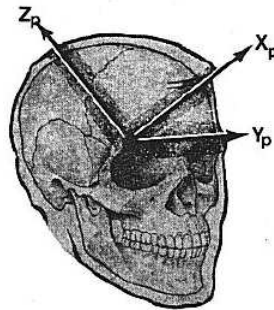


Figure B.3: Head link.

	Mass	Moments		
		X	Y	Z
SMALL	0.9	13	16	19
MID-SIZE	1.1	18	22	28
LARGE	1.2	23	27	35

Table B.2: Neck properties. The principal axes are rotated 22.2 degrees on the Y_r axis.

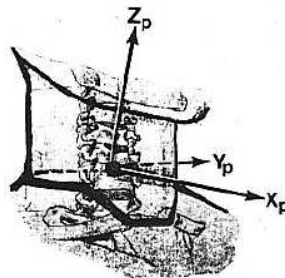


Figure B.4: Neck link.

	Mass	Moments		
		X	Y	Z
SMALL	18.6	3233	2347	1975
MID-SIZE	24.9	5224	3857	3284
LARGE	30.5	7002	5202	4432

Table B.3: Thorax properties. The principal axes are rotated -12 degrees on the Y_r axis.

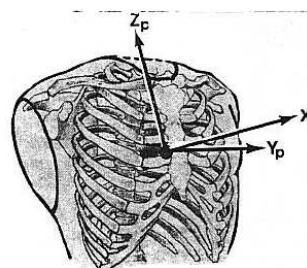


Figure B.5: Thorax link.

	Mass	Moments		
		X	Y	Z
SMALL	1.9	108	58	160
MID-SIZE	2.4	175	99	266
LARGE	2.9	233	133	356

Table B.4: Abdomen properties. The principal axes are coincident with the reference axes.

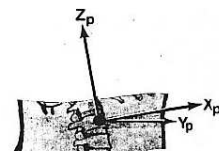


Figure B.6: Abdomen link.

	Mass	Moments		
		X	Y	Z
SMALL	8.6	651	587	746
MID-SIZE	11.8	1116	1028	1298
LARGE	14.6	1519	1408	1773

Table B.5: Pelvis properties. The principal axes are rotated -24 degrees on the Y_r axis.

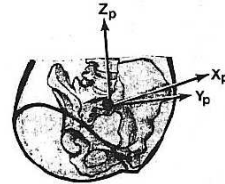


Figure B.7: Pelvis link.

	Mass	Moments		
		X	Y	Z
SMALL	1.5	85	85	17
MID-SIZE	2.0	141	141	29
LARGE	2.4	192	192	39

Table B.6: Upper arm properties. The Z_p axis is coincident with the Z_r axis and the X_p and Y_p axes are degenerate.

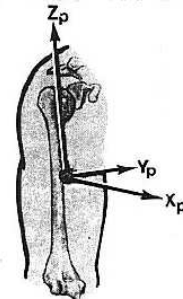


Figure B.8: Upper arm link.

	Mass	Moments		
		X	Y	Z
SMALL	1.1	61	61	9
MID-SIZE	1.4	90	90	14
LARGE	1.6	117	117	18

Table B.7: Forearm properties. The Z_p axis is coincident with the Z_r axis and the X_p and Y_p axes are degenerate.

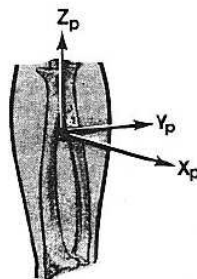


Figure B.9: Fore arm link.

Body Linkage and Center of Mass (COM) Locations

Figure B.14 illustrates the location of the centers of mass and joint centers for body segments for the mid-sized male aviator. The centers of mass of the body segments with respect to their adjacent joint centers are assumed not to change from the standing to the seated position.

With the exception of the head, the centers of mass locations are based on the stereophotometric assessments of McConville et al. (1980). The location of

	Mass	Moments		
	X	Y	Z	
SMALL	0.5	10	8	3
MID-SIZE	0.5	13	11	4
LARGE	0.6	16	13	5

Table B.8: Hand properties. The principal axes are coincident with the reference axes with the hand aligned, as shown in Figure 3.1.

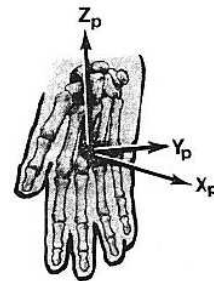


Figure B.10: Hand link.

	Mass	Moments		
	X	Y	Z	
SMALL	7.7	1093	1093	289
MID-SIZE	9.8	1652	1652	452
LARGE	11.8	2175	2175	595

Table B.9: Thigh properties. The Z_p axis is coincident with the Z_r axis and the X_p and Y_p axes are degenerate.

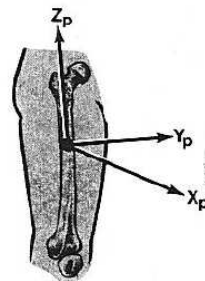


Figure B.11: Thigh link.

	Mass	Moments		
	X	Y	Z	
SMALL	3.1	406	406	48
MID-SIZE	3.8	606	406	71
LARGE	4.5	798	798	92

Table B.10: Calf properties. The Z_p axis is coincident with the Z_r axis and the X_p and Y_p axes are degenerate.

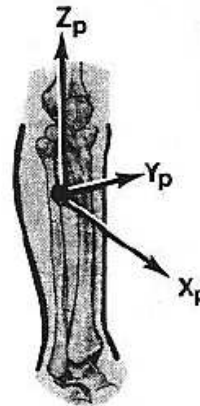


Figure B.12: Calf link.

the head center of mass is based on both the McConville data and that of Beier et al. (1979) and is similar to that derived by Robbins (1983).

The inserts in Figure B.14 show the estimated location of the trochanterion landmark with respect to the seated surface and a vertical plane tangent to the posterior surface of the buttock for an erect, seated posture.

These data are based upon the data developed by Geoffrey (1961), [49].

	Mass	Moments		
		X	Y	Z
SMALL	0.8	6	31	33
MID-SIZE	1.0	8	44	46
LARGE	1.1	11	56	59

Table B.11: Foot properties. The principal axes are coincident with the reference axes with the feet aligned as shown in Figure 3.1.

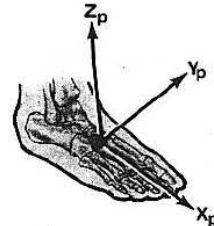


Figure B.13: Foot link.

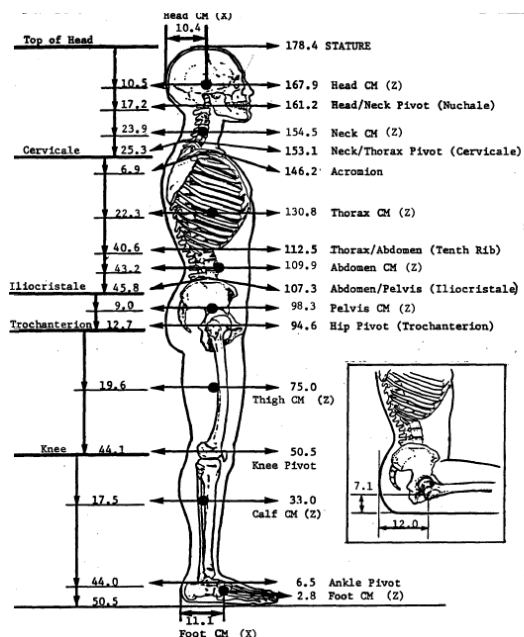


Figure B.14: Body linkage and centers of mass for the mid-sized male aviator. Units are in centimeters.

Bibliography

- [1] Biped robot johnnie (<http://www.amm.mw.tum.de/index.php?id=182&l=1>).
- [2] Hubo lab (<http://hubolab.co.kr/alberthubo.php>).
- [3] Kawada industries inc. (<http://www.kawada.co.jp/global/ams/index.html>).
- [4] *MatLab. The Language of Technical Computing. Creating Graphical User Interfaces. Version 6.*
- [5] Qrio (<http://www.sony.net/sonyinfo/news/pressarchive/200312/03-060e/>).
- [6] Toyota partner robots (<http://www.toyota.co.jp/en/special/robot/>).
- [7] Waseda humanoid lab (<http://www.humanoid.waseda.ac.jp/>).
- [8] R. Abraham and Marsden J. E. *Foundations of Mechanics*. Addison-Wesley Publishing Company, Inc., Redwood City, CA. ISBN 080530102X, 1987.
- [9] A. Albert and W. Gerth. Analytic path planning algorithms for bipedal robots without trunk. *Journal of Intelligent and Robotic Systems*, 36:109–127, 2003.
- [10] Inc. Corporate Affairs & Communications American Honda Motor Co. Technical information. Technical report, Honda Motor Co., Inc., 2003.
- [11] R. Aracil, M. Armada, C. Bosch, A. Caramagno, Casals A., S. Dormido, J. Arenas, L. Francisco, G. Ojea, A. Ollero, V. Pastor, J. Paniagua, C. Prada, M. Poza, R. Salichs, and C. Balaguer. *Fundacion Cotec para la innovacion tecnologica*. 2006.
- [12] M. Arbulu and C. Balaguer. Real time gait planning for Rh-1 humanoid robot, using local axis gait algorithm. In *7th IEEE-RAS International Conference on Humanoid Robots*, Pittsburg, USA, Nov. 29-Dec. 2 2007.
- [13] M. Arbulu and C. Balaguer. Human-humanoid robot cooperation in collaborative transportation tasks. In *Clawar 2008*, 2008.
- [14] M. Arbulu and C. Balaguer. Inverse dynamics modelling for humanoid robots based in lie groups and screws. In *Clawar 2008*, 2008.

- [15] M. Arbulu and C. Balaguer. Real-time gait planning for rh-1 humanoid robot using local axis gait algorithm. *International Journal of Humanoid Robotics*, 2008.
- [16] M. Arbulu, L.M. Cabas, P. Staroverov, D. Kaynov, C. Perez, and C. Balaguer. On-line walking patterns generation for rh-1 humanoid robot using a simple three-dimensional inverted pendulum model. In *9th International Conference on Climbing and Walking Robots (Clawar 2006)*, 2006.
- [17] M. Arbulu, J. M. Pardos, L. Cabas, P. Staroverov, D. Kaynov, C. Perez, M. Rodriguez, and C. Balaguer. Rh-0 humanoid full size robot's control strategy based on the lie logic technique. In *5th IEEE-RAS International Conference on Humanoid Robots*, pages 271–276, Tsukuba, Japan, Dec. 4-6 2005.
- [18] M. Arbulu, F. Prieto, L. Cabas, P. Staroverov, D. Kaynov, and C. Balaguer. Zmp human measure system. In *Climbing and Walking Robots*, 2005.
- [19] M. Arbulu, K. Yokoi, A. Kheddar, and C. Balaguer. Dynamic acyclic motion from a planar contact-stance to another. In *IEEE/RSJ 2008 International Conference on Intelligent Robots and Systems (IROS 08)*, 2008.
- [20] H. G. Armstrong. Anthropometry and mass distribution for human analogues, volume i: Military male aviators. Technical report, Aerospace Medical Research Laboratory and Naval Aerospace Medical Research Laboratory and Naval Air Development Center and Naval Biodynamics Laboratory and U.S. Air Force School of Aerospace Medicine and U.S. Army Aeromedical Research Laboratory, 1988.
- [21] E. Ayyappa. Normal human locomotion, part 1: Basic concepts and terminology. *Journal of Prosthetics and Orthotics*, pages 10–17, 1997.
- [22] C. Balaguer. Humanoid robots' gait control strategy based on the lie logic technique and lipm model. In *IURS 2006 Robotics Summer School on Humanoid Robots*, 2006.
- [23] C. Balaguer. Why humanoid robots? In *IURS 2006 Robotics Summer School on Humanoid Robots*, 2006.
- [24] C. Balaguer. Robotica avanzada de servicios en aplicaciones personales y metropolitanas. In *Curso de Verano de la UNED*, 2007.
- [25] R. S. Ball. *A treatise on the theory of screws*. Cornell University Library, 1900.
- [26] S. Banach. Mechanics. Technical report, 1951.
- [27] A. Barrientos, L. Pen, C. Balaguer, and R. Aracil. *Fundamentos de robtica, 2 Ed.* McGraw-Hill, 2007.
- [28] N. A. Bernstein. *Study on Biodynamics of Locomotion*. 1935.
- [29] N. A. Bernstein. *On the Construction on Movements (in Russian)*. Medgiz, 1947.

- [30] N. A. Bernstein. *The coordination and regulation of movements*. Pergamon Press., 1967.
- [31] E Bizzi and FA Mussa-Ivaldi. Neural basis of motor control and its cognitive implications. *Trends in Cognitive Science*, 2:97–102, 1998.
- [32] W. Bluethmann, R. Ambrose, M. Diftler, E. Huber, A. Fagg, M. Rosenstein, R. Platt, R. Grupen, C. Breazeal, A. Brooks, and A. Lockerd. Building an autonomous humanoid tool user. In *Proce. IEEE-RAS International Conference on Humanoid Robotics, Los Angeles, CA*, 2004.
- [33] R. A. Brooks. The cog project. *Journal of Robotic Society of Japan*, 15, 1997.
- [34] R. A. Brooks, C. Breazeal, M. Marjanovic, B. Scassellati, and M. M. Williamson. The cog project: Building a humanoid robot. Technical report, MIT Artificial Intelligence Lab, 545 Technology Square, Cambridge MA 02139, USA, 1998.
- [35] T. Buschmann, S Lohmeier, M. Bachmayer, H. Ulbrich, and F. Pfeiffer. A collocation method for real-time walking pattern generation. In *IEEE-RAS 7th International Conference on Humanoid Robots*, 2007.
- [36] L.M. Cabas, R. Cabas, P. Staroverov, M. Arbulu, D. Kaynov, C. Perez, and C. Balaguer. Challenges in the design of the humanoid robot rh-1. In *9th International Conference on Climbing and Walking Robots (Clawar 2006)*, 2006.
- [37] C Capaday. The special nature of human walking and its neural control. *Trends Neurosci*, 25:370–376, 2002.
- [38] Y. Choi, B You, and S. Oh. On the stability of indirect zmp controller for biped robot systems. In *Proceedings of 2004 IEEE/RSJ International Conference on Intelligent Robots and Systems*, 2004.
- [39] S. H. Collins and Wisse M. Ruina A., Tedrake R. Efficient bipedal robots based on passive dynamic walkers. *Science*, 307:1082–1085, 2005.
- [40] H. Cruse, T. Kindermann, M. Schumm, J. Dean, and J. Schmitz. Walknet - a biologically inspired network to control six-legged walking. *Neural Networks*, 11:1435–1447, 1998.
- [41] A. Dasgupta and Y. Nakamura. Making feasible walking motion of humanoid robots from human motion capture data. In *IEEE Internat. Conf. on Robotics and Automation*, 1999.
- [42] Ivan De la Guia, P. Staroverov, M. Arbulu, and Balaguer. C. Fast algorithm for kinematics problems solving of the low-cost legged robot leroi. In *Climbing and Walking Robots*, 2002.
- [43] F. Delcomyn. Factors regulating insect walking. *Annual Rev. Entomol.*, 30:239–256, 1985.

- [44] W. T. Dempster, Gabel W. C., and Felts W. J. L. The antropometry of manual work space for the seated subjects. *American Journal of Physics and Athropometry.*, 17:289–317, 1959.
- [45] R. Drills and R. Contini. *Body Segment Parameters*. 1966.
- [46] N. Ee Sian, K. Yokoi, S. Kajita, and K. Tanie. Whole-body motion generation integrating operator’s intention and robot’s autonomy in controlling humanoid robots. *IEEE Transactions on robotics*, 23(4):763–775, August 2007.
- [47] Andrew A. F. and M. Vukobratovic. On the gait stability of biped machines. *IEEE Transactions on Automatic Control*, pages 678–679, 1970.
- [48] R. Featherstone. *Rigid Body Dynamics Algorithms*. Springer, 2007.
- [49] S.P. Geoffrey. A 2-d mannikin—the inside story, x-rays used to determine a new standard for a basic design tool. In *Preprint of paper presented at the 1961 SAE International Congress and Exposition of Automotive Engineering*, 1961.
- [50] P. Gorce, F. El Hafi, and J. Coronado. Dynamic control of walking cycle with initiation process for humanoid robot. *Journal of Intelligent Robotic Systems*, 31:321–337, 2001.
- [51] A. Goswami. Postural stability of biped robots and the foot rotation indicator (fri) point. *International Journal of Robotics Research*, 18:523–533, 1999.
- [52] K. Hirai and Honda R&D Co. Ltd. Wako Research Center. Current and future perspective of honda humanoid robot. In *Proc. International Conference on Intelligent Robots and Systems*, 1997.
- [53] K. Hirai, M. Hirose, Y. Hikawa, and T. Takanaka. The development of honda humanoid robot. 1998.
- [54] Hirose. Hirose-fukushima robotics lab (<http://www-robot.mes.titech.ac.jp/>).
- [55] S. Hirose and Y. Umetani. Kinematic control of an active cord mechanism with tactile sensors. In *2nd CISM-IFToMM Symp. on Theory and Practice of Robots and Manipulators*, pages 241–252, 1977.
- [56] H. Hirukawa, S. Hattori, K. Harada, S. Kajita, K. Kaneko, F. Kanehiro, K. Fujiwara, and M. Morisawa. A universal stability criterion of the foot contact of legged robots - adios zmp. In *IEEE International Conference on Robotics and Automation*, pages 1976–1983, Orlando and Florida, May 2006 2006.
- [57] H. Hirukawa, S. Hattori, S. Kajita, K. Harada, K. Kaneko, F. Kanehiro, M. Morisawa, and S. Nakao. A pattern generator of humanoid robots walking on a rough terrain. In *IEEE International Conference on Robotics and Automation*, pages 2781–2187, Roma and Italy, April 10-14 2007.
- [58] Honda. Asimo website (<http://asimo.honda.com/>).

- [59] Q. Huang, K. Kaneko, K. Yokoi, S. Kajita, T. Kotoku, N. Koyachi, H. Arai, N. Imamura, K. Komoriya, and K. Tanie. Balance control of a biped robot combining off-line pattern with real-time modification. In *Proceedings of the 2000 IEEE International Conference on Robotics & Automation, San Francisco*, 2000.
- [60] A.C. Hutchinson. Machines can walk. *The Chartered Mechanical Engineer*, pages 480–484, 1967.
- [61] H. Inoue. Overview of the humanoid project of meti. In *Proc. of the 32rd International Symposium on Robotics*, pages 1478–1482, 2000.
- [62] CA 91109 Jet Propulsion Laboratory California Institute of Technology Pasadena. Nasa facts, mars exploration rover. Technical report, NASA, National Aeronautics and Space Administration, 2004.
- [63] S. Kajita, F. Kanehiro, K. Kaneko, K. Fujiwara, K. Harada, K. Yokoi, and H. Hirukawa. Biped walking pattern generation by using preview control of zero-moment point. In *IEEE International Conference on Robotics & Automation*, pages 162–1626, Taipei and Taiwan, September 14-19 2003.
- [64] S. Kajita, F. Kanehiro, K. Kaneko, K. Fujiwara, K. Yokoi, and H. Hirukawa. A realtime pattern generator for biped walking. In *IEEE International Conference on Robotics & Automation*, pages 31–37, Washington and DC, May 2002.
- [65] S. Kajita, F. Kanehiro, K. Kaneko, Fujiwara. K., K. Harada, K. Yokoi, and H. Hirukawa. Resolved momentum control: Humanoid motion planning based on the linear and angular momentum. In *IEEE/RSJ Intl. Conference on Intelligent Robots and Systems*, pages 1644–1650, Las Vegas and Nevada, October 2003.
- [66] S. Kajita, T. Nagasaki, K. Kaneko, K. Yokoi, and K. Tanie. A hop towards running humanoid biped. In *IEEE and International Conference on Robotics & Automation*, pages 629–635, New Orleans, LA, April 2004.
- [67] S. Kajita and K.: Tani. Study of dynamic biped locomotion on rugged terrain. In *IEEE Internat. Conf. on Robotics and Automation, ICRA*, 1991.
- [68] F. Kanehiro, K. Kaneko, K. Fujiwara, K. Harada, S. Kajita, K. Yokoi, H. Hirukawa, K. Akachi, and T. Isozumi. The first humanoid robot that has the same size as a human and that can lie down and get up. In *Proc. IEEE Int. Conference on Robotics and Automation*, 2003.
- [69] K. Kaneko, S. Kajita, F. Kanehiro, K. Yokoi, K. Fujiwara, H. Hirukawa, T. Kawasaki, M. Hirata, and T. Isozumi. Design of advanced leg module for humanoid robotics project of meti. In *Proc. IEEE Int. Conference on Robotics and Automation*, 2002.
- [70] K. Kaneko, F. Kanehiro, S. Kajita, H. Hirukawa, T. Kawasaki, M. Hirata, K. Akachi, and T. Isozumi. Humanoid robot HRP-2. In *IEEE International Conference on Robotics & Automation*, pages 1083–1090, New Orleans and LA, April 2004.

- [71] T. Katayama, T. Ohkis, T. Tnoues, and T. Kato. Design of an optimal controller for a discrete-time system subject to previewable demand. *International Journal of Control*, 41(3):677–699, 1985.
- [72] I. Kato, S. Ohteru, H. Kobayashi, K. Shirai, and A. Uchiyama. Information-power machine with senses and limbs (wabot -1). In *1st CISM-IFTOMM Symposium on theory and practice of Robots and Manipulators*, 1973.
- [73] D. Kaynov, M. Arbulu, L.M. Cabas, C. Staroverov, P. andPerez, and C. Balaguer. Control architecture for the dynamic humanoid robot walking. application to the rh-1 robot. In *9th International Conference on Climbing and Walking Robots (Clawar 2006)*.
- [74] O. Khatib. A unified approach for motion and force control of robot manipulators: the operational space formulation. *IEEE Journal of Robotics and Automation*, RA-3(3):43–53, February 1987.
- [75] O. Khatib, J. Warren, V. De Sapiro, and L. Sentis. Human-like motion from physiologically-based potential energies. *Advances in Robot Kinematics and Kluwer Academic Publishers and first edition and 2004*, pages 149–163, 2004.
- [76] J. Kim. Walking pattern generation of a biped walking robot using convolution sum. In *IEEE-RAS 7th International Conference on Humanoid Robots*, 2007.
- [77] Y. Koga, K. Kondo, J. Kuffner, and J. Latombe. Planning motions with intentions. 1994.
- [78] J. Kuffner, K. Nishiwaki, S. Kagami, M. Inaba, and H. Inoue. Motion planning for humanoid robots. 2003.
- [79] W. Lee and M. Raibert. Control of hoof rolling in an articulated leg. In *Proc. of the IEEE Conf. on Robot. and Automat*, 1991.
- [80] K. Loeffler, M. Gienger, F. Pfeiffer, and H. Ulbrich. Sensors and control concept of a biped robot. *IEEE TRANSACTIONS ON INDUSTRIAL ELECTRONICS*, 51:1–9, 2004.
- [81] P. Manoonpong, T Geng, T Kulvicius, B. Porr, and F. Worgotter. Adaptive, fast walking in a biped robot under neuronal control and learning. *The official journal of the International Society for Computational Biology*, 2007.
- [82] N. Mansard, O. Stasse, F. Chaumette, and K. Yokoi. Visually-guided grasping while walking on a humanoid robot. In *2007 IEEE International Conference on Robotics and Automation Roma and Italy and 10-14 April 2007*, pages 3041–3047, 2007.
- [83] J. T. McConville and Lloyd L. L. *Anthropometry. Chapter III in Anthropometric Source Book, Volume I: Anthropometry for Designers*. NASA Reference Publication No. 1024 (NTIS - HC A99hlF A01 CSCL 05H). National Aeronautics and Space Administration, Scientific and Technical Information Office., 1978.

- [84] T. McGeer. Passive walking with knees. In *Robotics and Automation proceedings*, 1990.
- [85] M. Mori and S. Hirose. Three-dimensional serpentine motion and lateral rolling by active cord mechanism acm-r3. In *Proc. of IEEE/RSJ Int. Conf. on intelligent Robots and Systems*, 2002.
- [86] R. M. Murray, Z. Li, and S. S. Sastry. *Mathematical Introduction To Robotic Manipulation*. CRC Press, 1994.
- [87] F. A. Mussa-Ivaldi and E. Bizzi. Motor learning through the combination of primitives. *Philos Trans R Soc Lond B Biol Sci.*, 355:1755–1769, 2000.
- [88] Yoshihiko Nakamura. *Advanced Robotics: Redundancy and Optimization*. Addison-Wesley, 1991.
- [89] J Nakanishi, J Morimoto, G Endo, G Cheng, and S Schaal. Learning from demonstration and adaptation of biped locomotion. *Robotics and Autonomous Systems* 47, 47:79–91, 2004.
- [90] NASA. Man-systems integration standards. Technical report, NATIONAL AERONAUTICS AND SPACE ADMINISTRATION, 1995.
- [91] Y. Ogura, H. Aikawa, K. Shimomura, H. Kondo, A. Morishima, H. Lim, and A. Takanishi. Development of a new humanoid robot to realize various walking pattern using waist motions. In *Proceedings of the sixteenth CISM-IFTOMM Symposium on Robot Design, Dynamics, and Control (ROMANSY16)*, 2006.
- [92] J. M. Pardos and C. Balaguer. Rh-0 humanoid robot bipedal locomotion and navigation using lie groups and geometric algorithms. In *International Conference on Intelligent Robots and Systems (IROS 2005)*, Edmonton, Canada, Aug. 2005.
- [93] J.M. Pardos. *Geometrical Algorithms for Mechanics, Control and Navigation of Humanoids Robots. Application to Rh-0 Robot*. PhD thesis, University Carlos III of Madrid, 2005.
- [94] F.C. Park, J.E. Bobrow, and S.R. Ploen. A lie group formulation of robot dynamics. *Int. J. Robotics Research*, 14, No. 6:609–618, 1995.
- [95] S.R. Ploen. *Geometric Algorithms for the Dynamics and Control of Multi-body Systems*. PhD thesis, University of California, Irvine, 1997.
- [96] J. Pratt, J. Carff, S. Drakunov, and A. Goswami. Capture point: A step toward humanoid push recovery. In *Humanoids 06*, 2006.
- [97] J. Pratt, C. Chee-Meng, A. Torres, P. Dilworth, and G. Pratt. Virtual model control: An intuitive approach for bipedal locomotion. *The International Journal of Robotics Research*, 20, N2:129–143, 2001.
- [98] M. H. Raibert. Hopping in legged systems: Modeling and simulation for the 2d one-legged case. *IEEE Transactions on Systems, Man, and Cybernetics*, 14:451–463, 1984.

- [99] M. H. Raibert. *Legged robots that balance*. 1986.
- [100] M. Russel. The first functionoid. *Robotics Age*, 5:12–18, 1983.
- [101] Y. Sakagami, R. Watanabe, C. Aoyama, S. Matsunaga, N. Higaki, and K. Fujimura. The intelligent asimo: System overview and integration. In *Proceedings of the 2002 IEEE/RSJ International Conference on Intelligent Robots & Systems*, 2002.
- [102] J. B. Saunders, V. T. Inman, and Eberhart H. D. The major determinants in normal and pathological gait. *JBJS*, 35-A:543–58, 1953.
- [103] R. D. Schraft and Gernot Schmieder. *Service Robots Products Scenarios Visions*. AK Peters; 1st edition, 2000.
- [104] L. Sentis and O. Khatib. Synthesis of whole-body behaviors through hierarchical control of behavioral primitives. *International Journal of Humanoid Robotics*, pages 1–15, 2005.
- [105] B. Siciliano and O. Khatib. *Handbook of Robotics*. Springer, 2008.
- [106] O. Sporns and G. M. Edelman. Solving bernstein’s problem: A proposal for the development of coordinated movement by selection. *Child Development*, 64:960–981, 1993.
- [107] P. Staroverov, D. Kaynov, M. Arbulu, L.M. Cabas, C. Perez, and C. Balaguer. A voice controlled image recognition system. In *9th Internacional Conference on Climbing and Walking Robots (Clawar 2006)*, 2006.
- [108] T. Takenaka, T. Matsumoto, and T. Yoshike. Gait generation device for legged mobile robot. Technical report, HONDA MOTOR CO., Ltd, 2006.
- [109] K. Tanie. New trends of walking robotics research and its application possibilities. Technical report, The National Institute of Industrial Science and Technology (AIST), Tsukuba, Ibaraki, Japan, 2001.
- [110] K. Tanie and FNR. Toward a platform based humanoid project, robotics research. *Eds. Y. Shirai and S. Hirose, Springer*, pages 439–450, 1998.
- [111] K. Terada and Y. Kuniyoshi. Online gait planning with dynamical 3d-symmetrization method. In *IEEE-RAS 7th International Conference on Humanoid Robots*, 2007.
- [112] M.W. Thring. *Robots and Telechirs*. Ellis Horwood, 1983.
- [113] D.J. Todd. *Walking Machines an Introduction to legged robots*. Kogan Page Ltd., 1985.
- [114] R. Tomovic and R.B. McGhee. A finite state approach to the synthesis of bioengineering control systems:. *IEEE Transactions on Human Factors in Electronics*, 7:65–69, 1966.
- [115] MT Turvey. Coordination. *American Psychologist*, 45:938–953.

- [116] Y. Umetani and K. Yoshida. Resolved motion rate control of space manipulators with generalized jacobian matrix. *IEEE TRANSACTIONS ON ROBOTICS and VOL. 5 and NO. 3 and JUNE 1989*, pages 303–314, 1989.
- [117] B. Verrelst, K. Yokoi, O. Stasse, Vanderborght; B., and H. Arisumi. Mobility of humanoid robots: Stepping over large obstacles dynamically. In *IEEE International Conference on Mechatronics and Automation*, pages 1072–1079, Luoyang and China, June 25 - 28 2006.
- [118] M. Vukobratovic and B. Borovac. Zero-moment point - thirty five years of its life. *International Journal of Humanoid Robotics*, 1:157–173, 2004.
- [119] M. Vukobratovic, B. Borovac, and V. Potkonjak. Zmp: A review of some basic misunderstandings. *International Journal of Humanoid Robotics*, 2:153–175, 2006.
- [120] M. Vukobratovic, B. Borovac, D. Surla, and D. Stokic. *BIPED LOCOMOTION: DYNAMICS, STABILITY, CONTROL AND APPLICATION*, Springer-Verlag, 1989.
- [121] M. Vukobratovic, D. Hristic, and Z. Stojiljkovic. Development of active anthropomorphic exoskeletons. *Medical and Biological Engineering*, pages 66–80, 1974.
- [122] M. Vukobratovic and D. Juric. Contribution to the synthesis of biped gait. *IEEE Transactions on Biomedical Engineering*, 16, 1969.
- [123] K. Waldron. Configuration design of the adaptive suspension vehicle. *The International Journal of Robotics Research*, 3:37–47, 1984.
- [124] Pierre-Brice Wieber. Trajectory free linear model predictive control for stable walking in the presence of strong perturbations. In *Humanoids 2006*, pages 137–142, 2006.
- [125] David A. Winter. *Biomechanics And Motor Control of Human Movement*. A Wiley-Interscience Publication, 1990.
- [126] I. Yamaguchi, A. Takanishi, and I. Kato. Development of a biped walking robot compensation for three - axis moment by trunk motion. In *Proc. IEEE/RSJ Int. Conf. Intelligent Robot and Systems*, 1993.
- [127] S. Ylnen, I. Leppnen, S. Salmi, and A. Halme. Hybrid locomotion of the workpartner service robot. In *FSR 2001*, 2001.
- [128] K. Yokoi. Human-humanoid teamwork. In *Workshop on "Collaborative Human-Robot Teamwork" in ICRA2006, May 19, 2006*. AIST-CNRS Joint Robotics Laboratory (JRL) National Institute of Advanced Industrial Science and Technology(AIST), 2006.
- [129] E. Yoshida, O. Kanoun, C. Esteves, and J. P. Laumond. Task-driven support polygon reshaping for humanoids. In *Humanoids 2006*, 2006.

- [130] J. W. Young, R. F. Chandler, C. C. Snow, K. M. Robinette, G. F. Zehner, and M. S.. Lofberg. Anthropometric and mass distribution characteristics of the adult female. technical report no. faa-am-83-16. Technical report, Civil Aeromedical Institute, Federal Aviation Administration, Oklahoma City, 1983.